TRANSPORTATION RESEARCH RECORD 1087

Durability, Strength, and Analysis of Culverts and Tunneling Machines

TRB
TRANSPORTATION RESEARCH BOARD
NATIONAL RESEARCH COUNCIL
WASHINGTON, D.C. 1986

Transportation Research Record 1087
Price $12.00
Editor: Elizabeth W. Kaplan
Compositor: Joan G. Zubal
Layout: Theresa L. Johnson

modes
1 highway transportation
3 rail transportation

subject areas
25 structures design and performance
63 soil and rock mechanics

Transportation Research Board publications are available by ordering directly from TRB. They may also be obtained on a regular basis through organizational or individual affiliation with TRB; affiliates or library subscribers are eligible for substantial discounts. For further information, write to the Transportation Research Board, National Research Council, 2101 Constitution Avenue, N.W., Washington, D.C. 20418.

Printed in the United States of America

Library of Congress Cataloging-in-Publication Data
National Research Council. Transportation Research Board.

Durability, strength, and analysis of culverts and tunneling machines

(Transportation research record, ISSN 0361-1981 ; 1087)
1. Culverts. 2. Tunneling—Equipment and supplies. I. National Research Council (U.S.). Transportation Research Board. II. Series.
TE7.H5 no. 1087 380.5 s 86-33154
[TE213] [625.7'342]
ISBN 0-309-04107-4

Transportation Research Record 1087

The **Transportation Research Record** series consists of collections of papers on a given subject. Most of the papers in a Transportation Research Record were originally prepared for presentation at a TRB Annual Meeting. All papers (both Annual Meeting papers and those submitted solely for publication) have been reviewed and accepted for publication by TRB's peer review process according to procedures approved by a Report Review Committee consisting of members of the National Academy of Sciences, the National Academy of Engineering, and the Institute of Medicine.

The views expressed in these papers are those of the authors and do not necessarily reflect those of the sponsoring committee, the Transportation Research Board, the National Research Council, or the sponsors of TRB activities.

Transportation Research Records are issued irregularly; approximately 50 are released each year. Each is classified according to the modes and subject areas dealt with in the individual papers it contains. TRB publications are available on direct order from TRB, or they may be obtained on a regular basis through organizational or individual affiliation with TRB. Affiliates or library subscribers are eligible for substantial discounts. For further information, write to the Transportation Research Board, National Research Council, 2101 Constitution Avenue, N.W., Washington, D.C. 20418.

Contents

Field Performance of Corrugated Polyethylene Pipe Culverts in Ohio

JOHN O. HURD

A total of 172 corrugated polyethylene pipe culverts 12 through 24 in. in diameter and ranging in age from 0 to 4 years were inspected in Ohio in the summer of 1985. Data pertinent to structural performance and durability of the culverts were collected at each site. These data were pipe diameter, cover over the pipe, type of backfill, culvert age, average daily traffic, pipe deflection, flow depth and velocity, bed load depth and size, water pH, and pipe slope. No culvert showed any signs of wear even at sites with abrasive flow. One 4-year-old site had constant low pH dry weather flow with a bed load of large cobbles. The incidence of large maximum deflections or wall flattening and buckling, or both, was significantly greater for 12- and 15-in. pipes than for 18- and 24-in. pipes. The only instances of wall flattening or buckling were limited to the 12- and 15-in. culverts. Large deflections, flattening, and buckling were generally due to bending of the pipe wall in both the circumferential and longitudinal directions. The greater flexibility and thinner walls of the 12- and 15-in. culverts were the only apparent reasons for the difference in performance.

Because of recent concern of governmental agencies about the nation's deteriorating infrastructure *(1–3)* many highway agencies have placed increased emphasis on repairing or replacing deteriorating bridges and roadway culverts. This concern has been reflected by the numerous recent reports on culvert durability *(4–8)*.

Corrugated polyethylene pipe has been suggested as a feasible material for small culvert replacement because of its ease of handling and corrosion resistance to most normal stream flows. Current available culvert pipe sizes range to 24 in. in diameter. The pipe is normally provided in 20-ft lengths. The most common concern about the use of corrugated polyethylene pipe for culvert replacements is its structural performance under highway loadings.

Considerable laboratory testing of tubing and pipe, and field testing of pipe installed with controlled backfill procedures, has been carried out *(9–14)*. The results of this work have been used to establish a theoretical required ring stiffness ($53.77EI/D^3$, as defined in the Iowa deflection formula) for various pipe diameters based on an allowable deflection of 5 percent. Deflections in excess of 25 percent can occur without buckling (reversal of curvature); failure of the ring occurs if adequate sidewall support is available. However, there is still concern about the use of these design criteria for real-world culvert installations with less than optimal "uncontrolled" backfill procedures.

Several Ohio Department of Transportation (ODOT) districts and Ohio county engineers have been using corrugated polyethylene pipe for small culvert replacements on a provisional basis since 1981. Use of this material by ODOT and the county engineers contacted has been limited to 12- through 24-in. sizes. Most culvert installations have been on secondary highways with no more than 6 ft of shallow cover.

Because there was concern regarding the structural capability of corrugated polyethylene pipe installed under pavement with uncontrolled backfill procedures, seven of the early culvert installations in Ohio were measured shortly after construction to determine deflection. There were no structural problems observed in any of the culverts measured. Measured deflections ranged from negative (i.e., crowning of the pipe) to approximately 8 percent.

Because the few corrugated polyethylene pipe culverts previously evaluated were nearly new when measurements were taken, there was still some question regarding the longer-term effects of live loading on the structural performance of these culverts. Updated measurements on these culverts would be required to determine if there was any effect of long-term live loading. That these culverts were also the first of their type installed may also have led to "more careful" than normal installation procedures. Thus there was some question whether these installations were representative of true maintenance replacement procedures. A broader data base would be required to determine to what degree corrugated polyethylene pipe culverts were "installation proof." In addition to structural performance, the ability of the pipe material to withstand abrasive flows was of interest because of the questionable performance of polymeric coatings of metal pipe at abrasive flow sites *(5–8)*.

Therefore, as part of ODOT's continuing culvert performance evaluation program, the structural and durability performance of all existing known corrugated polyethylene pipe culverts installed in the state of Ohio was evaluated. This study was undertaken in February 1985 and completed in August 1985.

CULVERT INVENTORY

To provide a data base for the study, all ODOT district maintenance engineers and Ohio county engineers who had purchased corrugated polyethylene pipe from a local supplier were contacted and asked to provide a list of culvert locations. Culvert locations were obtained from five ODOT field districts and five county engineers.

A total of 172 culverts were inspected in 21 counties in Ohio. Twenty-eight 12-in., ninety-two 15-in., thirty-one 18-in., and twenty-one 24-in. culverts were inspected. The number of culverts of each specific size in each county is shown in Figures 1 and 2.

DATA COLLECTION

A total of 3 weeks of field work by a two-man team was required to collect field data for the 172 culverts inspected. In addition to the culvert site inspection several members of ODOT district and local

Ohio Department of Transportation, 25 South Front Street, Columbus, Ohio 43215.

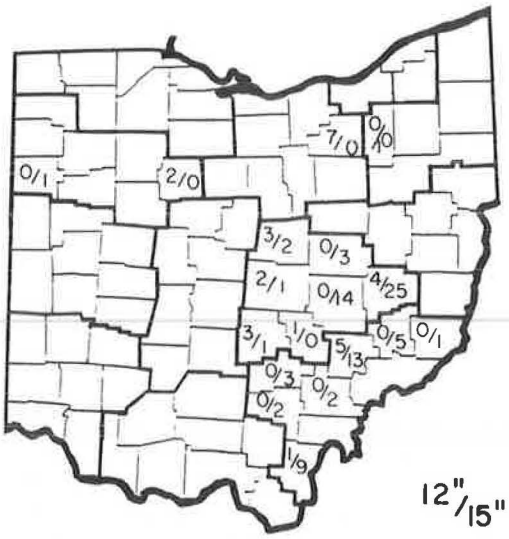

FIGURE 1 12- and 15-in. corrugated polyethylene pipe culverts in Ohio.

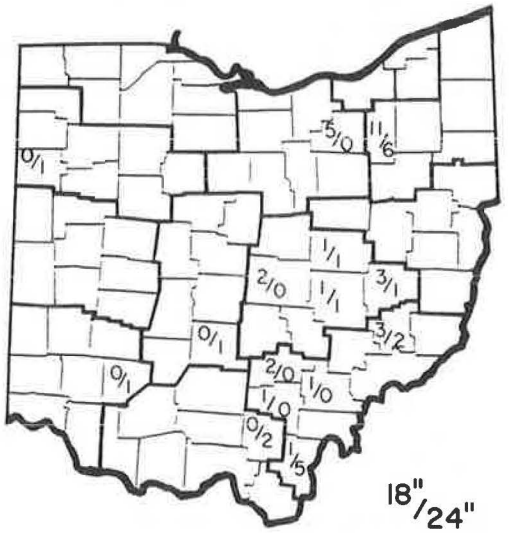

FIGURE 2 18- and 24-in. corrugated polyethylene pipe culverts in Ohio.

county engineers' staffs were contacted in person or by telephone to obtain traffic counts and other additional information regarding culvert installations. The following information, pertinent to the structural performance and durability of corrugated polyethylene pipe culverts, was obtained during the field data collection phase.

Pipe Diameter

The pipe diameter of each culvert provided on the culvert inventory was verified at the site. As previously indicated, pipe sizes were 12, 15, 18, and 24 in.

Cover over Pipe

The cover from crown to road surface over each culvert provided on the culvert inventory was visually verified at the site. If this information was not provided on the inventory or provided incorrectly, the cover was measured at the site. Pipe covers ranged from less than 6 in. to 6 ft. Various installation specifications require a minimum cover of from 12 to 18 in.

Type of Backfill

The type of culvert backfill or bedding material, or both, was obtained from ODOT or county personnel or visually determined at each site. Additional specific information related to bedding and backfill procedures at each site was not available because the culverts inspected were "real-world" maintenance installations. The installations are usually done hurriedly under maintained traffic. Conformance with ODOT construction specifications varies from site to site even within an individual county. Normally mechanically tamped backfill in shallow lifts is not used as often as large lifts "compacted" by saturation with water. A distinction was made among five different types of backfill material: crushed limestone, sand and gravel, a mixture of ash and stone, miscellaneous granular material, and native soil.

Age of Culvert

The installation dates of culverts were obtained from the culvert inventory. If the site inspection indicated a gross error in the inventory, the age was adjusted. New installations were considered to be installed in late spring of 1985. Ages ranged from 0 to 4 years.

Average Daily Traffic

The average daily traffic total of cars and trucks was obtained from ODOT published traffic counts for state highways and from county engineers for county highways. Average daily truck traffic ranged from 2 to 480 vehicles per day. Average daily car traffic ranged from 20 to 4,800 vehicles per day. One section of highway with several installations had frequent coal truck traffic. None of the culverts observed on this section of highway showed any sign of structural problems. Several culverts were inspected when coal trucks passed over them and no apparent movement was observed. Cover over these culverts ranged from less than 1 to 4 ft.

Culvert Alignment

Changes in vertical or horizontal alignment, or both, of the culverts were noted. Because of the longitudinal flexibility of corrugated polyethylene pipe, minor changes in culvert grade or direction can be accomplished by "bending the pipe." An increase in pipe deflection was not noticed with a gradual transition accomplished by a long bend. However, a slight increase in deflection was observed at quick changes in grade. Shear loading points such as soil settlement behind retaining walls or soil slip planes were also noted (Figure 3). Considerable increases in deflection were observed at these points. Buckling of the ring section was observed at a soil slip plane on one culvert, but the remainder of the pipe had no deflection. Alignment changes were observed much more often in 12- and 15-in. pipe than in 18- and 24-in. pipe. District and county personnel noted difficulties in maintaining alignment of the 12- and 15-in. pipes during backfill procedures.

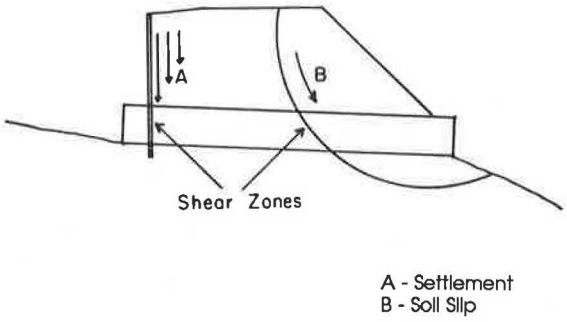

FIGURE 3 Schematic representation of shear loading.

County of Installation

The county of installation was used as representative of the installation crew. Alignment changes and deflection varied considerably among the various counties.

Deflection and Buckling

Three primary indices were used in the evaluation of the structural performance of corrugated polyethylene pipe culverts: average deflection, maximum deflection, and the presence of wall flattening or buckling. Average deflection is the average observed or measured deflection throughout the length of the culvert, excluding the ends. Average deflection is representative of culvert performance under "uniform" loadings and backfill conditions that are in general conformance with ring compression-deflection theory. Maximum deflection is the deflection at the point within the culvert where deflection is greatest, excluding the ends. Maximum deflection is more representative of culvert reaction to variable spot loadings and backfill conditions often encountered in actual installations. Flattening is the loss of curvature in the pipe wall, and buckling is the reversal of curvature in the pipe wall. Deflection, flattening, and buckling are shown schematically in Figure 4.

Because all the culverts were relatively short, the interiors could be easily observed from the ends with the aid of a high-intensity flashlight powered from an automobile cigarette lighter. Where no vertical deflection or slight vertical deflection was observed, it was so recorded. Where significant vertical deflection was observed and the interior of the pipe was accessible for measurement, the rise of the pipe was measured with a deflectometer developed by a local corrugated polyethylene pipe manufacturer. Where the pipe interior was not accessible vertical deflections were estimated. In general there was concurrent increase in the horizontal dimension with decrease in the vertical dimension. Deflectometers were available for 15-, 18-, and 24-in. culverts. The 24-in. deflectometer is shown in Figure 5. All seven culverts previously measured were remeasured even if no significant deflection was observed. There was no increase in pipe deflection in any of these seven culverts.

FIGURE 5 Direct-reading deflectometer for measuring deflection in 24-in. culverts.

Significant deflection to the point of wall flattening or buckling through a significant portion of the culvert length was observed in four culverts. Flattening occurred at deflections exceeding approximately 15 percent. Buckling occurred at deflections exceeding 25 percent. Where significant deflection occurred throughout the pipe length, it was not constant but occurred in waves as shown in Figure 6. Large deflections, flattening, and buckling appeared in general to be caused by bending of the pipe wall inward in both the circumferential and longitudinal directions. In three cases flattening of the wall was more prevalent in the invert than on the crown

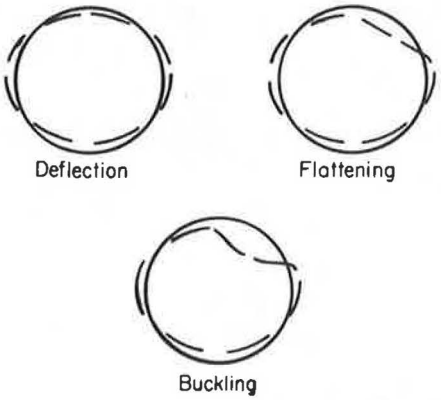

FIGURE 4 Schematic representation of flexible pipe deflection, flattening, and buckling.

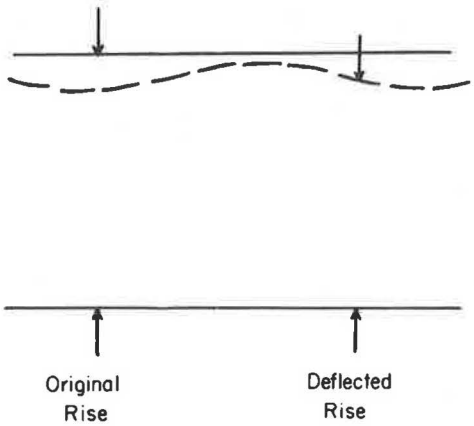

FIGURE 6 Varying deflection observed in corrugated polyethylene pipe culverts.

of the culvert, which suggests poor foundation. Two of the culverts had buckled to the point of being cracked and needing repair. Apparently the internal corrugation crests had been stressed by bending moment to the point of tearing apart.

Seven additional culverts had single flattened or buckled spots less than 1 ft long. These spots on three culverts were at shear points or severe vertical bends. Buckled spots on the other four culverts appeared to be just dents in the crown of the pipe, possibly caused by the dropping of a heavy object on the pipe.

All of these cases were limited to 12- and 15-in. culverts. Although the dented spots do not cause structural problems for the culvert as a whole, they produce a constriction within the barrel of the pipe and are not desirable hydraulically. Care should be taken to avoid denting the pipe.

Deflections in the rest of the culverts ranged from negative (i.e., crowning) to approximately 10 percent. The deflections at pipe joints were in general slightly larger than the deflections throughout the rest of the culvert.

On the basis of field observations only, it appears that pipe culvert performance is related only to pipe size and county of installation.

Condition of Pavement

The pavement surface above the culverts was observed at each site and any significant dips were noted. In general there was no concurrent dip in the roadway surface over culverts with larger deflections. This suggests that the deflections observed were built into the culverts rather than produced by live load on the pipe.

Durability Data

The condition of the culvert invert was observed at each site. It was planned to take coupons from pipes with noticeable wear. Because none of the culverts inspected showed any visible signs of loss of materials, no coupons were taken. Flow depth, observed flow velocity, sediment depth, and bed load size were recorded at each site as indicators of abrasiveness of flow. Water pH was taken at sites where there was significant flow. Pipe slopes were obtained from the inventory or estimated at the site for most of the culverts. Water pH ranged from 3.5 to 8.3 and flows ranged from nonabrasive to extremely abrasive.

Although no estimate of service life could be made because of the small age range of the culverts studied, an indication of the durability of corrugated polyethylene pipe can be obtained by looking at the worst-case installation. A 24-in. corrugated polyethylene pipe culvert was installed at NOB–145–3.58 in 1981. This culvert is shown in Figure 7. There is constant acidic dry weather flow at the site, and storm flows carry a bed load of abrasive cobbles. The pile of sediment on the bank of the outlet channel shown in Figure 8 is indicative of the force generated by the storm water flowing through the culvert. After 4 years this culvert is in good condition. The invert of the polymeric-coated galvanized corrugated steel pipe previously at this location completely deteriorated in less than 1 year.

Additional Observations

Damaged ends were observed on seven of the culverts inspected. Three appeared to have been damaged during installation. Three appeared to have been run over by errant vehicles or mowers. The tops of the corrugations on the end of one culvert with minimal cover on a side road appeared to have been sheared off by a snowplow. Although damaged ends do not present a structural problem, they could affect hydraulic performance. Therefore, vulnerable culvert ends should be delineated or protected, or both. This is especially true for shallow installations. There was no apparent deterioration of exposed ends due to ultraviolet sunlight rays.

FIGURE 7 24-in. corrugated polyethylene pipe culvert at NOB–145–3.58: low pH and severely abrasive flow.

FIGURE 8 Outlet channel debris at NOB–145–3.58 indicative of force of storm flow.

ANALYSES OF DATA

Various statistical analysis procedures including regression analysis, analysis of variance, and χ^2 tests were applied to the data to determine if deflection, flattening, or buckling was affected by any site parameters. Those parameters were pipe diameter, pipe cover, backfill type, culvert age, average daily truck traffic, average daily car traffic, culvert alignment, and county of installation.

None of the parameters studied had any quantifiable effect on average deflection. There was slight correlation between average deflection and average daily car traffic. As car traffic increased so did average deflection. However, this correlation accounted for only 2 percent of the scatter in the average deflection data. It is questionable whether light automobile loadings would affect deflection. County personnel interviewed indicated that installations were in general more rapid on highways with greater traffic. This could result in less dense backfill and thus greater average deflection.

None of the parameters studied had any quantifiable effect on maximum deflection or buckling. However, there was strong correlation between maximum deflection and culvert size and between occurrence of buckling and culvert size. As observed in the field, the incidence of large maximum deflections and buckling was significantly greater for 12- and 15-in. culverts than for 18- and 24-in. culverts. This is contrary to standard flexible pipe deflection theory, which is the basis for ASTM structural requirements for corrugated polyethylene pipe. Theoretical ring stiffnesses (53.77 EI/D^3) of 12- and 15-in. corrugated polyethylene pipe are greater than those of 18- and 24-in. pipe, and measured ring stiffnesses of the various sizes are about the same *(10–14)*.

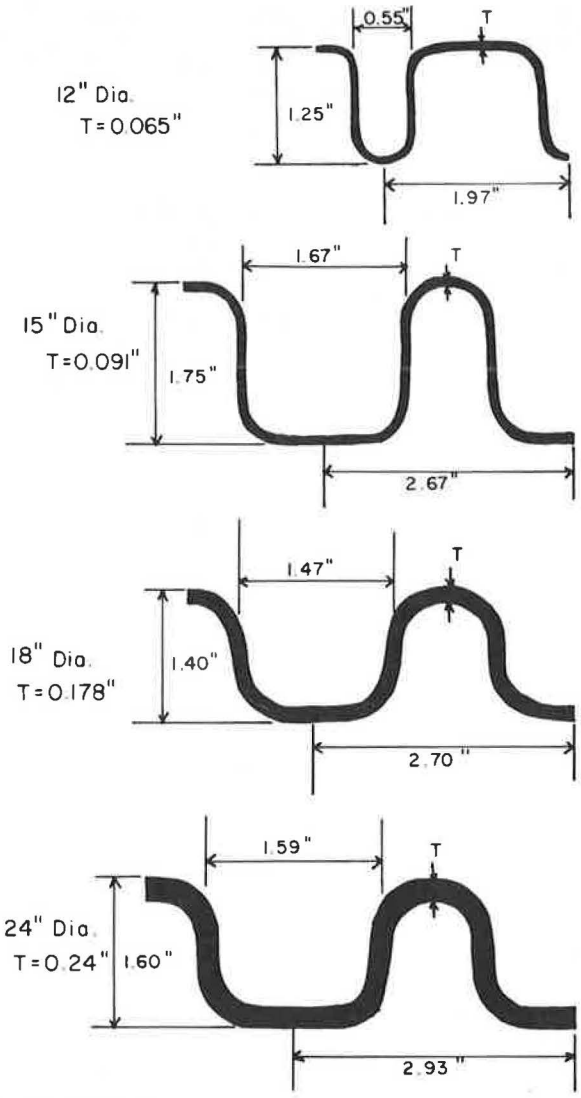

FIGURE 9 Corrugated polyethylene pipe corrugation profiles.

However, it can be seen in Figure 9 that the wall thicknesses of the 12- and 15-in. pipes are considerably thinner than those of the 18- and 24-in. pipes. Although theoretical flexibility factors (D^2/EI) for 12- and 15-in. pipe are slightly less than those for 18- and 24-in. pipe, actual measured flexibility factors for the smaller pipes were larger *(10–14)*. It was previously noted that the 12- and 15-in. pipe was much more difficult to handle than the 18- and 24-in. pipe. It is possible that with variable loadings and large local deflections as shown in Figure 6 the thinner walls of the "more flexible" 12- and 15-in. pipe allow a flattening (reduction in the rise) of the corrugation profile during bending in the longitudinal direction. This in turn would significantly reduce the ring stiffness of the pipe and allow bending in the circumferential direction. Observation of culverts with severe deflection and buckling showed a definite flattening of corrugation profile at points of maximum deflection.

The incidence of alignment changes was significantly greater for 12- and 15-in. pipe than for 18- and 24-in. pipe. Accomplishing an alignment change requires a flattening of the corrugation profile on the outside of the bend. The thinner walls of the more flexible 12- and 15-in. pipe allow this much more readily than in 18- and 24-in. pipe. Movement of the pipe during backfill will lead to differential loadings, causing the culvert not to behave in a theoretical ring compression-deflection manner.

The incidence of large maximum deflection and buckling was significantly greater in two counties than in the rest. This would indicate that large deflections and buckling are caused by backfill compaction quality control problems. These differences were most noticeable in the 12- and 15-in. culverts.

CONCLUSIONS

On the basis of field observations and data analyses the following conclusions can be drawn:

1. Because of their greater flexibility and much thinner walls, 12- and 15-in. corrugated polyethylene pipe culverts are more susceptible to bending moment stresses in both the circumferential and longitudinal directions. Thus the smaller pipes are much less installation proof than 18- and 24-in. corrugated polyethylene pipe culverts.
2. There is no increase in pipe deflection after 2 to 4 years in corrugated polyethylene culverts with small to moderate initial deflections (less than 10 percent deflection).
3. Four years' data indicate that corrugated polyethylene pipe appears to be resistant to abrasive flows.
4. Shallow cover and heavy truck traffic do not appear to be detrimental to the structural performance of corrugated polyethylene pipe culverts. Deflection appears to be built into the culverts instead of caused by highway loadings.
5. Exposed culvert ends are vulnerable to damage by mowing machines and other maintenance equipment. Exposure to sunlight did not appear to affect the condition of the exposed ends.

RECOMMENDATIONS

On the basis of these conclusions, the following recommendations are made:

1. The wall thickness of 12- and 15-in. corrugated polyethylene pipe should be increased, or pipes of these sizes should be securely anchored in the trench during backfill operations to provide a larger factor of safety against less than optimal installation methods.
2. Revision of ASTM structural requirements for corrugated polyethylene pipe to include consideration of flexibility and resistance to bending moment should be considered.
3. Culverts with moderate to large initial deflections (10 percent or greater) under the roadway should be observed periodically to determine if any increase in deflection occurs with time for this range of initial deflections.
4. Corrugated polyethylene pipe culvert ends should be delineated and protected with headwalls under minimal cover conditions.

ACKNOWLEDGMENT

The author wishes to thank all of the ODOT and county personnel who aided in the data collection phase of the study. Special thanks are given to James B. Goddard of ADS, Inc., for providing field equipment and assistance in data collection.

REFERENCES

1. R. Hanson. *Perspectives on Urban Infrastructure*. National Research Council, Washington, D.C., 1984.
2. H. C. Heldenfels. How Bad Are Things for America's Infrastructure? *Professional Engineer*, Vol. 52, No. 4, 1982.
3. America's Infrastructure. *Constructor*, Vol. 65, No. 5, 1983.
4. P. J.Bellair and J. P. Ewing. *Metal Loss Rates of Uncoated Steel and Aluminum Culverts in New York*. FHWA/NY/RR–84/115. New York State Department of Transportation, Albany; FHWA, U.S. Department of Transportation, 1984.
5. D. G. Meacham, J. O. Hurd, and W. W. Shisler. *Ohio Culvert Durability Study*. ODOT/L&D/82–1. Ohio Department of Transportation, Columbus, 1982.
6. W. H.Temple, S. L. Cumbaa, and B. J. Gueho. *Evaluation of Drainage Pipe by Field Experimentation and Supplemental Laboratory Experimentation*. FHWA/LA–85/174. Louisiana Department of Transportation and Development, Baton Rouge; FHWA, U.S. Department of Transportation, 1985.
7. W. T. Young. *Evaluation of Highway Culvert Coating Performance*. FHWA/RD–80/059. FHWA, U.S. Department of Transportation, 1980.
8. *Transportation Research Record 1001: Symposium on Durability of Culverts and Storm Drains*. TRB, National Research Council, Washington, D.C., 1984.
9. R. W. Cully. *Structure Test on Large Diameter Polyethylene Culvert Pipe*. Saskatchewan Highways and Transportation Department, Regina, Saskatchewan, Canada, 1982.
10. J. L. Fouss. *Structural Design Procedure for Corrugated Plastic Drainage Tubing*. Technical Bulletin 1466. Agricultural Research Service, U.S. Department of Agriculture, 1973.
11. J. B. Goddard. *Structural Design of Plastic Pipes*. ADS, Inc., Columbus, Ohio, 1983.
12. R. K. Watkins and R. C. Reeve. *Structural Performance of Buried Corrugated Polyethylene Tubing*. 30th Annual Highway Geology Symposium, Portland, Ore., 1979.
13. R. K. Watkins and R. C. Reeve. *Effect of Heavy Loads on Buried Corrugated Polyethylene Pipe*. ADS, Inc., Columbus, Ohio, 1982.
14. R. K. Watkins, R. C. Reeve, and J. B. Goddard. *Effect of Heavy Loads on Buried Corrugated Polyethylene Pipe*. ADS, Inc., Columbus, Ohio, 1982.

This study was funded by the Ohio Department of Transportation. The findings and opinions expressed herein are those of the author and do not constitute a standard or policy of the Ohio Department of Transportation.

Publication of this paper sponsored by Committee on Culverts and Hydraulic Structures.

Evaluation of Metal Drainage Pipe Durability After Ten Years

WILLIAM H. TEMPLE AND STEVEN L. CUMBAA

This study represents an investigation of the comparative performance of coated and uncoated, corrugated, galvanized steel and aluminum drainage pipe in Louisiana. The highly corrosive environments in some areas of the state make durability requirements of metal pipe as critical as strength requirements. Department personnel installed 10 types of metal drainage pipes at each of 10 locations in 1973. The test sites were selected on the basis of the pH and the electrical resistivity of the soil and the effluent. One pair of each type of culvert was installed at each site. Every 2 years one designated culvert of each of the pairs was removed and subjectively rated by a panel. The final (10-year) panel ratings reflect the condition of the undisturbed culverts in each pair. It was found that, in general, the 16-gauge asphalt-coated aluminum; the 14-gauge asbestos-bonded, asphalt-coated galvanized steel; and the 16-gauge galvanized steel with a 12-mil interior and a 5-mil exterior polyethylene coating were the test pipes with the most resistance to corrosion at the majority of the test sites. It was also found that, although all of the coatings provided added resistance to corrosion to some degree, the thicker coatings tested provided increased protection to the base metal. Comparisons of actual versus predicted years to perforation are made for galvanized steel in the harsher environments where test culverts actually experienced perforation.

The state of Louisiana annually receives approximately 60 in. of rainfall. The Louisiana Department of Transportation and Development (DOTD) road design engineer assigns a cross-slope and texture to the highways to rid them of this deluge of water. Drainage pipe is often used to remove the ensuing runoff from the highway right-of-way.

The hydraulics engineer can generally choose either reinforced concrete pipe or corrugated metal pipe in his designs. Concrete pipe is durable and with stable bedding conditions can normally serve effectively for the life of a highway.

The department also recognizes that metal pipe has its place in the field of hydraulics and maintains an interest in innovations in metal pipe. Metal pipe is relatively lightweight, an advantage that gains significance as the size of pipe increases. Metal pipe is relatively flexible, an advantage that could preclude failure under certain heavy loads. The major drawback with metal pipe is its tendency to corrode in the presence of moisture, oxygen, and salt. Additional information is needed on the rates at which galvanized steel and aluminum (with the various types of coatings recently introduced) will corrode.

In 1972 Louisiana found itself with a continuing need for drainage, a diverse set of environments, and a wide array of remedies offered by the metal culvert industry. The state responded with a major 10-year field study to determine the ability of available aluminum and galvanized steel culverts to resist corrosion while serving in moderate, acidic, and low-resistivity environments. A limited laboratory study parallels the field evaluations.

Research and Development Section, Louisiana Department of Transportation and Development, P.O. Box 94245, Capitol Station, Baton Rouge, La. 70804.

PROCEDURE

Site Selection

Research engineers selected 10 locations across the state as test sites to be representative of the seven general soil classifications found within Louisiana. The sites were expected to represent soil conditions normally encountered across the state as follows:

	Minimum Soil Resistivity (ohm-cm)	
Soil pH	*Less than 2000*	*Greater than 2000*
5.0–6.0	Site 1	Sites 4 and 8
7.0–8.0	Sites 2 and 3	Site 5
8.0–9.0	Sites 6, 7, 9, and 10	

Table 1 gives the actual characteristics of the soil and effluent at the test sites. Figure 1 is a map showing the locations of the test sites. Sites 6 and 7 are ditch and canal installations, respectively, located on opposite sides of the highway at that location. The pipes at Site 6 were accidentally destroyed during a utility relocation and were not available for the final evaluation. An 11th site representing a pH of less than 5.0 was added later, in 1977.

Materials Tested

Originally there were 10 varieties of coated and uncoated galvanized steel and aluminum culverts to be evaluated. During the course of the study several other types of pipes were installed at different times and locations. The types of pipes according to total field exposure time are as follows:

Ten Years of Field Exposure, Sites 1 Through 10

1. Uncoated, 16-gauge galvanized steel
2. Asphalt-coated, 16-gauge galvanized steel
3. Asbestos-bonded, asphalt-coated, 14-gauge galvanized steel
4. Uncoated, 16-gauge aluminum pipe, Alclad 3004
5. Asphalt-coated, 16-gauge aluminum pipe, Alclad 3004
6. 5052 structural aluminum plate arch
7. Sixteen-gauge galvanized steel with a 12-mil, coal-tar-based laminate applied to the interior and 0.3-mil modified epoxy coating on the reverse side
8. Sixteen-gauge galvanized steel with a 20-mil, coal-tar-based laminate applied to interior or exterior with a 0.3-mil, modified epoxy coating on the reverse side
9. Sixteen-gauge galvanized steel with a 10-mil interior and 3-mil exterior polyethylene coating
10. Sixteen-gauge galvanized steel with a 12-mil interior and a 5-mil exterior polyethylene coating

TABLE 1 pH AND ELECTRICAL RESISTIVITY

Site No.	Location	Soil Type	Soil Resistivity (ohm-cm)	Soil pH	Effluent Resistivity (ohm-cm)	Effluent pH
1	New Roads	Clay	1 023	6.5	9 500	6.7
2	Breaux Bridge	Silty clay	881	7.6	5 175	7.3
3	Kaplan	Silty clay	1 593	6.7	5 200	5.8
4	Simpson	Silty clay	11 169	5.5	18 333	6.2
5	Winnfield	Sand	3 720	6.7	3 375	6.9
6	Hackberry	Sandy clay	292	8.2	107	7.0
7	Hackberry	Sandy silt	281	8.0	123	7.0
8	Starks	Silty clay	3 786	5.7	15 833	6.7
9	Grand Isle	Sand	365	8.4	300	7.7
10	Leeville	Silty clay	219	7.9	121	7.2
11	Kisatchie	Sandy loam	2 083	4.9	4 400	7.4

Eight Years of Field Exposure, Sites 1 Through 10

11. Sixteen-gauge galvanized steel pipe with 10-mil interior and 3-mil exterior polymeric coating

Six Years of Field Exposure, Site 11

Pipes 1, 2, 3, 4, 6, and 11 were installed along with two additional types of pipes selected for evaluation. They are as follows:

12. Sixteen-gauge galvanized steel with a 10-mil, coal-tar-based laminate applied to interior and exterior
13. Sixteen-gauge galvanized steel with an 8-mil interior and 4-mil exterior polyethylene coating

Four Years of Field Exposure, Sites 4, 9, and 10

14. Sixteen-gauge steel with a 1.5-mil aluminum coating applied to the interior and exterior

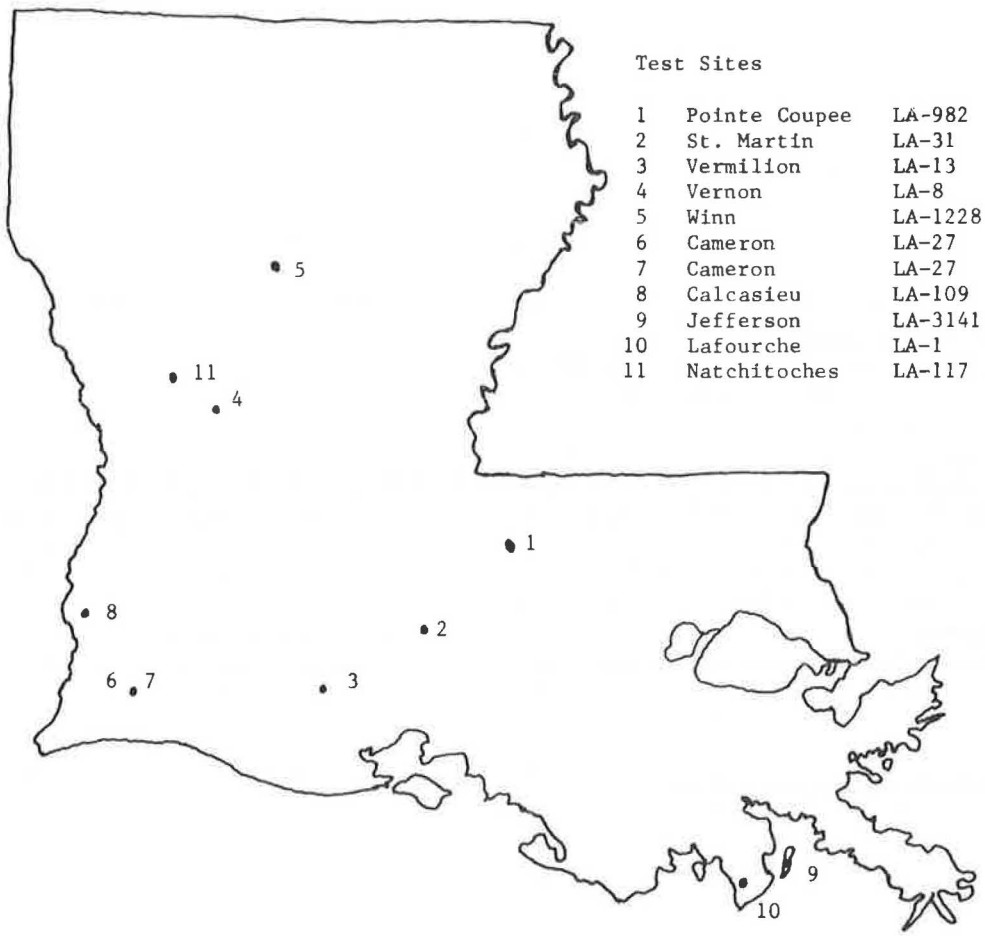

FIGURE 1 Location of test sites.

Four Years of Field Exposure, Sites 4 and 10

15. Sixteen-gauge galvanized steel with a 10-mil interior and a 7-mil exterior epoxy coating

Four Years of Field Exposure, Sites 7, 9, and 10

16. Fourteen-gauge aluminum pipe, Alclad 3004, with 10-mil interior and 5-mil exterior polymeric coating

Field Inspection

During the months of October and November 1983, the fourth and final field inspection of pipes with a maximum of 10 years of exposure was conducted. All of the pipes at each site were removed for inspection using a chain hooked to both ends of the pipe and to a "Gradall" bucket. The 4-ft sections were then washed clean, removing as much of the soil as possible without contributing to the removal of the coatings.

After the pipes were cleaned, photographs were taken from several angles to document the condition of each. Next, a panel consisting of highway engineers and highway engineering technicians visually rated the interior and exterior of the pipes and defined the total condition of a pipe using the following criteria:

1. Excellent condition—if, under visual observation, there were no signs of deterioration;
2. Good condition—if, under visual observation, there were slight signs of deterioration and pitting;
3. Fair condition—if, under visual observation, there were moderate signs of deterioration and pitting;
4. Poor condition—if, under visual observation, there were extreme signs of deterioration and pitting; and
5. Very poor condition—if, under visual observation, there were signs of complete deterioration and the pipe was no longer useful as a drainage tool.

The rating method was selected to provide a fair indication of the culverts' usefulness as drainage tools in addition to providing a relative indication of corrosion. This procedure was thought to be more relatable to actual field service life than time to first perforation. Time to first perforation was recorded, however, because many available design methods predict pipe life using this parameter.

Laboratory Analysis of Soil, Water, and Unexposed Culverts

Soil and water samples were initially collected from each installation site semiannually. Sampling frequency was later reduced to once a year because the results from the semiannual samples showed little change in pH and resistivity. These samples were tested for pH in accordance with Louisiana DOTD:TR 430–67 and for resistivity in accordance with Louisiana DOTD:TR 429–77. The two laboratory procedures require the use of a pH meter and a

TABLE 2 PANEL RATINGS (fourth evaluation) FOR EACH PIPE AND EACH TEST SITE GROUPED BY CORROSIVE CONDITIONS

		Sites by Corrosiveness									
		Mildly					Moderately			Very	
Type of Pipe	Age (yr)	1	2	4	5	11	3	8	9	7	10
Uncoated galvanized steel	6					1.5					
	10	2.6	1.8	3.0	1.8		4.4	3.8	4.1	5.0	5.0
Asphalt-coated galvanized steel	6					1.0					
	10	1.5	1.0	1.8	1.4		3.0	2.9	3.0	5.0	5.0
Asbestos-bonded asphalt-coated galvanized steel	6					1.0					
	10	1.4	1.0	1.0	1.0		1.9	1.1	2.9	3.1	3.2
Uncoated aluminum	6					1.6					
	10	1.4	1.5	1.9	1.8		2.5	1.8	2.1	4.4	4.1
Asphalt-coated aluminum	6										
	10	1.1	1.2	1.2	1.1		2.0	1.5	2.6	2.2	2.6
Structural aluminum plate arch	6					2.5					
	10	2.1	1.5	1.5	3.2		1.4	1.9	4.2	5.0	4.9
10-mil coal-tar-based polymer-coated galvanized steel	6										
	10	1.6	1.4	2.1	2.2		2.6	2.6	3.5	5.0	5.0
20-mil coal-tar-based polymer-coated galvanized steel	6										
	10	1.2	1.2	1.9	1.4		2.2	2.1	3.2	5.0	5.0
10-mil polyethylene-coated galvanized steel	6										
	10	1.1	1.2	1.8	1.8		1.8	1.8	2.9	4.2	4.4
12-mil polyethylene-coated galvanized steel	6										
	10	1.2	1.2	1.6	1.6		1.5	1.6	2.6	3.2	3.6
10-mil polymeric-coated galvanized steel	6					1.0					
	8	1.0	1.0	1.0			1.5	1.5	2.5	2.8	3.2
12-mil coal-tar-based polymer-coated galvanized steel	6					1.1					
8-mil polyethylene-coated galvanized steel	6					1.6					
Aluminized steel	4			2.2					2.8		3.6
Epoxy-coated galvanized steel	4			1.0							2.6
10-mil plastic-coated aluminum	4								1.1	1.1	2.1

resistivity meter. The soil samples were classified by laboratory technicians in accordance with Louisiana DOTD:TR 423–71.

Initially, the culvert-testing program dealt with determination of the physical characteristics of the various metals and their protective coatings as manufactured. The amount of zinc coating, expressed in ounces per square foot, was determined by measured weight loss as the zinc coating was dissolved in an acid solution. Thicknesses of the bituminous, asbestos, and various organic coatings were measured with a micrometer. The composition of steel and aluminum used in the culverts was determined by X-ray fluorescence, a process that provides a quantitative analysis of each element present in the metal alloys. Composition and thickness data are presented elsewhere *(1)*.

The durability of the culvert materials as manufactured has been evaluated in the laboratory by two primary methods, the salt fog exposure and the Weather-Ometer exposure tests. The salt fog exposure (Louisiana DOTD:TR 1011–74) consists of a closed salt spray cabinet equipped with a cyclic temperature control. This test was originally designed to test zinc-rich paint systems. The Weather-Ometer exposure (Louisiana DOTD:TR 611–75) consists of a carbon arc Weather-Ometer with automatic humidity controls. The evaluation of salt fog and Weather-Ometer exposure results is subjective and normally reported as satisfactory or unsatisfactory for the specified number of hours exposed. Initial durability test results are presented elsewhere *(1)*.

DISCUSSION OF RESULTS

The average panel ratings given to each pipe at each site for this fourth and final evaluation are given in Table 2. The ratings reflect the collective opinions of a panel of Louisiana DOTD employees who examined the culverts and assigned a numerical rating ranging from one (excellent) to five (very poor). The panel thought that, because of improper handling and lack of protection, the ends of many of the pipes indicated excessive corrosion and distress. The panel members were therefore asked to provide their ratings without considering the condition of the pipe ends. This is a departure from previous evaluations in which the entire pipe was rated but is believed to be a better representation of actual in-service conditions and performance.

To help in analyzing the data obtained during this study, the locations at which the pipes were installed were grouped in three categories, mildly corrosive, moderately corrosive, and very corrosive. These groupings were based on the environmental conditions at the sites represented by the minimum resistivity of the soil and the effluent. The limits of each group were selected in an effort to categorize the corrosive effect of the minimum resistivity on the galvanized steel base metal. This categorization placed Sites 4, 5, and 8 in mildly corrosive environments, Sites 1, 2, and 3 in moderately corrosive environments, and Sites 6, 7, 9, and 10 in very corrosive environments. Site 11 was considered very corrosive because of the low pH of the soil in conjunction with moderate resistivity.

Figure 2 indicates that the ratings assigned to the uncoated galvanized steel pipe (Pipe 1) are not consistent with the expected performance when based on minimum resistivities only [i.e., some galvanized steel pipes located at an assumed moderately corrosive site have a rating lower (better) than the same pipe at what was thought to be a mildy corrosive site]. Because of these inconsistencies, a different criterion for categorization or grouping of the 11 separate sites was established. This different grouping is based on the combined effect of all environmental influences on corrosion of uncoated galvanized steel as indicated by the assigned rating. In other words, the relative condition of 10-year-old uncoated galvanized steel pipe was used to place the sites in categories of increasing corrosion potential. Figure 3 shows the ratings of the uncoated galvanized steel when the sites are placed in the new categories. The limits of each category were established as follows:

Corrosive Condition	*Uncoated Galvanized Steel Rating (10 years)*
Mild	1.0–3.4
Moderate	3.5–4.5
Very	4.6–5.0

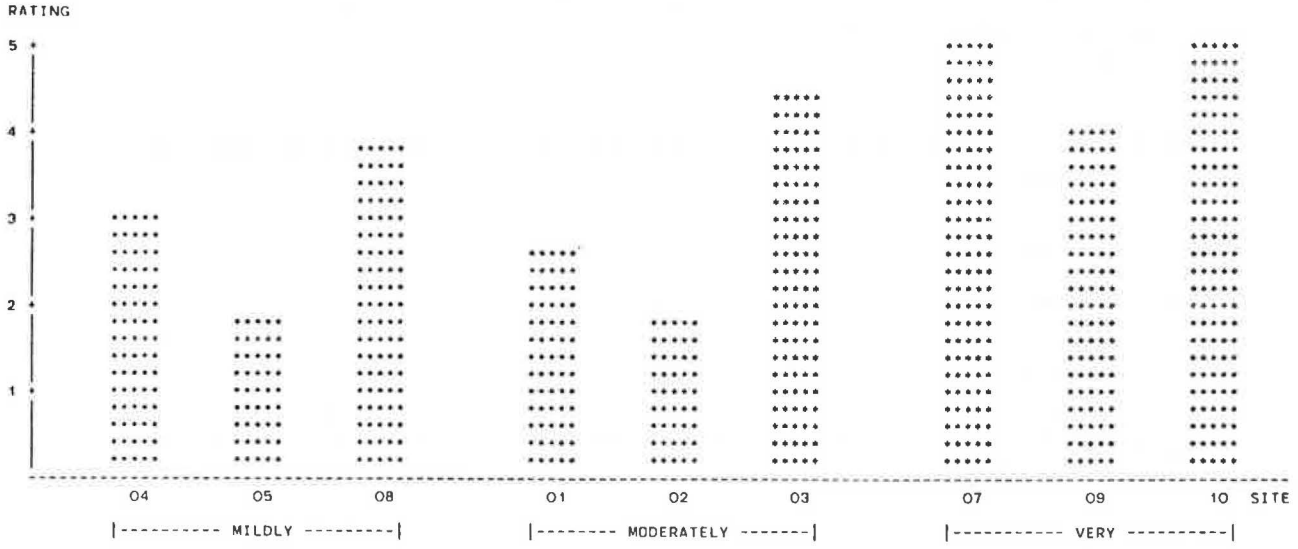

FIGURE 2 Ratings for 16-gauge galvanized steel pipe, original grouping (based on resistivity only).

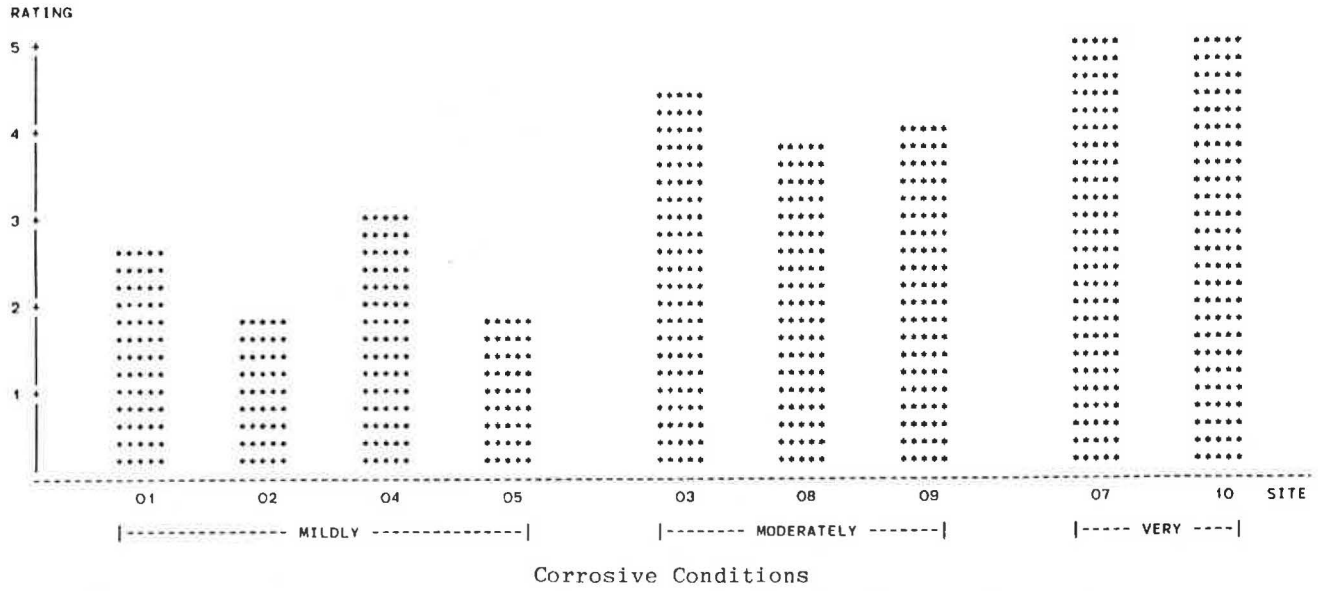

FIGURE 3 Ratings for 16-gauge galvanized steel pipe, new grouping (based on 10-year performance).

TABLE 3 AVERAGE 10-YEAR RATING BY ENVIRONMENTAL CONDITION

Pipe No.	Description	Avg Rating
Mildly Corrosive		
03	Asbestos-bonded, asphalt-coated galvanized steel	1.1
05	Asphalt-coated aluminum	1.1
10	12-mil polyethylene-coated galvanized steel	1.4
02	Asphalt-coated galvanized steel	1.4
08	20-mil coal-tar-based polymer-coated galvanized steel	1.4
09	10-mil polyethylene-coated galvanized steel	1.5
04	Uncoated aluminum	1.6
07	12-mil coal-tar-based polymer-coated galvanized steel	1.8
06	Structural aluminum plate arch	2.1
01	Uncoated galvanized steel	2.3
Moderately Corrosive		
10	12-mil polyethylene-coated galvanized steel	1.9
03	Asbestos-bonded, asphalt-coated galvanized steel	2.0
05	Asphalt-coated aluminum	2.0
04	Uncoated aluminum	2.1
09	10-mil polyethylene-coated galvanized steel	2.2
06	Structural aluminum plate arch	2.5
08	20-mil coal-tar-based polymer-coated galvanized steel	2.5
07	12-mil coal-tar-based polymer-coated galvanized steel	2.9
02	Asphalt-coated galvanized steel	3.0
01	Uncoated galvanized steel	4.1
Very Corrosive		
05	Asphalt-coated aluminum	2.4
03	Asbestos-bonded, asphalt-coated galvanized steel	3.1
10	12-mil polyethylene-coated galvanized steel	3.4
04	Uncoated aluminum	4.2
09	10-mil polyethylene-coated galvanized steel	4.3
01	Uncoated galvanized steel	5.0
02	Asphalt-coated galvanized steel	5.0
06	Structural aluminum plate arch	5.0
07	12-mil coal-tar-based polymer-coated galvanized steel	5.0
08	20-mil coal-tar-based polymer-coated galvanized steel	5.0

TABLE 4 ACTUAL VERSUS PREDICTED LIFE FOR 16-GAUGE GALVANIZED STEEL

Site Locations Where 16-Gauge Galvanized Steel Perforated	Actual Age to Perforation (yr)	Predicted Years to Perforation by California Chart by		
		Soil	Effluent	Combined
3	6-10	21	23	22
7	2-4	19	6	12.5
8	6-10	20	38	29
9	6-10	29	19	24
10	2-4	17	12	14.5

These limits are based on the previously outlined criteria established and used for the 1 to 5 rating scale.

The panel ratings of Table 2 represent each pipe and each site grouped according to these limits. Site 11 was placed under mildly corrosive conditions because of the relatively good rating of the uncoated galvanized steel pipe after 6 years of exposure. The average rating of each pipe (10 year) within the three corrosive conditions is given in Table 3.

Indications based on the average (10-year) ratings within the three corrosive environments are discussed in the following subsections.

Mildly Corrosive Environments

The asbestos-bonded asphalt-coated galvanized steel and the asphalt-coated aluminum pipes are the best-performing pipes tested, with an average rating of 1.1. The 10-year average rating for all pipes ranges from a best of 1.1 to a worst of 2.3. This indicates that all pipes tested performed well under mild environmental conditions.

Moderately Corrosive Environments

The asphalt-coated aluminum, the 12-mil polyethylene-coated galvanized steel, and the asbestos-bonded asphalt-coated galvanized steel are among the best-performing pipes evaluated with 10-year average ratings of 1.9 and 2.0. All pipes with the exception of the uncoated galvanized steel performed reasonably well in moderately corrosive environments.

Very Corrosive Environments

The asphalt-coated aluminum (rating of 2.4), the asbestos-bonded asphalt-coated galvanized steel (rating of 3.1) and the 12-mil polyethylene-coated galvanized steel (rating of 3.4) are the best-performing pipes in the very corrosive environments; these pipes stand out in their ability to resist corrosion under very harsh conditions and have some additional life remaining. The other pipes tested are at, or near, their end of life.

The only pipe with a maximum of 8 years of field exposure as of this final evaluation is the 10-mil polymeric-coated galvanized steel. This pipe performed well in the mildly and moderately corrosive environments and had an average rating of 3.0 in the highly corrosive environments.

Eight pipe types that were installed at Site 11 (mild environment) had a maximum of 6 years field exposure as of this final evaluation. The pipes that performed the best at this site, with a rating of 1.0 after 6 years, are the asphalt-coated galvanized steel, the asbestos-bonded asphalt-coated galvanized steel, and the 10-mil polymeric-coated galvanized steel.

Three pipe types had a maximum of 4 years of field exposure as of this final evaluation. The 10-mil plastic-coated aluminum was the pipe with the best performance in all three environments.

Table 4 is a list of sites at which 16-gauge uncoated galvanized steel pipes have perforated or reached a rating of 5.0 and the corresponding number of years elapsed to reach this end condition. Also included in this table is the pipes' expected life (years to perforation) as predicted by the California Chart *(2)* for the existing site conditions. The California Chart relates expected years to perforation versus minimum resistivity and pH of the site environment. As the data in Table 4 indicate and as is shown in Figure 4,

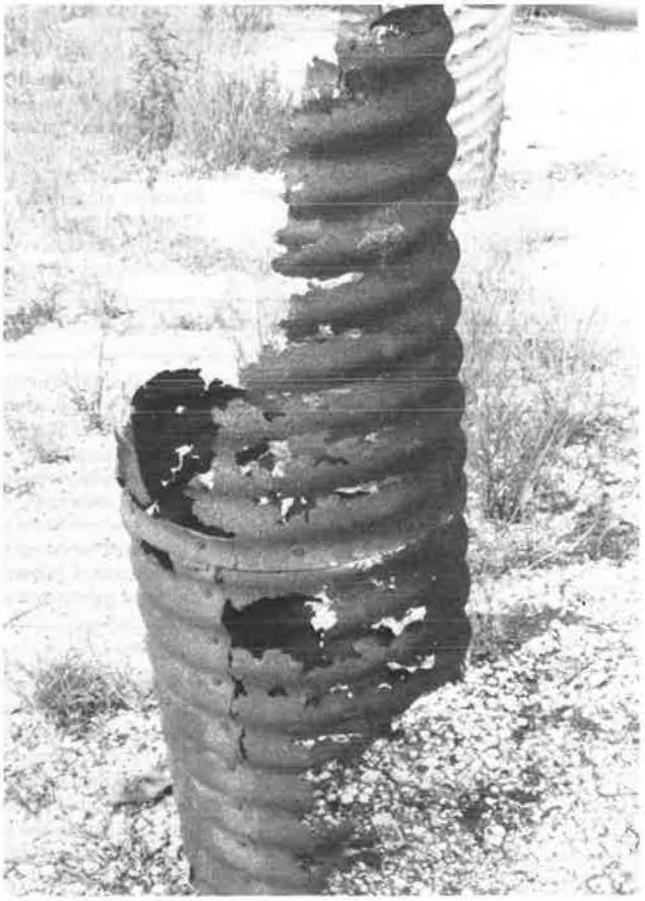

FIGURE 4 16-gauge galvanized steel after 10 years of exposure at Site 7.

TABLE 5 PREDICTED YEARS TO PERFORATION, ALL SITES

Site No.	Years to Perforation
Mildy Corrosive	
1	15.0
2	30.0
4	27.0
5	27.0
	25.0 avg
Moderately Corrosive	
3	21.0
8	20.0
9	19.0
	20.0 avg
Very Corrosive	
7	6.0
10	12.0
	9.0 avg

Note: Predicted years to perforation for uncoated, 16-gauge galvanized steel pipe utilizing the California Chart and worst-case environmental condition.

the California Chart overestimates the anticipated life of 16-gauge uncoated galvanized steel at those sites where perforation or failure has occurred during this study. The chart does, however, appear to provide predicted life relative to the available range of pH and resistivities when sites are grouped by performance of galvanized steel as indicated by the data in Table 5. It is impossible to accurately estimate or predict pipe life in all of the various environments on the basis of the ratings obtained during this study because of the nonlinearity of the 1 to 5 rating scale. For example, a rating of 3.0 (midpoint of the rating scale) does not necessarily indicate that one-half of the life or usefulness of the pipe is gone. All pipes tested would require field exposure times of such length that the pipes reach a rating of 5.0 before any accurate determination of pipe life or additional life due to the various pipe coatings could be made.

Three general types of coatings were used to protect the base metal of some of the (10-year) test pipes. The results of the ratings of coated and uncoated pipes indicate that all coatings provided some degree of additional life by reducing corrosion of the base metal. The three coatings fall into the following categories:

1. Asphalt,
2. Asbestos-bonded with asphalt coating, and
3. Polymeric.

The asphalt coatings tended to be removed during handling and tended to be removed or cracked from exposure to the environment (Figure 5). In harsh environments, rust stains, which indicate corrosion of the base metal, appeared in the asbestos (Figure 6). The polymers tended to blister in harsh environments and tended to peel (separate from the base) in moderate and harsh environments (Figure 7). The thicker polymeric coatings appeared to protect the base metal better than the thin coatings.

Maximum pit depths were measured on the aluminum test culverts because pitting was the principal mode of distress for the

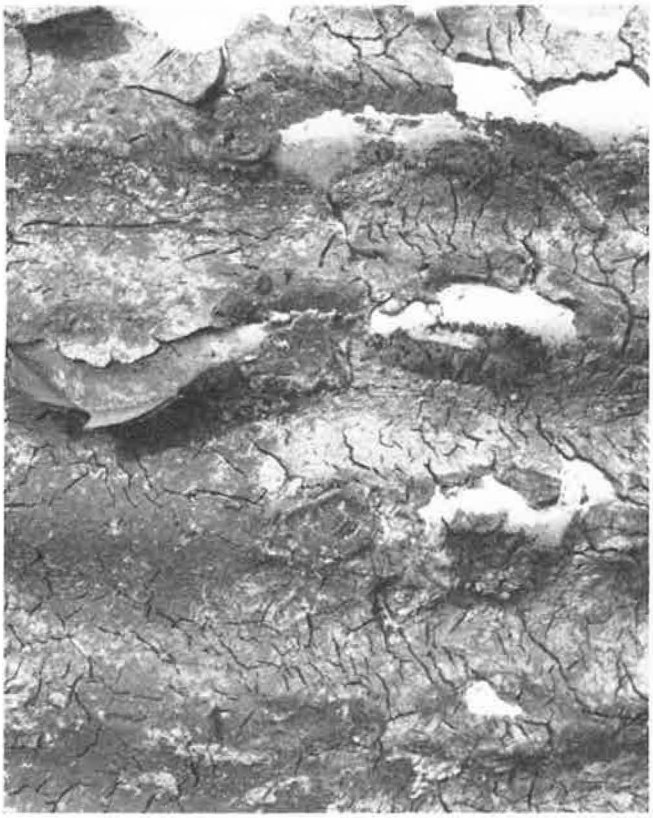

FIGURE 5 Asphalt coating cracked and removed.

FIGURE 6 Corrosion between asbestos and base metal—Site 10.

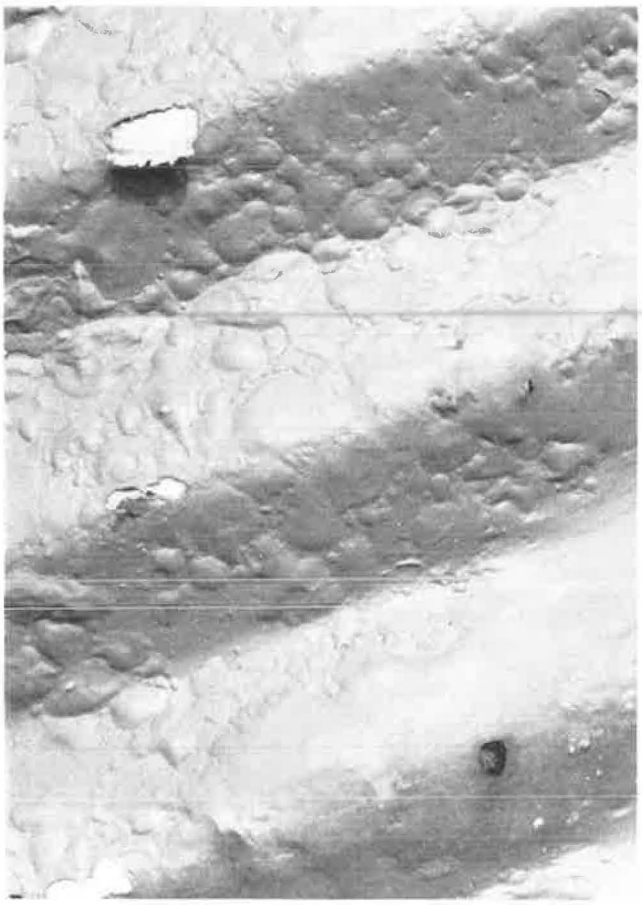

FIGURE 7 Polymeric coatings—blisters and peeling in harsh environments.

aluminum products. Pit depth values measured after 10 years of service are given in Table 6. It is evident that the observed rate of corrosion is significantly different for the aluminum 3004 and 5052 alloys.

TABLE 6 PIT DEPTH VALUES

Site No.	Alloy 3004[a] Depth (mils)	Alloy 3004[a] Rate (mils/yr)	Alloy 5052[b] Depth (mils)	Alloy 5052[b] Rate (mils/yr)
Mildly Corrosive				
1	2	0.2	40	4
2	3	0.3	16	1.6
4	2	0.2	16	1.6
5	3	0.3	100	10
Moderately Corrosive				
3	3	0.3	16	1.6
8	2	0.2	20	2
9	3	0.3	100	10
Very Corrosive				
7	60	6	100	10
10	60	6	100	10

[a] Nominal thickness = 60 mils.
[b] Nominal thickness = 100 mils.

CONCLUSIONS

Ten years of field exposure have provided much information on the in-service comparative performance of the various types of test culverts. The following conclusions have been reached at this time:

1. The pipe types that provide the best overall performance after 10 years of exposure to the various environments are the 16-gauge asphalt-coated aluminum, the 14-gauge asbestos-bonded asphalt-coated galvanized steel, and the 16-gauge 12-mil polyethylene-coated galvanized steel.

2. Under the environmental conditions (moderately and very corrosive) encountered during this study, the California Chart overestimates predicted pipe life (years to perforation). The chart does, however, combine pH and resistivities to correctly predict life in a relative sense for the mildly, moderately, and very corrosive environments.

3. All coatings provided some degree of protection to the pipe base metal. The thicker polymeric coatings provided more protection against corrosion than the thinner polymeric coatings.

4. Pitting rates for aluminum culverts with the 3004 alloy were found to be significantly less than pitting rates for aluminum plate with the 5052 alloy.

REFERENCES

1. W. H. Temple and S. L. Cumbaa. *Evaluation of Drainage Pipe by Field Experimentation and Supplemental Laboratory Experimentation.* Final Report. Louisiana Department of Transportation and Development, Baton Rouge, March 1985.
2. *Engineering Directives and Standards Manual.* Louisiana Department of Transportation and Development, Office of Highways, Baton Rouge, Nov. 1983, No. II.2.1.6, Figure 1.

Publication of this paper sponsored by Committee on Culverts and Hydraulic Structures.

Abrasion Resistance of Aluminum Culvert Based on Long-Term Field Performance

A. H. KOEPF AND P. H. RYAN

Culvert pipes not only are placed to drain water but are required to carry bed load materials including rocks. The flow and energy characteristics of bed load materials and their effect on culvert pipes are not well understood. Analysis of mechanics can provide a format for comparing predicted characteristics with field experience data, and results confirm the validity of the assumptions. In 1968 an initial study was reported on 229 aluminum culverts that had been exposed to abrasion for from 4 to 7 years. That study proposed a form of energy level for bed load materials and rated the abrasion performance of aluminum culvert through a series of energy ratings. The energy level and abrasion predictions were compared with actual field experience, and long-term culvert abrasion can be predicted when culvert geometry, installation arrangement, and content of bed load materials are established. In 1984 and 1985 the field experience of the originally reported culvert group averaged 20 years of exposure to abrasion. In this paper are presented the results of the 1984–1985 study. The basic method of determining abrasion energy levels has been retained and simplified to emphasize key variables that affect abrasion. The 1985 study indicates that abrasion of aluminum culvert follows the patterns of the previous work. Long-life abrasion typically does not continue at a linear wastage rate but levels off to a much reduced rate, reflecting reductions in total energy as the flow channel stabilizes with age. Abrasion and service life for aluminum culvert inverts may be predicted as a function of water flow, culvert entrance arrangement, culvert slope, and rock content of streambed load.

There have been few comprehensive studies on the resistance of metal culvert pipe to abrasion caused by normal streambed loads. Shortly after commercial introduction of aluminum alloy culvert in 1960, laboratory sample abrasion tests were conducted by several state highway departments. These tests resulted in selective agency specifications restricting the use of metal culvert, generally by limiting water velocity only. One such specification limited use of aluminum culverts to a maximum entrance velocity of 5 ft/sec and recommended increasing steel culvert thickness when the water velocity exceeded 5 ft/sec *(1)*.

A detailed study of aluminum alloy culvert in locations subject to abrasion was reported by Koepf in 1968 *(2)*. In that report abrasion service life of aluminum pipe was discussed in terms of bed load energy levels and visual ratings for 229 aluminum culverts that had been in service for approximately 5 years. Velocity–impact energy relationships were developed, and abrasion ratings were established using visual rating and invert sample coupons. These were tabulated so that the culvert design engineer could relate predicted service life to abrasion-related conditions for proposed pipe installations.

The present study, some 15 years later, provided the opportunity to field inspect many of the original aluminum culverts that were in the 1968 test and thus extend actual service life data from 5 years to 20 years or more. In this paper are presented the results of the field inspections, abrasion ratings, and culvert invert metallographic cross sections. The results are compared with the 1968 results. The original formulas and relationships for determining impact energy and impact energy-to-velocity ratio are discussed and trends are compared.

Koepf & Lange, Inc., 971 Dewing Avenue, Lafayette, Calif. 94549.

The 1968 study was arranged to present the characteristics of aluminum culvert abrasion through a series of steps intended to describe bed load behavior and performance due to abrasion and match observed behavior to predictions. The steps are as follows:

1. Describe the long-term erosion-corrosion cycle in the presence of abrasive water flow causing wastage of aluminum surfaces and compare it with the same cycle causing wastage of galvanized steel surfaces.
2. Apply the mechanics of erosion to culvert including bed load material, culvert size, culvert slope, and resulting water and rock velocity to produce a form of bed load kinetic energy levels. Field observations were made of rock flow in culvert to confirm the validity of the bed load kinetic energy method as a means of predicting aluminum alloy culvert service behavior.
3. Undertake field investigation of approximately 200 aluminum alloy culverts located in abrasive exposures, report performance, and compare with predicted behavior.

EROSION-CORROSION CYCLE

Aluminum alloys develop corrosion resistance through maintenance of an aluminum oxide layer covering all exposed surfaces. The oxide layer is very thin, is substantially colorless, promptly restores itself when abraded off, is very tough, is adherent, and resists removal. Culvert sites that are considered abrasive do not normally contain water compositions that are extremely acidic or alkaline or any combination that is expected to be corrosive to aluminum *(3)*. Because the abrasive bed load is chemically inactive, abrasive sites are not corrosive sites for aluminum alloy. Consequently, loss of metal from aluminum alloy culvert becomes dependent on abrasion energy without the addition of corrosion effects.

Galvanized steel exposed to an abrasive flow follows an entirely different form of erosion-corrosion cycle. The abrasive action of the bed load flow removes the relatively soft zinc and zinc oxide coating and exposes the steel surface below. The rate of removal will depend on the frequency of bed load flow. When the steel surface has been exposed, iron oxide is then promptly formed. Iron oxide is not highly abrasion resistant and will be removed by further abrasive flow, reexposing the steel continuously for more oxide formation. This progressive mechanism of erosion-corrosion causes small but steady rates of wastage of steel culvert inverts. The long-term wastage rate on the average steel culvert appears to be governed more by the corrosion portion of the erosion-corrosion cycle than by abrasion. The progressive erosion-corrosion cycle proceeds on steel with all types of bed load flow including sand and gravel. In cases in which water may be acidic and

corrosive, wastage rates increase. The mechanism of wastage is frequently expressed in inches per year loss, which results in a lineal form for predicting steel culvert invert service life.

A generalized cumulative erosion-corrosion curve is shown in Figure 1 to illustrate the observed characteristic combined metal wastage patterns of both aluminum alloy and galvanized steel culvert.

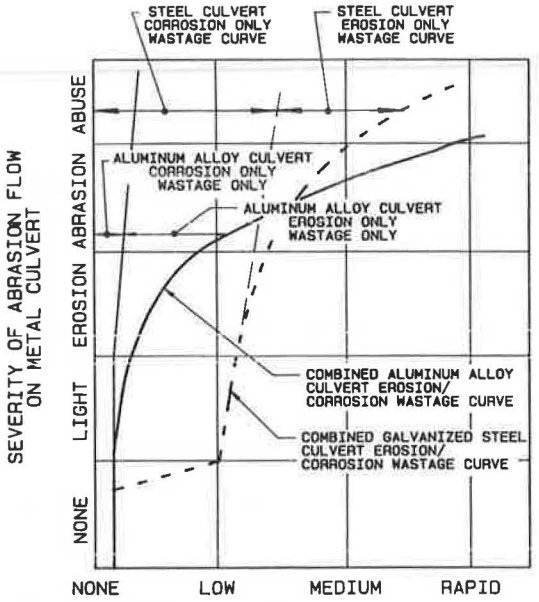

FIGURE 1 Representative rate of wastage of culvert pipe metal from an erosion-corrosion cycle.

Protective coatings are sometimes applied in abrasive site applications to extend service life. Culvert life may be lengthened only to the extent of the added resistance and integrity of the coating, and because the most common coatings are not highly resistant to abrasion the value of these coatings on either aluminum alloy or steel culverts is limited *(4, 5)*.

MECHANICS OF ABRASION APPLIED TO ALUMINUM ALLOYS

Surface abrasion on the invert of aluminum alloy culverts is the result of cumulative impact or scrubbing action by particles of hardness equal to, or greater than, the resistance of the aluminum oxide–protected metal surface. To evaluate or predict bed load abrasion it is desirable that abrasive action be reduced to a mathematical model. Observations show that culverts subjected to active flow are self-scrubbing (i.e., self-cleaning) including cleaning corrugation valleys so that buffer layers or smooth-line inverts are not established. Field observations of aluminum culvert installations show light peening and no significant evidence of abrasive metal wastage caused by sand or very small rock flows. Flows that contain increasing quantities and sizes of rock show increasing surface abrasion, peening, scarring, and ultimately metal wastage. From this it may be concluded that severity of abrasion is directly related to the cumulative kinetic energy of the bed load material rocks expressed as equivalent mass and velocity.

Figure 2 shows the force path of a single rock as it progresses through a culvert. When the driving force of water pressure exceeds the net resistance of gravity and friction of the example rock it will move and, when clear of the corrugation, continue to accelerate to a terminal velocity (U). Because culvert inverts are not smooth but a series of corrugated ridges, the actual path of a rock has been observed to follow a series of impact cycles as shown in Figure 2. During the initial portion of a flow cycle the rock is accelerated up the corrugation incline, moves within the water flow for one to several corrugation lengths, and then drops to strike the next corrugation incline, where impact reduces the rock velocity. A repeating cycle is obtained. The form of an abrasion energy level can be described by the equation

$$KE_u = (W/2g)U^2 \quad (1)$$

where

KE_u = kinetic energy of the "statistical" rock representing the bed load material in the foot-pounds,
W = weight of statistical rock in pounds,
g = acceleration due to gravity (32.2 ft/sec^2), and
U = average velocity of rock in culvert (ft/sec).

For a typical statistical rock of spherical shape weighing 150 pounds per cubic foot, the kinetic energy can be rewritten as

$$KE_u = 0.00071\, d^3U^2 \quad (2)$$

where d is rock diameter in inches.

The practical use of kinetic energy level as a means of describing abrasion levels must include a number of dimensional assumptions to streamline the form of solution. For example, a rock may be considered a sphere of uniform density, energy is expressed in translation motion, the most common culvert corrugation is 2 2/3 in. pitch by 1/2 in. height, and the rock velocity is the overall average time between impacts on the length of the culvert divided by the time to pass through.

Rock Size, Shape, and Availability

A basic assumption of the 1968 analysis was that progressive abrasion will follow a generally linear time rate pattern that reflects a uniform flow of bed load and rock sizes. Comparison of 20-year service data in the 1985 study with 5-year service data of the 1968 study shows that abrasion rates in average installations diminish. This is due principally to reduced number and sizes of available rock flow as the upstream drainage channels stabilize with age. Unfortunately, abusive and highly abrasive sites do not diminish substantially because their channels do not tend to stabilize.

The 1985 field investigation program also established that abrasion results are independent of geographic location as long as rock size, culvert size, and slope are similar. There are variations due to rock shape, hardness, terrain, and rainfall; however, variations are not excessive. These variations are patterned after routine observations of culvert in most geographic areas of the United States. Examples follow.

1. Areas with considerable vegetative ground cover restrict rock flow and thus cause less abrasion. Increased abrasion can be expected in areas with little ground cover and ample loose rock on the slopes.
2. Abrasion may be slightly greater than average in areas of consistent rainfall, steep slopes, and hard rocks with irregular shapes.

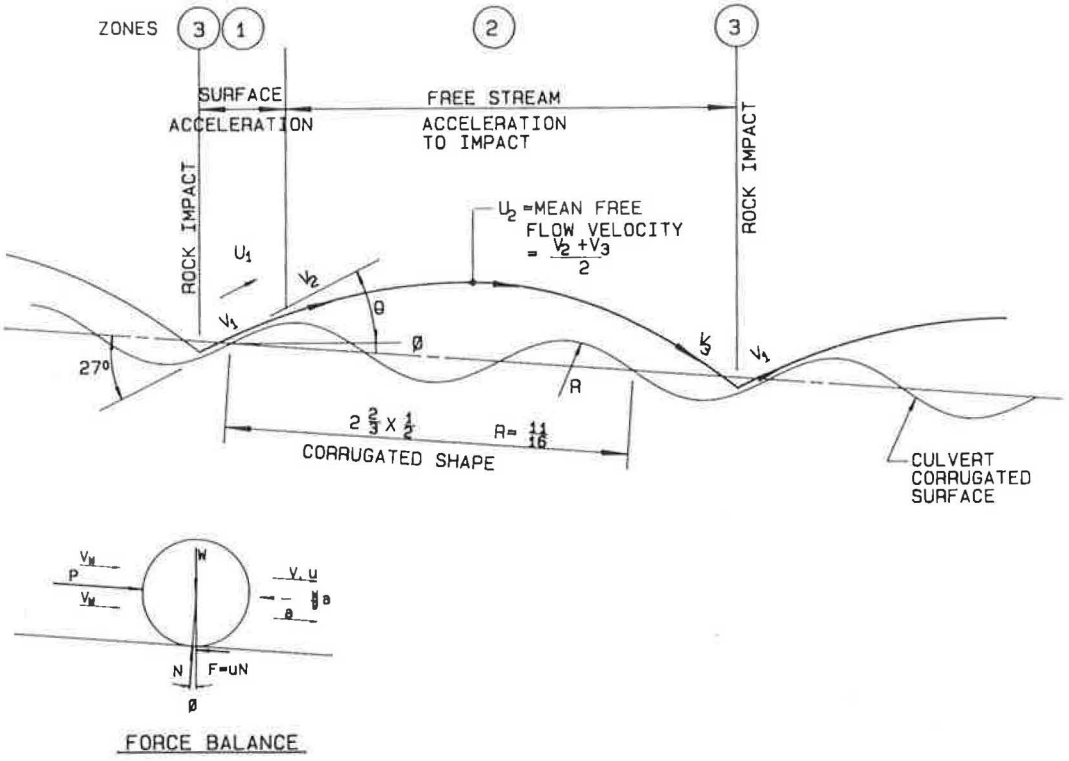

FIGURE 2 Representative rock cycle path.

The control culverts used for study are concentrated in the Pacific northwest, the California High Sierras, and northern New York and New Hampshire, which represent high expectations of abrasion. Where few rocks are naturally present, significant abrasion of aluminum alloys is not expected and has not been observed.

Velocity

The analysis is particularly dependent on the velocity of the rock, because the kinetic energy form contains a squared velocity term. Consequently, to best describe the velocity, it is necessary to review the different velocities that occur in specific locations of a typical culvert installation.

1. Culvert entrance water velocity (V_e) is the average velocity at the cross section entrance to a culvert. Entrance velocity is limited by upstream water level, culvert diameter, and geometry of the entry. Entrance water level usually governs the flow capacity of the installation. Designers frequently use flooded entrance water level flow calculations as a guide to selection of culvert size. Entrance velocity is not a satisfactory method of defining water velocity for establishing abrasion ratings because it does not describe actual water or rock velocity through the culvert.

2. Pipe water velocity (V_p) is the velocity of the water through the culvert after it has cleared the culvert entrance and is considerably higher than culvert entrance velocity. It is a function of culvert diameter, culvert slope, and corrugation shape. As an example, a 48-in. culvert with a flow of 63 ft^3/sec with a flooded projecting square entrance will develop an entrance velocity of 5.0 ft/sec and a pipe velocity of 13 ft/sec with a 21-in. depth on a 5 percent culvert slope, or 24 ft/sec with a 13-in. depth on a 30 percent culvert slope. Pipe velocity best describes the level of expected rock flow energy that can cause abrasion to culvert inverts.

3. Mean pipe water velocity (V_w) as defined for this study is the water velocity in a culvert for a water flow through a square end entrance ponded at half the depth of the culvert. This is a compromise velocity used to represent a reasonable combination of frequency of occurrence and velocity magnitude and is used in this study to establish rock kinetic energy levels. Design water velocity values for typical culvert sizes and slopes are given in Table 1.

4. Rock velocity (U) is the average velocity of a rock from entry to exit as it passes through the culvert when subjected to a forcing flow due to water velocity. The rock velocity may vary from zero, when water velocity is not sufficient to keep the rock moving or at an instant of total stopping impact, to approaching

TABLE 1 MEAN PIPE WATER VELOCITY (feet per second)

Diameter of Culvert (in.)	Water Flow,[a] Q (ft^3/sec)	Culvert Slope (%) 5	10	15	20	25	30
18	2.0	5.5	6.6	7.6	8.3	9.1	10.0
24	4.4	6.2	8.0	9.3	10.6	11.5	12.0
30	8.0	7.2	9.4	10.7	12.0	12.8	14.0
36	13.0	8.0	10.3	12.0	13.5	14.2	15.1
42	20.0	10.0	12.0	14.0	15.1	16.5	17.8
48	29.0	10.1	13.5	15.0	16.5	18.0	19.5
60	52.0	11.7	15.5	17.5	20.0	21.7	23.0
72	83.0	13.2	17.0	20.0	21.3	24.0	25.5
84	130	14.8	19.0	21.5	24.0	26.0	27.7
96	186	16.0	21.0	24.0	26.8	29.0	31.0

[a]Flow in cubic feet per second is based on square projecting entrance half full (H/D = 0.5). The velocity of the flow at indicated slope is based on Manning's equation with n = 0.024.

water velocity as if there were no impacts to slow it down. The ratio between rock velocity and pipe water velocity was determined from field tests by timing average rock velocity in culvert water flows. An empirical factor $(1 - e)$ may be added to the energy equations to relate mean rock velocity to water velocity. Field observations indicated that rock velocity peaked at about 83 percent of water velocity, which limits e to 0.17 minimum. This factor provides a means of describing the observed reaction of abrasion as culvert slope and rock sizes are reduced. Further, to focus on typical expected energy levels, it can be reasoned that small maximum rock sizes are typically found in smaller culvert installations and larger maximum rock sizes are found in larger culverts. These approximations and empirical data show that average water velocity can be related to a specific peak rock size and culvert installation slope. For this study, 2-in. peak rocks are matched to 18-in.-diameter culverts, and sizes are increased to 12-in. rocks for 60-in.-diameter culverts. Deviations in pipe water velocities related to culvert sizes are consistent with the other assumptions.

Mean Impact Energy

The kinetic energy level of a single spherical shaped rock available for impact as it passes through the culvert is represented by

$$KE = 0.00071\, d^3 V_w^2\, (1 - e)^2 \quad (3)$$

where e is a field-determined empirical factor from at rest to maximum velocity and is a function of rock size and pipe slope (Figure 3).

The total kinetic energy to which a culvert invert surface may be subjected over a long period of time can be considered proportional to such a unit rock equation.

The resulting composite rock energy equation is plotted in Figure 4. The lower cut-off line approximates the minimum flow and culvert slope necessary to maintain a given rock movement, generally with a threshold at 5.0 percent culvert slope.

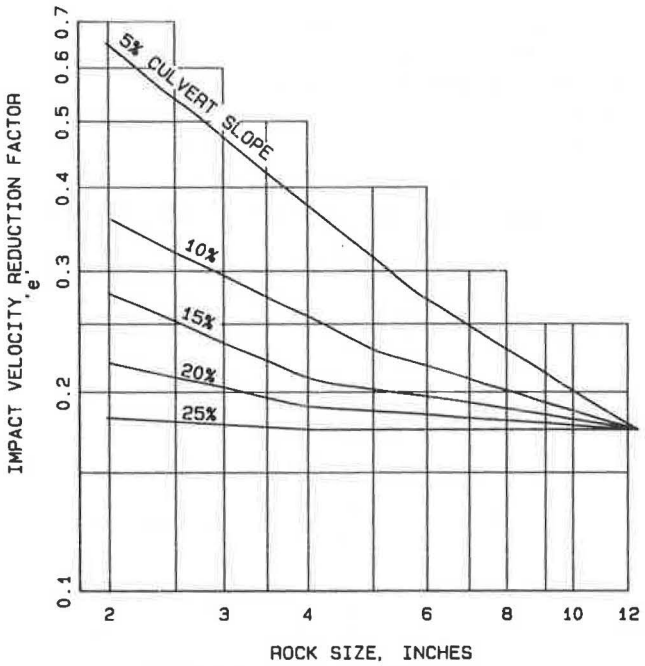

FIGURE 3 Field-determined impact velocity reduction factor versus rock size and culvert slope.

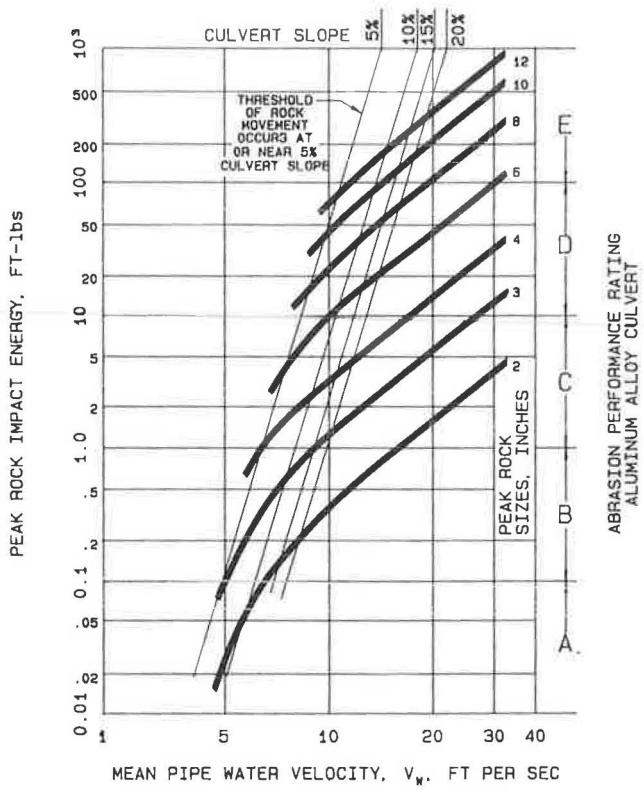

FIGURE 4 Rock energy curves.

Figure 4 also includes a series of abrasion ratings established from energy calculations and the observations from the 1968 survey. The observed levels were generally confirmed by the 1984 study. These rating levels serve as a basis for performance predictions. These data are also shown in tabular form in Table 2.

FIELD INVESTIGATION OF ALUMINUM ALLOY CULVERT SITES

The group of culverts selected for the 1968 abrasion report with an average of 4 to 5 years' service was reinspected during 1984 and

TABLE 2 SELECTED ABRASION RATING LIMITS FOR INDICATED ROCK SIZES AND CULVERT SLOPE

Abrasion Rating Limit	Rock Size[a] (in.)	Maximum Slopes (%) for Typical Culvert Sizes		
		24 in.	48 in.	72 in.
B	2	45	30	13
	3	20	5	5
	4	5	5	5
C	4	45	30	14
	6	25	10	5
	8	15	5	5
D	6	–	40	35
	8	–	30	15
	10	–	12	6

Note: Energy level predictions are those of Figure 4. Threshold of rock movement is approximately 5 percent.
[a]Statistical peak rock size expected.

1985 to obtain field data on culverts with an average service life of 20 years.

Some culverts are no longer in service as a result of road relocations or modifications or washouts, and some were not inspected. Approximately 77 percent of the 1968 group were reexamined. A selected number of additional culverts in abrasion sites with less than 20 years in service were added to this study to fill out the original control group. The field investigation group was thus 186 culverts.

The 1968 study used the control group as a basis for developing a suggested culvert abrasion rating performance system. This original rating system related experience to that date to equivalent wastage rates expressed in inches per year in an attempt to compare with typical forms of expressing corrosion rates. When the 1984 study compares 5-year exposure with 20-year exposure the results indicate that abrasion of aluminum culvert does not progress at a linear wastage rate but that total abrasion levels off at a much reduced rate. This reflects reduced cumulative impact energy from fewer rocks each season because of gradually stabilizing upstream channels. Because of this, the abrasion rating schedule description suggested for the 1968 study has been revised in the 1984 study by eliminating the lineal wastage factor. The revised schedule is given in Table 3. With 20 years of experience as support, generalized projected culvert service life data have been suggested in the abrasion rating schedule.

Culvert Inspection Procedure

The method of examining and sampling used previously was repeated in the 1984 survey. Each culvert site inspected was given an in-place overall visual abrasion rating from Table 3, using abrasion rating schedule letters A through E to represent severity of abrasion site. The original rating levels were used arbitrarily to describe observed conditions. Subsequent analysis and observed conditions made the ratings generally reproducible. Peak rock size was determined in the field by visual inspection of the streambed and the culvert inverts. Size was selected to represent not the largest possible rock to pass through but the estimated largest "statistical" rock that may pass through the culvert repeatedly at a "significant" frequency during periods of substantial water flow. This size selection is intended to represent the size typical of 25 percent of the rock flow is approximate only, but is important and calls for the exercise of judgment to simulate the exposure to abrasion expected over many years. Observations have suggested that a peak rock size of some frequency would not exceed 8 in. This approximation is necessary to the rating and it proved to be manageable with some experience.

Culverts were also sampled by drilling out 1-in.-diameter coupons from the invert crowns and subjecting them to laboratory examination. Each separate culvert or culvert group with similar exposure was sampled. Coupons were cleaned and surface photographed at 2.5X, then cross sectioned, mounted, etched, and photomicrographed at 5X. These photographs permitted a more detailed examination of surface and cross section to confirm the on-site visual abrasion ratings. Not all culverts were sampled, and actual coupons selected for photomicrographs are representative of examples of each abrasion rating. Field investigation showed that abrasion on aluminum culvert is generally limited to the upstream portion of the crown radius of the corrugations in the area of the invert line only.

Background data containing visual abrasion ratings for the 1967–1968 and the 1984–1985 inspections are available from the author.

RESULTS AND DISCUSSION

Figures 5–12 show examples of abrasion ratings A through E, including the abrasion test sites of both the 1968 and the 1984–1985 studies. In some instances the same pipe was not inspected, but a similar nearby pipe in the same exposure was selected to log the observed abrasion ratings. Figure 13 shows the observed effect of abrasion wear on fasteners.

A cross section rated A shows no effect of abrasion. The photos show the thin layer of the aluminum cladding alloy 7072 on both

TABLE 3 ABRASION PERFORMANCE RATING SCHEDULE FOR ALUMINUM ALLOY CULVERT PIPE

Performance Zone Rating	Effect on Surface of Crown of Corrugation, Invert Only[a]
A	No surface effect; no reduction in service life due to bed load; abrasion service life 100 years
B	Nonerosive; some slight roughening of the metal surface but no metal removal by erosion action; no reduction in normal service life of aluminum culvert; projected abrasion service life 75 years or more
C	Erosion; surface roughening and slight progressive removal of metal from culvert; some gouging may be noted if rocks tend to be large; projected abrasion service life 50 years or more
D	Abrasion; surface roughening and slow removal of metal from culvert; definite reduction in pipe life due to abrasion; gouging of surface may be expected; projected abrasion service life 25 to to 50 years
E	Abusive; surface roughening and rapid removal of metal from culvert; definite reduction in pipe life due to abrasion; projected abrasion service life 25 years or less

[a]Abrasion effects only this portion of the surface. The remainder of the culvert is usually unaffected by abrasion.

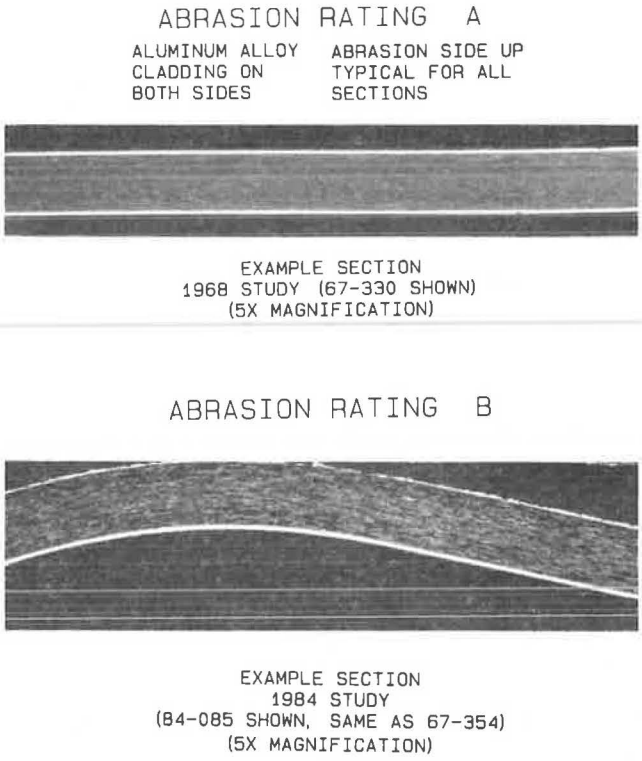

FIGURE 5 Photomicrographs of abrasion ratings A and B (sample sections).

sides of the 3004 core alloy. Cladding is galvanically anodic to the core making it sacrificial in a corrosive environment. When corrosion is encountered it will usually be limited to the cladding thickness. The nominal cladding thickness is 5 percent of the total thickness on each side. For 16-gauge culvert pipe of 0.060 in. total thickness, the cladding thickness is about 0.003 in. on each surface. The cladding alloy is slightly softer than the core alloy.

The "nonerosion" rating (A/B or B) samples show characteristic light surface pebbling but not significant removal of cladding. There is virtually no loss of culvert metal or strength.

The "erosion" rating (B/C or C) samples show the same pebbling texture plus a superimposed light random gouging from larger rock to a degree sufficient to visibly disturb and gradually remove metal. The long-term metal loss is small.

The "abrasion" rating (D) sample represents the cumulative result of pebbling and substantial gouging, which gradually reduces the overall metal thickness by removal. Long-term metal loss is significant and does limit expected culvert life.

The "abusive" rating (E) sample shows more rapid progressive removal of culvert invert metal by gouging and pounding than for abrasive rating D. Abusive energy levels can be large enough to wear through or flatten corrugations as part of the wastage process. Rivet projections are particularly vulnerable in abrasive and abusive flow and are rapidly worn flush where they project above the crown of the invert. Fortunately, the loss of an occasional rivet head in the invert area does not cause overall culvert distress once culverts are bedded. There are few sites that can qualify as abusive, and in such locations all pipe materials—aluminum, steel, and concrete—have been observed to deteriorate rapidly.

CONCLUSIONS

Aluminum alloy culvert has been shown by observation and analysis of the control group of culverts to be resistant to abrasion by bed load materials in culvert water flow. The abrasion rate of aluminum alloy culvert is not linear but decreases with time as demonstrated by the small changes in condition between the 1968 study and the 1985 study. Considering abrasion only, service life of aluminum alloy culverts can be related to rock impact energy levels, expressed by ranges of the abrasion rating schedule. The abrasion rating schedule ranges can be related to expected water flow, culvert entrance arrangement, culvert slope, and expected rock content in bed loads.

RECOMMENDATIONS FOR ESTIMATING SERVICE LIFE USING ENERGY CURVES

The established mathematical kinetic energy levels, substantiated by confirming field data, can be used as a basis for designing

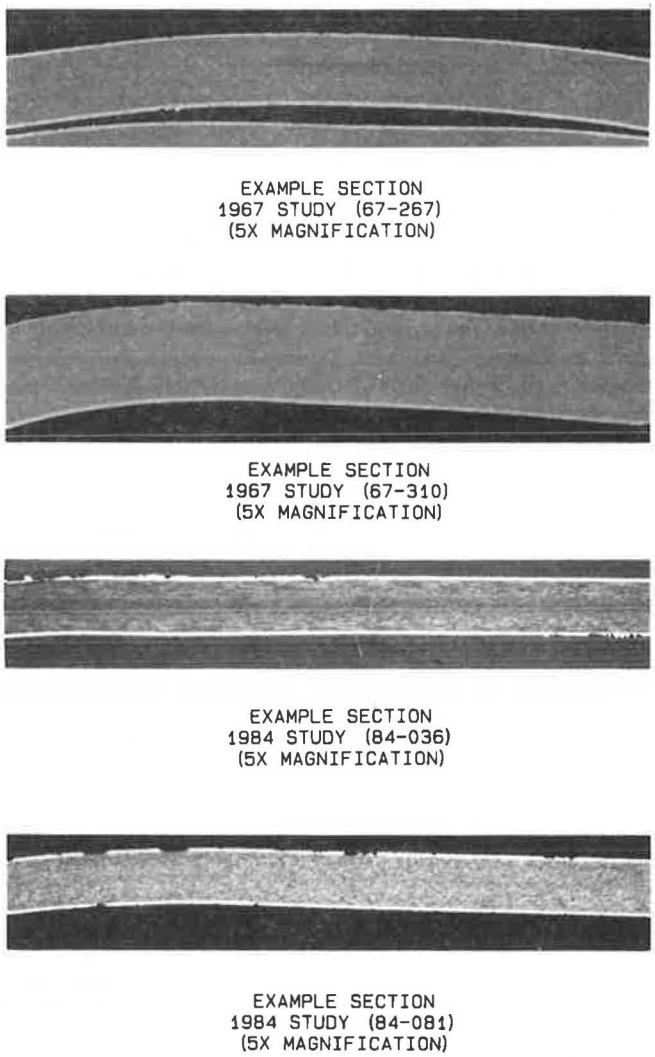

FIGURE 6 Photomicrographs of abrasion rating B/C (sample sections).

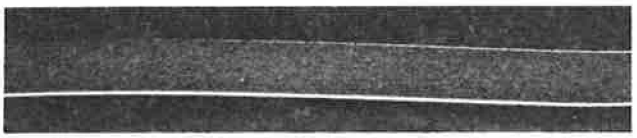

EXAMPLE SECTION
1984 STUDY (84-072)
(5X MAGNIFICATION)

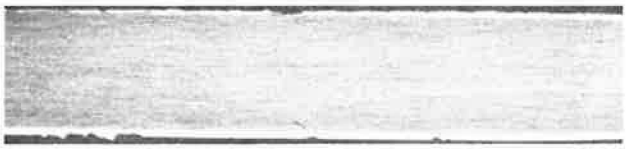

EXAMPLE SECTION
1984 STUDY (84-032)
(5X MAGNIFICATION)

SITE 84-072 RATED B/C

SITE 84-032 RATED B/C

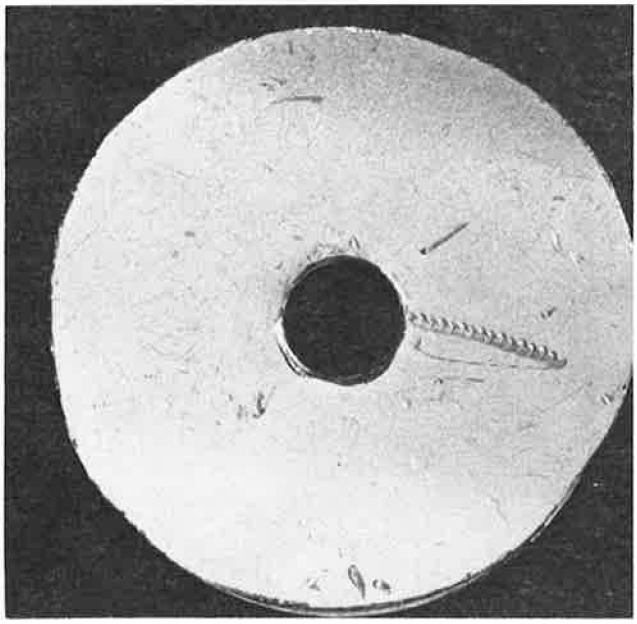

EXAMPLE FACE
1984 STUDY (84-072)
(2.5X MAGNIFICATION)

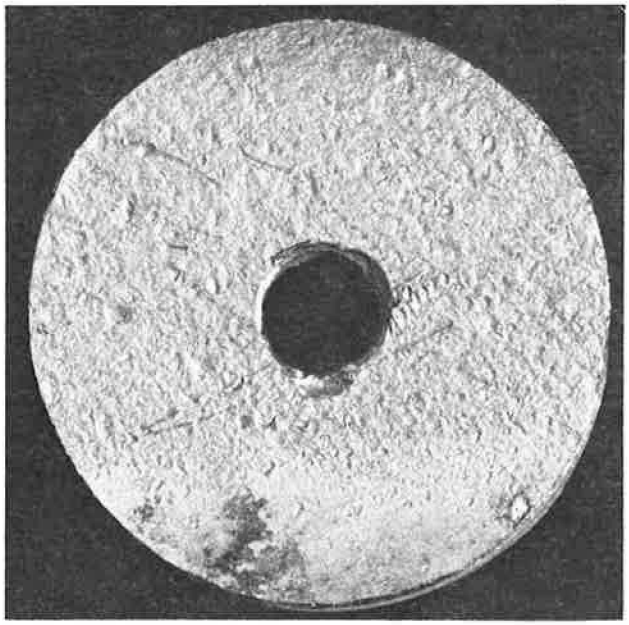

EXAMPLE FACE
1984 STUDY (84-032)
(2.5X MAGNIFICATION)

FIGURE 7 Photomicrographs of abrasion rating B/C (sample sections and faces).

EXAMPLE SECTION
1967 STUDY (67-316)
(5X MAGNIFICATION)
RATING B/C

EXAMPLE SECTION
1984 STUDY
(84-044 SAME AS 67-316)
(5X MAGNIFICATION)

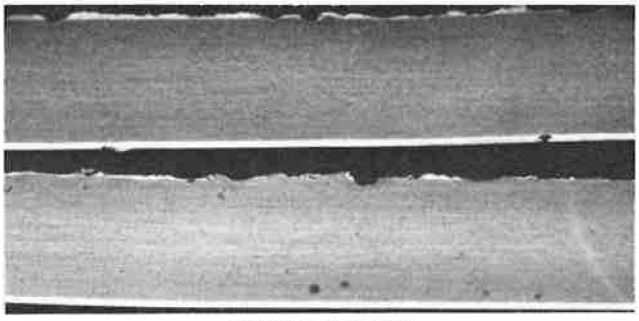

EXAMPLE SECTION
1967 STUDY (67-326, 327)
(5X MAGNIFICATION)

EXAMPLE SECTION
1984 STUDY
(84-079, SAME AS 67-326)
(5X MAGNIFICATION)

FIGURE 8 Photomicrographs of abrasion rating C (sample sections).

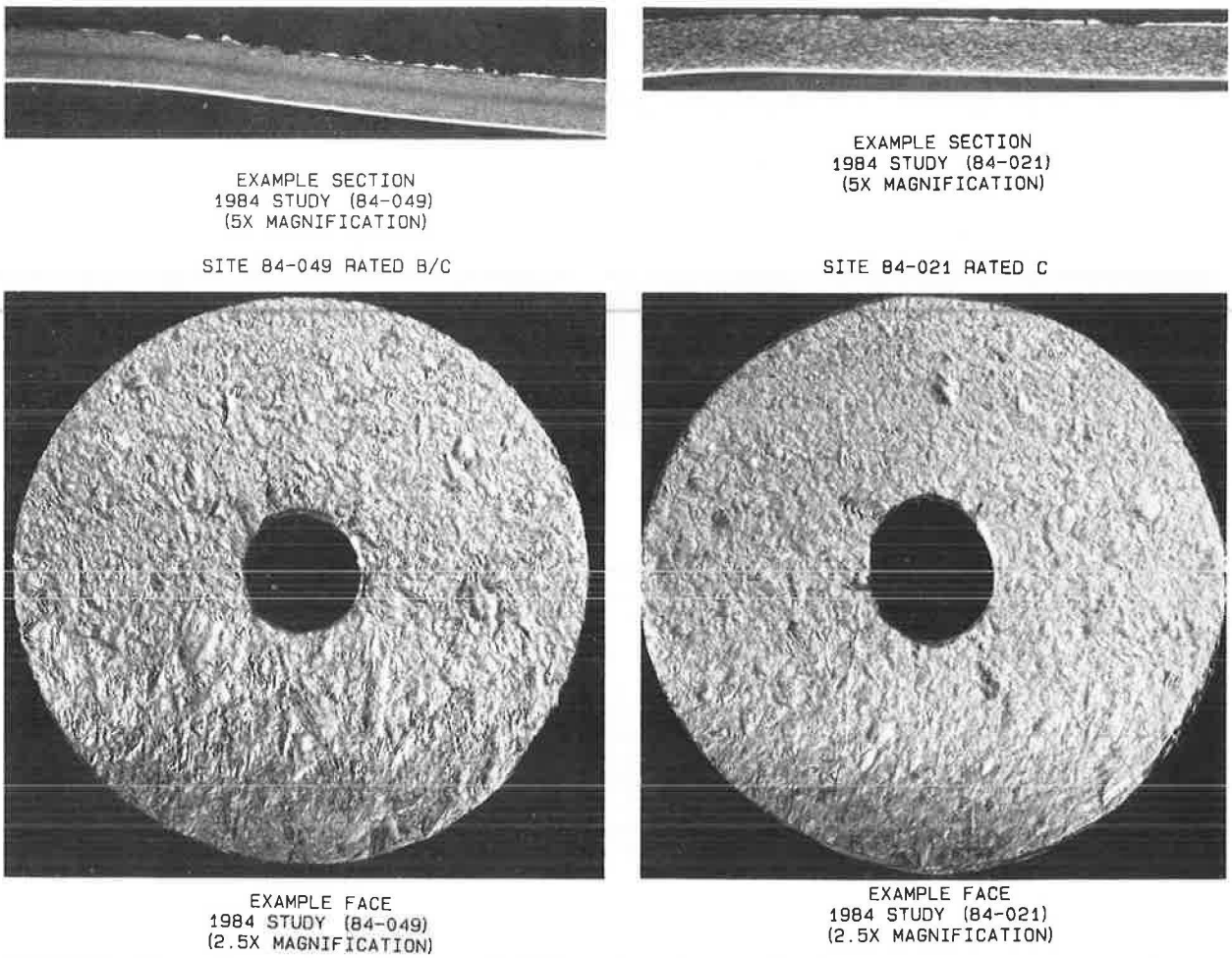

FIGURE 9 Photomicrographs of abrasion rating C (sample sections and faces).

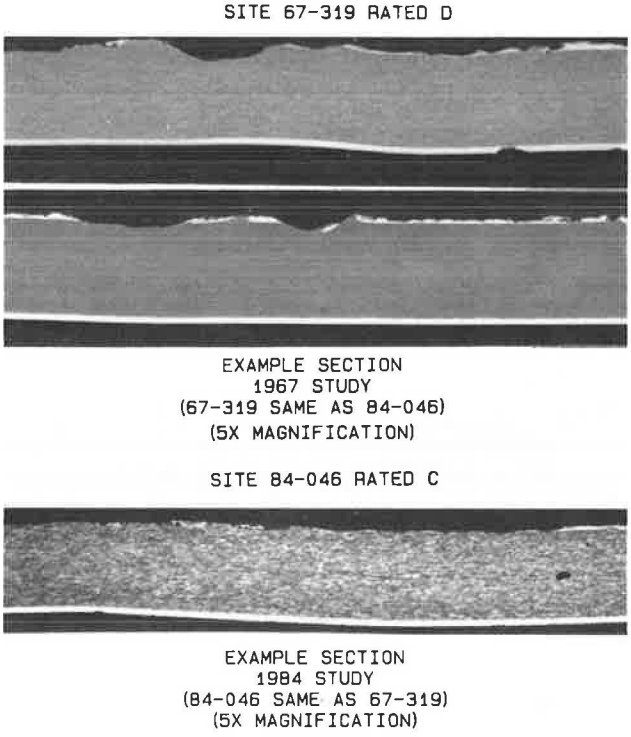

FIGURE 10 Photomicrographs of abrasion rating D (sample sections).

aluminum alloy culvert for abrasive conditions. Table 2 combines a series of culvert sizes, culvert slopes, and peak rock sizes that are representative of each abrasion rating level. Using these data from the current study, which represent more than 20 years of field service, a projected abrasion service life expectation can be added (Table 3).

Expected service life of a new installation can be predicted by determining the abrasion rating level by assessing the upstream bed load, maximum rock size expected, culvert size, and culvert slope. Figure 4 can be used to approximate the culvert abrasion rating. For example, a 36-in. culvert placed at a 15 percent slope develops an energy water velocity of 12.0 ft/sec according to Table 1. When these data are plotted on Figure 4 and peak rock size of 6 in. is selected, a D abrasion rating is indicated with a suggested service life of from 25 to 50 years.

In addition to the summary in Table 3, a number of other abrasion control possibilities should be considered:

1. Sheet gauge of the culvert is normally selected for structural considerations. The normal commercial structural gauge range will usually also fit well for abrasion selections. Where highly abrasive or abusive sites are encountered, consideration can be given to increasing culvert metal thickness.
2. Attention to channel shape and culvert entrance design can reduce rock flow. If the velocity of approach can be reduced the water forces are lowered and the bed load is relaxed. Consider installing culvert inlet above channel invert grade to provide a

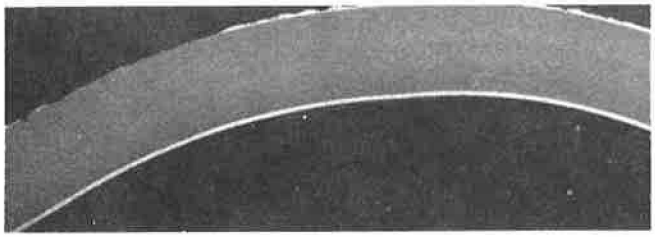

EXAMPLE SECTION
1984 STUDY (84-R-5)
(5X MAGNIFICATION)

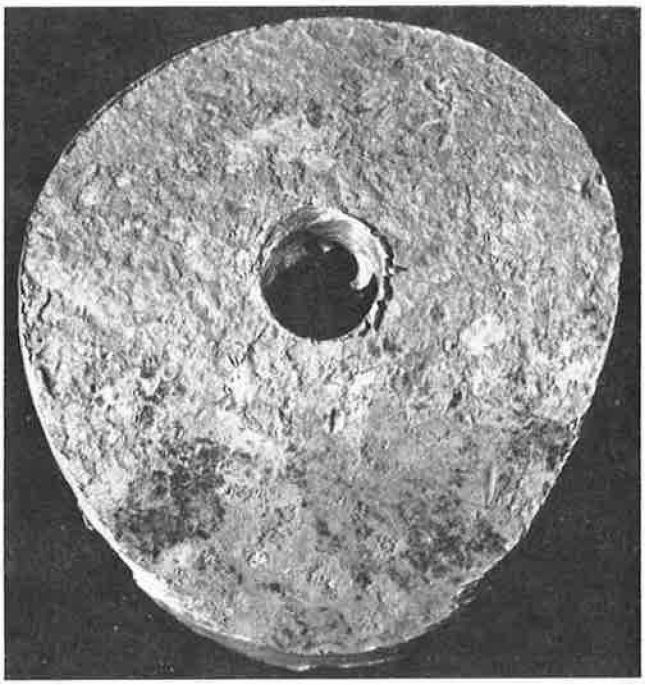

EXAMPLE FACE
1984 STUDY (84-R-5)
(2.5X MAGNIFICATION)

FIGURE 11 Photomicrographs of abrasion rating D (sample section and face).

settlement basin that will fill with larger rocks and reduce the entrance velocity. In time the basin will fill level and still permit fines and smaller rocks to pass.

3. Install trash racks or rock guards upstream of abusive or severe abrasive sites to retain heavy short-term rock and debris flows before they reach the culvert inlet. This practice would, of course, require periodic removal of accumulations.

4. Multiple culverts and arch-shape culverts widen the approach channel considerably, reducing approach velocity. Consider stepping the inlet elevations of multiple culverts to decrease possibilities of floating debris plugging.

5. Paving of inverts with softer materials such as bitumen, asphalt, or plastics is of limited value for use as abrasion control for culverts. Such coatings do not resist rock flow impacts for long periods. The filling of invert corrugations increases rock velocity and does not appear to alter rock flow patterns to improve resistance to abrasion *(4, 5)*. Coatings can be beneficial for nonabrasive mixed-flow exposures such as sanitary sewer systems.

6. Structural plate shapes or other deep corrugations slow rock flows by causing a small reduction in average velocities and resulting rock energies.

7. Where difficult abrasive conditions cannot be avoided, permanent or expendable invert liners can be installed in the invert. Liners should run longitudinally and particular care is necessary to eliminate projections or joints in the rock flow bed. Invert liners of reinforced concrete, railroad rail, or structural steel have been used.

8. Flared or apron entrances do not improve abrasion resistance of a culvert. On the contrary, such entrances actually induct more rocks.

9. Reducing culvert slopes will reduce water flow velocities, rock flow energy levels, and thus abrasion.

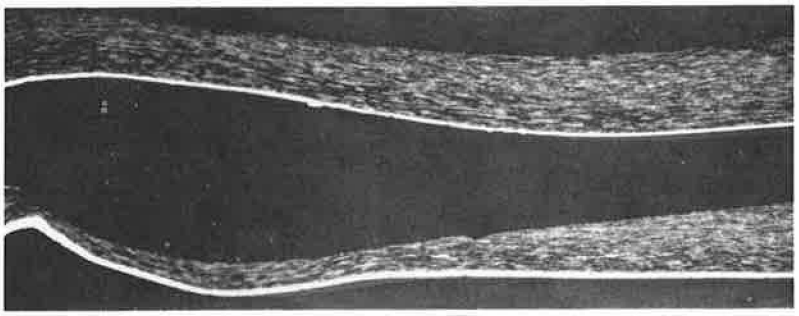

EXAMPLE SECTION
1984 STUDY (84-004)
(5X MAGNIFICATION)

FIGURE 12 Photomicrographs of abrasion rating E (sample section and face).

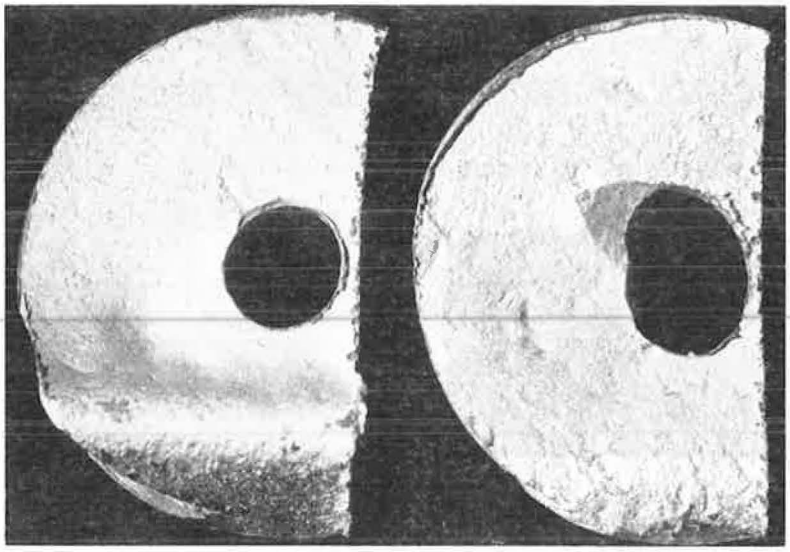

EXAMPLE FACE
1984 STUDY (84-004)
(2.5X MAGNIFICATION)

FIGURE 12 *continued.*

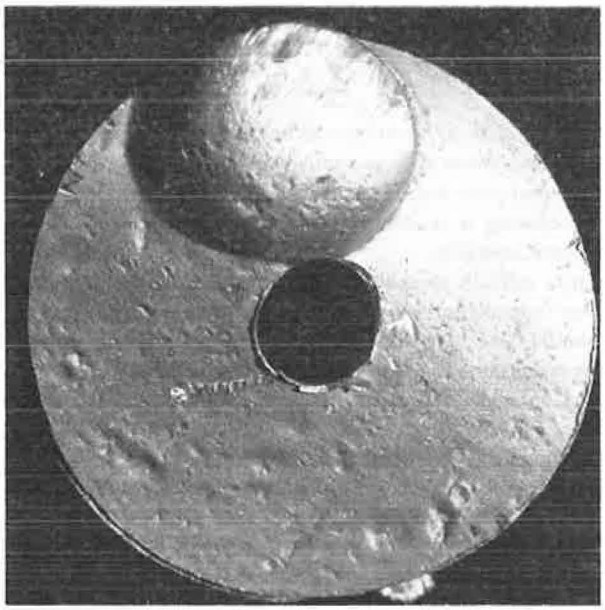

EXAMPLE FACE
ALUMINUM ALLOY RIVET
1984 STUDY (84-A-1)
(2.5X MAGNIFICATION)

(2.5X MAGNIFICATION)

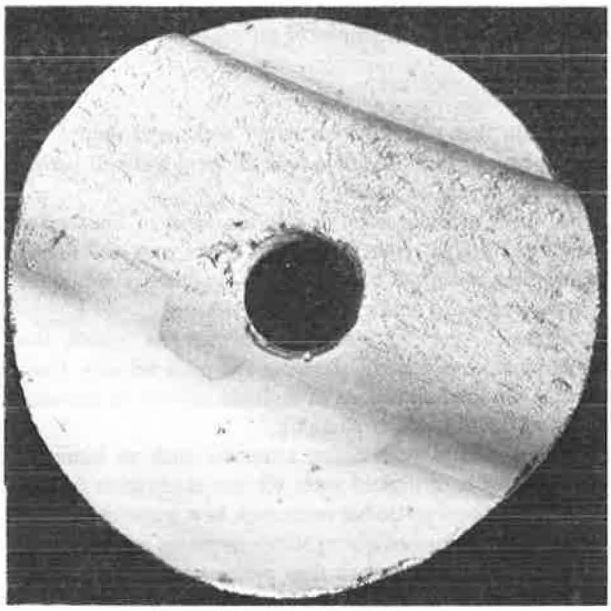

EXAMPLE FACE AND SECTION
ROLLED, FORMED LOCK SEAM
1984 STUDY (84-065)

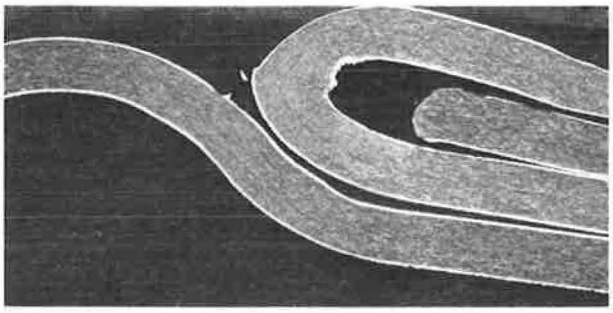

(5X MAGNIFICATION)

FIGURE 13 Abrasion of joints and fasteners.

ACKNOWLEDGMENTS

The author wishes to express appreciation for the support provided by the Aluminum Association in preparation of the material.

REFERENCES

1. *Highway Design Manual.* California Department of Transportation, Sacramento, Sept. 1, 1982.
2. A. H. Koepf. "The Mechanisms of Abrasion of Aluminum Alloy Culvert, Related Field Experiences, and a Method to Predict Culvert Performance." In *Highway Research Record 262*, HRB, National Research Council, Washington, D.C., pp. 44–55.
3. T. A. Lowe, R. H. Vaterlaus, R. I. Lindberg, and L. R. Lawrence. "Corrosion Evaluation of Aluminum Culvert Based on Field Performance." In *Highway Research Record 262*, HRB, National Research Council, Washington, D.C., 1969, pp. 56–68.
4. R. M. Pyskadlo and W. W. Renfrew. "Overview of Polymer Coatings for Corrugated Steel Pipe in New York State." In *Transportation Research Record 1001*, TRB, National Research Council, Washington, D.C., 1984, pp. 21–26.
5. J. O. Hurd. "Field Performance of Protective Liners of Concrete and CSP Culverts." In *Transportation Research Record 1001*, TRB, National Research Council, Washington, D.C., 1984, pp. 35–40.

Publication of this paper sponsored by Committee on Culverts and Hydraulic Structures.

Corrugated Steel Plate Structures with Continuous Longitudinal Stiffeners: Live Load Research and Recommended Design Features for Short-Span Bridges

A. E. BACHER AND D. E. KIRKLAND

The deformation of longitudinally stiffened long-span corrugated steel culverts (beneath shallow overfills) due to live load, backfill, and overfill conditions is investigated. A culvert's structural configuration was monitored from installation through the introduction of live loads. The results of this research at Stenner Creek, and the P–13 proof test loading at Weir Canyon, have led to the conclusions that are recommended herein for incorporation in the design phase. Long-span corrugated metal structures that successfully incorporate these recommended design features are noted.

In 1963 the California Department of Transportation (Caltrans), in cooperation with the Federal Highway Administration, initiated a $3.5 million culvert research program to assess structural behavior of culverts embedded in deep embankments. Included in this extensive culvert research program were three structural steel plate pipes: Chadd Creek, Apple Canyon, and DB Culvert, previously reported *(1–6)*.

Caltrans has also completed a Category 2 (construction evaluated) research project of a super span design at Stenner Creek. Most recently, a proof test for P–13 loading was performed on a multiple super span at Weir Canyon.

Special features for long-span corrugated steel plate structures (with continuous longitudinal stiffeners) have been implemented on subsequent Caltrans projects as a consequence of the Category 2 Caltrans culvert research project at Stenner Creek. Four permanent super spans and one permanent maxi span as well as two temporary super span corrugated steel plate bridges have been successfully installed in California. In addition, Caltrans has reviewed approximately 30 super span city and county installations.

California Department of Highways, 1120 N Street, Sacramento, Calif. 95814.

STENNER CREEK RESEARCH

Caltrans completed a Category 2 culvert research project at Stenner Creek, Bridge 49–146, in 1978, which included significant live load research findings (Figures 1 and 2). Live load design has been, and continues to be, a design consideration for minimum overfills on underground steel structures. The objective at Stenner Creek was to monitor (Figures 3 and 4) the shape changes due to backfilling and to live load in combination with incremental increases in overfill. It is apparent that live load can be a factor on a long-span culvert under shallow fill. The culvert is subject to flexing movement as the load passes over it.

Peripheral Shape Changes

Each of the six transverse sections (Figure 5) had a designated point on either side and a point on top that corresponded to points

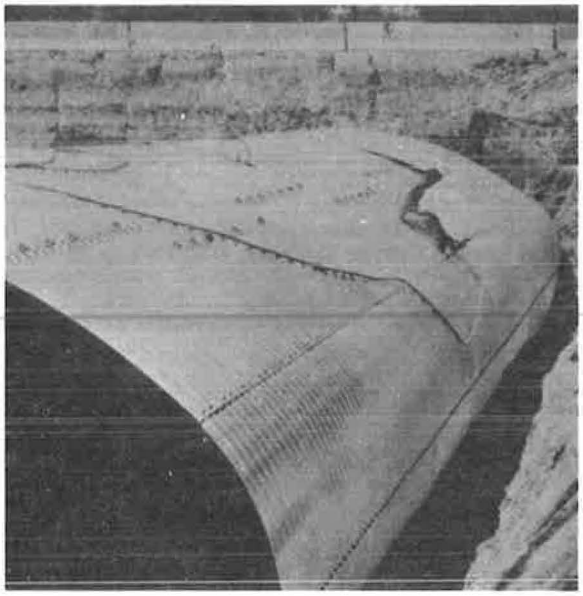

FIGURE 1 Stenner Creek—structural plate assembly.

FIGURE 3 Stenner Creek—backfilling.

on the existing invert slab to facilitate the measurement of the span and rise.

Measurement was accomplished by using a 50-ft tape between the horizontal points. Vertical dimensions were measured using an extended rod. Measurements were taken to the nearest ⅛ in.

Five points between the thrust beams were carefully located and hooks were welded to the structural plate. At these points the Caltrans Transportation Laboratory used deflection gauges to automatically record the peripheral shape changes as the (Figures 6 and 7) wheel load moved across the culvert. Tape switches (Figures 8 and 9) were placed across the wheel load path for the center and outer deflection gauges to reference the truck with respect to these gauges.

Soil Load Geometry

Horizontal and vertical dimensions were measured after the assembly of the structural plates, again after the thrust beam was placed and backfilled, and finally after backfilling to grade (Figure 10).

The variations in both vertical and horizontal dimensions were found to be within specified limits and will provide guidelines for future long-span culvert installations. The maximum variation in both the horizontal and the vertical dimensions during backfilling was 6 in. for all observed locations.

Between initial assembly of all the plates and backfilling behind the thrust beam, the rise increased approximately 5 in. accompanied by a corresponding 6-in. decrease in span width. Subse-

FIGURE 2 Stenner Creek—scaffolding for deflection gauges.

FIGURE 4 Stenner Creek—compacting structure backfill.

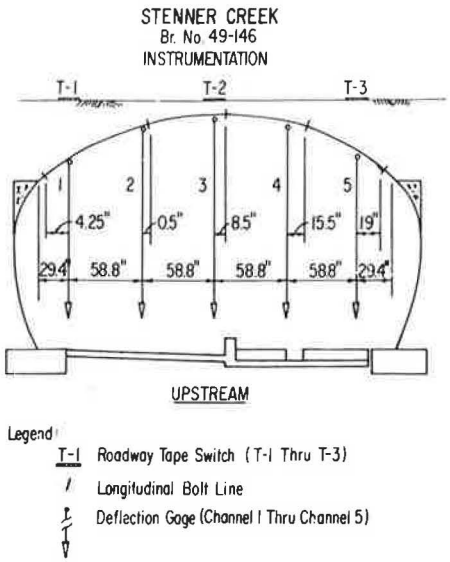

FIGURE 5 Stenner Creek—instrumentation.

quent to backfilling behind the thrust beam, there was an additional 1-in. increase in the rise, and the span had variations of ½ in. or less. The design span and rise dimensions were 35 ft 4 in. and 20 ft 0 in. The completed structure span and rise dimensions ranged between 35 ft 2 in. and 35 ft 4 in. for the span and 19 ft 11 in. and 20 ft 1 in. for the rise.

Live Load

An H20 loading (Figure 11, run 5) of 32 kips with 1 ft of overfill resulted in a maximum deflection of 0.40 in. Although the magnitude of the deflection was only ½ in., the more significant factor was the apparent reversal of stress because of the ripple effect as the load passed over the long-span culvert. Subsequent incremental fill height increases of 1 ft reduced the corresponding live load deflection to approximately 50 percent of those that occurred at the preceding lower fill heights (i.e., 0.20 in. for 2 ft, 0.10 in. for 3 ft, and 0.05 in. for 4 ft). Because only 0.05-in. or 1/16-in. deflection occurred with 4 ft of overfill, the minimum overfill height of span length/8, which corresponds to 4.5 ft of overfill, is considered by Caltrans to be a reasonable minimum. The 6-ft minimum cover at Stenner Creek, therefore, provides assurance that, on a long-term basis, the live load will not adversely affect the long-span culvert design.

FIGURE 7 Stenner Creek—measuring wheel load.

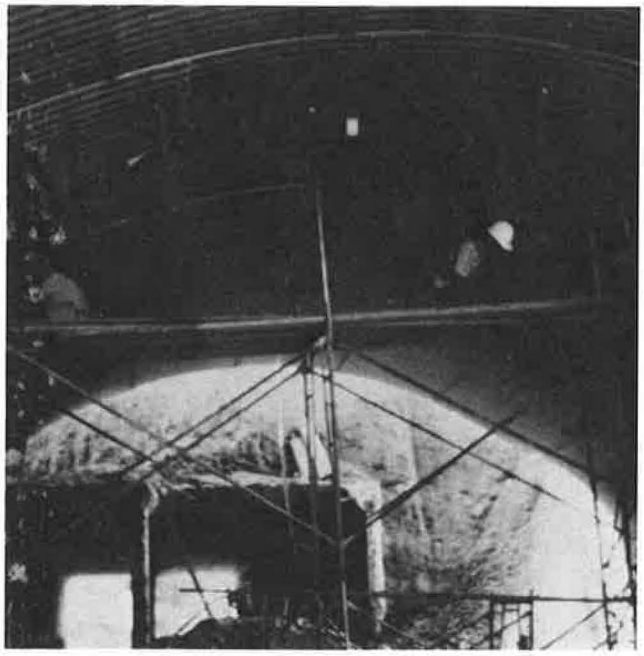

FIGURE 6 Stenner Creek—placing deflection gauges.

FIGURE 8 Stenner Creek—placing tape switches.

FIGURE 9 Stenner Creek—Transportation Laboratory vehicle.

The actual plot of the change in the peripheral configuration of the upper structural plate was of extreme significance. At the 1-ft overfill, a moment was induced in the structural plate. The plate was deflected upward in a ripple effect. It was not a case of pure downward deflection. Consequently, live load moment is a definite design consideration when design overfills are as shallow as 1 or 2 ft. It should be further noted that at the 4-ft overfill (Figure 12, run 15), the structural plate peripheral shape exhibited minimum deflection only. This indicates that with these overfills there is compatibility between the observed loading conditions and the design assumption that moment is not a design consideration, and ring compression becomes the primary design concern for the structural plates.

For live load (Figures 13 and 14), based on the research at Stenner Creek where the minimum overfill is less than span length/8, a 2-ft layer of three-sack concrete is placed between the thrust beams or steel wings.

STENNER CREEK
Br. No. 49-146
DISPLACEMENTS

Sta	No Backfill		Zone A Complete		Zone B Complete		L.L.Test 1' Overfill		Backfill Complete
	Rise	Span	Rise	Span	Rise	Span	Rise	Span	
1	19.74	35.83	—	35.32	20.07	35.27	—	35.28	—
2	19.60	35.67	20.02	35.19	20.09	35.18	20.11	35.18	20.11
3	19.62	35.70	20.02	35.23	20.09	35.22	20.11	35.23	20.09
4	19.60	35.65	19.94	35.18	19.99	35.18	20.00	35.22	19.96
5	19.64	35.78	19.98	35.36	20.03	35.24	20.05	35.37	20.00
6	19.66	35.68	19.95	35.28	20.00	35.28	—	35.32	—
7	19.76	35.63	19.88	35.27	19.97	35.25	—	35.28	—

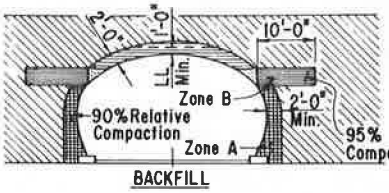

Station 1, Downstream end; Station 7 Upstream end; Station 2-6 at Each Intevening Circumferentral Seam of the Top Arch.

FIGURE 10 Stenner Creek—displacements.

STENNER CREEK
Br. No. 49-146
Live Load Deflection-Run 5
1' Overfill

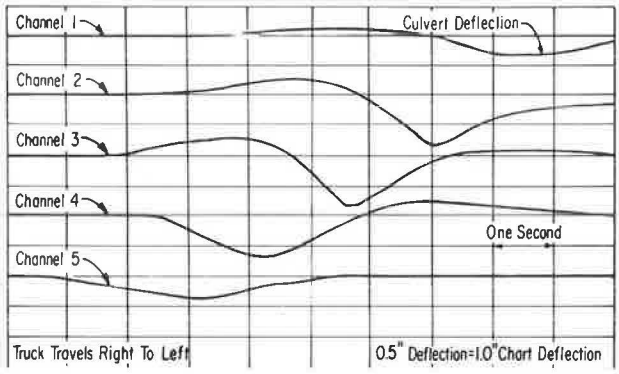

FIGURE 11 Stenner Creek—live load deflection, 1 ft of overfill.

STENNER CREEK
Br. No. 49-146
Live Load Deflection-Run 15
4' Overfill

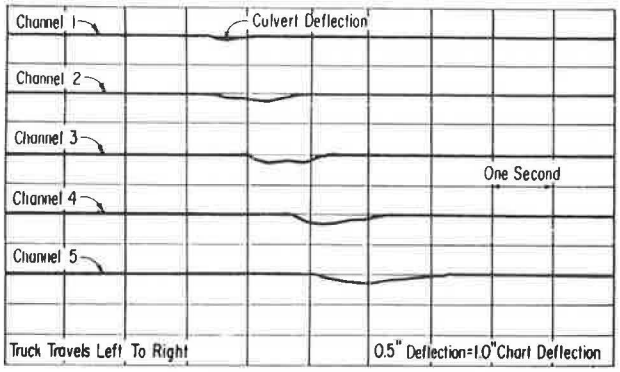

FIGURE 12 Stenner Creek—live load deflection, 4 ft of overfill.

FIGURE 13 Stenner Creek—test vehicle.

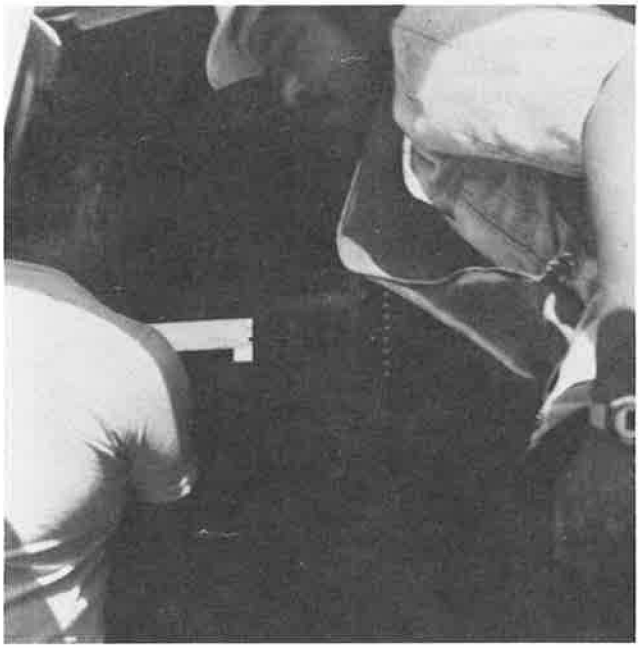

FIGURE 14 Stenner Creek—monitoring deflection plots.

ORANGE COUNTY RESEARCH

A super span in Orange County (Figures 15–17) was proof tested using P–13 loading on a double 38 ft 3 in. × 18 ft ellipse at Weir Canyon on July 4, 1984. The structure is a special design outside the standard AASHTO acceptable limits for minimum cover and top radius. Minimum cover is only 1.7 ft and top arc radius is 29 ft, whereas AASHTO standards limit radius to 25 ft with 4 ft of cover. There was no observable movement evident on any monitoring run. This result confirms the effectiveness of the Caltrans method of using concrete over the top when cover height is below minimum.

Implementation

Since the Stenner Creek research was completed, Caltrans has successfully installed six additional long-span corrugated steel structures. Of the seven total installations, five are permanent and two are temporary (Figure 18)—in use only during the duration of the stage construction. Incidentally, there has been concern for their structural integrity because failures of long-span structures have occurred, as reported in FHWA–RD–77–131, August 1977.

Caltrans has developed special features to ensure the safety and integrity of these cost-effective alternatives to bridges in the 20- to 40-ft span range.

FIGURE 15 Weir Canyon—completed multiple super span.

FIGURE 16 Weir Canyon—monitoring deflection.

Recommended Special Features

The special features that assure safety and structural integrity include (Figure 19) *(a)* providing concrete headwalls or slope

FIGURE 17 Weir Canyon—P–13 loading.

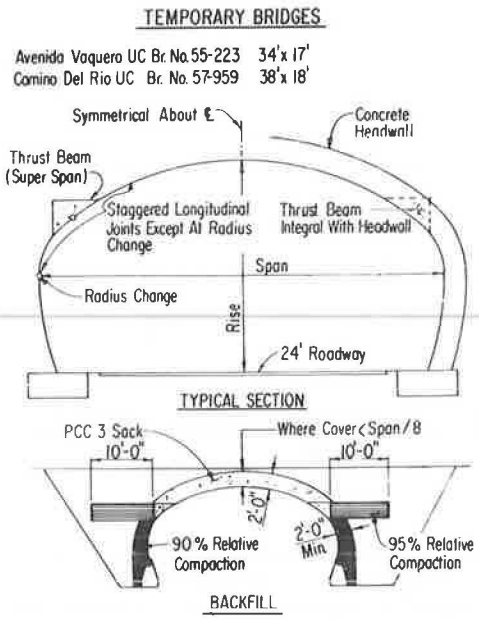

FIGURE 18 Temporary bridges—super span.

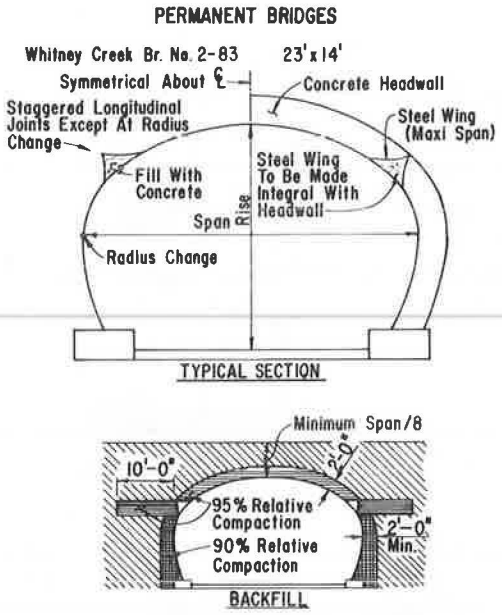

FIGURE 20 Permanent bridge—maxi span.

collars; *(b)* requiring the longitudinal joints to be staggered except at the point of radius change; *(c)* specifying a crown angle of 80 degrees; *(d)* specifying a maximum radius of the crown arch of 25 ft; *(e)* providing for a minimum 2-ft thickness of structural backfill at 90 and 95 percent compaction around the periphery (Caltrans specification); *(f)* limiting the skew to 20 degrees; *(g)* for live load, where the cover is less than span length/8, a 2-ft layer of concrete (three sack) shall be placed between the super span thrust beams or maxi span steel wings; and *(h)* extending the thrust beam on super spans into the headwall or slope collar at each end of the structure, and filling the steel wings of maxi spans (Figure 20) with concrete, and providing for an integral connection into the headwalls or slope collars.

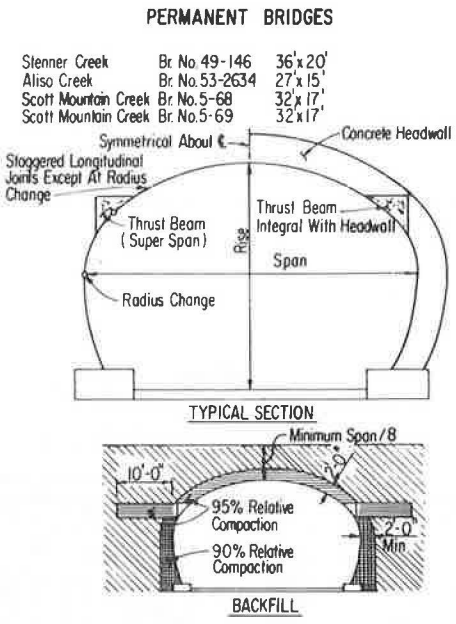

FIGURE 19 Permanent bridges—super span.

Design

The requirement to make the thrust beam or steel wings integral with the headwall provides a composite type of structure with the corrugated steel plate receiving an additional structural restraint by its attachment to the continuous thrust beams or the concrete-filled steel wings. Span-to-rise ratios less than 0.18 may require special design including moment calculations.

Application of ring compression design will provide adequate assurance of the structural competence of either the super span or the maxi span, provided the special features detailed are provided for these structures.

DIMENSION RATIO

Another interesting observation by Caltrans designers (Figure 21) has been the relationship of dimension ratio and structural steel plate pipe performance and design. Dimension ratio is defined as the inside diameter in inches divided by the depth of corrugation profile in inches. Based on Caltrans' experience, standard plans for Caltrans structural steel plate designs require internal strutting where the dimension ratio varies between 100 and 150. As a consequence of Caltrans' structural steel plate research, special pipe designs, and successful usage of long span designs, it appears that dimension ratios exceeding 150 require that special features (i.e., longitudinal stiffeners) be incorporated into the design of long-span structures.

SUMMARY

In conclusion, to date, the state of California has realized a total savings of approximately $1 million on the five permanent and two temporary structural steel plate long-span structures with the continuous longitudinal stiffeners. This type of structure can be an economical, structurally viable short-span bridge alternative.

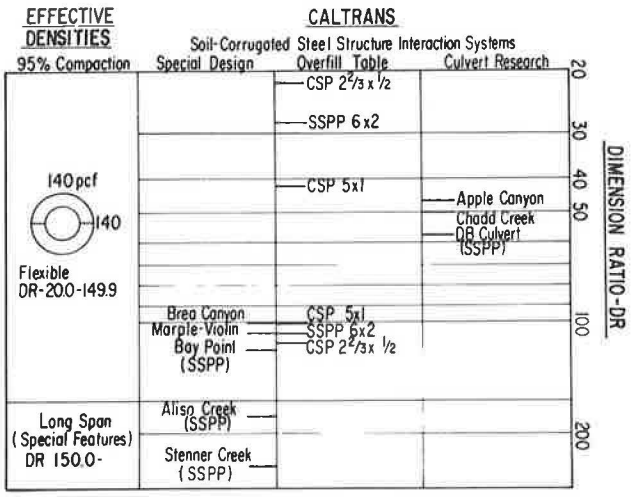

FIGURE 21 Corrugated steel pipe and structural steel plate pipe—dimension ratio.

REFERENCES

1. R. E. Davis and A. E. Bacher. "California's Culvert Research Program—Description, Current Status, and Observed Peripheral Pressures." In *Highway Research Record 249*, HRB, National Research Council, Washington, D.C., 1968, pp. 14–23.
2. R. E. Davis. *Structural Behavior of a Flexible Metal Culvert Under a Deep Earth Embankment Using Method B (Baled Straw) Backfill.* Report R&D 4–69. Bridge Department, California Division of Highways, Sacramento, 1969.
3. D. W. Spannagel, R. E. Davis, and A. E. Bacher. *Structural Behavior of a Flexible Metal Culvert Under a Deep Earth Embankment Using Method A Backfill.* Report CA–HY–BD–624111–73–6. Bridge Department, California Division of Highways, Sacramento, June 1973.
4. D. W. Spannagel, R. E. Davis, and A. E. Bacher. "Effects of Methods A and B Backfill on Flexible Culverts Under High Fills." In *Transportation Research Record 510*, TRB, National Research Council, Washington, D.C., 1974, pp. 41–55.
5. R. E. Davis and A. E. Bacher. *Prooftesting of a Structural Plate Pipe with Varying Bedding and Backfill Parameters.* Report FHWA/CA/SD–79/20. Office of Structures Design, California Department of Transportation; FHWA, U.S. Department of Transportation, Vols. 1–8, 1979–1983.
6. A. E. Bacher and D. E. Kirkland. "California Department of Transportation Structural Steel Plate Pipe Culvert Research: Design Summary and Implementation." In *Transportation Research Record 1008*, TRB, National Research Council, Washington, D.C., 1985, pp. 89–94.

Publication of this paper sponsored by Committee on Culverts and Hydraulic Structures.

Comparative Evaluation of Precast Concrete Pipe-Arch and Arch Structures

JAMES J. HILL AND ARUNPRAKASH M. SHIROLE

In this paper is presented a comparative evaluation of precast concrete pipe-arch and arch structures constructed in Minnesota during the past 20 years. Typical geometrics of these two types of structures are given. Design differences, structural details, load configurations, bedding materials, and foundation considerations for each type of structure are discussed. Comparative evaluation of features and problems associated with construction, maintenance, and repair of these structures is presented. Available information on initial and estimated life-cycle costs is covered in view of known performance history. Conclusions and recommendations are made for improvement in the design and construction of these two types of structures.

During the past two decades, precast concrete pipe-arch structures have been rather extensively used as replacement structures in Minnesota. Precast concrete (BEBO) arch structures were introduced in the United States in 1980–1981. Thirteen such structures have been installed in Minnesota so far and more are being planned. The wide use of precast pipe-arches has been attributed to their economy, ease of construction, and hydraulic efficiency. However, pipe-arches are limited to shorter spans of up to 16 ft. On the other hand, the precast arch structures, in addition to offering economy and ease of construction, can provide spans of up to 50 ft. As a result, their use is increasing.

In this paper are evaluated and compared geometric details, design features, construction techniques, and performance patterns based on construction and subsequent follow-up inspections of these two types of structures. Cost considerations are also examined, and comparative life-cycle costs are discussed.

GEOMETRIC DETAILS

Figure 1 shows typical geometric details of precast concrete pipe-arch structures. Pipe-arches normally span between 6 and 14 ft, beyond which field handling and costs become limiting factors. They are horseshoe shaped in cross section with wall thicknesses that vary from 6 to 11 in. depending on span length. The pipe-arch sections have tapered tongue and groove at their ends, which provide good joints and pipe continuity. Such sections are normally connected end to end with the upstream and downstream ends connected to a flared precast concrete section. Typical reinforcement for pipe-arches consists of two layers or cages of reinforcing bars or mesh, with 1 in. of concrete cover inside and outside. Reinforcement for shear stress, when necessary, is normally provided in the top and bottom floor areas. The lifting or handling hooks for pipe-arch sections are provided in the sides to minimize shear and tensile stresses. Sections of pipe-arches are such that they can be raised and positioned with minimal effort.

Figure 2 shows typical geometric details of precast concrete arch structures. These structures have spans of up to 50 ft, beyond which field handling and costs become prohibitive. Most commonly used spans are 24, 30, and 40 ft. The wall thickness of cross sections ranges between 10 and 12 in. Full-span arch sections, 5 to 6 ft wide, are placed side by side (butted together) on top of relatively shallow cast-in-place reinforced concrete footings.

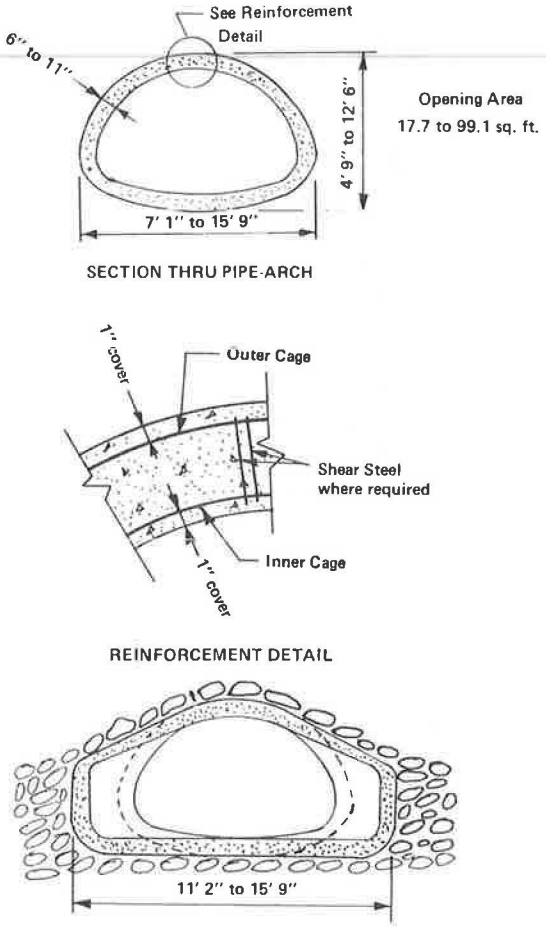

FIGURE 1 Typical geometric details of precast concrete pipe-arch structures.

Joints between arch sections are packed with mastic rope. Precast concrete headwall sections are connected to the end arch sections by 1-in.-diameter tie rods. A pair of wingwalls butt together with these headwalls in a notch. Typical reinforcement for arch structures consists of two layers of reinforcing bars or mesh, with 1½ in. of concrete cover on the inside and 2 in. on the outside. The height of fill above arch structures is normally maintained at such depths that shear reinforcement is not necessary. The lifting or handling hooks for arch structures are provided in the sides and top of the sections to minimize handling stresses. Sections of arch structures are such, especially because of their narrow widths and long spans, that their handling and placement have to be quite sophisticated.

Minnesota Department of Transportation, Transportation Building, St. Paul, Minn. 55155.

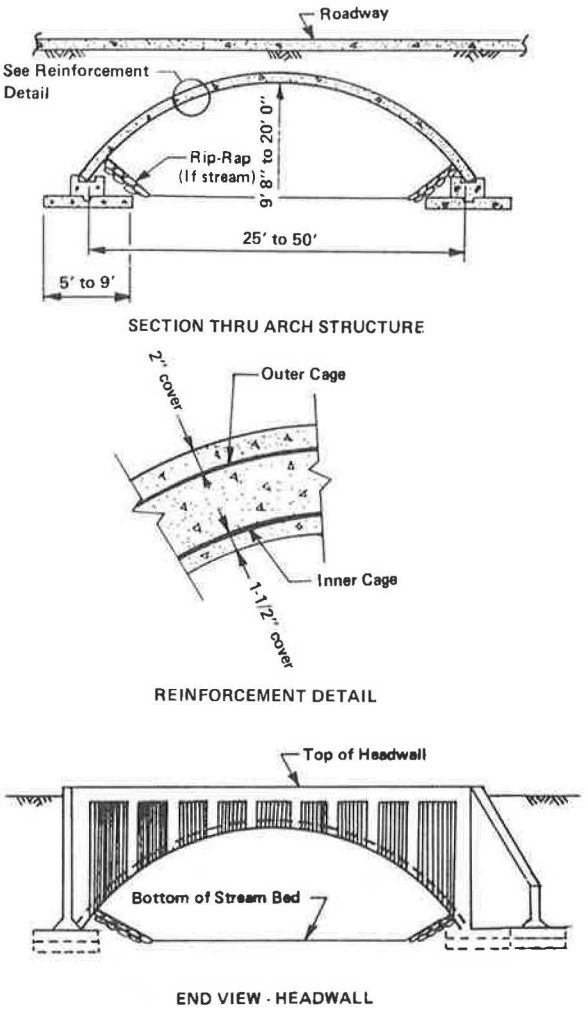

FIGURE 2 Typical geometric details of precast concrete arch structures.

COMPARATIVE EVALUATION

Design

Pipe-arches are designed as a closed-ring system with direct overburden and live loads from above and resisting soil pressures (Figure 3). Actual loads may result in unsymmetrical loading conditions over the life of the pipe-arches, which require greater shear reinforcement. The shape of a pipe-arch is such that the loads are distributed over a large area along its bottom. Typical load, shear, and bending moment diagrams are shown in Figure 3.

Arch structures are designed as two-hinged arches with overburden and live loads from above and resisting soil pressures under footings as well as passive soil pressures from sides. Footing loads consist of a vertical component and a horizontal thrust. The passive soil resistance needs to be mobilized to balance this horizontal thrust. Settlements and outward movements of footings have been found to be significant problems. The critical movements of the footing beneath the arch structures have been one of the major disadvantages in the design of arch structures. Imminent movement conditions have to exist in order to mobilize passive soil resistance that can balance horizontal thrust. Noticeable hairline cracks have been observed along the bottom of concrete at or near arch midspan. These cracks have run transverse to the span and have been located near the reinforcement. These can be attributed to the failure to develop adequate passive soil resistance to lateral movement or to inadequate bearing capacity of soil under the footings, or both. Subcuts as well as better quality and well-compacted bedding and fill materials are therefore necessary for arch structures.

Construction

Pipe-arch sections are normally cast in 4- to 10-ft lengths, weigh up to 15 tons, and are transported to site on flatbed trucks. In general, suitable bedding material for pipe-arches would have a safe bearing capacity of from 1,500 to 4,000 psf. This material is shaped to conform to the bottom of the section so that resulting soil pressures are uniform, thus preventing differential settlements and rotation of sections. A 40- to 50-ton crane is then used to lift, position, and place the sections. Because the pipe-arch sections are not match-cast, some difficulties can arise in achieving a proper fit at the tongue and groove between adjacent sections. A layer of geotextile is placed on top and sides, while a mastic rope is packed in the bottom, of joints to prevent leaking and piping action. Granular backfill is then placed symmetrically in 8-in. lifts and compacted to 95 percent of standard Proctor density to achieve balanced load conditions. A surface wearing course of asphalt or concrete is placed and compacted. A reinforced concrete slab is desirable with shallower overburdens of 2 ft or less to conform to AASHTO requirements.

Sections of arch structures are cast in 5- to 6-ft-wide full-span lengths, weigh up to 20 tons, and are transported to site lying on their side on flatbed trucks. Reinforced concrete footings are cast in place on properly excavated, backfilled, and well-compacted subgrade materials. Such bedding materials would normally be compacted to 100 percent of standard Proctor density and have a safe bearing capacity of 4,000 psf or better. A 75-ton crane, with heavy steel beam, is used to lift and place sections of arch structures on top of the cast-in-place footings. Under normal conditions, placement of an arch section takes from 10 to 15 min depending on construction worker skills and site conditions. Adjacent sections are just butted together with a mastic rope packed in the joints. A layer of geotextile is placed over the joints. Granular material is then placed symmetrically in 8-in. lifts and compacted to 95 percent of standard Proctor density to achieve balanced load conditions. A surface wearing course of asphalt or concrete is placed after all of the design overburden is placed and compacted. A reinforced concrete slab is desirable with shallower overburdens of 2 ft or less.

Erosion protection in the form of a filter material and rock riprap is placed in the channel bottom of arch structures immediately after the concrete footings have cured to the required strength of not less than 45 percent of the design strength. This sequence of operations saves costly hand placement later and permits use of lifting equipment from the stream level.

Maintenance and Repair

Pipe-Arches

Settlements and movements, in the case of pipe-arches, have been the result of inadequate preparation of bedding materials and inadequate compaction of backfill. However, in general, these problems have not caused any critical performance difficulties for pipe-arches.

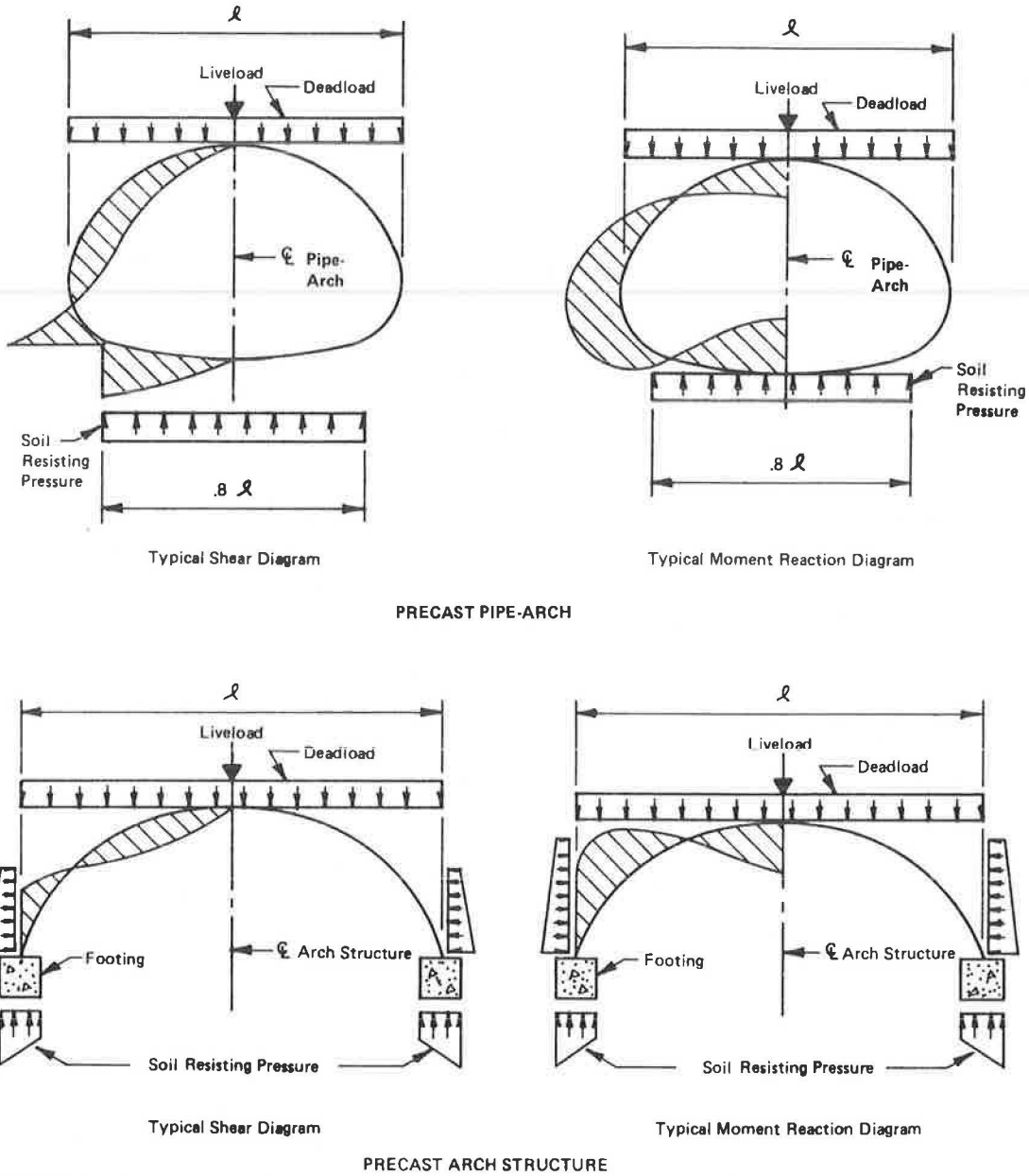

FIGURE 3 Load, shear, and moment diagrams.

The main problem with pipe-arches is scour at inlets and outlets because of excessive flows. Inadequate riprap protection at the base, sides, and top of arch aprons typically results in scour at the base, which progressively causes sliding of the upper soils, thereby enlarging the area of scour. Under extremely high flows scour would normally start further downstream and then progress to the outlet. Properly sizing the pipe-arches to high flows, such as 100-year floods, as well as properly sizing riprap and placing it on filter blankets or geotextiles can effectively minimize or even eliminate scour problems. In some places, where turf grows quickly and abundantly, scouring has not been a problem.

Another problem with pipe-arches is piping underneath the bottom, which erodes away the bedding material that supports it. This action may take place at the apron-inlet or between joints that have opened up. However, this problem has not been extensive for arch-pipes because of the sediment placed on the bottom during low flows that fills the joints. Piping at the inlet and outlet apron sections can be reduced by using a concrete dropwall or similar barrier.

The flat bottom of pipe-arch relates to wider stream flow; however, this wider bottom allows settlements of sediment that fill the waterway. This sediment normally gets washed away under rapid flow conditions. However, occasionally the pipe-arch has to be cleaned using labor-intensive methods that are costly.

Arch Structure

Settlements and movements, in the case of arch structures, have been the results of inadequate preparation of bedding materials under the footings and horizontal thrust as well as rotation at the footings. Cracking has been observed at the bottom of the arch at its crest. This can be explained by reviewing load, shear, and bending moment diagrams (Figure 3). Further, field measurements

indicate significant lateral movements as well as some rotation at the footings. This suggests that adequate lateral restraint by the passive earth pressure may not have been activated early enough to prevent lateral movements observed at the footings, thereby causing subsequent crack patterns.

Although differential settlements can be critical in the case of arch structures, no such cases have been identified in the present short performance history of these types of structures; although settlements of up to 2 in. have been noticed, differential settlements have been less than ½ in.

Arch structures have a circular type of opening without a bottom. The filter blanket and riprap materials are placed in the stream bed to prevent its erosion. To date, extensive scour problems have not occurred. However, settlement and scour around the wingwalls have caused some shear cracks in concrete interconnections. Placement of well-compacted granular material has deterred this problem. The flow through arch structures has been less turbulent and generally controlled by the riprap to prevent scour (Tables 1 and 2).

Total construction costs of pipe-arches and arch structures that have been estimated or are under contract for four sites in Minnesota are given in Table 3.

From the estimates in Table 3 it would appear that two-barrel pipe-arches are less expensive for certain spans and fill heights.

TABLE 1 DATA ON CONCRETE ARCH STRUCTURES

Arch Width	41'	31'	41'	31'	41'	41'	41'	31'	41'	41'	41'
Arch Height	9'-8"	13'-8"	9'-8"	11'-4"	9'-8"	9'-8"	9'-8"	11'-4"	9'-8"	9'-8"	9'-8"
Spreading Footing Width	8'-6"	8'-0"	7'-0"	5'-0"	8'-0"	6'-0"	6'-0"	5'-0"	8'-0"	8'-0"	8'-0"
Spread Footing Depth (Below arch section) (which includes pads)	2'-6"	2'-7"	3'-4"	1'-8"	2'-8"	1'-10"	1'-10"	1'-8"	2'-11"	3'-4"	3'-4"
Type of Scour Protection	Rock Rip Rap	Not Req'd	6' Wide/ Sloped Rip Rap	Rock Rip Rap	Rock Rip Rap	Rock Rip Rap	Rock Rip Rap	Rock Rip Rap	Rock Rip Rap	Rock Rip Rap	Rock Rip Rap
Hydraulic Flow Q_{100}	1350 cfs. @ 5.0 fps.	(None)	1440 cfs. @ 5.1 fps.	860 cfs. @ 4.8 fps.	2200 cfs. @ 7.6 fps.	1450 cfs. @ 5.6 fps.	1700 cfs. @ 6.5 fps.	860 cfs. @ 4.5 fps.	1000 cfs. @ 3.6 fps.	6980 cfs.* @ 5.9 fps.	3710 @ 10.8 fps.
Barrel Length	72'	90'	66'	84'	66'	58'	54'	90'	90'	42'	84'
Cover Over Arch Sections at C/L Roadway	2'-8"	4'-7"	4'-9"	2'-0"	3'-0"	1'-6"	3'-6"	9'-9"	1'-8"	1'-8"	5'-8"
Type Roadway Over	5-1/2" Bit.	Bit.	Bit.	Bit.	Bit.	Bit.	Bit.	Bit.	Bit.	Gravel	Bit.
Traffic Over: ADT	5200 (81)	1750 (80)	472 (99)	400 (87)	475 (82)	1750 (82)	1800 (82)	4850 (81)	6300 (82)	43 (71)	
Angle of Wingwalls to Barrel	Square	Square	Square	Square	30° Flare	30° Flare	30° Flare	Square	30° Flare	30° Flare Parallel	30° Flare
Soil Condition	Peat and Silty Sand	Generally clay loam till	SC stiff to very stiff	Medium to Coarse Sand	Sl. Pl. SiL.	Very Stiff to hard clay loam till	Sand and gravel	Si Clay Very Stiff trace of Sand	Silty Sand Loose to Medium Dense	Silty Sand to Stiff Clay Loam	Gray Clay Till
Subcut Depth Under Ftg.	6 to 8'	4' on North ftg. & 8' on South ftg.	2'	None	Subcut to Elev. 769 3'	2'	1'	None	6'	1'	2'
Backfill Placed Under Footings	Select Granular Borrow Spec. ∅ 3149.2B 100% Density	Select Granular Borrow Spec. 3149.2B 100% Density	Select Granular Borrow Spec. 3149.2B 100% Density	Granular Bedding Spec. 3149.2F 100% Density	Granular Bedding Spec. θ 3149.2F 100% Density	Granular Bedding Spec. 3149.2F 100% Density	Granular Bedding Spec. 3149.2F 100% Density	Granular Bedding Spec. 3149.2F 100% Density	Granular Bedding Spec. 3149.2F 100% Density	Granular Bedding Spec. 3149.2F 100% Density	Granular Bedding Spec. 3149.2F 100% Density

* An overflow channel is used to handle the 6980 cfs. flow.

∅ Specification 3149.2B allows select granular borrow material (one inch maximum size down to a maximum of 15% passing a #200 sieve) to be used in backfill.

θ Specification 3149.2F is the same as Spec. 3149.2B, except that only a maximum of 10% may pass a #200 sieve and the material is a graded aggregate product.

TABLE 2 DATA ON CONCRETE PIPE-ARCHES

Width (Inches) (Clearance span)	102	115	115	138	138	154	154	169	169
Height (Inches) (Clear Height)	62	72	72	87	87	97	97	107	107
Hydraulic Flow Q_{100} (CFS)	460/	717/	763/	640/	762/	1300/	1483/	1495/	1920/
V_{100} (FPS)	6.5	5.5	8.71	5.9	7.47	8.0	9.06	7.54	10.7
No. of Barrels	2	3	2	2	2	2	2	2	2
Barrel Length (Feet)	44	50	40	50	64	38	76	72	52
Cover over Pipe (Feet)	2.38	1.00	2.30	2.60	1.95	2.39	5.0	7.5	3.50
Type of Roadway Surface	Gravel	Gravel	Gravel	Bit.	Gravel	Gravel	Gravel	Gravel	Bit.
Subcut Depth Under Pipe (Ft.)	1.0	4.0	2.0	1.5	2.0	2.0	1.0	2.0	2.0
Type Backfill Under Pipe*	Class A	Class A	Class A	Class A	Class A	Class B	Class A	Class A	Class A

*Per specification 2451

All pipe-arches Class A riprap as scour protection.

TABLE 3 CONSTRUCTION COSTS

Fill Height Above Arch (ft)	Site (county)	Length of Pipe-Arch (ft)	No. of Barrels	Size (in.)	Water Way Area (ft^2)	Total Cost ($)	Size (ft)	Water Way Area (ft^2)	Cost ($)
7.0	Lake	122	2	154	163	129,470	24	190	150,700
2.5	Dakota	86	3	169	297	130,100	40	300	109,210
15.0	Murray	152	3	169	297	289,755	30	330	181,388
12.0	Clearwater	120	3	169	297	181,100	30	330	129,050

Note: Length of pipe-arch includes the aprons.

However, when three-barrel pipe-arches are used, the arch structure appears to be less costly. When long spans and deep fills are encountered, the arch structure is definitely more economical than pipe-arches. Additional comparisons need to be made to determine the competitiveness of two-barrel pipe-arches and the 24-ft arch structure.

No significant maintenance and repair costs related to the structure of the pipe-arches have yet been experienced. There have been costs associated with erosion and sedimentation. However, these can be substantially minimized by adequate sizing of the pipe-arch to handle extreme flow conditions, such as the 100-year flood, and proper selection as well as placement of appropriate erosion protection.

Significant problems related to settlement, movement, and rotation of footings have come to light in the short performance history of arch structures. Should current design practices for arch structures be maintained, the levels of maintenance and repair activities can be expected to be greater than those for the pipe-arches. The crack patterns may become more serious. Another area for maintenance would be the connections with the headwall and between the headwall and wingwalls. Cracking and spalling of concrete sections can be expected to develop in those areas.

Another area of concern is the potential damage to footing support due to scour under extreme flow conditions. Settlement and movements can worsen unless stronger requirements for bearing capacity, depth of burial to reduce adverse effects of potential scour, and better means of preventing footing movements and rotations are specified. Consideration of piling support would be in order. Under the current practice, however, maintenance costs can be expected to be higher than those for pipe-arches.

CONCLUSIONS

1. Pipe-arches with low, wide bottoms are suitable for flat, shallow stream crossings, and arch structures are more adaptive to narrow, deep channels.

2. Pipe-arches have not experienced structural or scour problems of any significance. There has been some localized scour at their inlet and outlet apron sections.

Arch structures have settled and moved horizontally outward at their footing lines, until the passive soil resistance has been activated. These conditions have caused hairline cracks at the midspan of the arches. Use of piling in the concrete footings should be considered.

3. Use of adequate scour protection is essential to arch structures that have spread concrete footings.

4. Pipe-arches are easy to place using normal construction equipment. Arch structures require more sophisticated handling equipment and techniques because of their size, shape, and weight.

5. Pipe-arches have only experienced some scour and sedimentation problems. Arch structures are relatively new and somewhat experimental in nature, but to date they have not directly presented similar maintenance or repair problems.

6. It appears that up to two lines of pipe-arches are as economical to use as a single arch structure. However, three or more lines of pipe-arches are significantly more expensive than a single arch structure.

Publication of this paper sponsored by Committee on Culverts and Hydraulic Structures.

Measurements and Analyses of Compaction Effects on a Long-Span Culvert

RAYMOND B. SEED AND CHANG-YU OU

Earth pressures that result from compaction of backfill can induce stresses and deformations, which are not amenable to analysis by conventional analytical methods, in flexible metal culverts. In this paper are presented the results of a study in which deformations of a 39-ft-span flexible metal culvert were measured at various stages of backfill placement and compaction. These field measurements were then compared with the results of finite element analyses in order to investigate the influence of compaction effects on culvert stresses and deformations. Two types of finite element analyses were performed: *(a)* conventional analyses that make no provision for modeling compaction effects and *(b)* analyses that incorporate recently developed models and analytical procedures that permit modeling of compaction-induced stresses and deformations. The results of these finite element analyses indicate that compaction effects significantly increased structural deformations during backfilling and also significantly affected bending moments within the culvert. Axial thrust around the culvert perimeter was also affected by compaction-induced earth pressures, but to a lesser degree. The results of this study provide a basis for assessing the potential importance of considering compaction effects in evaluating culvert stresses and deformations during and after backfill placement and compaction.

Earth pressures that result from compaction of backfill can produce stresses and deformations, which are not amenable to analysis by conventional analytical methods, in flexible metal culverts. These compaction-induced stresses and deformations can significantly influence the stress state and geometry of a culvert at various stages of backfill placement and compaction.

In this paper are presented the results of a study in which deformations of a large-span flexible metal culvert structure were measured during backfill operations. Detailed records of backfill placement procedures were maintained and care was taken to prevent the operation of large construction equipment in close proximity to the culvert, so this field study represents a case in which the influence of compaction effects on culvert stresses and deformations was less pronounced than for more typical cases in which the proximity of large equipment to the culvert structure is less rigorously controlled.

Two types of finite element analyses were performed: (*a*) conventional analyses that are well able to model incremental placement of backfill in layers but that cannot model compaction-induced stresses and deformations and (*b*) analyses that incorporate recently developed models and analytical procedures that permit modeling of compaction effects (*1*, *2*). Comparison of the results of these two types of analyses with each other, as well as with field measurements, provides a basis for assessing the potential importance of considering compaction effects in analyzing culvert stresses and deformations.

PROMONTORY CULVERT STRUCTURE

The Promontory culvert structure is located in Mesa, California, and is designed to perform as a bridge providing grade separation between two otherwise intersecting roadways. Figure 1 (top) shows a cross section through the structure. The culvert is a low-profile arch, with a span of 38 ft 5 in., a rise of 15 ft 9 in., and a length of 80 ft, founded on 3-ft-high reinforced concrete stem walls with a reinforced concrete base slab. The culvert consists of 9- x 2 1/2-in. corrugated aluminum structural plate 0.175 in. thick, and the crown section is reinforced with Type IV aluminum bulb angle stiffener ribs that occur at a spacing of 9 in. The culvert haunches are grouted into a slot at the top of the stem walls, providing a rigid connection for moment transfer at this point.

The existing foundation soil at the site was a stiff, silty, sandy clay of low plasticity (CL-SC). Chemical tests indicated that this sandy clay was potentially corrosive with respect to the culvert structure. As a result, a crushed basalt material (select fill) was imported for use as a protective backfill envelope within 3 to 4 ft of the culvert. This crushed basalt was an angular silty sand (SM) and was placed to a minimum width of 4 ft at both sides of the culvert and continued to the final fill surface as shown in Figure 1 (top).

Department of Civil Engineering, Stanford University, Stanford, Calif. 94305.

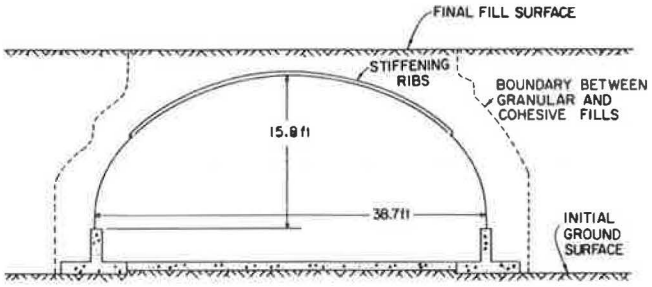

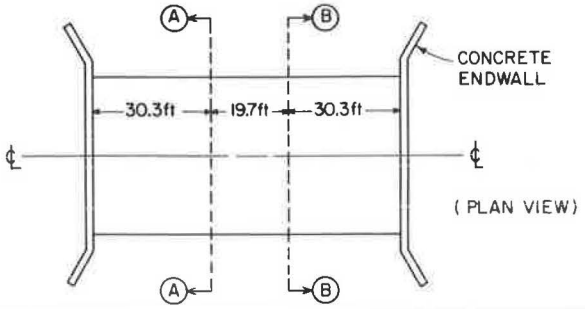

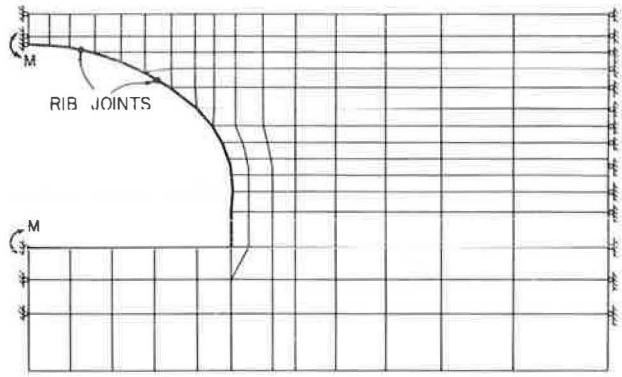

FIGURE 1 Promontory overpass structure.

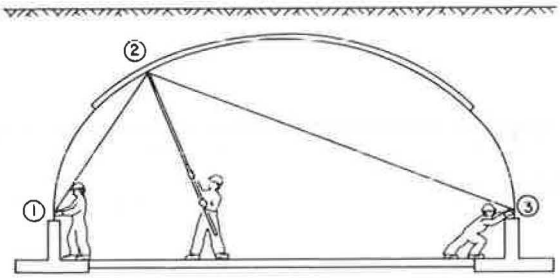

FIGURE 2 Measurements of culvert deformations during backfilling.

The existing sandy clay was used as backfill outside of this select fill zone. Both materials were compacted to a minimum of 95 percent of the maximum dry density determined by a standard Proctor compaction test (ASTM 698–D). Backfill placement and compaction procedures will be discussed later in detail. The final depth of soil cover over the crown of the structure was 2.5 ft.

FIELD MEASUREMENTS OF DEFORMATIONS DURING BACKFILLING

Culvert deformations were monitored at two culvert sections during backfill placement and compaction. As shown in Figure 2 (top), these sections (A-A and B-B) were separated by 19.7 ft and were both located 30.3 ft from the ends of the culvert to avoid any influence of restraint provided by the two reinforced concrete end walls. At both cross sections, the displacements of 13 measurement points were monitored relative to a pair of reference points at the base of the culvert haunches, as shown in Figure 2 (bottom). The change in span between the two reference points was also measured, and all relative displacements were corrected accordingly. Monitoring the relative displacements of these 15 points permitted determination of the deformed shape of each of the full cross sections at any given stage of backfill operations.

The distances between the measuring points and each of the two reference points at each section were measured using lightweight steel tapes. The measuring points were permanently established by means of marker bolts, and the ends of the steel tapes were held to the ends of these bolts by means of a fixture at the end of a pole that was designed to mate consistently with the measuring points. Tape tension was kept constant, and no correction was made for thermal expansion or contraction of the tape because the estimated maximum correction was less than 1/16 in. under the least favorable conditions encountered. Numerous practice measurements were taken before backfill operations began until it was demonstrated that all measurements could be repeated consistently within ± 3/32 in., with readings taken to the nearest 1/32 in. At the end of each day of construction operations a number of the most recent measurements were repeated at random to verify that this level of accuracy was maintained.

Backfill operations were well controlled and measured deformations at Sections A-A and B-B were nearly identical at all backfill stages, as shown in Figure 3, which shows the final deformed culvert shapes at both measured sections on completion of backfill placement and compaction. In this figure, deformations are exaggerated by a scaling factor of 5 for clarity. Throughout the remainder of this paper, all "measured" deformations reported will represent averaged deformations for the two measured sections.

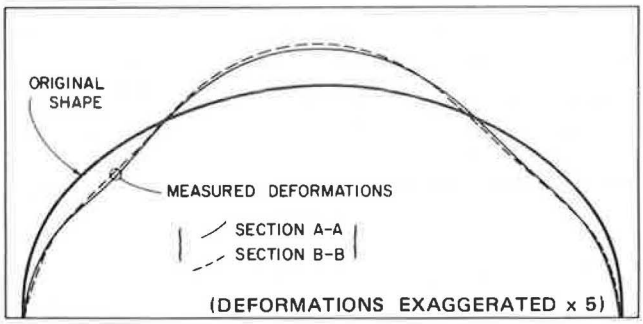

FIGURE 3 Final deformed shapes of Measurement Sections A-A and B-B.

Figure 4 shows measured deformations at three backfill stages: (*a*) backfill midway up the haunches, (*b*) backfill approximately 1.5 ft below the crown, and (*c*) final soil cover depth of 2.5 ft. Deformations are again exaggerated by a factor of 5. The general

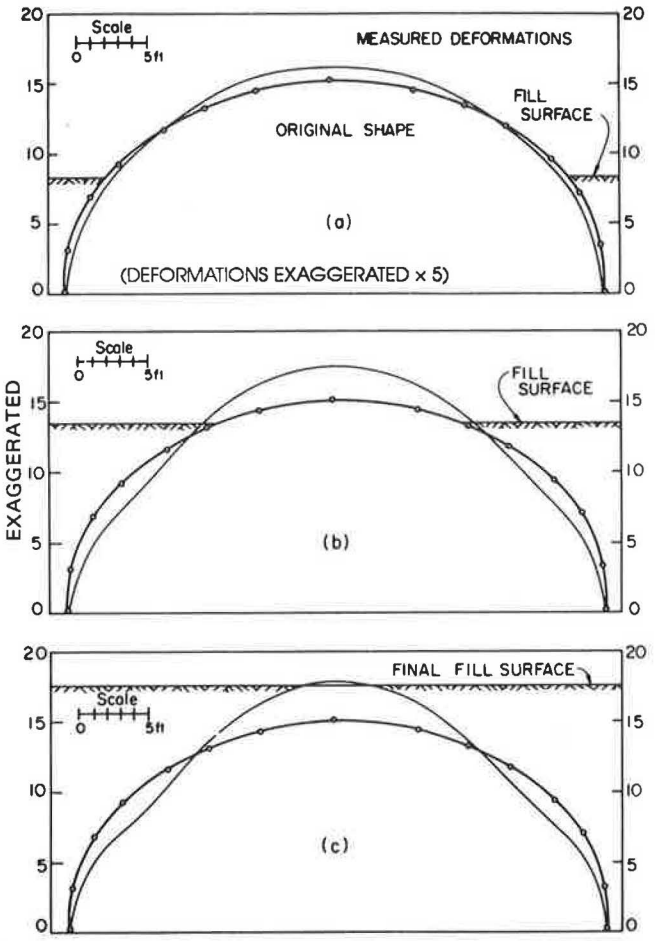

FIGURE 4 Measured deformations at various backfill stages.

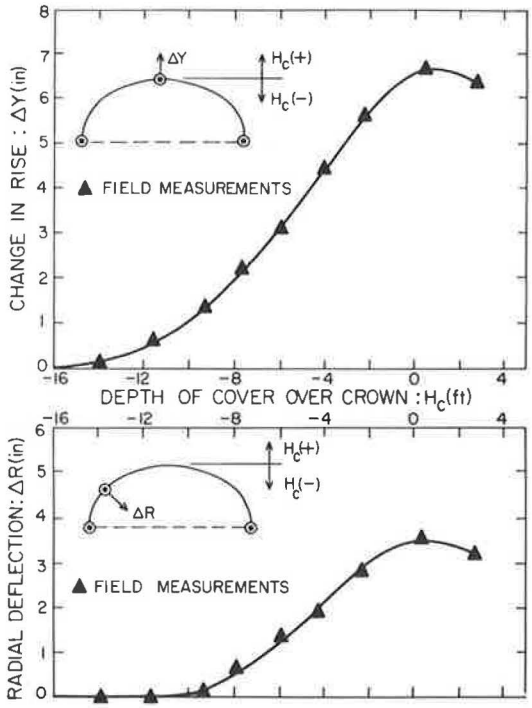

FIGURE 5 Measured crown rise and radial quarter point deflection versus fill height.

pattern of culvert deformations consisted of decreasing span and inward flexure of the quarter points at the juncture of the haunch and crown sections with increasing fill height, accompanied by an upward movement of the crown ("peaking"). The backfill elevation was carefully maintained at nearly the same level on both sides of the culvert at all fill stages, and placement and compaction operations were nearly identical on both sides of the culvert at any given fill stage, which resulted in essentially symmetric deformations of both sides of the culvert as shown in Figure 4. Maximum peaking of the crowns of both measured culvert sections were approximately 6.6 in., and the maximum inward radial deflection at the upper haunches was approximately 3.6 in.

The measured culvert deformations can be well characterized by monitoring the vertical deflection of the crown point and the radial deformation of the quarter point, as shown in Figures 4 and 5. In Figure 5, which shows crown and quarter point deflections as a function of backfill level, it can be seen that, as backfill was placed above the crown of the structure, peaking reversed and the crown began to descend slightly under the weight of the new crown cover fill.

FIELD OBSERVATIONS DURING BACKFILL OPERATIONS

Several important factors that affect the magnitude of compaction-induced soil stresses at any given point in the ground are contact pressure, footprint geometry, and closest proximity to the point of interest achieved by any given compaction (or other construction) vehicle. This is because these factors control the peak stress increase induced at the point of interest during application of the transient surface load represented by the most critical positioning of the compaction vehicle, and residual compaction-induced stresses remaining after departure of this transient vehicle load are a direct function of this peak stress increase (*1*).

During backfill placement and compaction, large equipment and vehicles were not allowed to operate in close proximity to the culvert structure. As a result, compaction-induced earth pressures acting against the culvert were quite sensitive to the closest proximity to the culvert achieved by each piece of compaction equipment at each backfill stage. To properly model compaction-induced earth pressures acting against the culvert, it was thus necessary to continuously monitor the closest proximity to the culvert achieved by each construction vehicle at each stage of backfill placement and compaction, and field observers maintained a detailed record of this.

Six types of construction equipment were used during backfill operations: (*a*) a small pan or scraper, (*b*) a tracked bulldozer, (*c*) a front loader with four rubber wheels, (*d*) a 2,000-gal water truck, (*e*) a two-drum vibratory hand roller, and (*f*) a medium-sized single-drum vibratory roller. Table 1 gives the significant characteristics of each of these pieces of equipment that affect the magnitude of compaction-induced soil stresses within the backfill.

Backfill operations began with the initial ground surface at the base of the concrete stem walls. Up to an elevation of 10 ft above the stem wall bases (near the top of the culvert haunches) the select backfill envelope was maintained at a width of from 4 to 4.5 ft and was placed and compacted in 6-in. lifts. The select fill was dumped by the front loader operating at some distance from the culvert and was spread by hand before being compacted by the two-drum vibratory hand roller, so that the hand roller was the only equipment operated close to the culvert. The native backfill was brought

TABLE 1 EQUIPMENT USED FOR BACKFILL PLACEMENT AND COMPACTION

Attribute	Measurement
John Deere JD-672 scraper	
Wheel type	4 rubber tires
Lateral tire separation	7.5 ft (center to center)
Axle spacing	26 ft
Operating weight modeled	62 kips (60% on rear axle)
Caterpiller CAT D6D dozer	
Tread spacing	74 in. (center to center)
Tread contact length	93 in.
Operating weight modeled	32 kips
Case W20-C front loader	
Wheel type	4 rubber tires
Lateral tire separation	73 in.
Axle spacing	108 in.
Operating weight modeled	23 kips (60% on front axle)
2,000-gal water truck	
Front axle	2 rubber tires at 6.5 ft
Rear axle	4 rubber tires (total width = 8.5 ft)
Axle spacing	10 ft
Operating weight modeled	47 kips
Wacker WDH 86-110(758) two-drum vibratory roller	
Drum length	32 in.
Drum spacing	40 in. (center to center)
Total weight	2.8 kips
Peak dynamic thrust	Modeled at 6.3 kips/drum
Raygo SF-54A single-drum vibratory roller	
Drum length	54 in.
Total weight	4.8 kips
Peak dynamic thrust	15 kips

up roughly concurrently with the select fill envelope and was rolled right to the point of contact with the select fill by both the water truck and the scraper, so that both of these heavy vehicles operated over the full fill surface to within a proximity of approximately 4 to 4.5 ft to the culvert haunches.

As the fill began to rise above the haunches and onto the ribbed crown section, the select fill envelope began to follow the culvert contour, as shown in Figure 1 (top). Until the fill reached an elevation approximately 1 ft below the crown, the select fill continued to be hand leveled and compacted with the hand roller, though the bulldozer began to operate on the outer edges of the select zone. The native soil lifts at this stage were again rolled by the scraper and water truck, and both vehicles made occasional (documented) incursions onto the select fill zone.

At a fill elevation approximately 1 ft below the crown, the larger single-drum vibratory roller (towed by the bulldozer) began to be used to compact the outer portions of the select fill zone, while the central portion was compacted with the hand roller. The front loader operated well onto the select zone at this stage. Finally, when fill covered the crown to a depth of approximately 1.5 ft, the bulldozer began to make compaction passes transversely across the crown of the structure while towing the single-drum vibratory roller. During the last 2 to 3 ft of fill placement both the water truck and the scraper also operated up to several feet onto the select fill zone on a random and occasional basis.

These carefully controlled fill placement and compaction procedures, with care being taken to prevent the occurrence of large vehicular loads in close proximity to the flexible culvert structure, represent a case in which the effects of compaction on culvert deformations and stresses will be significantly less than for more "typical" conditions in which procedural controls are less conscientiously enforced.

The degree of compaction achieved has only a minor effect on the magnitude of soil stresses induced by compaction, but it has a significant influence on the stiffness of the backfill (*1, 2*). For this reason it was also necessary to closely monitor the degree of compaction achieved at all points in order to properly model backfill stress-deformation behavior in the finite element analyses performed. On the basis of constant observation of field operations, as well as 26 in situ density tests, it was judged that compaction control was excellent and resulted in uniformly compacted backfill in both the select fill and the sandy clay fill zones. The average density achieved was approximately 96 percent of the standard Proctor maximum dry density in the select fill zone and 97 percent (at an average water content of 12 percent) in the sandy clay zone. Density variations within each zone were judged to be small.

CONVENTIONAL FINITE ELEMENT ANALYSES

Two types of finite element analyses were performed to evaluate the significance of compaction effects on culvert deformations and stresses: (*a*) conventional analyses without any capacity for consideration of compaction-induced stresses and (*b*) analyses that incorporate recently developed finite element models and algorithms that allow consideration of compaction-induced soil stresses and associated deformations.

Both types of analysis used the hyperbolic formulation proposed by Duncan et al. (*3*) as modified by Seed and Duncan (*1*) to model

nonlinear stress-strain and volumetric strain behavior of the soils involved, varying the values of Young's modulus and bulk modulus in each soil element as a function of the stress state within that element at any given stage of the analysis.

The conventional analyses, without compaction effects, consisted of modeling placement of fill in successive layers or increments. A two-iteration solution process was used for each increment to establish appropriate soil moduli in each element in order to model nonlinear soil behavior. These analyses were performed using the computer program SSCOMP (*4*), a two-dimensional plane strain finite element code.

Figure 1 (bottom) shows the finite element mesh used for these analyses. Only one-half of the culvert and backfill was modeled because of the symmetric nature of both the backfill operations and the measured deformations. Soil elements were modeled with four-node isoparametric elements and the culvert structure and underlying concrete members were modeled with piecewise-linear beam elements. Nodal points at the right and left boundaries of the mesh were free to translate vertically but were rigidly fixed against rotation or lateral translation, which provided full moment transfer at the culvert crown and the centerline of the concrete base slab.

The program SSCOMP models all structural elements as deforming in linear elastic fashion. Table 2 gives the properties used to model the various components of the culvert structure. The concrete footings and base slab were interconnected by reinforcing steel and were modeled as a continuous section. Elastic section moduli for the corrugated aluminum structural plate culvert sections represent values 20 percent less than the theoretical values calculated for these sections. This 20 percent reduction is based on large-scale flexural test data and provides a reasonably accurate model of stress-deformation behavior for 9- x 2 1/2-in. aluminum plate of 0.175-in. thickness at stress levels representing a factor of safety greater than 2.0 with respect to plastic failure in flexure.

TABLE 2 STRUCTURAL PROPERTIES MODELED

Structural Component	E (kip/ft^2)	Area (ft^2/ft)	I (x 10^{-4}) (ft^4/ft)
Concrete walls and invert	464,000	0.75	352.0
Culvert haunch (no ribs)	1,468,800	0.017	0.676
Culvert crown (with ribs)	1,468,800	0.033	4.74
Culvert crown "hinges"	1,468,800	0.033	2.37

Section moduli of the ribbed crown section were modeled as intermediate between the theoretical value for the crown plate and ribs functioning as a composite beam and the theoretical value for the ribs and crown plate each functioning independently. This is again based on large-scale flexural test data and represents the effects of shear slippage at the plate-rib connection. Every alternate crown rib was spliced at one of two locations, and each of these splice locations was modeled as a partial "hinge" of reduced flexural stiffness with a length of 0.1 ft as indicated in Figure 1 (bottom) and Table 2.

Table 3 gives the hyperbolic soil model parameters used to model the select and native backfill zones as well as the existing foundation soils. These parameters were based on triaxial tests of these soils. A series of isotropically consolidated, drained triaxial tests with volume change measurements was performed on the crushed basalt select fill. Samples were compacted to approximately 96 percent of the standard Proctor maximum dry density, taken as representative of field conditions, and were tested at effective confining stresses of between 6.4 and 20.2 psi. Figure 6 shows the results of these tests, as well as the modeled soil behavior based on the soil parameters listed in Table 3. Modeled stress-strain behavior is in excellent agreement with the test results. Modeled volumetric strain behavior agrees well with the test data at low stress levels but provides poor modeling at high stress levels because the hyperbolic soil model cannot model dilatency. An additional pair of triaxial tests was performed to provide a basis for evaluation of unloading-reloading behavior, as shown in Figure 7.

A second series of unconsolidated, undrained triaxial tests was performed to evaluate the behavior of the native backfill. Samples were compacted to approximately 97 percent of the standard Proctor maximum dry density at a water content of 12 percent, again representative of field conditions, and were tested under undrained conditions at confining stresses of between 5.0 and 16.9 psi. Figure 8 shows the results of these tests as well as the modeled soil behavior based on the parameters listed in Table 3. In the absence of volume change data, the two bulk modulus parameters K_b and m were estimated from typical values for similar soils. Two additional tests were performed to evaluate unloading-reloading behavior as shown in Figure 9. The soil model parameters generated for the native backfill zone were also considered suitable for representation of the existing native foundation soil, which was partly desiccated with an in situ water content of approximately 6 to 10 percent.

Figure 10 shows the results of incrementally modeling fill placement without compaction-induced stresses using the program SSCOMP. As shown in this figure, calculated culvert displacements at the crown point are only approximately one-third of the measured values at all fill stages, and the maximum calculated radial deflection of the quarter point is only one-quarter of that measured in the field. It is unlikely that this magnitude of discrepancy between deformations calculated without consideration of compaction effect and the actual field measurements is due to poor modeling of soil or structural stiffnesses, because these are all based on reliable test data, and it thus appears likely that compaction-induced earth pressures significantly influenced the measured field deformations, even though compaction operations were carefully controlled to minimize this influence.

TABLE 3 HYPERBOLIC SOIL MODEL PARAMETERS

Soil Type	γ (kip/ft3)	c (kip/ft2)	ϕ (degrees)	$\Delta\phi$ (degrees)	K	n	R_f	K_b	m	K_{ur}	K_o
Select backfill	0.138	0.0	47.0	0.0	580	0.50	0.63	350	−.15	1080	0.27
Native backfill	0.126	0.85	14.5	0.0	260	0.26	0.81	175	0.30	505	0.70
Native foundation	0.126	0.85	14.5	0.0	260	0.26	0.81	175	0.30	505	0.70

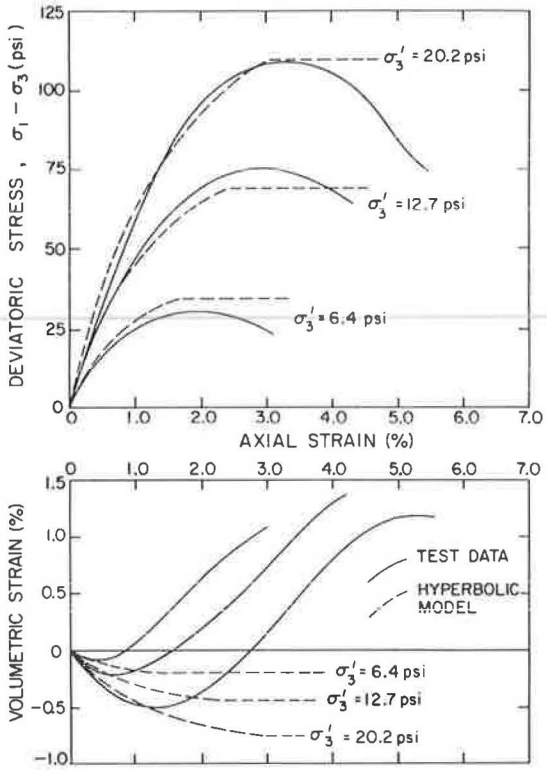

FIGURE 6 Modeled nonlinear stress-strain and volumetric strain behavior of the select backfill versus triaxial test results.

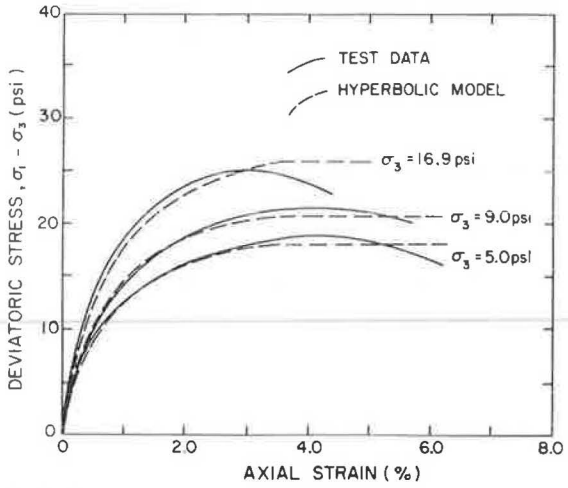

FIGURE 8 Modeled nonlinear stress-strain behavior of the native sandy clay versus triaxial test results.

FINITE ELEMENT ANALYSES WITH COMPACTION EFFECTS

A second set of finite element analyses was performed, again using the program SSCOMP, to model the effects of compaction-induced earth pressures. These analyses again incrementally modeled the placement of backfill in layers, but after each backfill placement increment an additional two-iteration solution increment was used to model the effects of compaction operations at the surface of the new backfill layer. The models and analytical procedures used to simulate compaction effects are described in detail by Seed and Duncan (*1, 2*). Because these are rather complex, only a brief general description follows.

Two soil behavior models are employed in these analyses. Nonlinear stress-strain and volumetric strain behavior are again modeled with the hyperbolic formulation used for the conventional analyses without compaction. The second soil behavior model is a model for stresses generated by hysteretic loading and unloading of soil. This hysteretic model performs two roles during the analyses: (*a*) it provides a basis for the controlled introduction of compaction-induced soil stresses at the beginning of each compaction increment and (*b*) it acts as a "filter" controlling and modifying the compaction-induced fraction of soil stresses during all stages of analysis.

Horizontal stresses within a given soil element are considered to consist of two types or fractions defined as (*a*) geostatic lateral stresses ($\sigma_{x,o}$), which include all stresses arising because of increased overburden loads and deformations that result in lateral stress increases, and (*b*) compaction-induced lateral stresses ($\sigma_{x,c}$), which are the additional lateral stresses arising at the beginning of each compaction increment as a result of transient compaction

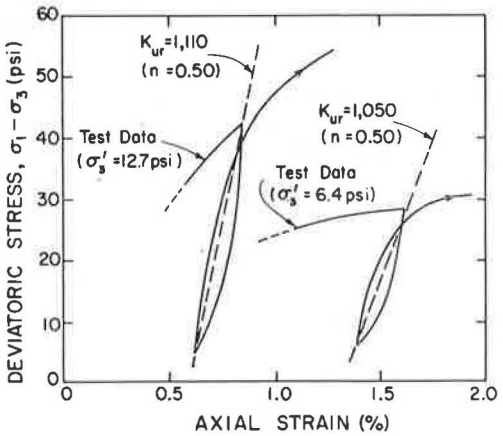

FIGURE 7 Select backfill unloading-reloading stress-strain behavior.

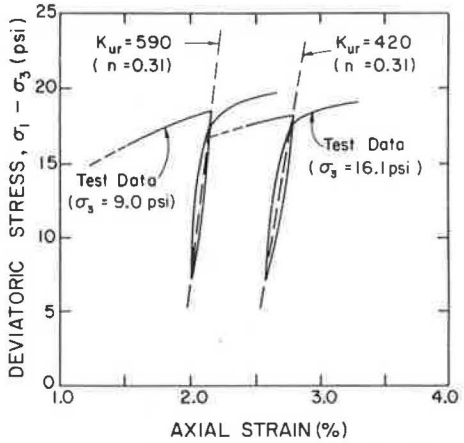

FIGURE 9 Native sandy clay unloading-reloading stress-strain behavior.

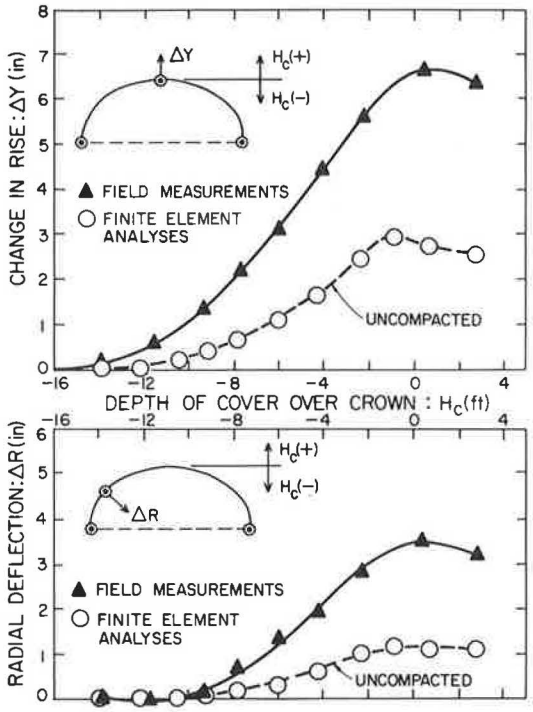

FIGURE 10 Field measurements versus culvert deformations calculated by finite element analyses without modeling compaction effects.

loading. The overall lateral soil stress (σ_x) at any point is then the sum of the geostatic and compaction-induced stresses.

Compaction-induced lateral stresses are introduced into an analysis during "compaction" increments. Both the peak and the residual compaction-induced lateral stresses at any point are modeled based on the peak, virgin compaction-induced horizontal stress increase ($\Delta\sigma_{x,vc,p}$), which is defined as the maximum (temporary) increase in horizontal stress that would occur at any given point as a result of the most critical positioning of any surficial compaction plant loading actually occurring if the soil mass was previously uncompacted (virgin soil). This use of $\Delta\sigma_{x,vc,p}$ allows consideration of compaction vehicle loading as a set of transient surficial loads of finite lateral extent that pass one or more times over specified portions of the fill surface, properly modeling the three-dimensional nature of this transient concentrated surface loading within the framework of the two-dimensional analyses performed. The need to model the most critical positioning actually achieved by each compaction vehicle relative to each soil element at each backfill stage necessitated the constant monitoring of vehicle movements during backfill operations.

$\Delta\sigma_{x,vc,p}$, which is independent of previous hysteretic stress history effects, can be evaluated using three-dimensional linear elastic analyses (*1*) and is directly input for each soil element at the beginning of each compaction increment. The hysteretic soil behavior model then accounts for previous hysteretic loading-unloading cycles (e.g., previous compaction increments) and calculates both the actual peak and residual lateral stress increases on planes of all orientations within a soil element (residual vertical stress remains constant) based on $\Delta\sigma_{x,vc,p}$ and the previous hysteretic stress history of the soil element.

In addition to establishing the magnitude of residual compaction-induced lateral stresses introduced at the beginning of each compaction increment (before nodal displacements and associated stress redistribution), the hysteretic soil behavior model also acts as a "filter" controlling and modifying the compaction-induced component of stress in soil elements at all stages of analysis. All calculated increases in σ_x at any stage during an analysis are considered to represent an increase in geostatic lateral stress and represent hysteretic "reloading" if a compaction-induced stress component is present. Subsequent to the solution of the global stiffness and displacement equations for any increment, therefore, the resulting calculated increases in σ_x are used as a basis for calculating an associated decrease in the compaction-induced fraction of lateral stress ($\sigma_{x,c}$). This progressive erasure or "overwriting" of compaction-induced lateral stresses by increased geostatic lateral stresses results in an overall increase of σ_x less than the calculated increase in $\sigma_{x,o}$ for soil with some previously "locked-in" compaction-induced lateral stress component and corresponds to hysteretic "reloading." When solution of the global stiffness and displacement equations results in a calculated decrease in σ_x, it is assumed that this decrease is borne by both the geostatic and the compaction-induced fractions of the preexisting lateral stress in direct proportion to their contributions to the overall lateral effective stress.

Compaction-induced lateral stress increases in a soil mass can exert increased pressure against adjacent structures, which results in structural deflections that may in turn partly alleviate the increased lateral stresses. Multiple passes of a surficial compaction plant, however, continually reintroduce the lateral stresses relaxed by deflections and result in progressive rearrangement of soil particles at shallow depths. To approximate this process with a single solution increment, both the compaction-induced lateral stresses and the corresponding nodal point forces for a given compaction increment are assumed to represent "following" loading from the current ground surface down to the depth at which $\sigma_{x,c}$ exceeds $\sigma_{x,o}$. All soil elements above this depth are assigned negligible moduli, resulting in calculation of displacements at all locations as a result of compaction-induced lateral forces, but (*a*) no changes in soil stresses result from displacements in soil elements above the specified depth of "following" compaction loading and (*b*) compaction-induced nodal forces in this upper region are also undiminished by deflections.

Four additional soil parameters are needed for the hysteretic model controlling compaction-induced soil stresses, and these may be evaluated by correlation with the soil strength parameters c and ϕ. Seed and Duncan (*1, 2*) provide a detailed description of methods for determining these four parameters, and Table 4 gives the parameters used to model the select fill and native soil zones in the analyses performed. Two parameters $K_{1,\phi,B}$ and c_B define the maximum residual compaction-induced lateral stress that can retained by soil at shallow depth as controlled by potential passive soil failure. The parameter F controls the fraction of peak (transient) lateral stress ($\Delta\sigma_{x,vc,p}$) retained as residual compaction-induced stress. The final parameter (K_3) defines the rate at which geostatic stress increases "overwrite" compaction-induced stresses during hysteretic reloading.

TABLE 4 HYSTERETIC SOIL MODEL PARAMETERS

Soil Type	c_B (kip/ft^2)	$K_{1,\phi,B}$	K_3	F
Select backfill	0.00	4.30	0.11	0.61
Native backfill	0.67	1.11	0.45	0.40
Native foundation	0.67	1.11	0.45	0.40

There is significant scatter in the relationship between F and ϕ for cohesionless soils, and the mean value of F based on correlation with ϕ was used to model the select fill (*1*, 2). There is currently little reliable data on which to base evaluation of F for cohesive soils under short-term conditions, but F in the cohesive native soil zones does not significantly affect stresses and deformations near the Promontory culvert structure, and a value of F = 0.40 was judged to be suitable for modeling the native soil zones in the analyses performed.

Calculation of the peak, virgin compaction-induced lateral stress ($\Delta\sigma_{x,vc,p}$) to be input into each soil element at the beginning of each compaction increment is a time-consuming process. In the "free field" away from the culvert, three-dimensional linear elastic analyses were performed using Boussinesq closed-form solutions to calculate the peak lateral stresses induced at any given depth by each piece of construction equipment. These values were then enveloped to produce a single profile of $\Delta\sigma_{x,vc,p}$ versus depth that was used for all soil elements occurring at a distance of more than a few feet from the culvert at all fill stages.

For soil elements near the culvert it was necessary to carefully review the recorded field observations in order to model peak stresses arising as a result of the most critical positioning (closest proximity) achieved by each piece of compaction equipment at each fill level. At fill levels up to the top of the haunches, the small two-drum vibratory roller controlled peak transient lateral stresses ($\Delta\sigma_{x,vc,p}$) adjacent to the culvert. At fill levels above the hanches, however, larger vehicles began to exert increasing influence on values of $\Delta\sigma_{x,vc,p}$ for soil elements in the region of the quarter point midway between the haunch and crown. If compaction operations had been less carefully controlled and larger vehicles had operated nearer the culvert, the influence of compaction on culvert stresses and deformations would have been greatly increased.

Figure 11 shows the results of incrementally modeling both backfill placement and compaction. Modeling of compaction effects has resulted in significantly improved agreement between calculated and measured culvert deflections at all backfill stages compared with the earlier analyses without compaction. The calculated maximum crown rise (peaking) of 5 in. represents an increase of 80 percent over the maximum peaking of 2.8 in. calculated by conventional analyses without consideration of compaction effects and is only 25 percent less than the value actually measured. Modeling compaction effects also doubled the maximum calculated radial displacement of the quarter point to more than 2 in., and this new value is within 40 percent of the value actually measured.

Whereas the modeling of compaction effects significantly improved agreement between calculated and measured deformations, it must also be noted that peak calculated displacements of the crown and quarter points are still 25 and 40 percent less, respectively, than the values measured in the field. It is likely that this remaining discrepancy is due in large part to the modeling of culvert deformation behavior as linear elastic using the properties listed in Table 2. As was noted previously, this provides fairly accurate modeling of flexural stiffness for the various culvert elements as long as stress levels remain low (representing a factor of safety greater than 2.0 with respect to plastic failure in flexure). Calculated culvert stresses were all well within this range for the earlier analyses performed without modeling compaction effects, but, when compaction was modeled in this second set of analyses,

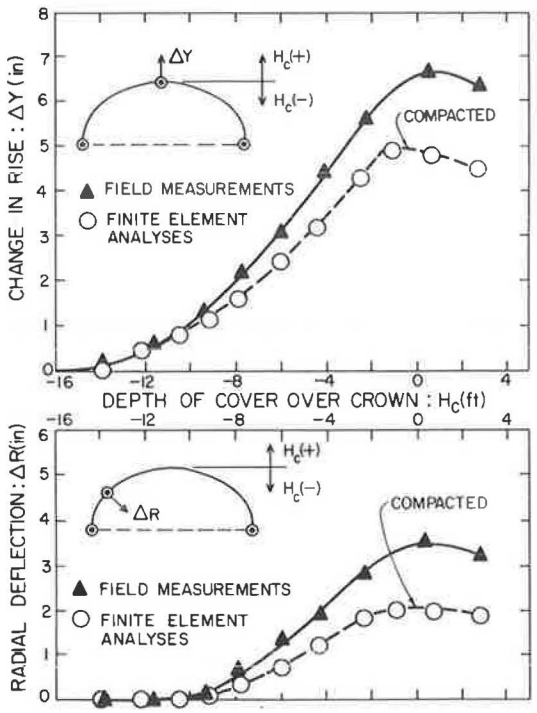

FIGURE 11 Field measurements versus culvert deformations calculated by finite element analyses including modeling of compaction effects.

bending moments calculated in the haunch region were significantly increased to the extent that this linear elastic modeling of culvert behavior greatly overestimated culvert stiffness during the later stages of backfilling.

Figure 12 shows culvert bending moments and axial thrust around the culvert perimeter following completion of backfill operations as calculated in both sets of finite element analyses performed (with and without compaction). In Figure 12*a* it can be seen that modeling compaction effects resulted in increased bending moments in both the crown and the haunch regions. The increased positive crown moment is not of serious concern for design purposes because it is well below the level required for onset of plastic yield (factor of safety = 3.9) and represents an increase in the ability of the crown section to withstand subsequent negative moments that will arise due to live traffic loads. The increased bending moments at the top and base of the unreinforced haunch region are potentially more serious. Without compaction effects the calculated minimum factor of safety with regard to exceeding the plastic moment capacity in the haunch region was 7.4, apparently representing overconservative design. Modeling compaction effects reduced this factor of safety to only 1.4 at the top of the haunch region and 2.0 at the base, and both of these moments correspond to flexure in directions representing potential failure modes.

In Figure 12*b* it can be seen that modeling compaction-induced earth pressures also resulted in calculation of increased thrust around the perimeter of the culvert. This increase, which was between 10 and 25 percent around the culvert perimeter, was much less pronounced than was the effect of modeling compaction on calculated culvert bending moments.

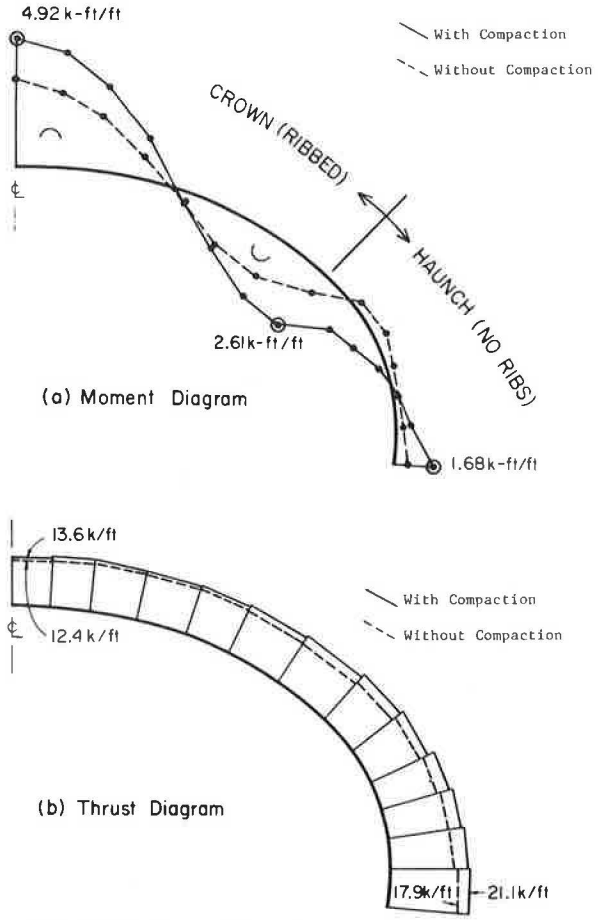

FIGURE 12 Culvert bending moments and perimeter axial thrust calculated by finite element analyses with and without modeling compaction effects.

SUMMARY AND CONCLUSIONS

Incorporation of analytical models and methods for consideration of compaction effects significantly improved the agreement between culvert deformations calculated by finite element analyses and actual field measurements at all stages of backfill placement and compaction. Conventional finite element analyses, which did not model compaction effects, greatly underestimated culvert deformations at all fill stages. Analyses modeling compaction effects produced much better agreement with field measurements, and it was shown that the remaining underestimation of culvert deformations in these analyses may have been due in large part to linear elastic modeling of culvert stress-deformation behavior, which overestimated culvert stiffnesses at the higher culvert stress levels calculated by the analyses that modeled compaction effects.

Calculated culvert stresses were also significantly affected by the modeling of compaction-induced earth pressures. Analyses that included modeling of compaction effects resulted in calculation of higher bending moments at both the culvert crown and the haunch sections, with the increased haunch moments representing the potentially most serious condition. Calculated thrust around the perimeter of the culvert was also increased by inclusion of compaction-induced earth pressures in these analyses, but this effect was less pronounced than the effect of compaction on calculated bending moments.

The results of these analyses, along with the full-scale field measurements, strongly suggest that compaction-induced earth pressures had a significant effect on both the deformations and the final stress state of the Promontory culvert structure. Conventional analyses, without modeling of compaction effects, appear to have resulted in a somewhat unconservative assessment of both culvert stresses and deformations for this case, which involved a very long-span flexible metal culvert structure with relatively shallow final crown cover.

ACKNOWLEDGMENTS

Support for this research was provided by Kaiser Aluminum and Chemical Corporation as well as by the National Science Foundation. This support is gratefully acknowledged. The authors also wish to extend their thanks to Mony Antoun of Kaiser Aluminum and Chemical Corporation for his valuable assistance during the field operations involved in this project.

REFERENCES

1. R. B. Seed and J. M. Duncan. *Soil-Structure Interaction Effects of Compaction-Induced Stresses and Deflections*. Geotechnical Engineering Research Report UCB/GT/83–06. University of California, Berkeley, 1983.
2. R. B. Seed and J. M. Duncan. FE Analyses: Compaction-Induced Stresses and Deformations. *Journal of the Geotechnical Engineering Division*, ASCE, Vol. 112, No. 1, Jan. 1986, pp. 23–43.
3. J. M. Duncan, P. Byrne, K. S. Wong, and P. Mabry. *Strength, Stress-Strain and Bulk Modulus Parameters for Finite Element Analyses of Stresses and Movements in Soil Masses*. Geotechnical Engineering Research Report UCB/GT/80–01. University of California, Berkeley, 1980.
4. R. B. Seed and J. M. Duncan. *SSCOMP: A Finite Element Program for Evaluation of Soil-Structure Interaction and Compaction Effects*. Geotechnical Engineering Research Report UCB/GT/84–02. University of California, Berkeley, 1984.

Publication of this paper sponsored by Committees on Subsurface Soil-Structure Interaction and on Culverts and Hydraulic Structures.

Soil-Structure Interaction of Flexible Pipe Under Pressure

MEHDI S. ZARGHAMEE AND DAVID B. TIGUE

This paper contains the results of a finite element analysis of the soil-structure interaction of a buried flexible pipe subjected to internal pressure. The analysis is performed using a fine mesh so that *(a)* an accurate representation is made of the highly variable soil stiffness in some installations, similar to that of a pipe with poorly supported haunches resting on a hard bedding, and *(b)* an accurate model is made of the pipe wall stresses in light of the rapid attenuation of local deformations and strains in flexible pipe buried in stiff soils. In addition, the nonlinear behavior of pressurized flexible pipe, including large deflections and the flexural stiffening effect of the pressure-induced membrane stresses, is modeled. A special purpose program, FLEXPIPE, is developed. The program uses Duncan's soil model and considers the step-by-step nature of construction. It is used to calculate the stresses and strains in a buried flexible pipe with improper haunch support and hard bedding. It is shown that significant flexural stresses are developed at the invert of the pipe after installation and that internal pressure magnifies the flexural stresses and strains thus developed.

In the early stages of the development of flexible pipe for underground installation, there was a general consensus that installation-induced pipe wall stresses and strains were small because the serviceability requirement limits the deflection of the installed pipe to a fraction of the total deflection that the flexible pipe can withstand without fracture. This consensus was contingent on a popular belief that pipe wall stresses are proportional to the deflection of the pipe. However, numerous failures of flexible pipe due to an obvious overstress at the invert of the pipe in some installations accompanied by the successful performance of the pipes in other installations demonstrated that pipe wall stresses and strains were not always small. Interestingly, the deflection of the pipe that failed was not necessarily large. It appeared that improper installation and compaction procedures may have led to high localized stresses and strains and resulted in the fracture of the pipe wall.

The state-of-the-art design formulas for predicting pipe wall stresses in flexible pipe are developed primarily for stiffer pipe and are based on the assumption that pipe wall stresses are proportional to deflections. New tools for analysis are required for the prediction of pipe wall stresses in flexible pipe, particularly when subjected to internal pressure. The sensitivity of flexible pipe to installation suggests the use of finite element soil-structure interaction methods. Although much work has been performed on the analysis of the behavior of buried conduits using soil-structure interaction models *(1–3)*, the behavior of buried pressurized pipe has been little explored with the aid of soil-structure models. Recently, two major efforts were made to introduce finite element soil-structure methodology to the analysis and design of flexible pipe. The American Concrete Pipe Association sponsored the development of a soil-pipe interaction design and analysis (SPIDA) program as a tool for the design of buried reinforced concrete pipe *(4, 5)*. Concurrently, Owens-Corning Fiberglas embarked on a program to investigate the behavior of buried flexible pipe, including the development of a finite element soil-structure interaction model *(6–8)*. Both of these programs are supposed to have the capability to predict pipe wall stresses in nonideal installation conditions and to handle internal pressure; however, no results have been published by which the adequacy of these programs for predicting the stresses and the strains in pressurized flexible pipe installed in less than ideal conditions can be judged.

Simpson Gumpertz & Heger, Inc., Consulting Engineers, 297 Broadway, Arlington, Mass. 02174.

In this paper is described a finite element, soil-structure interaction method for predicting the pipe wall stresses and strains in a buried flexible pipe subjected to internal pressure.

The behavior of a buried flexible pipe depends to a large extent on the uniformity of the soil stiffness provided by the bedding and the backfill for the pipe. Nonuniformity of support can result in local deformations and flexural stresses in the pipe wall, in addition to the pipe wall stresses that result from the ovaling deflection of the pipe. The local deformation and flexural stresses are developed as the stiffer soil inhibits the outward radial movement of the pipe wall while the softer soil permits it. For example, when a flexible pipe is installed on hard bedding with inadequate haunch support, significant local deformation (i.e., flattening and a high flexural stress at the invert) is to be expected.

When a buried flexible pipe with uniform soil support is subjected to internal pressure, membrane stresses will develop in the pipe wall and the pipe will expand radially. In addition, internal pressure will reround the pipe and thus alleviate much of the flexural stresses and strains developed in the pipe wall as a result of the ovaling deflection of the pipe. This behavior has little resemblance to the behavior of the same pipe when the soil support does not provide a uniform support for the pipe. When a flexible pipe with nonuniform soil support is subjected to internal pressure, the deformation of the pipe before pressurization results in a larger radius of curvature locally (e.g., at the invert of the pipe), which, in turn, causes higher membrane stresses there. In addition, the internal pressure causes radial movement of the pipe wall that if inhibited by the stiffer soil will increase the local flexural stresses. As the pipe becomes more flexible, the additional stresses that result from the nonuniformity of the soil support become more significant.

Deformations induced in a flexible pipe buried in relatively stiff backfill tend to attenuate rapidly. Using the analogy of a ring embedded in an elastic foundation (*9*, p. 157), the attenuation length for a half wavelength may be approximately expressed as $\pi[(EI/E'r^3)^{1/4}]$ where E is the pipe wall stiffness (lb-in.^{2}/in.), r is the pipe radius (in./in.), and E' is soil stiffness (psi); therefore deformations induced in a flexible pipe with a stiffness of 10 psi buried in moderately stiff backfill are expected to attenuate in about 30 degrees. (Pipe stiffness is defined as the stiffness of the

pipe when subjected to two diametrically opposed loads similar to those imparted to the pipe in a parallel plate test, whereas pipe wall stiffness is the stiffness of the pipe wall when subjected to a bending moment.) Obviously the mesh size must be sufficiently fine to permit an accurate prediction of pipe wall stresses.

Certain installation conditions can result in highly localized soil reactions on the pipe. In addition, when such a pipe is pressurized, additional reaction forces can develop on the pipe and thus exacerbate the situation. The stresses in the pipe wall are significantly affected by the spread of the localized reaction. A hard bedding is expected to provide only a narrow reaction at the invert, and a soft bedding is expected to distribute the reaction over a wider region and thus relieve pipe wall stresses.

To model these phenomena in such a way that a reasonable estimate of pipe wall stresses can be obtained, a much finer mesh than those used by the existing finite element, soil-structure interaction programs is needed.

To properly simulate the effects of internal pressure acting on a flexible pipe, the nonlinear effects of the deformed configuration of the pipe and of the internal pressure must be taken into account. The nonlinear effects of the deformed configuration of the pipe and of the internal pressure are incorporated in the program by applying the internal pressure incrementally to the deformed geometry of the pipe. In addition, the stiffening effect of the membrane stress resultant developed as a result of the internal pressure on the flexural stiffness of the pipe is considered.

The program has been applied to a number of buried flexible pipes with and without internal pressure. The results indicate that in the absence of a soil support of uniform stiffness, large flexural strains can develop in a buried flexible pipe. The magnitude of such flexural strains cannot be predicted from the deflection of the pipe. For all practical purposes, they may be considered additional to the strains that would result when soil provides an approximately uniform support for the pipe. Internal pressure not only does not alleviate the flexural strains that result from the nonuniformity of soil support, it also exacerbates the situation by increasing the flexural strains at the invert of the pipe. Furthermore, local deformations of the pipe that result from the nonuniformity of the supporting soil stiffness and the consequent local changes in the radius of curvature of the deformed pipe give rise to higher pressure-induced membrane stresses.

PIPE-SOIL INTERACTION MODEL

The mathematical model developed for the pipe-soil interaction is one in which the pipe and the surrounding soil are discretized in finite elements with specific load-deformation characteristics. The model has a mesh geometry that makes possible accurate analysis of flexible pipe in nonideal installations observed in the field that, in some instances, have led to the failure of the pipe wall. The model thus developed simulates the characteristics of the actual installation condition, of the soil, and of the flexible pipe and considers the step-by-step construction sequence of the pipe. The model as it stands now assumes a vertical plane of symmetry. It does not account for the method of compaction of the backfill at the time of its placement. Furthermore, it does not consider the soil compaction that may ensue after installation of the pipe such as the settlement that is expected from a collapsible backfill (e.g., an inadequately compacted sandy silt subjected to the simultaneous action of load and groundwater).

Finite Element Mesh

The mesh geometry adopted for the finite element model of pipe-soil interaction is shown in Figure 1. The general layout of the mesh is designed to analyze pipe installed in trench-type installations, considered to be the most common type of installation of flexible pipe. The mesh element size is fine enough that significant discretization errors are not expected in cases in which a buried flexible pipe is resting on a hard bedding and has loosely supported haunches. In addition, because the flexural stresses that result from highly localized soil reactions are significantly affected by the spread of the load, the mesh layout and fineness provide an adequate representation for predicting the actual pipe wall stresses for different bedding thicknesses including the installation condition in which the pipe is laid directly on a hard foundation.

The program allows the user to specify several mesh geometry parameters that will define the specific geometric profile of the trench that the user desires to analyze. The pipe may be placed

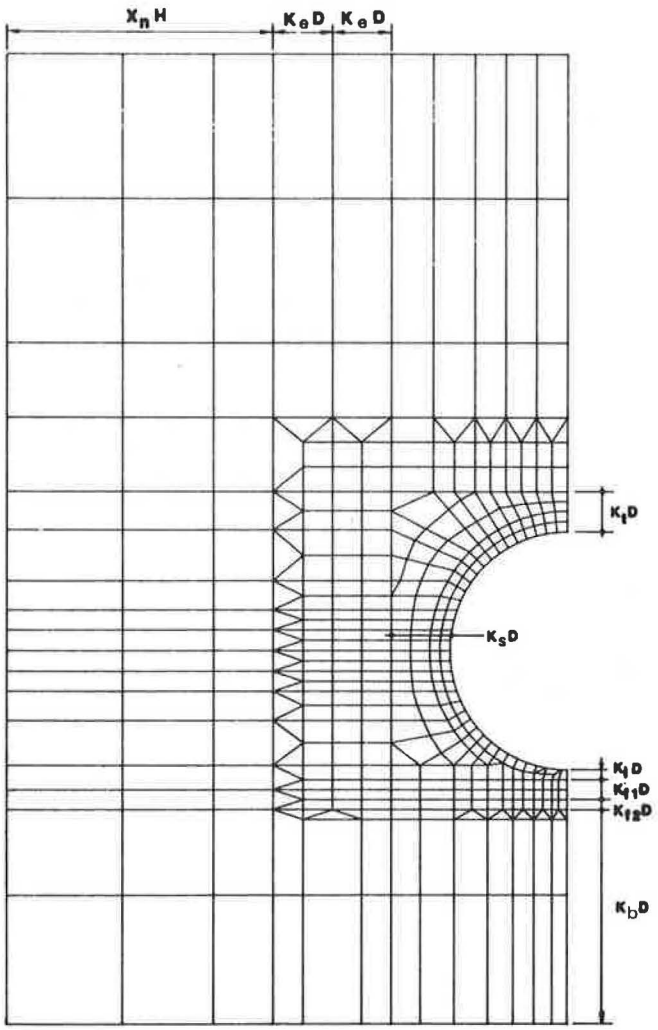

FIGURE 1 Fine mesh geometry of the finite element model of soil-structure interaction for flexible pressurized pipe, program FLEXPIPE.

either on native material or on backfill material the thickness of which can be varied. In addition, the mesh is adjustable through input parameters to facilitate analysis of pipe installed in different trench widths. Other parameters that can be specified define the pipe zone region immediately above the pipe and the overall mesh dimensions. The parameters that are not specified by the user will default to values defined in the program. The specific input parameters that the user can specify are shown in Figure 1. The mesh is designed in such a way that it can be deformed to any reasonable trench geometry while retaining good geometric proportions.

Characteristics of Pipe Element

The half circular arch of the pipe is discretized into 37 prismatic beam elements. The lengths of the beam elements range from a minimum that appears at the invert and subtends an angle of 2.5 degrees to a maximum that subtends an angle of 5 degrees away from the invert of the pipe. The 5-degree elements are approximately one-sixth of the attentuation interval of 30 degrees, calculated in the first section of this paper for a flexible pipe with a stiffness of 10 psi buried in a moderately stiff backfill. This element size is expected to yield sufficiently accurate results for pipe the stiffness of which is not much less than 10 psi based on the results of tests conducted on discretization of beams on elastic foundations. Obviously, the accuracy of analysis will deteriorate as pipe stiffness decreases below 10 psi. The beam elements are connected together so that full continuity of displacements and rotations is ensured. The material of the beam elements is linearly elastic. The stiffness matrix of the beam elements is modified incrementally, as construction progresses in steps and as pressure is incrementally applied, to incorporate *(a)* the effect of pipe deformation on the geometry of the pipe and *(b)* the stiffening effect of the axial force in the element, such as the tensile force that results from internal pressure, on the flexural stiffness of the elements. The first effect is modeled by modifying the coordinates of the joints by the magnitude of their displacements. The second effect is modeled by adding to the stiffness matrix of the beam elements a correction matrix described elsewhere (*10*, p. 262; *11*).

Characteristics of Soil Elements

The model employs two kinds of soil elements, an in situ element and a constructed soil element.

In situ soils are the preexisting natural soils in the foundation and the walls of the trench. In situ soils are undisturbed through installation and have been consolidated under the natural overburden. The in situ soil elements are assumed to be linear in the sense that their elastic constants do not vary with stress. This is believed to be a valid approximation because the final state of stress that results from pipe backfill is not expected to be significantly different from the natural state.

Constructed soils are soils used for bedding underneath the pipe and the backfill around and over the pipe. They are usually placed in layers and compacted mechanically or through the application of the subsequent layers. The constructed soil elements have a hyperbolic stress-strain relationship *(12)*. This relationship implies that the constructed soil stiffness decreases with increasing stress but increases with confining pressure. The properties of the constructed soil elements, which characterize the hyperbolic stress-strain relationship, are based on those proposed for several soil types in Duncan et al. *(13)*. Tables 1 and 2 give the soil properties used in the program. Note that the soil types studied in Duncan et al. *(13)* do not constitute the entire range of compactions that has been encountered in the field. In many cases, the constructed soil beneath the haunches of the pipe is much looser than the "loose" soil properties presented by Duncan et al. *(13)*. The elastic properties of the improperly compacted soils used for the installation of the pipe need to be established. This, however, must be performed separately for each soil type encountered in the field. Table 1 gives the properties of the soil used in the haunch areas of the flexible pipe with improper haunch support presented herein. In specific applications, these properties must be established on the basis of field observation and testing.

The constructed soil elements are elastic in the sense that loading and unloading are assumed to follow the same path on the stress-strain diagram. The soil elements are connected to each other and to the pipe elements so that full continuity of all of the components of displacement is ensured. In other words, no slip is permitted between the constructed soil elements and the pipe elements.

Loads

There are several sources of loads that the pipe-soil system may be subjected to, such as the weights of the soil, pipe, and water inside the pipe; internal pressure; the live load of a truck; and surcharge.

TABLE 1 SOIL PROPERTIES OF CONSTRUCTED SOIL (backfill)

Soil No.	Unified Classification	Compaction	γ_m (lb/ft^3)	K	n	R_f	K_b	m	C (psi)	ϕ (degrees)	$\Delta\phi$ (degrees)	k_0
1	GW, GP	H	145	550	0.4	0.7	150	0.2	0	42	8	1.5
2	SW, SP	M	135	300	0.4	0.7	75	0.2	0	35	5	1.0
3		L	125	100	0.4	0.9	25	0.2	0	30	2	0.5
4	SM	H	135	650	0.25	0.7	500	0	0	36	8	1.3
5		M	125	400	0.25	0.7	350	0	0	33	5	0.9
6		L	115	150	0.25	0.9	150	0	0	30	2	0.5
7	SM–SC	H	135	400	0.6	0.7	200	0.5	3.5	33	0	1.1
8		M	125	200	0.6	0.7	100	0.5	2.5	33	0	0.8
9		L	115	100	0.6	0.9	50	0.5	1.4	33	0	0.5
10	CL	H	130	250	0.45	0.7	150	0.2	2.8	30	0	0.9
11		M	120	150	0.45	0.7	100	0.2	1.8	30	0	0.6
12		L	110	50	0.45	0.9	50	0.2	0.6	30	0	0.3
19	(haunch voids)	VL	10	5	0.25	0.9	0.2	0.0	0.0	20	0.2	0.2

TABLE 2 SOIL PROPERTIES OF PREEXISTING SOIL (in situ)

Soil No.	State	γ_m (lb/ft^3)	K	n	R_f	K_b	m	C (psi)	ϕ (degree)	$\Delta\phi$ (degree)	k_0
Coarse-Grained Soils											
13	A	145	680	0	0	22,000	0	0	0	0	1.0
14	B	130	408	0	0	453	0	0	0	0	1.0
15	C	115	136	0	0	76	0	0	0	0	1.0
Fine-Grained Soils											
16	D	125	408	0	0	340	0	0	0	0	1.0
17	E	117	238	0	0	393	0	0	0	0	1.0
18	F	110	68	0	0	2,200	0	0	0	0	1.0

The dead weights are applied with each construction layer. When all layers have been placed, the pipe is subjected to the weight of the water and internal pressure. The internal pressure is applied incrementally; the number of increments is dependent on the extent of nonlinearity expected in the behavior of the pressurized pipe. A larger number of pressure increments are expected for a pipe with an installation-induced deformation configuration that results in a significant change in the local radius of curvature of the pipe before pressurization. This condition occurs when, for example, a flexible pipe has an improper haunch support and is installed directly on hard bedding.

Construction Sequence

The model considers the step-by-step sequence of construction. It starts with the assemblage of the in situ soil elements and in each step adds a layer of the constructed soil. The pipe may be placed either on in situ soil or on constructed backfill the thickness of which may be specified by the user. After the pipe is placed, five additional layers of backfill are placed in sequence until the backfill just covers the crown of the pipe. The number of layers applied after this is dependent on the height of the fill that the user specified. Above the pipe zone regions, layers are constructed that have a thickness of approximately one-half the pipe diameter. In each construction step, a soil layer is applied by adding new nodes and elements to the previously constructed finite element model. The weight of the soil layer increases the confining pressure of the previous soil elements. The increase in the confining pressure increases the stiffness of the constructed soil elements. (At any stage of construction, the top layer of soil is not confined and therefore initially lacks stiffness; care must be exercised not to unduly load the flexible pipe by the weight of the soil elements that lack the necessary stiffness to support the pipe, particularly when the construction reaches pipe haunches.)

At each step of construction, the pipe-soil system is subjected to a two-iteration analysis. In the first iteration the solution before the application of the load increment is used to approximate the states of stress and deformation of the pipe-soil system after the application of the load increment. The results of the first iteration are then used to estimate the average states of stress and deformation of the pipe-soil system during the application of the load increment, which are in turn used to modify the stiffness matrix and the geometry of the deformed pipe-soil system. This iterative procedure has been shown to give results that are sufficiently accurate for all practical purposes when load increments are not very big. However, for problems for which experience does not justify the two-iteration analysis, a larger number of iterations is unavoidable.

Pressurization

When the last construction layer is applied, the pipe is subjected to the weight of the water and the pressure increments. At each pressure increment, the pipe-soil system is subjected to two-iteration analysis. In the first iteration, the state of stress and deformation of the pipe-soil system at the end of the pressure increment is approximated. The results are then used to calculate the average stresses and deformations in that load increment. These average values are used to modify the soil and the pipe stiffnesses that are in turn used to calculate the state of stress and strain in the pipe-soil system at the end of the pressure increment.

As the flexible pipe is subjected to internal pressure, the pipe expands and moves against the surrounding soil. This increases the radial load on the soil elements around the pipe. In addition, with increasing pressure, a larger share of the weight of the cover will be picked up by the pipe, thus reducing the confining stress on some soil elements near the springline. The program ignores any inelastic behavior of the soil resulting from such a reduction of the confining stress and assumes that the loading and unloading paths are coincident. The effects of this approximation on the accuracy of the results obtained have not been evaluated.

Note that the geometric nonlinearity of the pipe, resulting from large deformation and from the effect of the axial force in the elements on the flexural stiffness of the pipe elements, and the nonlinearity of the stress-strain relationship of the soil render the problem highly nonlinear and sensitive to pressure increment size.

PROGRAM

The computer program FLEXPIPE is developed for the finite element analysis of soil-structure interaction of a flexible pipe subjected to internal pressure. The soil model is a variant of the Nonlinear Soil-Structure Interaction Program (NLSSIP), a general-purpose finite element soil-structure interaction program developed originally at the University of California at Berkeley and modified at the University of Massachusetts at Amherst for application to SPIDA *(4)*. It generates the mesh geometry and construction sequence internally from a limited input. It computes the stiffness of the pipe elements considering large displacement and the nonlinear effects of the axial force in the element on its flexural stiffness. The results are printed as deformations and stress resultants in the pipe wall. The input to this program consists of the following parameters:

- Trench geometry. Specifications for trench geometry include height of fill, trench width, bedding thickness, height of pipe zone region, and overall mesh dimensions.

- Pipe parameters. These include pipe diameter, wall thickness, material density, and elastic modulus.
- Construction sequence. The construction sequence is by and large internally specified. The user may only specify whether the pipe is to be placed on in situ material or on constructed backfill.
- Soil properties. The soil properties are built into the program, but the user may choose to define his own. To facilitate the assignment of soil properties to each element, the finite elements are grouped into zones that are typical of present engineering and construction practices. The user simply assigns a number that represents the desired soil properties to each zone. In addition, he may override soil properties for any element in any given zone and specify the properties he desires for that particular element.
- Pressure. The user may specify the magnitude of pressure and the number of increments in which the pressure is to be applied.
- Additional loads. The user may specify additional loadings such as AASHTO truck loading and surface surcharge loads.

The output consists of the following items:

- Summary of installation data, pipe properties, deflections, thrusts, moments, shear stresses, and arching factors;
- Soil properties;
- Finite element node geometry, connectivity, and construction layer information; and
- Incremental node forces, deformations, axial forces, shears, moments, and normal and tangential soil pressures on the pipe elements.

The user may specify as much or as little output as is desired. In addition, the user may specify at what construction layers the detailed information should be printed. In addition, a summary table of the pipe deformations and the stress resultants and strains in the pipe wall are printed at the end of the analysis for all construction layers.

At present, the program is privately maintained on a CDC Cyber 176 computer at the Control Data Corporation Eastern Cybernet Service Center, 6006 Executive Boulevard, Rockville, Maryland.

RESULTS OF ANALYSIS

The program was used to investigate the effects of inadequate haunch support and hard bedding on the stresses and the strains induced in flexible pipe subjected to internal pressure. For this purpose, a flexible pipe with a pipe stiffness of 10 psi was selected for analysis. The pipe diameter is assumed to be 36 in. with a thickness of 0.4 in. and a modulus of elasticity of 1.63×10^6 psi. The pipe is installed with 6 ft of cover and is subjected to 100 psi of internal pressure after installation.

Installation is in a narrow trench, only a foot wider than the pipe, with vertical walls. The in situ soil of the walls of the side trenches and the foundation is a moderately dense coarse-grained soil. The backfill adjacent to the pipe is a moderately dense loose gravel and sand mixture with silt fines, and the cover over the pipe is loose sand. The haunches are supported by extremely loose soil with a very low bulk modulus. The pipe is placed directly on the hard coarse-grained native soil supported only by the 2.5-degree element at the invert of the pipe. Figure 2 shows the soil types and construction layers used in this analysis. The soil properties for each soil number shown are those given in Tables 1 and 2.

The results of the analysis are shown in Figures 3 and 4. Figure 3 shows the deformed configuration of the pipe before and after pressurization. The bending moments, or equivalently the flexural strains, before and after pressurization are shown in Figure 4.

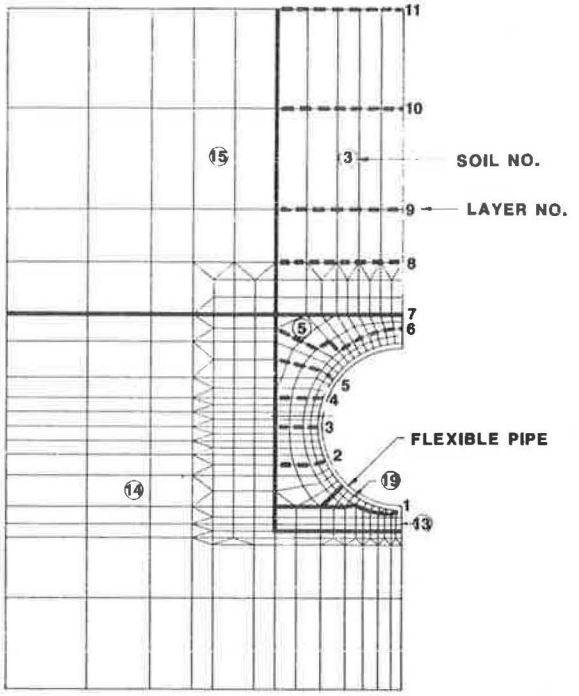

FIGURE 2 Mesh geometry, soil types, and construction layers used in analysis of buried flexible pipe with poorly supported haunches and hard bedding.

In addition, a second analysis in which the same flexible pipe was installed properly was performed. In this analysis, a 4-in.-thick bedding was provided underneath the pipe and the pipe

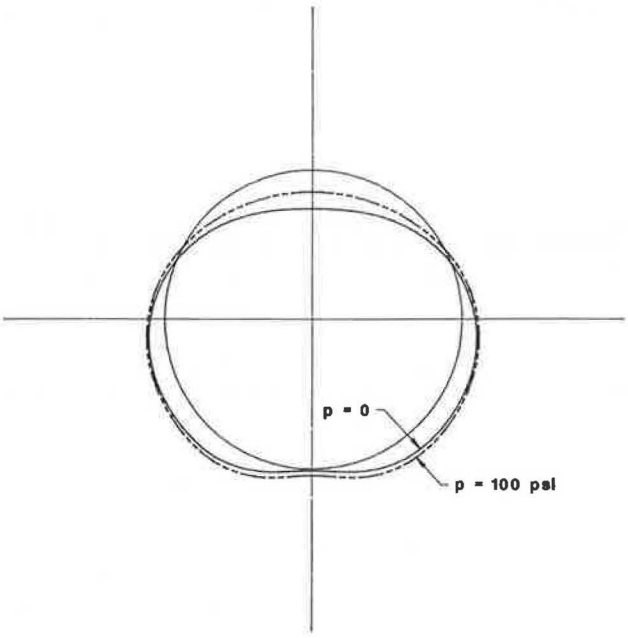

FIGURE 3 Deformed shape of a buried flexible pipe with improper haunch support and hard bedding before and after pressurization.

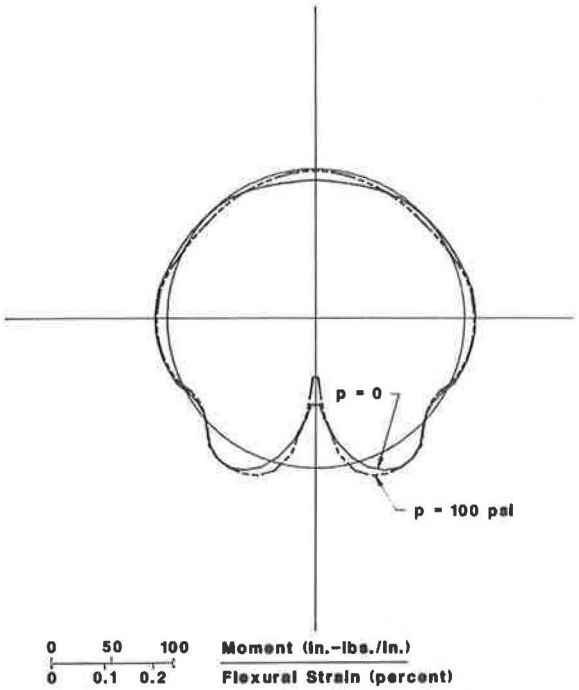

FIGURE 4 Bending moment, or flexural strain, of a buried flexible pipe with improper haunch support and hard bedding before and after pressurization.

haunches were supported by the backfill material with the same compaction as the sidefills. The soil types and construction layers used in this analysis are shown in Figure 5. Note that the pipe in this case is laid on a soil layer modeled as a region subtending a 10-degree angle. The resulting deformations of the pipe and the moments (or strains) in the pipe wall are shown in Figures 6 and 7.

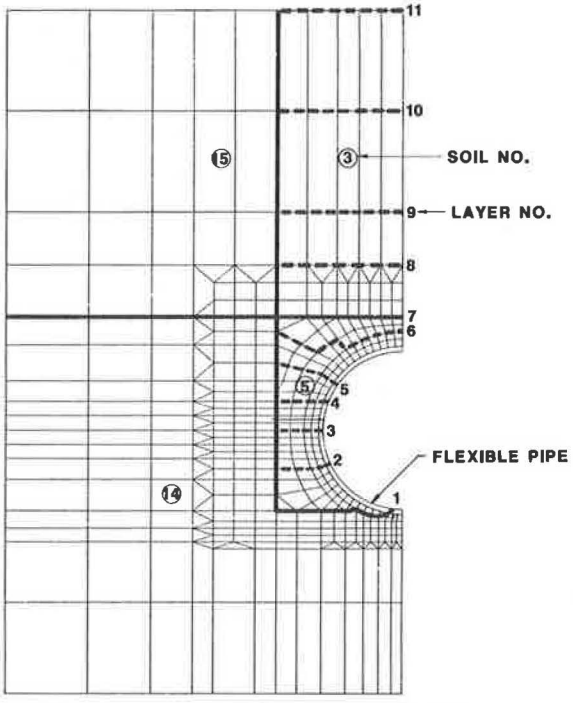

FIGURE 5 Mesh geometry, soil types, and construction layers used in analysis of buried flexible pipe with haunches and invert properly supported.

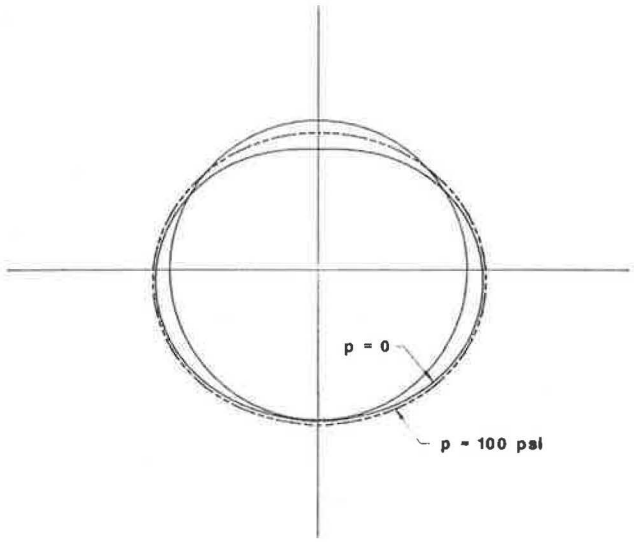

FIGURE 6 Deformed shape of a buried flexible pipe with proper haunch support and bedding before and after pressurization.

Table 3 gives a summary of the results of the analyses performed on the flexible pipe with inadequate haunch support laid on hard bedding and for the same pipe installed on a 4-in. bedding with adequate haunch support. The results are presented for the empty pipe immediately after installation and for the water-filled pipe before and after pressurization.

The following statements, based on the review of the numerical results obtained, can be made:

1. A comparison of the flexural strains at the invert of a flexible pipe with improperly supported haunches laid on hard bedding and

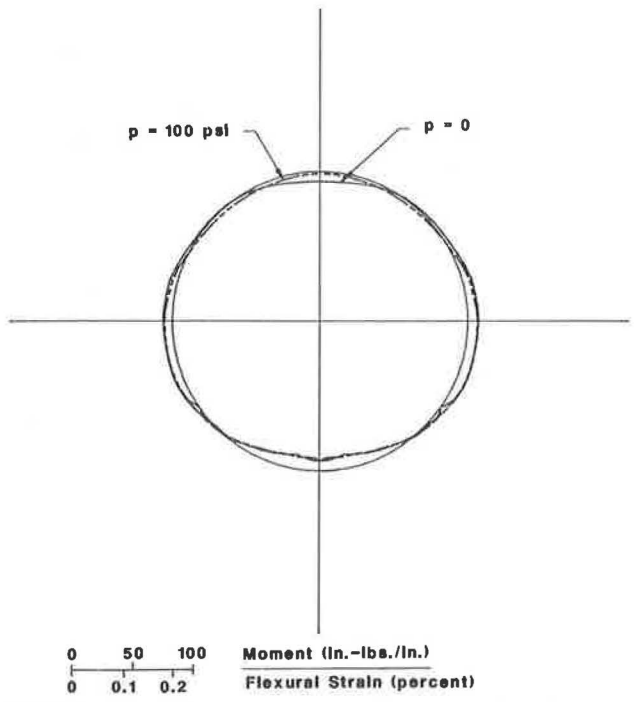

FIGURE 7 Bending moment, or flexural strain, of a buried flexible pipe with proper haunch support and bedding before and after pressurization.

TABLE 3 SUMMARY OF RESULTS OF FINITE ELEMENT SOIL-STRUCTURE INTERACTION ANALYSIS FOR FLEXIBLE PIPE IN PROPER AND IMPROPER INSTALLATIONS

Item	Hard Bedding and Poor Haunch Support			4-in. Bedding and Supported Haunches		
	After Installation	Before Internal Pressure	After Internal Pressure	After Installation	Before Internal Pressure	After Internal Pressure
Arching factor	0.44	0.36	0.56	0.55	0.50	0.77
Vertical deflection (in.)	-0.29	-0.30	-0.13	-0.22	-0.23	0.06
Horizontal deflection (in.)	0.23	0.23	0.27	0.21	0.21	0.26
Approximate invert reaction (lb/in.)	27	35	148	–	–	–
Bending moment (in.-lb/in.)						
At crown	8.7	8.9	1.3	8.1	8.3	1.8
At springline	-9.6	-9.7	-8.8	-8.3	-8.3	-7.1
At invert	44.1	52.8	76.5	8.4	8.5	10.6
Flexural strain (%) at invert	0.101	0.121	0.176	0.019	0.020	0.024
Membrane strain (%) at invert	-0.003	-0.001	0.267	-0.004	-0.003	0.266
Combined strain (%) at invert	0.104	0.122	0.443	0.023	0.023	0.290
Nominal hoop strain (%)	–	–	0.28	–	–	0.28

of the same pipe properly installed suggests that the deformation configuration of the installed pipe, and consequently the resulting installation-induced strains in the pipe wall, may be visualized as the sum of two distinct configurations, an ovaling deformation that would have been obtained if the pipe had been installed on a soft bedding with haunches adequately supported (Figure 6) and a pear-shaped configuration resulting from the localized soil reaction at the invert of the buried pipe, such as the shape corresponding to the difference or deformations shown in Figures 3 and 6. The magnitude of the deformation that results from the pear-shaped component is roughly proportional to the magnitude of the reaction at the invert of the pipe and, therefore, depends on several factors such as the size of the haunch area with inadequate support, the stiffness of the bedding material, the arching factor (i.e., the fraction of the total weight of cover supported by the pipe), and the depth of cover.

This result suggests a generalization that the deformed configuration of any pipe with less-than-ideal installation condition may be considered as the sum of an oval-shaped configuration, which would be obtained if the invert were properly supported, and a pear-shaped configuration resulting from the deviation of the installation from the ideal condition (i.e., the localized soil reaction at the invert) (Figure 8).

Because the oval configuration contributes more to pipe deflection and the pear-shaped configuration to moment, the strain cannot be defined uniquely in terms of the deflection unless a unique mix of the two configurations is assumed. Molin's formula for strain *(14)*, used by most standards including those of AWWA, expresses the flexural strain in the pipe wall as $6(\Delta/d)(t/d)$, where Δ is the deflection, t is the thickness, and d is the diameter of the pipe. For the pipe analyzed herein, this formula yields a value for strain of less than 0.06 percent, underestimating it by almost an order of magnitude.

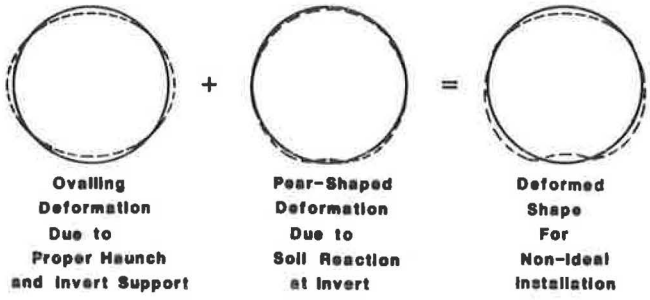

FIGURE 8 Schematics.

2. High flexural strains can develop at the invert of a flexible pipe installed with improper haunch support and on hard bedding. For the problem analyzed, the resulting flexural strain before pressurization is between one-third and one-half of the nominal strain in the pipe wall resulting from internal pressure (pr/Et). Such high flexural strains are not present when the pipe is installed on a softer bedding with proper haunch support.

Comparison of the flexural strains developed in the flexible pipe installed with inadequate haunch support and on hard bedding with those developed in the same pipe installed properly demonstrates the supreme importance of proper installation to the performance of buried flexible pipe. In other words, design of flexible pipe in accordance with the requirements of the AWWA specification is contingent on adequate assurance of the quality of installation.

3. The calculated arching factors after installation and before pressurization indicate that only a fraction of the total weight of the column of the soil above the pipe is supported by the pipe. With time and under the action of the fluctuating groundwater level, the arching factor will increase and more of the weight of the cover will rest on the pipe. This is expected to increase the soil reaction at the invert of the pipe laid on hard bedding with poor haunch support and to increase the flexural strain at the invert of the pipe significantly. For pipe with proper haunch and invert support, the increase in arching factor is expected to have a much smaller effect on pipe wall strains.

4. Internal pressure affects the two components of the deformation in different ways. Its effect on the ovaling deformation component is to reround the pipe. However, the flexural strains in the pipe wall will not decrease as the pipe rerounds even for the flexible pipe installed with proper haunch and invert support because of the nonuniformity of the support that the soil provides for the pipe in the radial direction. The effect of the internal pressure on the pear-shaped deformation component, which results from the improper haunch support and hard bedding, is totally different. As the pressure-induced radial expansion of the pipe is inhibited by the hard invert while permitted into the loose haunch support areas, the pipe will flatten and the flexural strains will increase at the invert. The data in Table 3 indicate that the flexural strain at the invert of the pipe is increased significantly when the pipe is pressurized to 100 psi.

5. In the cases analyzed, the rerounding of the flexible pipe with internal pressure was not accompanied by an unloading of the sidefills; therefore, the assumption of elastic behavior of soil used in the program is not expected to entail large errors.
6. The quality control procedure for the installation of flexible pipe must include steps to ensure that the compaction of the backfill supporting the haunches of the pipe is adequate and that the bedding is not very hard. Note that the deflections of the pipe analyzed are quite small, not exceeding 1 percent of the diameter, and the sidefills have adequate compaction, but the strain in the pipe wall is extremely high. In other words, the quality of installation cannot be ensured by checking pipe deflection and sidefill compaction.
7. In the examples presented herein, the flattening at the invert of the pipe is not large enough to give rise to higher pressure-induced membrane stresses. This is not always the case and higher membrane stresses can result when the invert flattens in a more pronounced way *(15)*. Obviously, a larger arching factor or a lower pipe stiffness could result in larger flattening of the invert.

CONCLUSIONS

The analysis of buried flexible pipe subjected to internal pressure is performed by a finite element soil-structure interaction program. The program has a fine mesh geometry to enable accurate modeling of the variability of soil stiffness around the pipe and of the rapid attenuation of the flexural stresses of flexible pipe installed in stiff backfills. In addition, the program considers the nonlinear behavior of the pipe resulting from large deflection and from the flexural stiffening effect of the pressure-induced membrane stresses. The program provides for the hyperbolic stress-strain relationship of the soil and for the step-by-step nature of construction. Using the program, the stresses and the strains for a buried flexible pipe subjected to internal pressure with improper haunch support and hard bedding have been calculated and compared with those calculated for the same pipe installed properly.

The results show that the deformed configuration of a flexible pipe in less-than-ideal installation conditions may be visualized as the sum of two components. One component is an ovaling configuration, such as that which results from installation with proper haunch and invert supports, and the other is a pear-shaped configuration, which results from the deviation of installation from the ideal configuration, caused by a localized soil reaction at the invert of the buried pipe. Molin's formula, used in most of the present standards, gives a fixed ratio of strain to deflection in terms of pipe deflection. It may be considered to be based on a fixed mix of these two configurations and, therefore, may not be valid for general application (i.e., improper installation cases). High flexural strains can develop in a flexible pipe laid on hard bedding with improper haunch support, although the deflection of the pipe is small. The results demonstrate the supreme importance of proper installation to the performance of buried flexible pipe. In addition, the quality of an installation for a flexible pipe cannot be ensured by checking the deflection of the pipe and the compaction of sidefills. Steps must be taken to ensure that the haunch support areas are well compacted and that a proper bedding is provided.

Internal pressure is shown to reround the buried flexible pipe, but, even when the haunches and the invert are properly supported, it may not alleviate the flexural stresses in the pipe wall. In the case of a flexible pipe with an improper haunch support and a hard bedding, internal pressure increases the installation-induced flexural stresses significantly.

The program cannot at the present time simulate the time-dependent behavior of the soil and the resulting higher stresses in the pipe wall that are expected to occur with time. Therefore the results of the finite element analysis of soil-structure interaction should be reviewed in light of the expected increase in the arching factor.

ACKNOWLEDGMENT

The authors are indebted to Ernest T. Selig of the University of Massachusetts in Amherst and to Atis A. Liepins of Simpson Gumpertz & Heger, Inc., for their invaluable assistance and many useful discussions.

REFERENCES

1. J. M. Duncan. "A Design Method for Metal Culvert Structures Based on Finite Element Analyses." Presented at 55th Annual Meeting of the Transportation Research Board, Washington, D.C., 1976.
2. J. M Duncan. Behavior and Design of Long-Span Metal Culverts. *Journal of the Geotechnical Engineering Division*, ASCE, Vol. 105, No. GT3, March 1979, pp. 399–418.
3. M. G. Katona, J. M. Smith, R. S. Odella, and J. R. Allgood. *CANDE—Engineering Manual—A Modern Approach for Structural Design and Analysis of Buried Culverts*. Report FHWA–RD–77–5. FHWA, U.S. Department of Transportation, Oct. 1976.
4. E. T. Selig, M. C. McVay, and C. S. Chang. "Finite-Element Modeling of Buried Concrete Pipe Installation." In *Transportation Research Record 878*, TRB, National Research Council, Washington, D.C., 1982, pp. 17–23.
5. F. J. Heger, A. A. Liepins, and E. T. Selig. "SPIDA: An Analysis and Design System for Buried Concrete Pipe." Presented at the International Conference on Advances in Pipeline Engineering, Madison, Wis., Aug. 27–29, 1985.
6. A. P. Moser, R. R. Bishop, O. K. Shupe, and D. R. Bair. "Deflection and Strains in Buried FRP Pipes Subjected to Various Installation Conditions." In *Transportation Research Record 1008*, TRB, National Research Council, Washington, D.C., 1985, pp. 109–116.
7. K. D. Sharp, L. R. Anderson, A. P. Moser, and R. R. Bishop. "Finite-Element Analysis Applied to the Response of Buried FRP Pipe Under Various Installation Conditions." In *Transportation Research Record 1008*, TRB, National Research Council, Washington, D.C., 1985, pp. 63–72.
8. R. R. Bishop and D. C. Lang. "Design and Performance of Buried Fiberglass Reinforced Plastic Pipe—A New Perspective." In *Pipeline Materials and Design* (Jay Schrock, ed.), *Proc., ASCE National Convention*, San Francisco, Calif., Oct. 1984, pp. 1–12.
9. M. Hetenyi. *Beams on Elastic Foundations*. The University of Michigan Press, Ann Arbor, 1946.
10. R. D. Cook. *Concepts and Applications of Finite Element Analysis*. John Wiley & Sons, Inc., New York, 1974.
11. M. S. Zarghamee and J. M. Shah. Stability of Spaceframes. *Journal of the Engineering Mechanics Division*, ASCE, Vol. 94, No. EM2, April 1968, pp. 371–384.
12. J. M. Duncan and C.-Y. Chang. Nonlinear Analysis of Stress and Strain in Soils. *Journal of Soil Mechanics and Foundations Division*, ASCE, Vol. 96, No. SM5, Sept. 1970, pp. 1629–1653.
13. J. M. Duncan, P. Byrne, K. S. Wong, and P. Marby. *Strength, Stress-Strain and Bulk Modulus Parameters for Finite Element Analyses of Stresses and Movements in Soil Masses*. Report UCB/GT/80–01. Department of Civil Engineering, University of California, Berkeley, Aug. 1980.
14. J. Molin. *Principles of Calculations for Underground Plastic Pipes—Loads, Deflections, and Strains*. International Organization for Standards, Oct. 1971. [Translated by British Standards Institute, Doc. No. ISO/TC 136/WG (Sweden-3) 47, 1977.]
15. M. S. Zarghamee. Buried Flexible Pipe with Nonuniform Soil Support. *Journal of Transportation Engineering*, ASCE, Vol. 112, No. 4, July 1986, pp. 400–415.

Publication of this paper sponsored by Committee on Subsurface Soil-Structure Interaction.

Enhancement of Membrane Action for Analysis and Design of Box Culverts

THEODOR KRAUTHAMMER, JAMES J. HILL, AND TONY S. FARES

Current design procedures for cast-in-place reinforced concrete box culverts are based on the load factor design approach, as recommended by AASHTO, or on the working-stress method and the fundamental assumption of rigid culvert behavior. Also, the interaction between the soil cover and the structure is not considered beyond the computation of the soil load that is to be added to the other live and dead loads that affect the design. Recent developments in the understanding of the structural behavior of reinforced concrete combined with a modified formulation of this behavior may provide some ideas for improvement in the design of box culverts. Membrane (in-plane) forces are often present in reinforced concrete slabs as a result of boundary conditions and the geometry of slab deformation. Box culverts can be viewed as composed of slabs, and the restraints will be introduced by the joints and the surrounding soil backfill. These conditions will introduce in-plane forces, initially in compression and ultimately in tension, that are capable of enhancing the load-carrying capacity of the individual slabs. Such enhancement, in the domain of compressive membrane behavior, is associated with a certain amount of deflection that in many cases does not affect serviceability requirements. In the present study, one-, two-, and three-barrel culverts were analyzed using this approach, and the results can be used to demonstrate the modified behavior of such structures. It was found that the stiffness of the lateral restraint around the structure makes a significant contribution to structural capacity, that the membrane enhancement of the load is more than 50 percent larger compared with the yield line approach for the same culverts, and that this enhancement could be improved further by a relatively simple redesign of the culverts that would increase their load capacity by as much as 74 percent.

Design guidelines for cast-in-place reinforced concrete box culverts are provided by the AASHTO code (*1*) and similar codes that are based on linear elastic frame analysis of the box cross section combined with an assumed load distribution. The design parameters are obtained by employing an ultimate strength approach that eventually leads to rather stiff structural members. In these design considerations, soil-structure interaction is not considered, and the soil contribution is only to the loads that act on the box structure. The limited analytical capabilities incorporated in the design approach can be enhanced significantly by employing advanced numerical techniques such as the finite element approach, as discussed by Katona and Vittes (*2*). Another approach to the analysis and the design of box culverts is based on the theory of enhancement of membrane action in reinforced concrete slabs combined with the yield line method, as proposed by Fares and Krauthammer (*3*).

Previous studies of the behavior of reinforced concrete slabs and the significant contribution of membrane action to structural performance in the static domain have been adequately tested and documented in the last 20 years (*4*). Similar effects were also noticed for reinforced concrete slabs in the dynamic domain of behavior, and the analytical procedures that incorporated membrane action enhancement have led to accurate assessments of structural performance (*5*). Membrane action is the development of in-plane forces, due to geometric conditions at the slab supports, combined with the lateral and rotational support stiffnesses and possibly also with externally applied forces that are transmitted to the slab plane. The contribution of such action both in tension and in compression can be well beyond the load-carrying capacity that is based on the yield line theory (*6, 7*). Initially, at low central deflections, slabs behave according to the assumed one- or two-way slab behavior, but, as the central deflections increase, the compressive membrane action becomes an important mechanism that tends to peak when the central deflection is between 0.25 and 0.5 of the total depth of the slab. Beyond that point a steep decline in load capacity was noticed until the central deflection reached about 1.0 times the total depth of the slab, and at that point there is a transition into the tensile membrane domain where the resistance increases almost linearly with added central deflections. The loads are carried essentially by the steel reinforcement acting as a plastic tensile membrane with the concrete fully cracked through the entire slab depth.

This paper is intended to demonstrate how membrane action can be incorporated into the analysis, and eventually the design, of box culverts. The methodology of the approach is presented next, followed by several examples and recommendations for future development.

STRUCTURAL MECHANISMS

Two fundamental assumptions can be employed for evaluating the load-carrying capacity of reinforced concrete slabs, as extensively discussed in the literature (*4, 8, 9*). These methods consist of the yield line theory for reinforced concrete slabs based on the approach proposed by Johansen (*10, 11*) and the membrane approach that combines the concept of yield lines with the in-plane force enhancement, as discussed by Park and Gamble (*4*). At this time, only the yield line approach can be incorporated explicitly into design procedures (*8*), but the advantages of the membrane mechanism provide clear incentives for considering such contributions during slab analysis and design. Here, it is assumed that structural engineers are quite familiar with the yield line method, and therefore the membrane mechanism will be emphasized in the following discussion.

Nevertheless, it should be mentioned that the yield line theory is based on a variational approach, such as virtual work, in which the analyst assumes a collapse pattern for the structure (i.e., yield lines in the slab) and requires that the work done by the external loads over the deflected shape equal the work performed by the resisting moments over the corresponding rotations along the yield lines. The resulting equations lead to the evaluation of the limit load-carrying capacity of the slab.

T. Krauthammer, Department of Civil and Mineral Engineering, University of Minnesota, Minneapolis, Minn. 55455. J. J. Hill, Minnesota Department of Transportation, Transportation Building, Room 615, St. Paul, Minn. 55155. T. S. Fares, Sargent and Lundy, 55 East Monroe Street, Chicago, Ill. 60603.

The load versus central deflection curve of a uniformly loaded reinforced concrete slab with laterally restrained edges is shown in Figure 1. At early loading stages the behavior is the same as that described by the theories for one- or two-way slabs. However, as the load is increased and the center of the slab is pushed downward, the slab edges must rotate and move outward to accommodate the central displacement. Because the edges are fixed (or restrained by the adjoining walls) such rotation and outward motion cannot occur, which causes an in-plane compression in the slab that increases its load-carrying capacity. The slab reaches its enhanced ultimate load at B with an associated central deflection of about one-half its effective depth (*4*). Beyond B the slab exhibits a decrease in load-carrying capacity with an increasing central deflection. The stage between B and C marks the transition from compressive to tensile membrane behavior. For slabs with rigid boundaries, the central deflection of the slab at C has been found to approximately equal the slab thickness. Beyond C the slab carries the load by the reinforcement acting as a plastic tensile membrane. The slab continues to carry further load until at D the reinforcement fails.

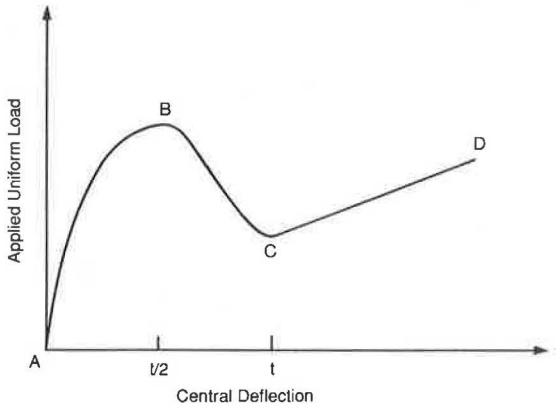

FIGURE 1 Load-deflection relationship for slab, after Park and Gamble (*4*).

The present approach is based on the model and the extensive discussion in Park and Gamble (*4*) in which a load-deflection relationship was derived for a reinforced concrete slab strip.

A fixed-end strip with developed plastic hinges is shown in Figure 2. The strip is initially of length L and is restrained against rotation and vertical translation at each end by the adjoining structural components. The ends are considered to be partly restrained against lateral displacement, and the outward lateral movement at each end is t. The strip in Figure 2 is considered to have symmetrically positioned plastic hinges. The portions of the strip between the critical sections (plastic hinges) are assumed to remain straight; it will be assumed that at each plastic hinge the tension steel has yielded, the compressive concrete has reached its uniaxial compressive strength, and the tensile strength of the concrete can be neglected. It also is assumed that the top steel at opposite supports has the same area per unit width, bottom steel is constant along the length of the strip, and top and bottom steel may be different. Because of the sensitivity of the theory to axial shortening, the axial strain (ε) will be assumed to have a constant value because the membrane force is constant along the length of the strip. The change in dimensions of end portion 1–2 due to ε and t is shown in Figure 3. It should be noted that ε is compatible with the introduction of in-plane forces to the slab and that such forces can exist only if the slab edges are effectively restrained by adjoining structural members, such as walls.

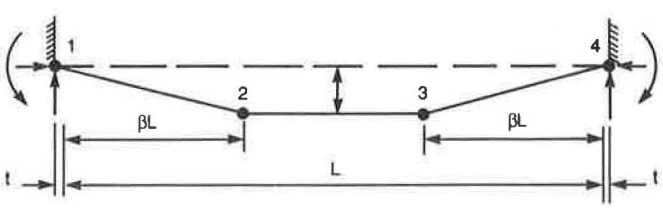

FIGURE 2 Deformation mechanism for slab strip, after Park and Gamble (*4*).

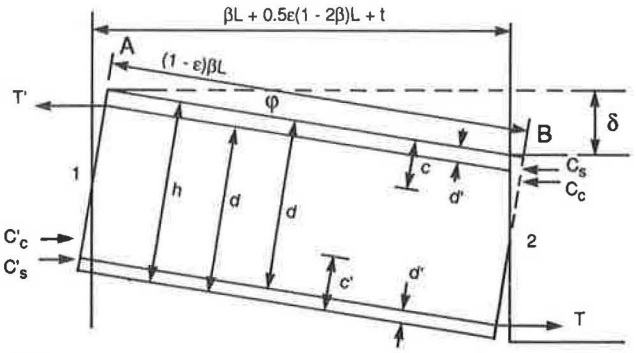

FIGURE 3 Free body diagram for strip segment, after Park and Gamble (*4*).

Employing the principle of equilibrium for this system, Park and Gamble (*4*) showed that the resulting equation for the end portions 1–2 or 3–4 of the strip in Figures 2 and 3 is

$$
\begin{aligned}
m'_u + m_u - n_u\delta = 0.85 f'_c \beta_1 h \; & \{(h/2)(1 - \beta_1/2) \\
& + (\delta/4)(\beta_1 - 3) + (\beta L^2/4\delta)(\beta_1 - 1) \\
& [\varepsilon + (2t/L)] + (\delta^2/8h)[2 - (\beta_1/2)] \\
& + (\beta L^2/4h)[1 - (\beta_1/2)][\varepsilon + (2t/L)] \\
& - (\beta_1 \beta^2 L^4/16h\delta^2)[\varepsilon + (2t/L)]^2\} \\
& - (1/3.4f'_c)(T' - T - C'_s + C_s)^2 \\
& + (C'_s + C_s)[(h/2) - d' - (\delta/2)] \\
& + (T' + T)[d - (h/2) + (\delta/2)] \qquad (1)
\end{aligned}
$$

where

L = initial length of the strip;
t = outward lateral displacement of each boundary;
ε = axial strain in the strip due to elasticity, creep, and shrinkage;
f'_c = uniaxial compressive strength for concrete;
βL = location of the middle hinges;
h = thickness of the strip;
c, c' = neutral axis depth at Sections 1 and 2, respectively;
d = distance from top compression fiber of the concrete to the steel in tension;
d' = distance from compression steel to the outer fiber of concrete in compression;

T, T' = steel tensile forces acting on Sections 1 and 2;
C_s, C'_s = steel compressive forces acting on Sections 1 and 2, respectively;
C_c, C'_c = concrete compressive forces acting on Sections 1 and 2, respectively;
m_u, m'_u = positive and negative ultimate moment capacity for strip, respectively;
n_u = membrane force corresponding to all in-plane forces on the strip at midspan;
β = constant, less than 1, defining hinge position from support as βL;
δ = deflection of the middle part of the strip;
ϕ = inclination of portion 1–2;

and

$$\beta_1 = \begin{cases} 0.85 & \text{for } f'_c \le 4{,}000 \text{ psi} \\ 0.85 - 0.05\,[(f'_c - 4000)/1000] \ge 0.65 & \text{for } f'_c > 4{,}000 \text{ psi} \end{cases} \quad (2)$$

It is also shown (*4*) that for a fixed-end reinforced concrete strip:

$$\varepsilon + 2t/L = \Big([(1/hE_c) + (2/LS)]\,[0.85f'_c\beta_1\,\{(h/2) - (\delta/4) - [(T' - T - C'_c + C_s)/1.7f'_c\,\beta_1]\} + C_s - T]\Big)/\{1 + 0.2125\,(f'_c\,\beta_1\,\beta\,L^2/\delta)\,[(1/hE_c) + (2/LS)]\} \quad (3)$$

where E_c is the elastic modulus for concrete and S is the lateral stiffness of the slab surroundings at each end in units of load per outward displacement of the support (i.e., support resistance function). The lateral stiffness is defined as a function of E_c and represents the primarily contributions of adjoining structural elements. The contribution of soil backfill to the lateral restraining of the slab may also be considered, but usually such contribution is rather limited. Furthermore, because the primary restraint is provided by structural components, the backfill effects can be ignored for the present model.

Employing the principle of virtual work for the strip under a uniform load *(w)* and a virtual rotation (Θ) for portions 1–2 or 3–4:

$$(wL/2)/(\Theta L/4) = (m'_u + m_u - n_u\,\delta)\,\Theta \quad (4)$$

from which

$$(wL^2/8) = m'_u + m_u - n_u\,\delta \quad (5)$$

The load on the slab (w) can be computed from Equation 1 after Equations 3 and 5 are introduced into it. It may be noticed that in Equation 1 w is a function of material properties of steel and concrete, geometry of the strip, and central deflection (δ). Therefore the load-carrying capacity (w) can be assessed as a function of the central deflection (δ) because all other parameters are known for a given slab.

The present study was limited to the compressive membrane range ($\delta < t$) because the peak load capacity is obtained in this range and because structural damage would be too severe in the tensile membrane domain, and, therefore, might not meet code deflection and cracking control requirements.

Furthermore, only uniformly distributed loading conditions were considered because the soil cover above the culverts transforms concentrated loads on the surface to distributed loads on the culvert, as recommended by AASHTO (*1*).

EFFECT OF SURROUND STIFFNESS

The model for membrane enhancement, as described by Equations 1 and 3, includes the parameter S, which was defined as the "surround" stiffness. The fundamental development of this model, as clearly discussed by Park and Gamble (*4*), is based on the assumption that such stiffness is provided by structural elements connected to the slab in question. To obtain an understanding of the magnitude of required surround restraint for achieving significant membrane action, S can be compared with the axial stiffness of a slab strip over each half span, S_b (where S_b is the load per unit shortening of the half span). When $S = S_b$, it was shown (*4*) that

$$S = (2h/L)\,E_c \quad (6)$$

where the parameters h, E_c, L, and S are as defined earlier. From this approximate model the magnitude of the restraint provided by the surround (i.e., the surround stiffness) can be assessed from the geometric and material properties for each case. For example, in the present case the information on the slabs is given in Table 1 from which it is found that for the top slab $h = 11.5$ in. and $L = 144$ in. When this information is introduced into Equation 6 it is found that S is practically equal to $0.16\,E_c$. Similarily, the bottom and side slabs will provide $S = 0.167\,E_c$ and $S = 0.11\,E_c$, respectively. Therefore, on the basis of this brief discussion, it is clear that for the present structure it should be expected that $0.11\,E_c < S < 0.167\,E_c$, which, as will be shown later, produces significant membrane enhancement. Also, the reader should realize that such values of surround restraint (stiffness) are present in the structure without the addition of any special design features, and, if required, S can be enhanced by providing stiffer boundary conditions to the slabs. However, in this paper, the slabs will be analyzed under regular conditions to illustrate the existing membrane enhancement.

COMPUTER PROGRAM

The information and behavioral model, as outlined previously, was programmed in FORTRAN on the IBM 4341 of the Department of Civil and Mineral Engineering at the University of Minnesota. It should be noted that the program was written for eliminating long manual computations, but the present approach does not require a computer program if only simple assessments are needed. At present the engineering data are in standard units, and an SI version can be prepared without difficulty. Figure 4 is a flow diagram of the program, and the following comments are keyed to the corresponding letters in the diagram.

A. The length and thickness of the strip are read. Reinforcement areas of compressive and tensile steel in both sections of the strip are read. Diameter of bars parallel to short span and stirrup diameter are read. Concrete protective cover and material properties of concrete and steel are read. Finally, location of the middle hinge and concrete ultimate strain are read. All units must be compatible (i.e., pounds and inches are used).

B. The program computes the effective depth of compressive and tensile reinforcement at both ends of the section.

TABLE 1 DESIGN DATA FOR SINGLE CAST-IN-PLACE BOX CULVERT

INSIDE HEIGHT	12.00 FEET
INSIDE WIDTH	12.00 FEET
DEPTH OF FILL	2.00 FEET
UNIT WT. FILL	130.0 LBS/CU.FT.
LATERAL SIDE PRESS. COEFF.	
MAXIMUM	0.75
INSIDE FACE SLAB	0.16
OUTSIDE FACE SIDEWALL	0.16
REINF. YIELD STRENGTH	60000. P.S.I.
ULTIMATE CONCRETE STRESS	4000. P.S.I.
SEGMENT LENGTH (INTERIOR)	40. FEET
SKEW ANGLE	0.0 DEGREES
REINF. COVER	2.0 INCHES
BEDDING CONDITION CLASS	- 1
LOAD FACTOR	1.30
LIVE LOAD COEFF.	1.67
TOTAL CONCRETE QUANTITY	62.4 CUBIC YARDS
SOIL BEARING PRESSURE	2145. POUNDS PER SQUARE FOOT

REINFORCING BARS

BAR	NO.	SIZE	LENGTH	SPACING	LOCATION	WEIGHT
B 603	97	6	13'0"	5.0 IN.	ROOF BOTTOM LONG	1894.02
B 404	49	4	12'1"	10.0 IN.	ROOF TOP LONG	395.51
B 607	87	6	13'0"	5.5 IN.	FLOOR TOP LONG	1698.76
B 409	49	4	12'1"	10.0 IN.	FLOOR BOTTOM LONG	395.51
B 510	130	5	12'5"	7.5 IN.	WALL VERTICAL INSIDE	1683.58
B 512	194	5	6'4"	5.0 IN.	CORNER TOP	1281.50
B 613	150	6	6'6"	6.5 IN.	CORNER BOTTOM	1464.45
B 414	98	4	2'2"	10.0 IN.	WALL DOWELL	141.84
B 420	122	4	7'10"	8.0 IN.	WALL VERTICAL OUTSIDE	638.39
B 421	34	4	44'0"	18.0 IN.	FLOOR AND ROOF LONG.	999.33
B 422	34	4	44'0"	18.0 IN.	WALL LONG.	999.33

STIRRUPS

BAR	NO.	DIM "A"	LENGTH	SPACING	RANGE X	LONG. SPACING	LOCATION	WEIGHT
B 446	148	7.50"	16.50"	4.50'	4.50"	13.00"	BD	135.94

TOTAL REINFORCEMENT WEIGHT 11728.12

RESULTS OF MN/DOT CALCULATIONS

REQUIRED THICKNESS

TOP 11.50 INCH BOTTOM 12.00 INCH SIDE 8.00 INCH

C. The stress block parameter and the concrete modulus of elasticity are computed.

D. The program then computes the tensile and compressive forces and the ultimate moments at both ends of the section.

E. Computation of the Johansen's load is executed using the values of ultimate moments computed in D.

F. The program computes the coefficients of lateral restraint stiffness (K_1) defined as the ratio S/E_c, which are successively incremented, and S is then inserted into Equation 3.

G. The middle-span central deflection is incremented starting from zero and reaching one slab thickness.

H. The program then finds the membrane action load for every deflection step by using compressive membrane action and plastic theory.

I. The maximum membrane load for every lateral restraint stiffness specified and the corresponding deflection are found.

J. The program then computes the ratio of membrane load to Johansen load and the corresponding ratio of central deflection to the strip depth.

K. The output provide numerical as well as graphic results.

ANALYSIS AND DESIGN CONSIDERATIONS

The present study (*3*) concentrated on three one-, two-, and three-barrel box culverts for which design data were obtained from the Minnesota Department of Transportation. These structures were analyzed to derive the ratio between the membrane-enhanced load-carrying capacity and the Johansen load as a function of the central deflection (normalized by the slab total depth, δ/h). The computations were performed for each slab of the three culverts and as a function of the lateral restraint stiffness (represented by the parameter S in Equation 3), as presented elsewhere (*3*), and in general the analytical approach for those cases is the same as that discussed in this paper for a simpler case. Here, the approach will be illustrated on a one-barrel box culvert 40 ft long with a 12-ft x 12-ft opening. The wall thicknesses are 11.5 in. for the top slab, 12 in. for the bottom slab, and 8 in. for the side slab (Table 1). The analytical results are provided for the top, bottom, and wall slabs in Figures 5–7. From these figures it is noticed that the membrane enhancement effects and the restraint stiffness contributions are significant. Furthermore, the culvert can be redesigned by employing the present approach, as explained next.

The same top slab for the one-barrel culvert (Table 1) will be designed using the yield line theory. This example is chosen to demonstrate how the proposed approach can be incorporated in the design procedure. The panel carries a uniformly distributed service line load of 640 psf (based on a simplified rectangular loading for a 2-ft soil cover and a 16,000-lb wheel load).

$$w = 16{,}000/2 + [2 * 1.75\ (1 + 2 * 1.75)] = 646$$

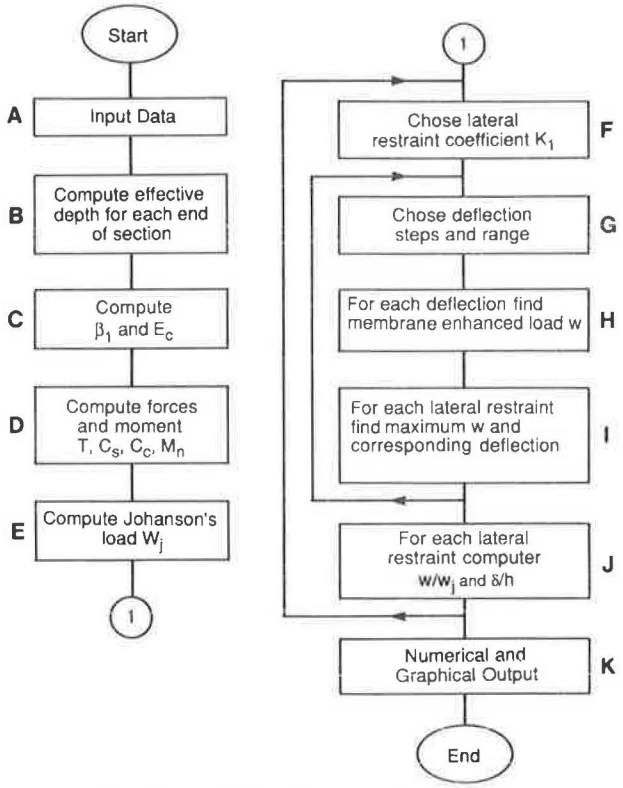

FIGURE 4 Computational approach.

In this case a 0 impact factor for 2 ft or more of fill was assumed. For this case it was assumed that w = 640 psf for purposes of illustration, but the designer may wish to perform more accurate computations.

The backfill dead load is 260 psf, and other conditions for concrete and steel are the same as for the data given in the actual design.

Select slab thickness of 11.5 in., the same as that employed in the existing structure.

Strength Requirement

Assuming that the concrete unit weight is 150 pcf, the service dead load is D = (11.5/12) 150 = 144 psf. Therefore the factored (ultimate) load according to AASHTO (*1*) is

$$w_u = \gamma [BdD + B_1 (L + I) + B_e E] \quad (7)$$

where

γ = 1.3 for rigid culverts,
B_d = 1.0 for rigid culverts,
B_1 = 1.67 for rigid culverts,
B_e = 1.0 for rigid culverts,
D = 144 psf,
$L+I$ = 640 psf,
E = 2(130) = 260 psf, and
w_u = 1.3 {144 + 1.67 (640) + 260} = 1,915 psf.

The yield line pattern for the strip is a hinge at each end and in the center. The ultimate load is given by the following equation:

$$w_u = [24/(L_x)2] [1/3 (L_y/L_x) - 1.0] [(L_y/L_x) (m'_{ux} + m_{ux}) + m'_{uy} + m_{uy}] \quad (8)$$

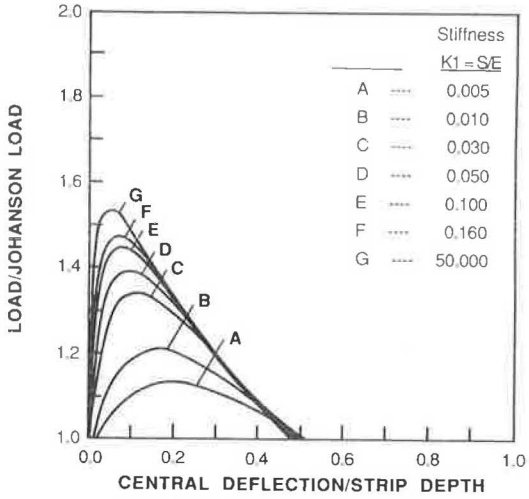

FIGURE 5 Analytical results for top slab.

Place the minimum steel in the y-direction because the load is carried effectively in the x-direction between the supported edges (where x is the direction from support to support, and y is along the culvert axis).

Use No. 4 bars with 2 in. of cover; therefore,

d = 11.5 − 2.00 − 0.25 − 0.375 = 8.875 in. in x-direction and

d = 11.5 − 2.00 − 0.50 − 0.375 − 0.25 = 8.375 in. in y-direction.

The amount of steel permitted is 0.0018 of the gross section, giving A_s = 0.0018(11.5) = 0.0207 in.2/in. width that requires No. 4 bars on 0.20/0.0207 = 9.66 in., say 9 in. on center. Therefore A_s = 0.022 in.2/in.

Place minimum steel in the y-direction at the bottom of the slab and compute the allowable moment capacity.

$$m_u = \phi A_s f_y (d - 0.59 A_s f_y / f'_c) \quad (9)$$

The moment is

$$m_{uy} = 0.9 (0.022) (60{,}000) [8.375 - (0.59) (0.022) (60{,}000/4{,}000)]$$
$$= 9{,}718 \text{ ft-lb/ft width.}$$

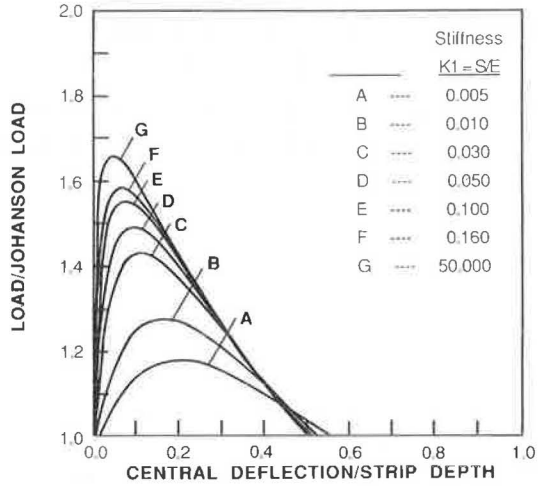

FIGURE 6 Analytical results for bottom slab.

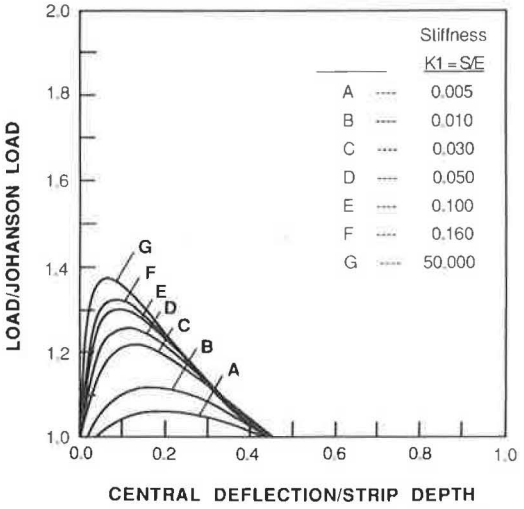

FIGURE 7 Analytical results for wall slab.

Certain assumptions about the induced moments in the x- and y-directions can be made in order to derive the required design parameters, and such assumptions can be adjusted for specific cases on the basis of better information about site and serviceability conditions. Here, such assumptions were made to enable the authors to continue with the example by introducing appropriate values into Equation 7, as follows.

If the x-direction positive moment is 1.5 times larger than the y-direction positive moment, and the x-direction negative moment is 1.5 times larger than the x-direction positive moment, then

$m_{ux} = 1.5(9{,}718) = 14{,}577$ ft-lb/ft width,

$m'_{ux} = 1.5(14{,}577) = 21{,}865$ ft-lb/ft width, and

$m_{ux} + m'_{ux} = 14{,}577 + 21{,}865 = 36{,}442$ ft-lb/ft,

which is larger than $w_u L^2/8 = 1{,}915(12)^2/8 = 34{,}470$ ft-lb/ft.

Therefore, from Equation 7

$$w_u = \{24/(12^2\,[3(40/12) - 1.0])\}\,\{9{,}178 + (40/12)\,(36{,}442)\}$$
$$= 2{,}419 \text{ psf},$$

which is larger than 1,915 psf. Therefore the design meets its ultimate load requirement.

For positive reinforcement

$$14{,}577 = 0.9A_s\,(60{,}000)\,[8.875 - 0.59A_s\,(60{,}000/4{,}000)].$$

Solving the quadratic equation for A_s, yields

$A_s = 0.0314$ in.2/in.

Using No. 4 bars on 0.20/0.0314 = 6.37 in., say 6 in., on centers. Then $A_s = 0.0333$ in.2/in. The resulting moment is

$$m_{ux} = 0.9\,(0.0333)\,(60{,}000)\,[8.875$$
$$- 0.59\,(0.0333)\,(60{,}000/4{,}000)] = 15{,}429 \text{ ft-lb/ft}.$$

For negative reinforcement

$A_s = 0.0483$ in.2/in.

Using No. 5 bar on 0.31/0.0483 = 6.4 in. Select 6 in. on centers; therefore, $A_s = 0.0517$ in.2/in. The resulting negative moment is

$m'_{ux} = 23{,}499$ ft-lb/ft.

Serviceability Check for Cracking

The elastic theory distribution of moments for a fixed-edge strip carrying a service load of (640 + 260) = 900 psf gives maximum x-direction moments.

Negative moment = $w_u L^2/12 = 900(12^2)/12 = 10{,}800$ ft-lb/ft

and

Positive moment = $w_u L^2/24 = 900(12^2)/24 = 5{,}400$ ft-lb/ft.

The maximum steel stress found from $f_s = M/jdA_s$ is

Top steel in x-direction $f_s = 10{,}800/[0.0517(12 - 5.5/3)] = 20.5$ ksi

and, from ACI 318–83 Section 10.6.4;

$z = 20.5[2.7(32.25)]^{1/3} = 91$ kips/in. and

Bottom steel in x-direction $f_s = 10.3$ ksi,

which is less than 20.5 ksi; therefore the design is adequate for both interior and exterior exposure according to AASHTO 8.16.8 (*1*) or ACI 318–83, Section 10.6.4 (*8*).

The new design for the one-barrel culvert was also analyzed by the present program, and the results for the top slab are shown in Figure 8. A comparison of the two designs for this culvert is provided in Table 2 from which it can be seen that the second design provides a higher load-carrying capacity, primarily because of the different reinforcement arrangement. It is important to notice in Table 2 that for $S/E_c = 0.16$ (i.e., the surround stiffness is 0.16 of the concrete elastic modulus) the membrane contributes an additional 47 percent to the original case and 66 percent to the redesigned case. Also, a significant increase in the surround stiffness will not provide much higher capacities, as is clearly indi-

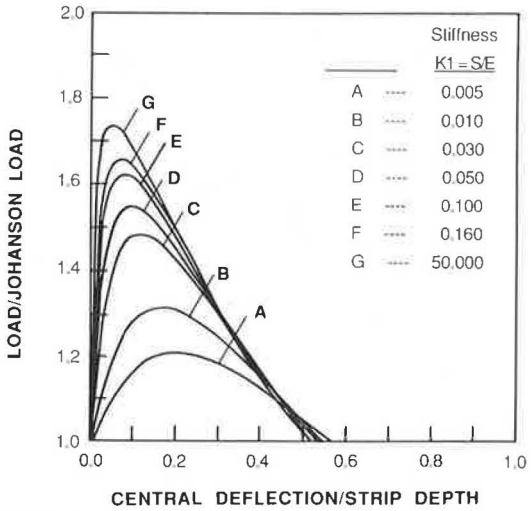

FIGURE 8 Analytical results for redesigned top slab.

TABLE 2 COMPARISON OF ELASTIC DESIGN AND DESIGN BY MEMBRANE APPROACH FOR THE TOP SLAB IN THE SINGLE-BARREL CULVERT

K1	Thickness, H1 (in.)	Span Length, L (in.)	Johansen Load Wj (lb/in.2)	Membrane Action Load, W (lb/in.2)	Strip Central Deflection, δ (in.)	Membrane Load, Johansen Load (W/Wj)	Central Deflection Thickness (δ/H1)
Elastic Design							
0.005	11.5	144	24.98	28.20	2.30	1.29	0.20
0.16	11.5	144	24.98	36.80	0.81	1.47	0.07
50.0	11.5	144	24.98	38.34	0.56	1.54	0.05
Membrane Design							
0.005	11.5	144	20.98	25.34	2.30	1.21	0.20
0.16	11.5	144	20.98	34.86	0.81	1.66	0.07
50.00	11.5	144	20.98	36.42	0.56	1.74	0.05

cated in Table 2 and shown in Figures 5–8. When the surround stiffness is increased from 0.16 to 50.0, the load capacity enhancement increases only from 1.66 to 1.74. The ratio S/E_c was chosen as a parameter for representing possible restraint conditions on in-plane slab motion. Here it is important to note that such restraint is actually not provided by the soil backfill; the end conditions of the slab are a major contributor (i.e., the connection and culvert walls have a major effect on the in-plane forces in the slab). As a result, a ratio of 0.16 is not extraordinarily high when all contributions to these restraining conditions are considered.

CONTROL OF CRACKING AND DEFLECTION

Structural serviceability is an important issue that needs to be addressed by the analyst and the designer. For cracking control (*1*, *8*), it was shown in the previous example that the modified design will assure that cracking will not become a problem. In the present case $z = 91$ kips/in., which is well below the limits (*1*, *8*), and therefore the design is acceptable. Nevertheless, the analyst should perform similar checks for other cases to verify that they meet code requirements.

It can be seen from Figures 5–8 that the deflections associated with the peak membrane capacity are approximately in the range $0.05 < \delta/h < 0.2$ depending on the surround restraint. For the top slab $h = 11.5$ in., which corresponds to a central deflection range of 0.57 in. $< \delta <$ 2.3 in. Because the span length is 144 in. these deflections lead to $0.004 < \delta/L < 0.016$. These values can be compared with recommended deflection control criteria (*1*, *8*) as follows: $L/180 = 0.8$ in. leads to δ/h values of about 0.07 for the top slab, 0.067 for the bottom slab, and 0.1 for the side slab. These values correspond to E/E_c ratios of about 0.16 for these slabs, as can be obtained from Figures 5–8. From the previous discussion on surround restraint (stiffness) it should be clear that these values are in line with existing conditions for the structure.

Another important comment that should be made is that under normal service conditions a structure is not loaded to its ultimate capacity. Therefore the anticipated normal deflections should be lower than those computed for peak resistance, and under such conditions there is no doubt that neither deflections nor cracking are serious problems when membrane action is considered.

CONCLUSIONS AND RECOMMENDATIONS

A modified analytical approach to the assessment of the behavior and design of cast-in-place reinforced concrete culverts was presented in this paper. This approach is based on the enhancement of the structural capacity of reinforced concrete slabs by the effects of in-plane forces that are provided through the jamming of the slab edges by adjoining structural elements. The membrane action mechanism was observed experimentally and is well documented (*4*).

The analytical method previously described can be employed for the analysis of cast-in-place reinforced concrete box culverts subjected to various loading conditions and encourages the user to employ engineering judgment before computer analyses. On the basis of information presented in the literature (*4*) and the results obtained in the present study (*3*), the following conclusions are drawn:

1. The present approach is simple for application to the design and behavioral assessment of cast-in-place reinforced concrete culverts. The consideration of membrane action enhancement provide good estimates of ultimate capacity and associated deflections.
2. Ultimate load is not reached at a sharp peak in the load-deflection curve, and structural capacity does not differ significantly from the ultimate value over a small range of deflections (Figures 5–8). Therefore the exact determination of the deflection at ultimate load may be unnecessary.
3. Strips with small L/h ratios are less sensitive to outward displacements at their ends than are strips with large L/h ratios. It is also evident that the surround stiffness (i.e., the restraint by adjoining structural elements) need not be enormous to achieve membrane action that is close in value to that for an infinitely rigid surround. Furthermore, the added load capacity on the order of about 10 percent does not justify the expense of providing a very stiff surround (i.e., $S/E_c = 50$ instead of 0.16, as shown in Figures 5–8).
4. The actual deflection cannot always be assumed to be accurate at maximum load. This is because the plastic theory curves do not hold for small deflections when the slab is acting elastically, or at greater deflections when the slab is acting elastically and partly plastically before the yield line pattern has fully formed. However,

this should not be a major problem if the slab is assessed to perform close to Point B in Figure 1.

5. The load-central deflection curves of Figures 5–8 for the strips tend to indicate the attainment of the maximum load at small central deflections. However, it should be noted that in the strip the whole of the positive moment yield section has the same deflection as the strip center. Thus strips (and one-way slabs) will reach ultimate loads at a smaller central deflection. Also, calculation of the ultimate load using the δ/h value of 0.15 may at first sight appear to be a crude approximation for these cases, but it can provide a practical estimate of loads and deflections. As briefly mentioned previously, the load-deflection curve is fairly flat near the ultimate load and the load is near ultimate load over a good range of deflections for stiff surrounds.

6. The use of compressive membrane action allows the designer to reduce the amount of reinforcement to less than that required by Johansen's yield line theory. For economical use of compressive membrane action, it is anticipated that the resulting reduction in the steel content of the slabs should be greater than the extra reinforcement that could be placed in the supports.

The results that were obtained by the present method demonstrate its effectiveness in evaluating the performance of the strips under consideration; however, further studies are needed to refine the approach and to evaluate it against experimental data. Also, the present approach should be reevaluated for complete slabs, rather than strips, and this should be performed by a combined experimental analytical study. The strength and safety of structures to be assessed by this approach need to be adjusted in light of similar requirements for other transportation structures (*1*). Furthermore, it is recommended that explicit contributions of the soil backfill in terms of surround stiffness be derived and a tool for optimal design of buried culverts be thus attained.

REFERENCES

1. *Standard Specification for Highway Bridges*, 13th ed. AASHTO, Washington, D.C., 1983.
2. M. G. Katona and P. D. Vittes. Soil-Structure Analysis and Evaluation of Buried Box-Culvert Designs. In *Transportation Research Record 878*, TRB, National Research Council, Washington, D.C., 1982, pp. 1–7.
3. T. S. Fares and T. Krauthammer. *Membrane Action Enhancement in Reinforced Concrete Slabs with Application for RC Box-Type Culverts.* Structural Engineering Report ST–85–01. Department of Civil and Mineral Engineering, University of Minnesota, Minneapolis, May 1985.
4. R. Park and W. L. Gamble. *Reinforced Concrete Slabs*. John Wiley and Sons, New York, 1980.
5. T. Krauthammer. Analysis of Shallow-Buried RC Box-Type Structures. *Journal of the Structural Engineering Division*, ASCE, Vol. 110, No. 3, 1984, pp. 637–651.
6. R. H. Wood. *Plastic and Elastic Design of Slabs and Plates*. Thames and Hudson; W.W. Norton Co., Inc., New York, 1961.
7. P. B. Hughes. *Limit State Theory for Reinforced Concrete Design*. Van Nostrand Reinhold Co., Inc., New York, 1976.
8. *Building Code Requirements for Reinforced Concrete*. ACI 318–83. American Concrete Institute, Detroit, Mich., 1983.
9. C. K. Wang and C. G. Salmon. *Reinforced Concrete Design*. Harper & Row, Inc., New York, 1985.
10. K. W. Johansen. *Yield-Line Theory*. Cement and Concrete Association, London, England, 1962.
11. K. W. Johansen. *Yield-Line Formulae for Slabs*. Cement and Concrete Association, London, England, 1968.

Publication of this paper sponsored by Committee on Subsurface Soil-Structure Interaction.

Practical Geotechnical and Engineering Properties for Tunnel-Boring Machine Performance Analysis and Prediction

PETER J. TARKOY

Given the ever-increasing range of geological conditions that can be and have been excavated by tunnel-boring machines (TBMs), both new and used, it behooves the industry to enhance the potential for mechanical excavation during the early stages of project conception and planning. Early planning will allow appropriate geological data and rock tests, necessary to clearly establish anticipated conditions, to be developed. Clear definition of anticipated conditions protects contractors from risk and owners from spurious claims. In this paper methods of estimating anticipated TBM performance are outlined and examples of analysis used on encountered TBM performance are presented. Methods outlined herein should only be used by persons who have appropriate TBM expertise. Analyses of past TBM performance are essential to prediction. In effect, prediction and analysis are related, one feeds the other.

More than 125 years have passed since the first tunnel-boring machine (TBM) was built and 30 years have passed since the first successful TBMs were built by Robbins and Jarva in the 1950s. In the last 15 years an increasing number of tunnel projects and the availability of used machines have made it possible to excavate marginal tunnel projects by TBM. The growing TBM lifespan is reflected by an increasing number of new ventures that specialize in rebuilding used TBMs.

After a method of predicting TBM penetration rates and cutter wear was provided by Tarkoy *(1–5)*, the focus shifted to the prediction of TBM utilization. Prediction of utilization was outlined in a paper by Tarkoy *(3)*. Since then, more refined methods based on extensive TBM performance data and analyses have been developed. Refined methods permit the preparation of accurate, reliable, and responsible estimates of TBM penetration rates, cutter costs, and as many as 20 categories of TBM downtime.

In the last 15 years, TBM case history data have been collected and microcomputers have been introduced. This combination of events has permitted detailed analyses of performance data, heretofore impractical. The microcomputer facilitated development of a large TBM data base with a wide variety of TBM performance, backup system, project management, and geotechnical variables.

Custom software, originally developed on mainframes for analyzing encountered TBM performance *(1, 2)* and later moved to microcomputers, was used to prepare detailed estimates of anticipated TBM performance *(3)*. With the development of generic software, such as electronic spreadsheets, it was possible to develop simpler, faster, and more flexible methods of estimating TBM performance on a microcomputer.

Estimating anticipated TBM performance with the microcomputer-based system relies on a large data base that represents a wide variety of conditions and produces estimates that would have been impractical to calculate otherwise.

102 North Main Street, Sherborn, Mass. 01770.

Unique and economical advantages of TBM excavation have been put to widespread use, even in marginal conditions, and the commensurate benefits are being reaped. The greatest benefits of TBM excavation can be enjoyed when mechanical excavation is considered during project conception and planning.

CONSIDERATIONS FOR TBM PROJECTS

TBM excavation must be considered at an early stage to

1. Establish accurate economic and technical TBM feasibility,
2. Plan exploration to provide information necessary to prepare an optimum design and a competitive bid for TBM excavation,
3. Design a project to enhance the capabilities of a TBM and minimize the effect of its limitations, and
4. Successfully execute TBM excavation and project completion.

During the various stages of project development, increasingly more complex and detailed information is necessary and becomes available. Consequently, TBM excavation feasibility, anticipated performance, project design, and costs can be recalculated and refined.

Project Feasibility Stage

Mechanical excavation is generally more economical than conventional tunneling, particularly on longer tunnels. Therefore it is essential to determine TBM excavation feasibility at project conception and enhance the planning, exploration, design, bidding, and construction for mechanical excavation. On the basis of simple feasibility-level exploration, it is possible to evaluate TBM feasibility and prepare comparative estimates of conventional and TBM excavation.

Decisions made by planners and designers in the early stages of conception have the greatest impact on project cost. Therefore it is essential that planners and designers avail themselves of current state-of-the-art knowledge and experience regarding exploration, design, contracting, bidding, and excavation using TBMs. It is important that

1. Exploration be appropriate to anticipated conditions and anticipated type of construction equipment and methods,
2. Geotechnical testing be appropriate to anticipated conditions and anticipated type of construction equipment and methods,
3. Rock testing include total hardness (H_T) for all rock units to be encountered, and

4. Construction expertise for anticipated conditions be utilized during project conception.

Feasibility Exploration

Feasibility exploration consists of a fact-finding survey that is generally limited to a literature search, simple establishment of route alignment, preliminary design and selection of preliminary construction methods, and preparation of a feasibility estimate. The exploration program is established on the basis of the information obtained from the fact-finding survey. Typical sources are summarized in Table 1.

General geology, lithologies, structure, water table, and major features can be determined during the feasibility phase to provide information adequate for evaluation of TBM (penetration, utilization, advance rate, cutter costs) feasibility. However, the preliminary exploratory program does not provide sufficient information for design or construction and further investigations are required.

Local and Pertinent Experience

Armed with fundamental and general knowledge of geology and geologic conditions of the proposed site and a catalog of local and similar tunneling and excavation experience, it is possible to establish

1. Experience in similar geological conditions,
2. Local tunnel excavation costs, and
3. Local experience with similar excavation methods.

It is important, however, to ascertain that conditions and methods are truly comparable. The types of excavations that may be surveyed include

1. Transportation (railroad, highway, subway) tunnels;
2. Water and sewer tunnels;
3. Hydroelectric and associated tunnels;
4. Mine access and development tunnels; and
5. Other applicable excavations.

Feasibility Estimate of TBM Performance

Rock hardness directly affects TBM penetration and cutter costs. Indirectly it also affects downtime, which in turn inversely affects utilization and advance rates. For very rough and general estimates, penetration rates and cutter costs can be determined from known average rock properties shown in Figure 1 and applied to empirical relationships between total hardness and TBM penetration rates (Figure 2) and between total hardness and cutter costs (Figure 3). Quantitative calculation of penetration rates and cutter costs may be supplemented by case histories, summaries of TBM experience, and reports of TBM performance to provide a rough estimate of utilization and to permit calculation of shift and daily advance rates.

Utilization is proportional to total hardness (Figure 4) and directly dependent on a variety of interrelated factors that are more difficult to define. These factors include various elements of project management and the TBM backup system available to deal with geotechnical conditions, both expected and unexpected. Utilization is also inversely proportional to TBM diameter.

Utilization greater than 30 percent should not be used for feasibility estimates unless a detailed study is carried out or specific utilization requirements are stated in the contract specifications, or both.

Project Exploration Stage

Exploration, design, and construction are inextricably intertwined and cannot be considered separately. Inasmuch as the design depends on geological conditions, the type of geological exploration necessary will depend on the design and construction methods envisioned.

Objectives and Scope of an Exploration Program

The objectives of an exploration program are simply to satisfy the needs of the parties involved. The owner's need is to have a facility that is suitable for the purpose intended, compatible with the existing environment (urban or rural), and constructable at the lowest possible cost.

The engineer's need is to have the information necessary to permit the selection of optimum location, design, and construction methods in order to provide the facility at the lowest cost.

The contractor's needs must be served to permit him to choose the most appropriate and cost-effective equipment and methods. In addition, a contractor must estimate progress and costs related to excavation, stabilization, support, lining, and any potential problems.

The primary goal of exploration has classically been to provide a minimal amount of information for design. The needs of the contractor require more detail than those of the owner or designer because construction is much more sensitive to geological conditions than is design.

Consideration of excavation by TBM, particularly under marginal, difficult, or challenging conditions, brings with it the added responsibility of providing geotechnical information essential to TBM performance prediction. In other words, TBM excavation requires that results of pertinent and appropriate rock testing be made available to bidders so that more competitive and responsible bids can be made.

The competitive bidding environment is conducive to optimism, particularly when information to the contrary is lacking. Therefore optimism may lead to unsupportable differing site condition claims, which can be prevented by leaving little to interpretation.

Professional geotechnical interpretation by the owner or his engineer, made available at bidding time, should define clear and reasonable anticipated conditions, methods of evaluating encountered conditions, and methods of establishing legitimate claims of differing site conditions, should they occur.

Factual data relevant to TBM excavation are not considered adequate for prebid interpretation. Providing professional interpretation of anticipated conditions and comments regarding TBM performance is considered essential to assure that all contractors are bidding the same conditions and have reasonable expectations. Presentation of factual data during bidding permits and promotes a wide variety of interpretations and optimism by individuals least familiar with the project and its geology and least qualified to interpret those data.

TABLE 1 SUMMARY OF FEASIBILITY EXPLORATION METHODS

Category	Specific Items
Archives	Plans of old civil structures, shorelines, former watercourses, swamps, and fill areas
Regional	Physiography; geomorphology; drainage patterns; geologic material characteristics; and soil, agricultural, glacial, bedrock, and structural maps
Literature	Textbooks (geomorphology, physiography); city search (original topography, shorelines, archive maps, etc.); county (soils and geologic maps, water well data); universities (geology, civil engineering, agricultural, mining and minerals); state (geological and water surveys, agricultural experiment station, mining and minerals, wells and boreholes for oil, gas, and minerals); tourist pamphlets; federal (U.S. Geological Survey, Bureau of Mines, Bureau of Reclamation, USDA Forest Service)
Maps	Country; airline (physiographic); highway (highway alignments, other features); American Association of Petroleum Geologists (geologic and highway); state geology and soils; county (agricultural experiment station, land use, topographic, geologic, landform analyses)
Remote sensing	Aerial photography, multispectral scanning, radar sensing imagery, infrared imagery (useful to determine lithology, structure, groundwater conditions)
Local experience	Excavation of any type, quarries and mines, road construction cuts, water wells, borings
Site visit	Geology, physiography, field mapping, surficial features, sources of water, highways, railroads, chemical plants, gas pipelines, structures

Ambiguities in such data promote either large contingencies or optimistic assessment of anticipated conditions. Optimism invariably results in differing site condition claims, which make the project costlier than when interpretations are provided.

Definition of anticipated ground behavior and comments about construction performance leave little room for interpretation and thus establish a common basis for all estimates, bids, and adjudication of bona fide differing site conditions.

It is clear that a great deal of the responsibility rests with the owner and his engineer. This is appropriate because they are involved from the inception, for the longest period of time, and throughout the project. They produce the geotechnical reports and contract documents and are most familiar with all relevant conditions. The contractor is generally involved only during the bidding period, which may be as short as 1 to 2 months.

Detailed geotechnical information will decrease the uncertainties to which mechanical excavation is uniquely sensitive. The magnitude and nature of an exploratory program should be determined on the basis of the

1. Importance (use and cost) of the project to be constructed,
2. Nature of site geology,
3. Sensitivity to construction methods and equipment, and
4. Evolution of exploration with project design to suit geotechnical conditions.

There is no standard scope for an exploration program; instead, its sophistication varies with the complexity of the project and its geology and with method of construction, funds available, and parties involved.

The responsibility for organizing and developing exploration for the design and construction of a project should lie with an individual who has qualifications that include knowledge of general geology, intimate knowledge of engineering geology, familiarity with geotechnical engineering associated with design of a structure, intimate familiarity with construction equipment and methods, and an understanding of costs associated with construction methods.

Exploration and Testing for TBM Excavation

It is important for the director of exploration to be familiar with the latest exploration, testing, and empirical relationships, particularly those relevant to TBM excavation equipment and methods. Table 2 gives a summary of common field exploration data that are pertinent and must be acquired for determining construction methods, equipment, and behavior. Laboratory tests relevant to construction and anticipated rock behavior must also be provided (Table 3).

Preliminary Selection of Construction Methods

During the initial stages of exploration, potential construction methods should be selected to tailor and provide appropriate exploration, preliminary design, and rock tests for all construction

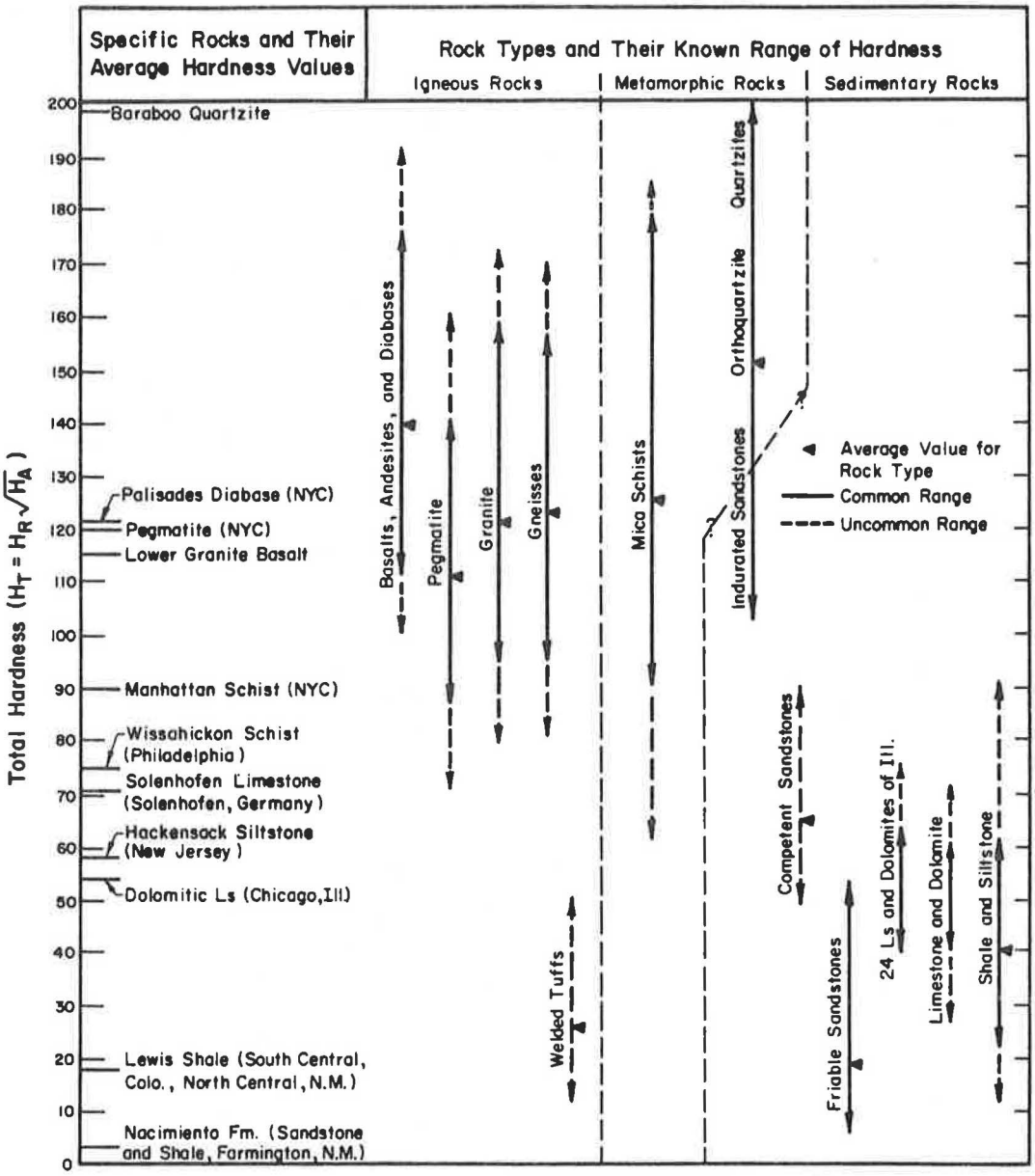

FIGURE 1 Total hardness for common rock types bored by TBM.

alternatives being considered. To assist with evaluating the appropriateness of TBM excavation on a particular project, the advantages and disadvantages can be summarized as follows:

- Advantages
  - High and predictable excavation rates
  - Continuous (noncyclical) excavation
  - Smooth bore, hydraulic advantage
  - Less disturbance of the rock
    - Negligible overbreak
    - Less support (about 10 to 20 percent of drill-and-blast support)
    - Less water inflow
    - Increased inherent safety
  - Tunnel may stand permanently unsupported
  - Concurrent concrete lining is possible
- Disadvantages
  - 6- to 12-month lead time to manufacture new TBM
  - High initial capital expenditure
  - Difficult or limited access to the face (probe drilling, grouting, presupport)
  - Impractical to change excavation method if problem develops

A preliminary selection of mechanical excavation, at an early stage of the project, will enhance the consideration of the inevitable savings for initial support, less overbreak, and final support. In competent rock, a lining may be unnecessary because it is possible to take advantage of the hydraulic properties of a smooth machine-bored tunnel. Support methods that are incompatible with TBM tunneling should be avoided. Exploration and testing must provide information required for predicting anticipated TBM penetration, downtime, and cutter wear.

Project Design Stage

The choice of design is interrelated with the method of construction. Unless the structure can be built (economically), the

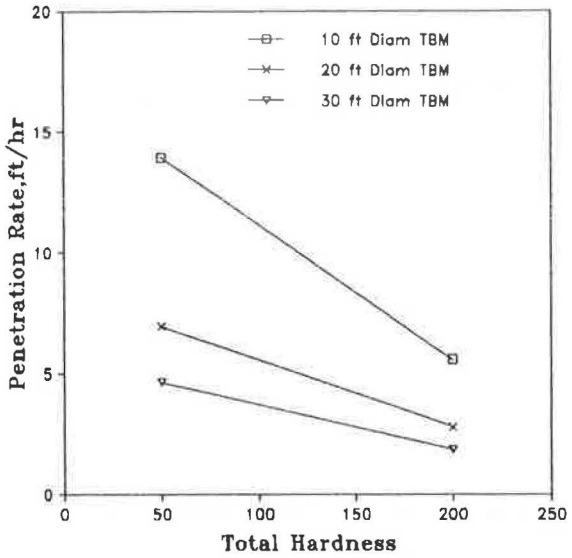

FIGURE 2 Empirical relationship between total hardness and TBM penetration.

REGRESSION EQUATION:
Cutter Cost, $/CY = (Total Hardness x .07) -- 0.46

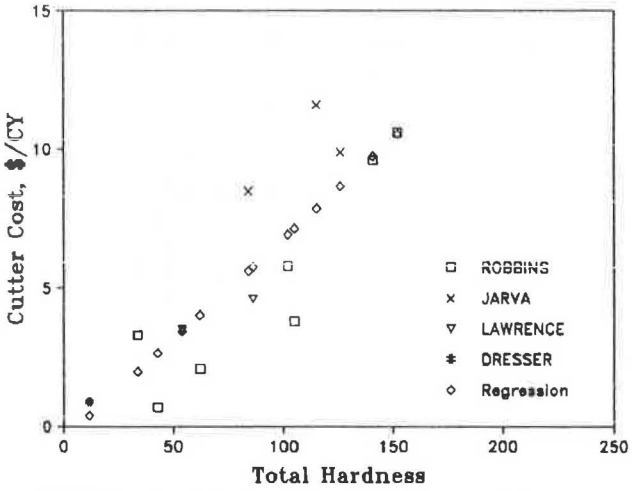

FIGURE 3 Empirical relationship between total hardness and TBM cutter costs.

design will never come to fruition. When the preliminary design is envisioned, anticipated construction methods should be selected and associated cost estimates prepared.

The design of a project is based on the requirements of the desired facility and the ability to construct the facility at a reasonable and lowest possible cost. In other words, design must reflect geological conditions as well as economic constructability. Consequently, it is clear that geology is the independent variable and design and construction are the dependent variables. As a result, the importance of geology and geotechnical properties of the site becomes much more apparent.

Selection of Excavation and Support Methods

Some of the major reasons why TBM excavation is commonly selected are

1. Economic considerations (faster and cheaper excavation),
2. Imposed time limitations (faster project completion),
3. Design advantages (unlined hydraulic properties),
4. Cost advantages (less initial and final support), and
5. Imposed environmental limitations (noise, vibrations).

Many choices can be made no later than the project design stage. These choices fix the cost and approach throughout exploration, design, and construction. Changes are costly and associated with delays and claims.

TBM excavation will generally require less support than conventional excavation for the same ground conditions. The effect of supports on costs in a TBM tunnel will be the result of decreased excavation rates and the cost of materials and installation. The method of support must be structurally adequate and compatible with the high penetration and advance rates common with TBM excavation. Compatibility of the support and excavation system can have a profound effect on excavation rates.

Common tunnel support systems, in decreasing order of desirability for TBM excavation, are as follows:

1. Unsupported,
2. Rock bolts,
3. Steel ribs and lagging,
4. Precast segments and liner plate,
5. Surficial protective epoxy and coatings,
6. Gunite and shotcrete, and
7. Spiling or forepoling.

An attempt should be made to select support that requires consistent crew sizes, occasions no delay or stoppage of the excavation system, and has no adverse effects on the equipment (shotcrete).

Unsupported tunnel requires no downtime for support. Spot bolting can generally be maintained without downtime by assigning one or more drillers. Pattern bolting will require a large enough crew of drillers and chucktenders with drills to handle twice the average anticipated penetration rate.

Precast segments and ribs and lagging will require a crew and support-erection equipment adequate to prevent downtime while advancing at double the average anticipated penetration rate. In the case of steel sets, the crew may have to be adjusted continuously, depending on rock hardness, penetration rate, and advance, to prevent downtime.

The placement of protective coatings to prevent deterioration of the rock may be performed without downtime only if an adequate crew and well-maintained equipment are provided.

Application of gunite or shotcrete, installation of spiling and forepoling, and installation of a combination of supports will generally require a total shutdown of TBM excavation.

Classification schemes are available for predicting support requirements in tunnels; however, few if any take into account the effect of mechanical excavation. For general purposes (no allowance was made for diameter), Table 4 may be used to establish anticipated TBM support. Common practice provides for pattern bolting in TBM tunnels larger than 15 ft in diameter.

Design Considerations for TBM Excavation

Design considerations to minimize construction cost, enhance successful excavation, and optimize advantages of TBM excavation are given in Table 5. Unusual anticipated conditions that may affect tunnel excavation should be identified early in project

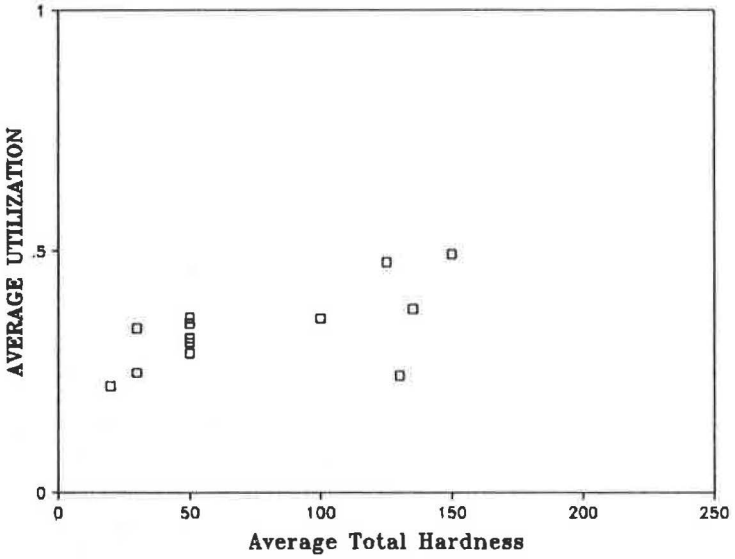

FIGURE 4 Experience with total hardness and TBM utilization.

TABLE 2 EXPLORATION DATA FOR TUNNEL CONSTRUCTION

Exploration Method	Useful Data Provided
Core logs	
Rock type	Inherent and unique rock characteristics
Core recovery	Quality of the rock mass
Fracture index	Rock rippability (*6*, p. A7)
Rock quality designation	Rock quality *(1)*, rippability (*8*, p. A47)
Drilling rate	Relative rock hardness for boreability, cuttability, and rippability *(2)*
Discontinuities	Rock structure, behavior, and stability
Core sampling	Necessary for determining rock properties by testing
Nx	Preferred core size for testing
Triple tube	Preferred samping equipment especially under marginal rock conditions
Field seismic velocity	Rippability and rock quality *(9, 10)*
Acoustic probing	Cost-effective method for locating top of rock
Water testing	Required for determining permeability, water quality for effect on structural concrete, and toxic gases

TABLE 3 ROCK PROPERTIES PERTINENT TO TUNNEL CONSTRUCTION

Test	Application
Thin section analysis	Lithology and fabric for hardness
Unit weight	Design of lining
Hardness	
Total hardness (H_T)	Boreability by TBM *(2, 3)*
Point load	Roadheader cuttability *(11)*
Uniaxial strength	Rippability *(12)*
	Rough estimates of TBM penetration *(2)*
Modulus	Deformability and design of lining
Shale durability	Stability of excavated surfaces
Laboratory sonic velocity	Rippability *(9)*

development. For example, the incidence of faults, shears, weathered and altered rock, high in situ stresses, water inflow, and infiltration of gasses along the tunnel alignment can have disastrous consequences on tunnel excavation unless they are taken into account in the design of tunnel, support, construction system, and TBM.

Project Bidding Stage

At the time of bidding the primary goal of the owner's and engineer's exploration is to produce clear, concise data to promote a narrow spread of low-cost construction bids devoid of large amounts allocated for contingencies. The contract documents and data should also serve to protect the contractor in the event that conditions worse than anticipated are encountered. Thus the risk (and contingencies) of encountering high-impact features without hope for compensation or the inclusion of costly allowances for contingencies is eliminated.

The objective is simply to have bidders bid the same geological conditions, to exclude contingencies for geological uncertainties,

TABLE 4 COMMON SUPPORT TYPES USED IN TBM-EXCAVATED TUNNELS

	Rock Quality Designation				
Rock type	0–25 (very poor)	25–50 (poor)	50–75 (fair)	75–90 (good)	90–100 (very good)
Igneous	E	D-E	C-D	B	A
Metamorphic					
Foliated	E	D-E	C-D	B-C	A-B
Nonfoliated	E	D-E	C-D	B	A
Sedimentary					
Sandstone	E	D-E	C-D	B	A
Shale	E	E	D-E	C	A-B
Limestone	E	D-E	C-D	B	A

Note: A = bald, unsupported; B = spot bolting; C = pattern bolts; D = pattern bolts and straps; and E = ribs and lagging, precast segments, etc.

TABLE 5 TUNNEL DESIGN TO ENHANCE TBM EXCAVATION

Consideration	Remarks
Tunnel length	Provide maximum length of tunnel per contract and per single run; minimum 5 to 15,000 ft
Adverse conditions	Avoid Faults Joints at adverse angles to tunnel alignment Faults at adverse angles to tunnel alignment Water inflow, salt water inflow
Geometric limitations	Avoid Sharp curves Downgrade excavation Steep inclines and declines Small-diameter access shafts Unusually large-diameter machines Noncircular tunnel section if possible, otherwise permit drill-and-blast over-excavation to desired shape
Undesirable methods	Shotcrete, gunite, forepoling, steel ribs Grouting ahead of the face Probe drilling ahead of the face
Access	Provide easy access to the work area and tunnel portal or shaft for installation of the TBM; for long tunnels, provide periodic access through shafts for mucking and utilities
Construction schedules	Construction schedules should provide for TBM manufacturing and delivery and permit access to development work to receive TBM; provide adequate power on site before bid
Mobilization cost	Part of the TBM cost should be allowed in the mobilization costs

and to protect the contractor from encountered conditions worse than anticipated.

Although by bidding time owners and engineers may be satisfied with their knowledge of anticipated site and project conditions, contractors are only beginning to familiarize themselves in the limited time of 1 to 2 months allowed for the bid. The contractor takes the risk that his conception, interpretation, and approach are reasonable. It is at this stage that communication between the owner or engineer and the contractor becomes crucial.

Essential Information

As stated earlier, it is essential to provide results of exploration and rock testing (total hardness), descriptions of geotechnical conditions (jointing, faulting, water inflow, etc.), project design, contract language, conditions, and considerations appropriate to TBM excavation.

Selection of Construction Methods

At the bidding stage, conventional and machine excavation alternatives may have been preselected. However, if alternatives still exist, the geotechnical consultant and estimators require information to evaluate the most economic alternative. The selection is usually made by the contractor on the basis of economy, scheduling, availability of equipment, and ability to deal with anticipated conditions.

Evaluation of Prebid Conditions

The estimator, engineering geologist, or geotechnical engineer must be intimately familiar with construction methods and equipment. Fundamental responsibilities for geotechnical assessment require

1. Review of all pertinent literature and available information;
2. Review of all contract documents, boring logs, material samples, test results, geological reports, and specifications;
3. A site visit to examine and photograph geological and physical conditions, alignment, perimeter, adjoining structures, and so forth;
4. Gathering of data, experience, and analytical methods pertinent to the project;
5. Additional investigation and testing, if necessary; and
6. Quantitative opinions regarding anticipated construction conditions, performance, and potential problems.

Data and methods used for evaluation of TBM feasibility are too general and rough for prebid estimating. Project-specific data and methods must be used to estimate construction performance. Project data should be provided in the contract documents. Case history experience and empirical relationships should be developed in-house by the contractor or the geotechnical consultant.

The contractor's need to know can be summarized by, "Where, what, and how much?" To answer this question, it is necessary to consider

1. Excavation methods and support requirements,
2. Rate of progress,
3. Water and gas infiltration,
4. Any other conditions affecting tunnel construction, and
5. Materials and equipment that will be required.

The quantitative answers to these questions will be the foundation of a responsible, accurate, reasonable bid.

MEASURE OF TBM PERFORMANCE

Universal terms established to measure TBM performance are as follows:

1. Penetration rate (ft/hr) = Length of tunnel bored (ft per shift)/Elapsed boring time (hr per shift)
2. Utilization (%) = Elapsed machine time (hr per shift)/Excavation shift time (hr per shift) = Total shift time − Downtime
3. Cutter costs, $\$/yd^3$ or \$/ft of tunnel

The term "downtime" is used to define the nonutilization of the TBM. The advance rate, a combination of the penetration rate and utilization, is the unit most commonly used in estimating.

4. Downtime (%) = Total shift time − Machine time
5. Advance rate (ft/day) = Penetration rate × 24 hr × Utiliza-

tion (for three 8-hr shifts). Ft/shift = Penetration rate × 8 hr × Utilization (for an 8-hr shift)

"Availability" was the term used in the past to imply reliability when TBM breakdowns were common. It is no longer used because there is no universal agreement on its definition and it is therefore misleading.

GEOTECHNICAL PROPERTIES THAT AFFECT TBM PERFORMANCE

Feasibility of TBM excavation is based on the ability of a TBM and associated backup system to perform under the average and the most adverse geological and tunneling conditions. Consequently, it is necessary to define both average and most adverse anticipated geotechnical conditions for the alignment. Project costs and conditions, TBM design, and backup system variables must be specified to accommodate these conditions.

Average Conditions

The average geological conditions are the basis for design of the TBM and preparation of the construction estimate. The TBM, excavation backup system, and project management are designed for the average anticipated conditions in terms of support requirements, utilities (e.g., water pumping and discharge facilities, ventilation for gassy tunnels, mucking system capacity), and crew sizes to deal with average anticipated conditions. Average conditions are used to calculate average performance (penetration, utilization, cutter consumption, and advance rate). Average performance is the basis on which the estimate is prepared.

Average conditions are defined by the intact rock properties in terms of the total hardness (H_T). Rock mass properties affected by the extent, orientation, and characteristics of rock structures (joints, faults, and shears); rock mass characteristics [weathering, alteration, rock quality designation (RQD), stress conditions] and permeability; and mass behavior (squeezing, swelling, slaking, water inflow, and gas infiltration) all intimately influence tunnel stability and support requirements.

Adverse Conditions

Adverse geological conditions are those that are worse than the average anticipated conditions. These conditions must be evaluated carefully because their spatial extent and their degree of severity will significantly affect TBM performance and may alter feasibility or even constructability. Adverse conditions may consist of intact as well as rock mass properties.

Harder-than-anticipated rock or more extensive hard rock than anticipated is effectively an adverse condition. Both will decrease penetration and increase cutter costs. Unusually high cutter loads will be required for efficient cutting of occurrences of hard rock.

Hard rock no longer has the disastrous effect that it did in the earlier history of TBM development. High rock hardness has had different effects on performance of TBMs depending on their mechanical design. Advances in the state-of-the-art TBM design (cutter bearings, cutter metallurgy, cutter profiles, maximum sustainable cutter loads) have extended the limit of rock materials that may be bored economically and successfully.

Intact Rock Properties

Rock hardness is the most relevant property for evaluating TBM excavation performance. The rock property that is most commonly used to predict TBM penetration rates and cutter costs is total hardness (H_T), which is based on Schmidt (L-type) hammer hardness (H_R) and the modified Taber abrasion hardness (H_A), supplemented by the Shore (D-type) scleroscope hardness (H_S). These tests are described elsewhere *(13, 14)* (Table 6).

A number of unsuccessful attempts have been made to use other mechanical rock properties to predict TBM performance. Many of the test methods are nonstandard, inapplicable to boreability, proprietary, and of limited use because the property and performance relationships are unproven in the literature.

Total Hardness

Total hardness is determined from two individual tests, namely, the rebound hardness (H_R) and abrasion hardness (H_A) tests. Total hardness (H_T) is equal to

$$H_T = H_R(H_A^{1/2})$$

The range of total hardness for common rock types is shown in Figure 1.

Total hardness has been empirically related to TBM penetration rates *(1, 2, 13–15)*, utilization *(3)*, and cutter costs *(3, 4)*. These relationships have been successfully used to predict accurate anticipated TBM performance for contractors' estimates.

Total hardness was developed specifically to make reliable predictions of TBM performance *(2)*. A study funded by the National Science Foundation was based on extensive field work (collection of cores from bored tunnels), field experience based on TBM shift reports, and laboratory testing of core collected from bored tunnels. The objectives of the study were to

1. Develop empirical relationships between rock properties and TBM performance,
2. Study the effects of mechanical design of machine and cutting structures on performance,
3. Document the effects of mechanical design of machine and cutting structures on performance, and
4. Document case history data for use in evaluation of TBM feasibility for future projects.

The results were reported in part by Tarkoy *(1, 13, 14)* and in their entirety by Tarkoy *(2)* and Tarkoy and Hendron *(15)*. Subsequent development through experience on more than 100 projects was incorporated in the estimating method reported by Tarkoy *(3)*.

Detailed test specifications have been described *(13)* and have also been submitted to the American Society for Testing and Materials for standardization.

The Schmidt rebound hardness (H_R) is determined by taking readings using a calibrated Schmidt (L-type) hammer on Nx core seated in a standard core cradle. H_R tests were designed to be performed on Nx (2⅛-in.-diameter) core. Although Nq (1⅞-in.-diameter) core may be used with inserts in the test anvil, it has been noted from experience *(2)* that the use of Nq core may yield

TABLE 6 SUMMARY OF ROCK HARDNESS TESTS FOR TBM PERFORMANCE, AFTER TARKOY *(13)*

	Hardness Test	Description	Remarks
H_R	Schmidt (L-type) hammer hardness (calibrate and determine correction factor)	10 readings taken with core mounted in standard anvil; five highest readings are averaged; use correction factor	Best for mass property measurements because contact point is (1.3 cm) larger than scleroscope point
H_S	Shore scleroscope (D-type) hardness (calibrate and determine correction factor)	20 readings taken with core mounted in standard anvil; 10 highest readings are averaged; use correction factor	Contact point is fine (1 mm); therefore measurements more accurately represent individual grains and crystals, but statistical sampling must be taken and averaged for mass properties; can be used to estimate H_R if necessary when sample breaks during H_R test
H_A	Modified Taber abrasion hardness	Two Nx-sized discs (0.6 cm thick) abraded for 400 revolutions on each side; determine weight loss; use average values of two discs; H_A = 1/ weight loss (g)	This test is sensitive to factors that influence small-scale strength, shearing, crushing, and abrasion
H_T	Total hardness	$H_T = H_R/(H_A^{1/2})$	The rock hardness properties that correlate best with TBM performance in terms of penetration rates, repair and maintenance, and cutter consumption

lower readings than does Nx core. For that reason, it is useful to determine the Shore scleroscope hardness (H_S) to estimate H_R.

H_S is useful as an indicator of rock hardness and has been related to TBM penetration rates *(2)* with limited success. H_S is also useful in estimating the Schmidt (L-type) hammer rebound hardness (H_R) when samples are too small for testing or when they break during testing with the Schmidt (L-type) hammer *(2)*.

To have a complete set of dependable total hardness (H_T) test results, in spite of rock breakage during testing and the effect of undersized (Nq instead of Nx) core, the values of H_R were projected from the H_S values as described by Tarkoy (2, pp. 74, 78, Figure 5.6). This method was used by Tarkoy *(2)* and is used as standard laboratory practice. The values of H_R thus determined were also used to calculate total hardness (H_T).

The modified Taber abrasion hardness (H_A) is determined by taking two ⅛-in.-thick slices of Nx core and abrading each side for 400 revolutions on a modified Taber abraser. The inverse of the average weight loss is taken as the abrasion hardness (H_A). The prescribed modifications of the equipment and the testing procedure must be followed to produce consistent and accurate results. Detailed specifications for the modification of the Taber abraser are available from the author.

To obtain consistent and accurate results, equipment, equipment modifications, and detailed testing procedure must be followed precisely according to prescribed methods. Detailed specifications for the fabrication of the core cradle are available from the author.

Other Tests

The unconfined compressive strength (q_u) is not reliable for predicting TBM performance, particularly in foliated or other relatively anisotropic rock. Empirical relationships nevertheless have been developed between strength and penetration rates *(2)* for relatively homogeneous rock such as limestones, sandstones, and horizontally bedded shale. Uniaxial strength (q_u) is unnecessary yet useful in high-strength rock as an indication of the normal cutter load (F_n) necessary for efficient rock breakage.

The point load index is a simple test often used in lieu of the unconfined compression test because it is easier to perform. The test was originally described by Broch and Franklin *(16)*. Descoeudres and Rechsteiner *(17)* used a modified version of the test to relate to penetration. The correlation was poor and considerable judgment had to be exercised to reduce the scatter.

Results from the point load test are less reliable and consistent than are those from the uniaxial strength test. Furthermore, the point load test was originally meant to be applied to rocks of low strength, less than 10,000 psi (68.9 MPa), and preferably 5,000 psi

(34.4 MPa). It has since been applied (with special redesign) to testing of lumps that have an index (I_s) as high as 58,000 psi.

Rock Mass Properties

Rock mass properties affect TBM performance directly by requiring downtime to deal with adverse conditions. Indirectly, familiarity with anticipated rock mass properties is essential in the design of the TBM and backup systems to minimize downtime associated with adverse geological conditions such as squeezing ground, support placement, and protection against and countermeasures for dealing with water inflow. TBM system design for adverse rock mass conditions is intended to eliminate downtime and adverse effects on performance.

Joint Spacing

Jointing has been considered, overoptimistically, beneficial to TBM boreability. The beneficial effect of discontinuities depends on their spacing, attitude, and characteristics as well as the cutter head (false face, scraper, muck bucket, cutter mounts) design. The characteristics and orientation of discontinuities continually change along the tunnel length, and they interact with and are masked by other variables. Thus the difficulty of quantitatively defining the effect of jointing on boreability is compounded by the scarcity of substantiating data.

Field experience confirms that, for all practical purposes, adverse effects of discontinuities overshadow beneficial effects. The adverse effect of jointing on boreability occurs when joints are totally absent or very closely spaced.

Faults, Shears, and Weathered and Altered Rock

When faults, shears, shear zones, and weathered and altered rock are encountered, the physical conditions include soft, blocky, squeezing, and swelling rock (causing the TBM to get stuck) and associated water inflow. These conditions generally require installation of heavy supports. When such conditions are anticipated, the facilities for shielded support, support placement behind the TBM, and protection against water must be included in the TBM design to avoid downtime and the inevitable decrease in TBM performance.

High-Stress Conditions

Stress conditions may be encountered by a TBM as a result of

1. High in situ stresses,
2. Squeezing rock,
3. Swelling rock,
4. Slaking rock, and
5. Loosening of rock blocks.

The loosening of rock blocks can generally be prevented by initial support if a shield and subsequent primary rock support are used. Similarly, slaking can be prevented by protection of the susceptible material with shotcrete; gunite; or, more economically, epoxy sealant.

High in situ stresses, squeezing, swelling, and slaking that cause inward movement generally cannot be prevented and should be included in TBM design. Tunneling in such rock results in

1. Stresses exceeding material strengths and causing rock failure,
2. Squeezing of material around the TBM, and
3. Stress relief failure on tunnel wall around the gripper.

Water Inflow

Intact rock is relatively impermeable and rock permeability is controlled by secondary features (discontinuities) that make the definition of rock permeability difficult. Consequently, prediction of water inflow from a rock mass is inevitably no more than an educated guess. Nevertheless, the following information is necessary to estimate anticipated water inflow:

1. Hydraulic head above the tunnel,
2. Intact and rock mass permeability,
3. Storage capacity of the rock mass,
4. Recharge potential, and
5. Location of major conduits or inflows in the tunnel.

A reasonable way of establishing the range of rock mass permeability is to use the intact rock permeability as a lower limit and the highest permeability test results (usually in a permeable discontinuity) as the upper limit.

The method proposed by Goodman et al. *(18)* can be used to take into account the average rock permeability and the high permeability of discontinuities. Using this method, an average "background" inflow can be calculated using the intact rock permeability and the tunnel surface area. Similarly, local high inflows can be calculated using the permeability of joints and faults, appropriate spacing, and surface areas on the tunnel wall. The two flows should be averaged proportionately. The process requires sound judgment and must be tempered with professional experience.

Because water inflow cannot be avoided, there are a number of countermeasures that can be incorporated in the TBM design to protect it from water and to minimize the effect that water may have on construction performance.

Infiltration of Gasses

The accumulation of hazardous (toxic, flammable, asphyxiating, and radioactive) gasses is the second leading cause of injuries and fatalities in underground construction. Although it is difficult to estimate rate of gas infiltration in typical civil construction, subjective judgments can only be developed with factual information about potential gas conditions.

Although little can be done to prevent gas infiltration, there are a number of countermeasures that can be incorporated in the design of the TBM and backup system to minimize the effect on TBM performance.

Tunneling by machine in gassy (and water-bearing) conditions is safer than by conventional methods because

1. There is less disturbance and fracturing of the surrounding rock,
2. Continuous and consistent ventilation is possible at the face,
3. A TBM can be manufactured to be explosion proof,
4. Continuous TBM excavation is less likely to produce gas concentrations, and
5. Continuous monitoring at the tunnel face is easy with a TBM.

Other Adverse Conditions

High rock temperatures are uncommon for most civil tunnels; however, TBMs have been used extensively in deep underground mining applications in which high temperatures are normal. Problems associated with existing high temperatures have been and can be solved through TBM and backup system design.

ESTIMATE OF ANTICIPATED TBM PERFORMANCE

Basis of Estimate

Estimates of TBM performance are based on empirical relationships that have been developed between total hardness (H_T) and

1. Penetration rates *(1, 2)*,
2. Utilization *(3)*,
3. Maintenance and repair *(3)*, and
4. Cutter consumption *(3, 4)*.

The method was enhanced by

1. Including subsequent experience with more than 100 projects,
2. Continuing research, and
3. Refining the method of estimating TBM performance.

The empirical relationships and the method of predicting TBM performance *(3)* have been used extensively to provide the basis for contractors' tunnel excavation estimates. Results have been field tested in a number of cases in which prebid and postbid data were available; results have been within 5 percent of anticipated performance.

Project and Construction Assumptions

Project, TBM, and backup system assumptions are the foundation of a performance analysis. TBM performance estimates rely strictly on these assumptions and must be consistent with anticipated conditions. Important assumptions, given in Table 7, strictly control TBM performance.

Calculation of Anticipated TBM Performance

Penetration rates and cutter wear may be determined from total hardness (H_T), machine design, and cutter design. Downtime prediction is based on backup system design and construction experience. An example of a detailed cost appraisal reported by Persson and Schmidt *(19)* has been computerized *(3)* for prebid evaluation of TBM performance.

The emergence of microcomputers has radically changed traditionally subjective and qualitative methods of estimating TBM performance. Availability of generic software, particularly spreadsheets, has facilitated the refinement of TBM performance-estimating methods.

TBM Penetration Rate

The rate of penetration is calculated from empirical relationships based on total hardness (H_T) as shown in Figure 2. The design configuration of the TBM (cutter head rotational rate, cutter gauge velocity, cutter forces, cutter spacing, cutter type and diameter, etc.) is selected from empirical relationships. The empirical relationships between rock properties and TBM performance associated with respective TBM design variables will assist in designing the TBM that has the highest penetration rate to deal with anticipated geotechnical conditions.

TBM Downtime

Total downtime may be calculated for as many as 26 different categories. However, downtime generally falls into the categories given in Table 8.

Calculated downtime and geological downtime are generally determined in units of minutes per shift hour. Downtime based on case history experience and prevented downtime are usually available as a percentage of total excavation shift time. All downtime is converted to minutes per shift hour and back into percentage of total excavation shift time to calculate utilization.

Determination of many of the downtimes requires circular calculations with numerous iterations to obtain a stable number. This is a result of interrelated variables and relationships. For example,

TABLE 7 PROJECT ASSUMPTIONS THAT AFFECT TBM PERFORMANCE

TBM	Cutters	Project	Backup System
Head diameter	Cutter type	Tunnel diameter	Cutter change
Stroke length	Gauge velocity	Lunch time	Stroke cycle
Total thrust	Cutter spacing	Shift change	Support
Total torque	Normal cutter load	Repair and maintenance	Mucking
Cutter head drive	Tangential cutter load	Precautions for gas	Utilities
Cutter head rpm	Cutter costs	Union regulations	Engineering
Gripper size	Cutter diameter		Electric delays
Gripper bearing	Cutter geometry		Conveyor delays
Weight/grip	Cutter material		Crew size
Structural strength			

TABLE 8 DETERMINATION OF TBM DOWNTIME

Determined by	Category of Downtime
Calculation	TBM regrip/stroke
	Change trains
Geology	Frequency of cutter changes
Experience	Time to change cutter
	Unpredictable (breakdowns) downtimes
Prevention	Backup system design
	Support system capacity double average rate
	Mucking system capacity double average rate
	Contractor's job setup (planned repair and maintenance, review of performance records, etc.)
	TBM construction experience

at a faster penetration rate, more tunnel is excavated per hour and the more often the TBM has to be regripped/restroked; thus the amount of time available for excavation decreases in that hour. Consequently, the less excavation time in an hour, the less often downtime is required to reset the machine.

The new generation of electronic spreadsheets available for microcomputers has made it possible to do these circular iterations easily. Penetration rate can thus be calculated for each geological unit along the tunnel alignment *(3)*.

TBM Utilization

Utilization is calculated by subtracting the total percentage of downtime from unity. Unity is a single shift, day, or excavation shift hour. However, utilization should be calculated on a daily basis if a daily maintenance shift or period is set aside from the excavation shift. Maintenance shifts or periods outside the normal 24-hr day, such as on weekends, are not included in the estimation of utilization.

Experience has shown that utilization can range from a low of 10 percent (TBM excavation in a mine environment with a low priority) to an average of 30 percent. Utilization as high as 75 percent has been achieved on a number of projects with careful backup system design, aggressive project management, positive preparation, and flexibility for the unanticipated.

For bidding purposes, utilization should not be estimated directly from Figure 4. A direct estimation of utilization is unacceptable for bid estimates because many variables, such as the effect of TBM diameter and backup system, cannot be taken into account.

TBM Advance

The advance rate is calculated by using the penetration rate and projecting it for the shift time during which the machine is operating. It is the common unit used for bidding and for determining feet per shift, day, week, or month.

TMB Cutter Wear and Costs

Cutter costs may be determined from the total hardness and the empirical relationships shown in Figure 3. More precise results require the contractor's proprietary experience and empirical relationships between total hardness and cutter rolling path life and complex relationships that include cutter gauge velocity, cutter forces, and cost of cutter parts. Cutter costs can then be calculated for each geological unit along the tunnel alignment *(3)*.

TBM Design Considerations

The design of the TBM is as important as the TBM performance estimate. TBM design must take into account all of the anticipated intact rock properties, rock mass properties, average conditions, and adverse conditions in order to perform as anticipated. TBM design must also be consistent with assumptions made during estimating the variables given in Table 7.

TBM Mechanical Variables

The mechanical variables that have the greatest influence on penetration rate and cutter costs are fixed at the time of manufacture and cannot be varied during the excavation of the tunnel. They are

1. Normal cutter load (F_n),
2. Tangential cutter load (F_t),
3. Cutting coefficient (F_t/F_n),
4. Cutter head rotational rate (rpm), and
5. Cutter spacing.

The penetration of a cutter is proportional to the cutter normal load (F_n). The thrust must be adequate to provide the required normal cutter load (F_n) for each of the cutters and the additional thrust load necessary for pulling the backup equipment.

After the cutter has penetrated the rock as a result of the normal force that has been applied to it, a tangential cutter load (F_t) must be applied for the cutter to continue to pass through the rock with the given depth of penetration. The torque necessary to provide the tangential force can be calculated by taking the sum of the tangential forces and their respective moment arms.

The cutter head rotational rate determines how often the cutters pass over the face in a given unit of time. The rotational rate is limited by the maximum allowable gauge cutter velocity, which results from mechanical considerations associated with available horsepower, and torque.

For all practical purposes, the cutter spacing is generally fixed within relatively narrow limits (2.5 to 4 in.) when the TBM is designed and built. Cutter spacing is determined on the basis of the strength and hardness of the rock. This variable should be determined in association with the TBM manufacturer.

The evaluation and selection of a TBM should be done on the basis of forces available at the cutter-rock interface, mechanical variables, machine structural strength, available optional equipment, cost, design and manufacturing experience, innovative expertise, and field performance of the manufacturer's equipment.

Backup System Variables

The backup system should be designed specifically for anticipated conditions and should include

1. Muck disposal (conveyor, gantry, track, train, and portal-shaft systems);

2. Installation of utilities (water, air, water discharge, ventilation, and track);
3. TBM shield for high stresses and swelling and squeezing ground;
4. Rock support facilities;
5. Protection against water (waterproofing, probing, and grouting);
6. Countermeasures for gassy ground;
7. Countermeasures for high temperatures;
8. Routine maintenance programs; and
9. Crew size.

To sustain average anticipated penetration rates, the capacity of the mucking system must be adequate to keep up with peak penetration rates. Similarly, high advance rates can only be sustained with a crew size adequate to install utilities (water, air, discharge, rail, electric) and support (drills, bolts, ribs, etc.) at peak advance rates.

In blocky, squeezing, swelling, and slaking ground that can cause loosening or inward movement, a slotted roof or full shield may be required for support until temporary support can be installed. Slotted roof shields are adequate for blocky rock; however, a full shield capable of a decrease in diameter is generally necessary in squeezing and swelling ground. Past experience in swelling and squeezing shales, in shears, and in faults has shown that the ability to decrease the diameter by 2.5 percent is inadquate. In one case in which a machine became lodged by squeezing ground, the TBM was redesigned to act as a walking blade shield capable of very-large-diameter changes in excess of 10 percent.

In blocky rock, fallout at the face may cause jamming of rock between the cutters and the face and in the muck openings. Damage to the cutters and buckets is usually controlled with a false face and grillwork on the buckets.

TBM design to protect components against damage by water inflow and adverse effects on excavation performance are given in Table 9. Countermeasures to deal with gassy underground excavation can be summarized as follows:

- Limit ignition sources by using explosion-proof equipment,
- Continuous probing for gas-producing features,
- Degasification by tunnel ventilation or predrainage,
- Provide air turbulence to prevent dangerous concentrations,
- Safety training of all engineers and personnel, and
- Provide monitoring of hazardous gasses at tunnel face with automatic shutoffs.

Countermeasures for excavation under high-temperature conditions include ventilation or the use of water heat exchangers for hydraulic oil and drive motors. In small-diameter tunnels with high TBM power requirements, drive motor cooling may also be used for dust suppression and cooling at the face.

Although routine maintenance is not an absolute requirement, it will minimize the occurrence of unexpected downtime at inopportune times. Routine maintenance is best carried out during the boring cycle and other extended and unavoidable downtimes. For example, during cutter changes that are limited to a few crew members, greasing, lubricating, and filling of hydraulic tanks can also be accomplished.

ANALYSIS OF ENCOUNTERED TBM PERFORMANCE

Analysis of encountered TBM performance is essential to maintaining case history data; TBM experience for evaluating feasibility; and reliable empirical relationships among geological conditions, rock properties, and TBM performance for estimating TBM performance and evaluating differing site condition claims.

TABLE 9 TBM DESIGN FOR ANTICIPATED WATER INFLOW

Objective	Design Component
Protection against water	Forced or pressurized main bearing seal lubrication
	Waterproof motors and electrical system
	Overhead protection from water
Limit effect of water	Ribbed low-angle conveyor at least for the TBM
	Deeply troughed and flashed conveyor
	Buckets designed to rescoop wet sloppy spilled muck
	Narrow bucket openings to prevent muck spillage
Countermeasures	TBM design for drilling probe and grout holes
	TBM design to permit easy access for grouting
	Enough water pump, discharge, and disposal capacity
Construction management	On site, closely monitoring construction
	Planned alternatives
	Maintenance of detailed construction records

Analyses provide a better understanding of TBM excavation and potential for TBM application and performance enhancement. Results of construction performance analyses have been and are used to predict, prevent, and focus on developing problems as well as to solve existing problems.

Analysis of performance concurrent with construction permits monitoring and improvement of TBM performance. Graphic performance data displays permit correlation with geological conditions, and planning of repair and maintenance allows project management to be the cause of efficiency rather than at the mercy of TBM downtime.

Four types of TBM performance analyses are commonly used:

1. Excavation progress and major delays;
2. Performance (penetration, utilization, advance, cutters);
3. Downtime; and
4. Excavation efficiency.

TBM Major Delay Analysis

The TBM major delay analysis is simply a velocity chart; that is, the cumulative length of tunnel (x-axis) excavated is plotted against cumulative shift time (y-axis). Any substantial vertical jog in the line indicates a major delay (generally more than 24 hr).

This type of plot is used to provide a summary of construction progress and identify major delays. It can also be prepared on the same scale as available surface or tunnel geological mapping for correlation with geological conditions. An example of such a plot is shown in Figure 5.

TBM Performance Analysis

Variables used to quantify TBM performance are penetration rate, utilization, advance rate, and cutter costs. Results of analyses consist of as many as 100 variables per day; thus graphic presentation is necessary for comprehension. A plot along tunnel length permits comparison of tunnel geology and performance. TBM performance variables may also be plotted against cumulative shift time to illustrate performance variables as a function of elapsed time as shown in Figure 6.

Penetration will often be related to changes in rock hardness and lithologies, particularly changing lithologies in a sequence of sedimentary rock.

Utilization is indirectly related to encountered geological conditions and directly related to the TBM backup system design for dealing with those conditions. Utilization reflects backup system design and construction management available to deal with encountered adverse conditions.

The cutter replacement plot lags behind cutter wear and cannot be related to concurrent geological conditions. The cutter plot has illustrated cutter damage sustained as a result of improper TBM operation in a small-radius curve. The cutter replacement data have also been instrumental in the identification of unusual cutter wear problems. Cutter rolling path life has also been graphed; however, cutter changes may have an inordinately high effect on

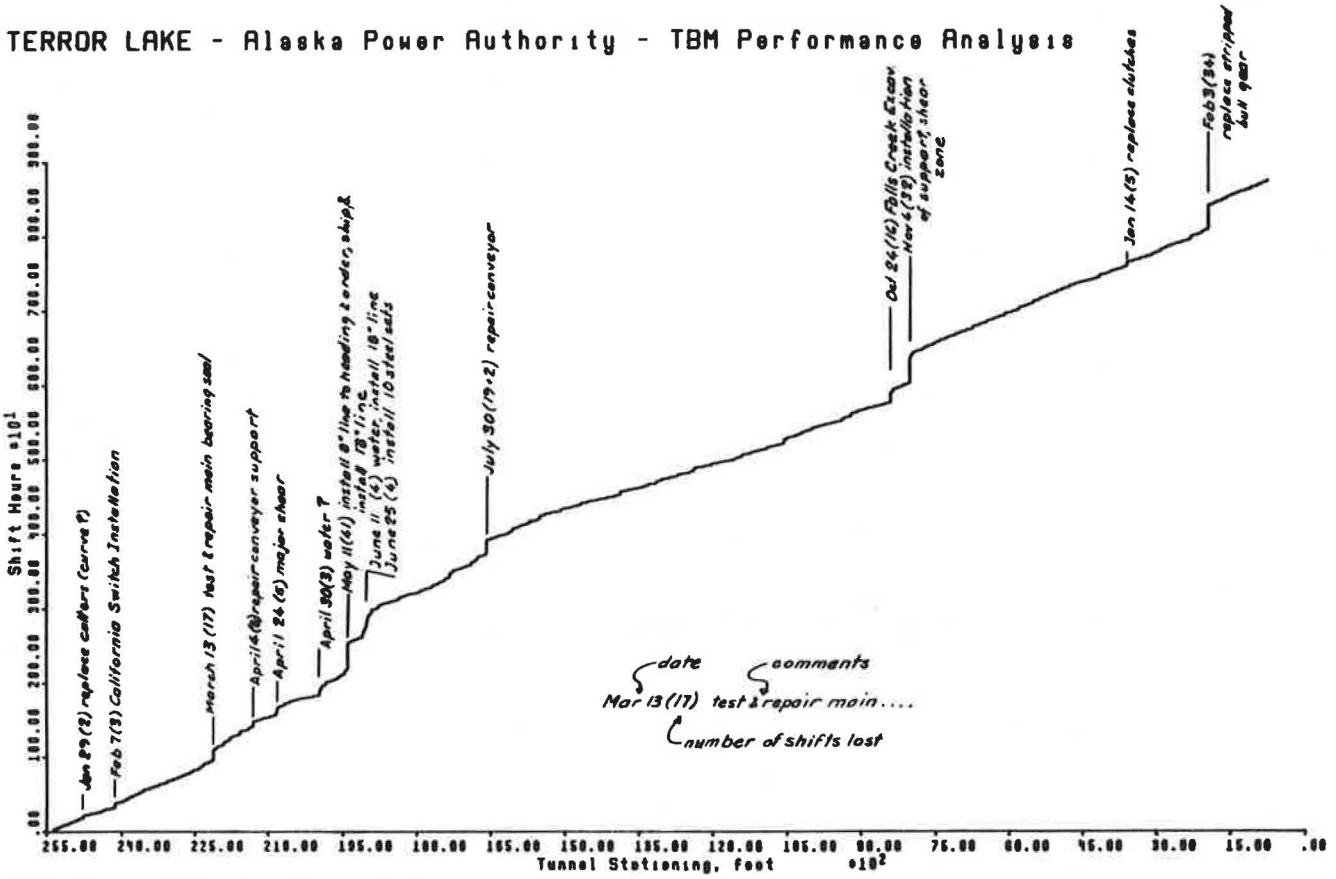

FIGURE 5 TBM major delay analysis.

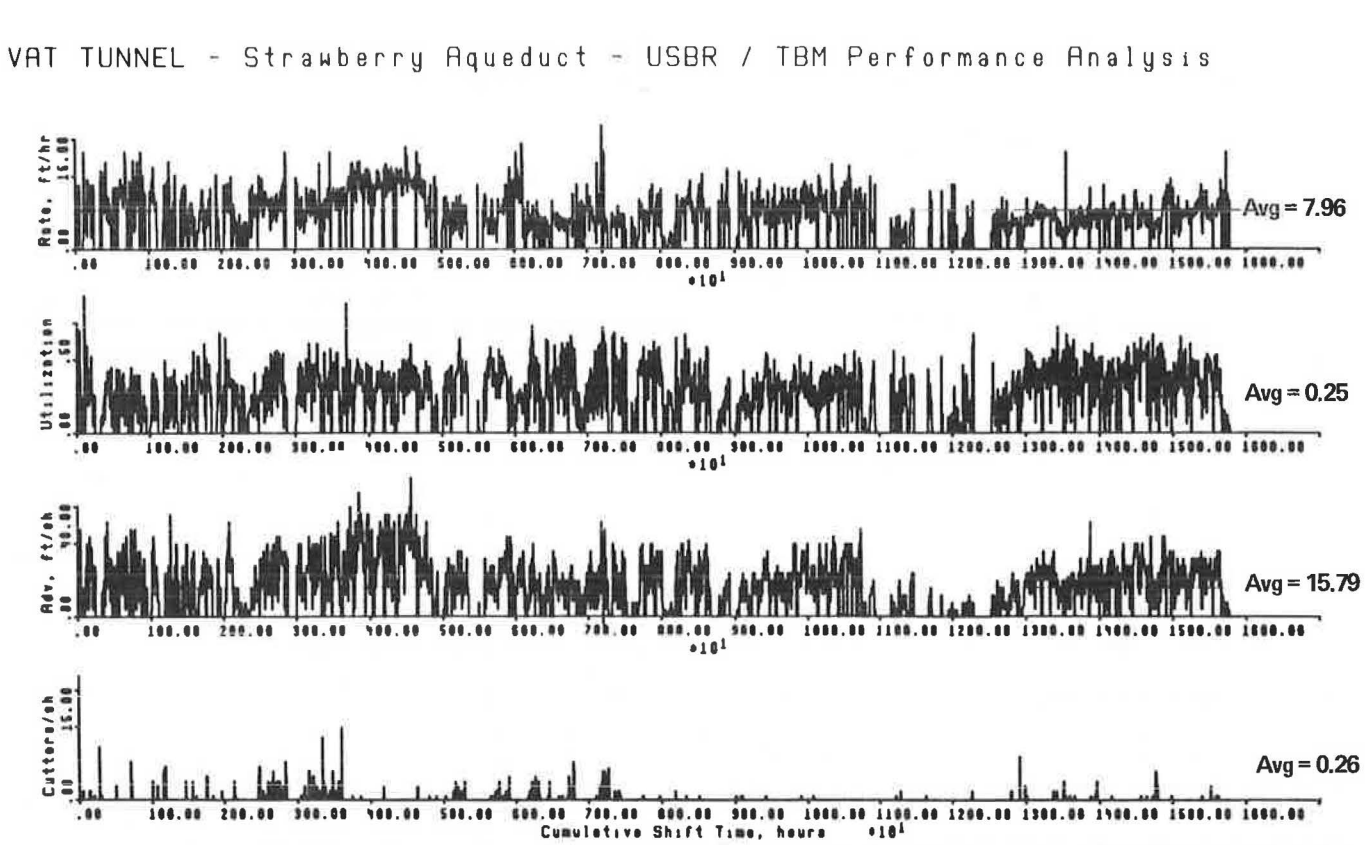

FIGURE 6 TBM performance analysis along tunnel alignment.

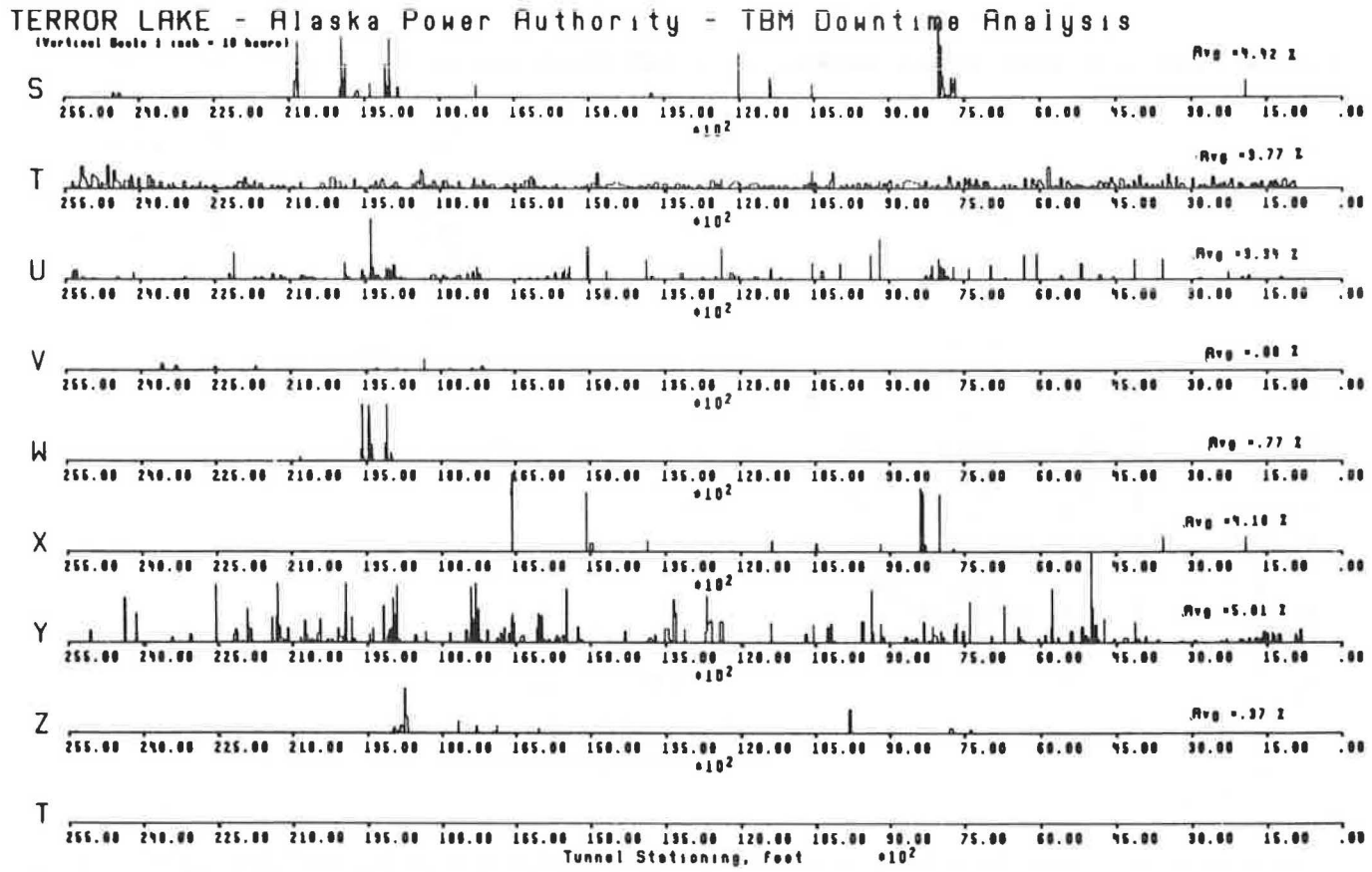

FIGURE 7 TBM downtime analysis along tunnel alignment.

average rolling path life in the early stages of the project and a subdued effect in later stages.

TBM Downtime Analysis

The analysis of downtime is used to define, identify, summarize, and illustrate the effect of specific operations and geological conditions as they relate to TBM downtime.

An example of TBM downtime sustained along a tunnel alignment is shown in Figure 7. It is easy to identify and relate geological conditions that are associated with downtime in this manner. A summary of total project downtime (in as many as 26 categories) is useful as case history data for estimating TBM downtime. It has also been used successfully to resolve differing site condition claims.

One such claim involved an 8-month delay caused by time lost to install additional and unanticipated support. Analysis of all shift records resulted in a summary of all downtime. The actual documented lost time for all support, including anticipated and unanticipated support, amounted to less than ½ month. Needless to say, the differing site condition claim was promptly resolved.

TBM Excavation Efficiency Analysis

TBM performance data in association with crew sizes and manhours worked are useful for evaluating construction efficiency during construction or later for evaluating differing site condition claims. For example, in one case it was alleged that water inflow was the cause of all delays. A plot of lineal feet of tunnel excavated per manshift illustrated that production efficiency was decreasing and continuing on a downward trend long before high water inflows were encountered in the 14th week, as shown in Figure 8.

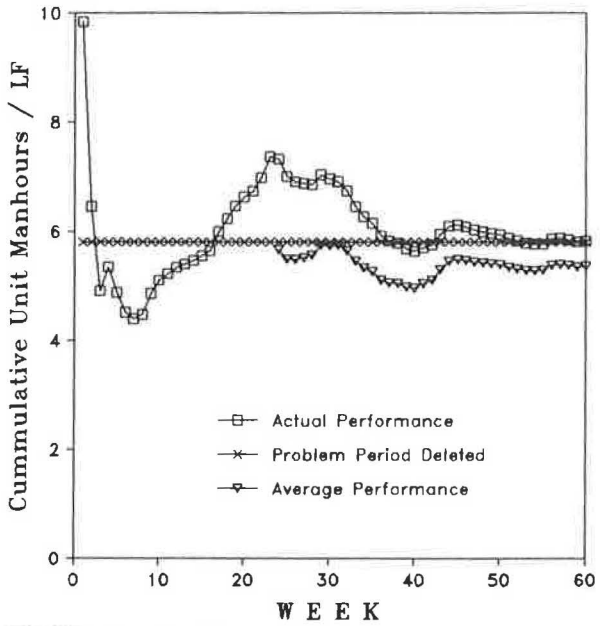

FIGURE 8 Tracking efficiency of tunnel construction.

CONCLUSIONS

Although an increasing number of projects have utilized TBMs, in many instances the design has not provided for mechanical excavation because of a lack of familiarity with TBM excavation and construction economics on the part of the designer. Similarly, many tunnel projects excavated by conventional methods could have been excavated more economically, expeditiously, and with less risk had the designers recognized the potential cost and time saving associated with a well-planned TBM excavation.

The future of TBM excavation lies in a wider application of TBMs in adverse ground conditions, an increase in backup system capacity for substantial increases in performance, ability to bore larger diameters and in harder rock, and lower cutter costs.

It is possible to increase the quantity and quality of bored tunnels by the application of state-of-the-art technology (geotechnical and TBM) at project conception and during initial planning.

REFERENCES

1. P. J. Tarkoy. "A Study of Rock Properties and TBM Advance Rates in Two Mica Schist Formations." *Proc., 15th ASCE Symposium on Rock Mechanics*, Custer State Park, South Dakota, Sept. 1973, pp. 415–447.
2. P. J. Tarkoy. *Rock Hardness Index Properties and Geotechnical Parameters for Predicting Tunnel Boring Machine Performance.* Ph.D. dissertation. University of Illinois, Urbana, Sept. 1975, 327 pp.
3. P. J Tarkoy. "Predicting Raise and Tunnel Boring Machine Performance: State of the Art." *Proc., 4th Rapid Excavation and Tunneling Conference*, Atlanta, Ga., June 1979, pp. 333–352.
4. P. J. Tarkoy. "Excavation in Hard Rock." In *Short Course on Engineering Geology in Construction Excavation*, Association of Engineering Geologists, Brentwood, Tenn., Oct. 1980.
5. P. J. Tarkoy. Tunneling Machine Performance as a Function of Local Geology. *Association of Engineering Geologists Bull.*, Vol. 18, No. 2, May 1981, pp. 169–186.
6. J. A. Franklin, E. Broch, and G. Walton. Logging the Mechanical Character of Rock. *Transactions of the Institution of Mining and Metallurgy* (Section A), Vol. 70, 1971.
7. D. U. Deere. Technical Description of Rock Cores for Engineering Purposes. *Rock Mechanics and Engineering Geology*, Vol. 1, 1963, pp. 18–22.
8. A. M. Muir-Wood. Discussion. *Transactions of the Institution of Mining and Metallurgy* (Section A), Vol. 81, 1972.
9. *Handbook of Ripping*, 5th ed. Caterpillar Tractor Co., Peoria, Ill., 1975, 33 pp.
10. D. U. Deere and R. P. Miller. *Engineering Classification and Index Properties for Intact Rock.* Technical Report AFWL–TR–65–116. Air Force Weapons Laboratory, Kirtland AFB, New Mexico, Dec. 1966, 308 pp.
11. I. McFeat-Smith. Rock Property Testing for the Assessment of Tunnelling Machine Performance. *Tunnels and Tunnelling*, March 1977.
12. B. Boden, G. West, and C. J. Harrad. Tunnels in Mining and Civil Engineering—Common Ground. *Tunnels and Tunnelling*, Vol. 7, No. 3, May 1975, pp. 61–67.
13. P. J. Tarkoy. "Predicting TBM Penetration Rates in Selected Rock Types." *Proc., 9th Canadian Symposium on Rock Mechanics*, Montreal, Quebec, Dec. 13–15, 1973.
14. P. J. Tarkoy. "Rock Index Properties to Predict Tunnel Boring Machine Penetration Rates." *Proc., 2nd Rapid Excavation and Tunneling Conference*, San Francisco, Calif., June 1974 (abstract only); complete paper available from National Technical Information Service, Springfield, Va. 22151.
15. P. J. Tarkoy and A. J. Hendron, Jr. *Rock Hardness Index Properties and Geotechnical Parameters for Predicting Tunnel Boring Machine Performance.* Available from National Technical Information Service, Springfield, Va. 22151, Document No. PB 246293 or RA–T–75–030.
16. E. Broch and J. A. Franklin. The Point-Load Strength Test. *Interna-*

tional Journal of Rock Mechanics and Mining Science, Vol. 9, 1972, pp. 669–697.
17. F. Descoeudres and G. Rechsteiner. Etude des correlations entre la geologie, les propriétés mecaniques et la forabilité des roches de Crespera-Gemmo. *Schweizerische Bauzeitung*, March 1973, pp. 9–16.
18. R. Goodman, D. G. Moye, A. Van Schalwyk, and I. Javandel. Groundwater Inflows During Tunnel Driving. *Association of Engineering Geologists Bull.*, Vol. 2, No. 1, Jan. 1965, pp. 39–56.
19. P. A. Persson and R. L. Schmidt. Mechanical Boring or Drill and Blast Tunneling. 1st U.S.-Swedish Underground Workshop, Swedish Detonic Research Foundation, Stockholm, Dec. 1976.

Publication of this paper sponsored by Committee on Tunnels and Underground Structures.

Experimental Study of Buried Fiber-Reinforced Plastic Pipe

NAFTALI GALILI AND ITZHAK SHMULEVICH

An experimental study of interaction between soil and fiberglass-reinforced plastic pipes was performed in a large laboratory soil box. Seven pipe specimens of different diameters and stiffnesses were tested at various loads and under various laying conditions. Sand and clay were the soil backfill. Five different and independent sets of measurements were taken in each test: vertical and horizontal pressures in the backfill soil, normal and tangential stresses at the pipe-soil interface, radii of curvature of the pipe, vertical and horizontal pipe deflections, and hoop strains at the internal and external perimeters of the pipes. Measurements were taken during backfilling and when superimposed pressures were applied. Short-term effects of load, soil type and density, split backfill, and installation quality on pipe performance were considered. The main findings of the study are analyzed and discussed in qualitative terms.

Flexible pipe-soil interaction has been studied extensively during the last decade. However, few experimental studies (*1, 2*) have been done on the response of fiberglass-reinforced plastic (FRP) pipes to different loads and laying conditions. Several numerical methods, all based on finite element analysis, have been developed to predict the behavior of buried pipes. These theoretical evaluations have to be proved experimentally, especially those of the range of flexible pipes the strains and deflections of which when buried may be considerably affected by uneven soil construction.

The purpose of the present study was to obtain data in well-controlled laboratory conditions as a contribution to the knowledge of the behavior of buried FRP pipes. In particular, it was intended to provide answers to some practical questions, such as the possibility of safely replacing the usually recommended granular backfill, entirely or partly ("split backfill"), by the available in situ cohesive soil and the effects of well-compacted or poorly compacted haunches.

Faculty of Agricultural Engineering, Technion-Israel Institute of Technology, Technion City, Haifa 32000, Israel.

METHOD

Experimental Setup

Seven pipe specimens, each 2.0 m (78.7 in.) long with outside diameters ranging from 400 to 1028 mm (15.75 to 40.47 in.), wall thicknesses of from 6.0 to 15.7 mm (0.24 to 0.62 in.), and stiffnesses ($STIS = EI/D^3$) of from 1.19 to 10.84 kPa (0.172 to 1.515 lb/in.^{2}) were tested in a large rigid laboratory soil box. A list of the tested pipes is given in Table 1. Two types of soil were used as backfill material: a fine uniform sand (SP) and a terra rossa clay (CH). Soil classifications are given in Table 2; details of the mechanical properties of the soils are given in Table 3.

TABLE 1 MECHANICAL PROPERTIES AND DIMENSIONS OF THE TESTED PIPES

Pipe Code	Outside Diameter, D_0 (mm)	Wall Thickness, t (mm)	Pipe Stiffness, $STIS$ (kPa)
A	400	6.0	1.35
B	618	8.0	1.19
C	1,028	13.4	1.24
D	616	15.7	10.84
E	616	8.2	1.27
F	630	13.5	5.28

Note: 1 mm = 0.039 in.; 1 kPa = 0.145 lb/in.2.

Superimposed loads were applied to the surface of the soil backfill through a rubber membrane at the bottom of a semicylindrical steel cupola fixed to the top of the box and filled with pressurized air. Measurements were taken close to the midway cross section of the pipes. The measuring instrumentation included

TABLE 2 SOIL CLASSIFICATION

Type of Soil	Uniform Classification	Specific Gravity	Liquid Limit (%)	Limit of Plasticity (%)	Plasticity Index (%)	Graduation: Percentage Passing by Weight Through Standard Size No. 4	No. 10	No. 20	No. 40	No. 100	No. 200
Clay	CH	2.69	71	25	46	99.6	98.2	97.1	96.3	95.1	94.2
Sand	SP	2.66	–	–	–		99.8	98.6	97.8	31.2	1.8

TABLE 3 SOIL PROPERTIES

Type of Soil	Compaction Standard Proctor (%)	Angle of Friction (degrees)	Cohesion (kN/m^2)	Unit Volume Weight (kN/m^3)	Confined Modulus, *Ms* (kPa)
Sand (SP)	85	29.7	–	14.48	4,100
	90	31.9	–	15.34	10,100
	98	33.7	–	16.70	18,800
Clay (CH)	80	14.0	23.1	13.72	910
	85	18.6	24.3	14.59	1,590

Note: 1 kN/m^3 = 6.24 lb/ft^3; 1 kPa = 0.145 $lb/in.^2$.

• Thirteen soil pressure transducers were placed in different locations in the soil box. The transducers were a commercial diaphragm strain gauge type with 88 mm (3.46 in.) sensitive surface diameter and 20 mm (0.89 in.) disk thickness. Six transducers were used to measure the vertical soil pressure distribution across the width of the soil box, 0.25 m (10 in.) above the crown of the pipe, as shown in Figure 1 (7–12 in the figure); six more (1–6) were used for measuring the horizontal soil pressure. An additional transducer (13) measured the pressure under the rubber membrane.

• Ten Cambridge-type plane-stress transducers (*3*) were used for measuring both normal and tangential stresses at the pipe-soil interface. The transducers were mounted so that the surfaces of the cells were flush with the surface of the pipe. Their location is shown in Section A-A of Figure 2.

• Twenty-four strain gauges were bonded to each pipe specimen to measure hoop strains (Section B-B in Figure 2). Special measures were taken to prevent temperature and moisture effects (*4*).

• Changes in diameter lengths were measured by a sliding, spring-loaded linear potentiometer. Two such gauges were installed in the pipe (Figure 2) to determine pipe deflections in vertical and horizontal directions. The vertical and horizontal deflections were also measured manually.

• A radius of curvature meter (RCM) was developed for measuring the radius of curvature of the deflected pipe. The RCM device consists of a commercial dial-gauge mounted on a small three-wheel carriage and moved on a premarked perspex strip that was bonded to the inner circumference of the pipe (Figure 3). This procedure was applied to ensure the correct location of the carriage

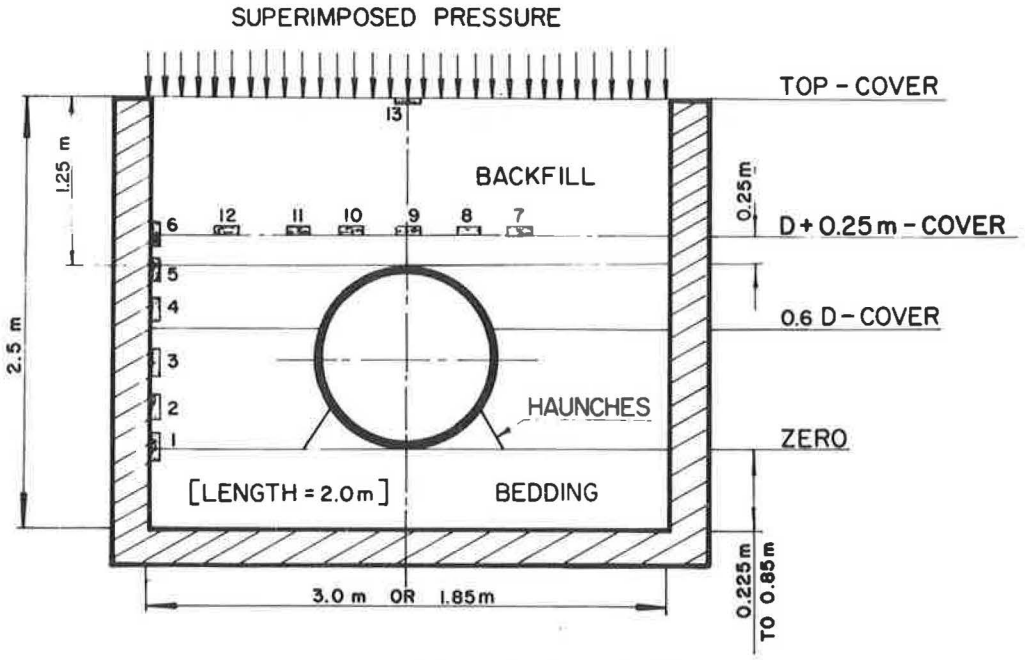

FIGURE 1 Cross-sectional view of soil box with pipe and soil-pressure transducers.

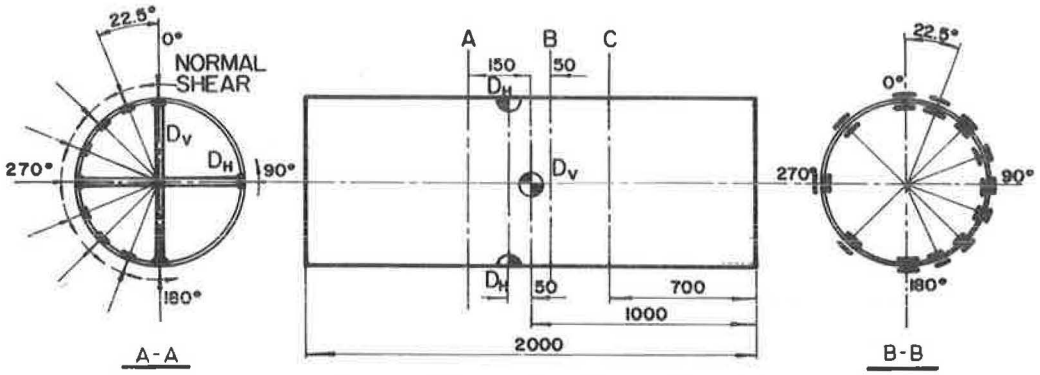

FIGURE 2 Sections of measurement: (A) normal and tangential soil-stress transducers, (B) internal and external hoop strain gauges, and (C) radius of curvature.

and the repeatability of the measurements. The RCM measurements were taken manually.

- A multichannel data logger system was used for calibration and recording, calculating, and storing measurements. The data were printed out and later transferred to a personal computer for further analysis.

Testing Procedure

The pipe segments were tested in the soil box 1.85 m (72.8 in.) wide except the pipe with 1.28-m (40.47-in.) outside diameter, which was tested at a width of 3.0 m (118 in.) to simulate wide trench conditions. The testing procedure began with preparation of the bedding. In all tests the rigid bottom of the soil box was covered with a layer of fine sand of a variable thickness compacted to about 98 percent standard Proctor so that the height of cover remained 50 in. (1.25 m) for all pipes. Three installation designs were used:

- Code A: Backfill compacted in layers to a height of 0.25 m (10 in.) above the crown of the pipe and the remaining soil box height backfilled with dumped soil,
- Code B: Backfill compacted in layers up to a height of 60 percent of the pipe's outer diameter and the rest with dumped soil as in Code A,
- Code C: Dumped soil backfill from the compacted foundation to the top of the soil box.

Compaction of the backfill above the pipe foundation (Codes A and B) was carried out in layers, starting from the soil box walls and moving toward the pipe, to reach 90 percent standard Proctor for sand and 85 percent standard Proctor for clay. The dumped soil (Code C) was slightly compacted to get a uniform backill. Hence, the actual degree of compaction of the Code C backfill was up to 85 percent of standard Proctor for sand and up to 80 percent of standard Proctor for clay. The quality of the installation was defined by the degree of compaction under the haunches of the pipe. Well-compacted haunches (Code ch) and dumped haunches (Code dh) were included.

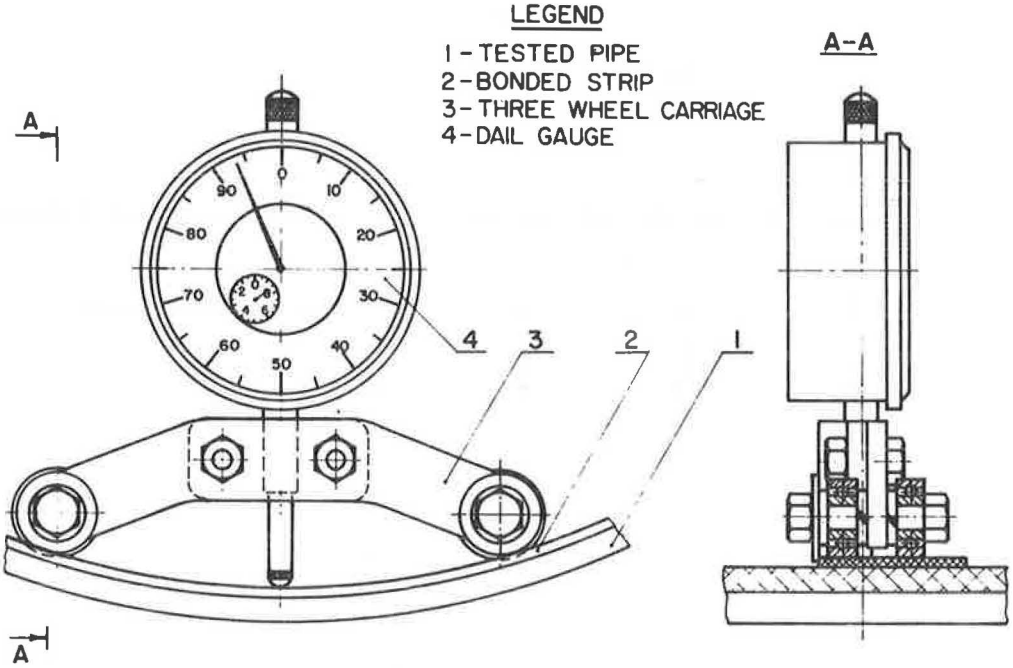

FIGURE 3 Radius of curvature meter.

The response of the pipe specimens to external loading was established by the previously mentioned measurements of soil stresses, pipe strains and deflections, and radii of curvature of the pipe. The measurements were recorded in eight stages in each test series:

- When the pipe was resting free on the foundation;
- When the backfill reached a height of 60 percent of the vertical pipe diameter;
- When the backfill reached a height of 0.25 m (10 in.) above crown level;
- When the backfill reached the top of the soil box, approximately 1.25 m (50 in.) above pipe crown;
- At up to four surcharge pressures of as much as 29 lb/in.2 (200 kPa) or until strain of up to 2000 microstrains was recorded.

All measurements were taken after a stabilization time of 1 hr at each stage in order to cancel short-term time effects.

DISCUSSION OF RESULTS

A total of 21 full-scale test series were performed within the framework of the study. Seventeen of these tests were short-term ones (up to 24 hr each); in each of the remaining test series, measurements were taken during 1 month under sustained load. The main findings of the short-term study are presented and discussed.

Normal and Tangential Stresses at Pipe-Soil Interface

Typical results of contact stresses at the pipe-soil interface are shown in Figures 4 and 5. In most of the tests soil stresses at the invert of the pipe were quite small, and vertical equilibrium of pipe load was not satisfied; this phenomenon could be the result of lifting the pipe during compaction of the bedding and backfill. For the same surcharge pressure and installation design, normal soil stresses at the pipe-soil interface were smaller in sand (Figure 4) than in clay (Figure 5) and increased with pipe stiffness. In general, tangential stresses reached up to half the magnitude of the normal ones, and therefore they cannot be ignored when soil loads are calculated. Similar results were reported in an earlier study of soil stress distribution around buried pipes (*3*).

Vertical and Horizontal Soil Pressure Distributions in the Soil Box

Typical soil pressure distributions along the vertical wall of the soil box, and in the horizontal plane 10 in. (0.25 m) above the crown of the pipe are shown in Figures 6 and 7. It can be seen that the stiffness of the FRP pipe affects the soil pressure distributions even though it was measured at a distance of half the diameter above the pipe and one diameter from its side. In the case of a low-stiffness pipe (Figure 6) the lateral soil pressure is greater and the vertical soil pressure is smaller than in the case of the high-stiffness pipe (Figure 7). Note that sometimes sharp changes occurred in soil pressure distribution. This could be the result of local arching, poor contact between a specific transducer and the surrounding soil, or other local effects.

Vertical and Horizontal Pipe Deflections

Vertical and horizontal diametral deflections, during installation and when surcharge pressure was applied to the top of the soil box, are shown in Figure 8. As expected, vertical and horizontal pipe deflections are greater in clay backfill and in installation design

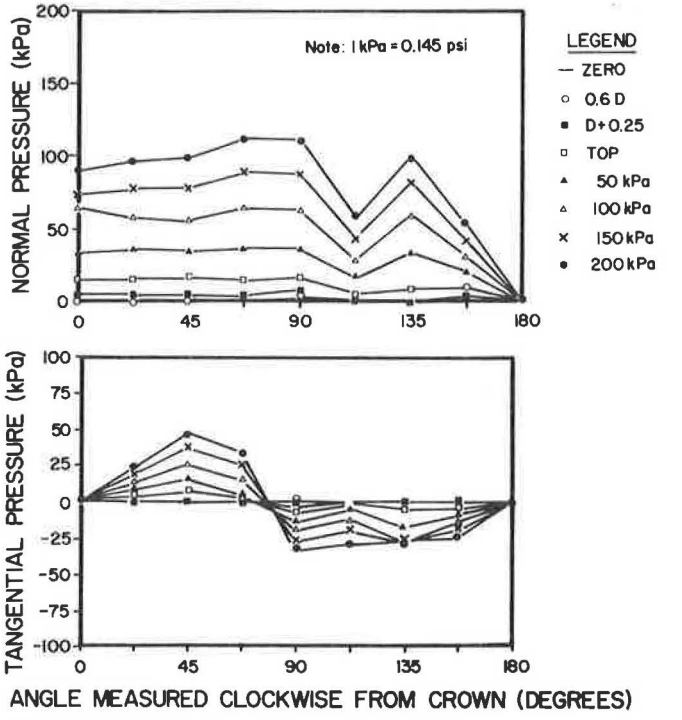

FIGURE 4 Normal and tangential soil stresses around 4.62-kPa pipe in sand, Code B/ch installation design.

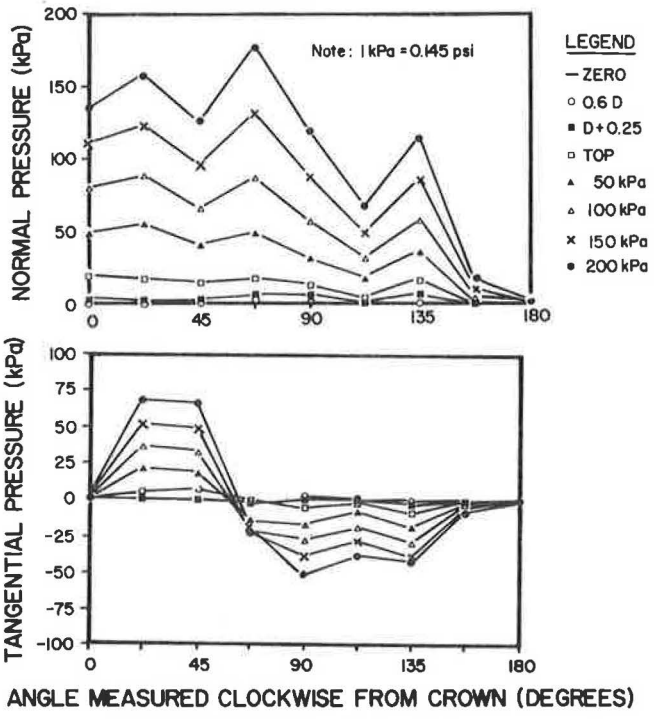

FIGURE 5 Normal and tangential soil stresses around 4.62-kPa pipe in clay, Code B/ch installation design.

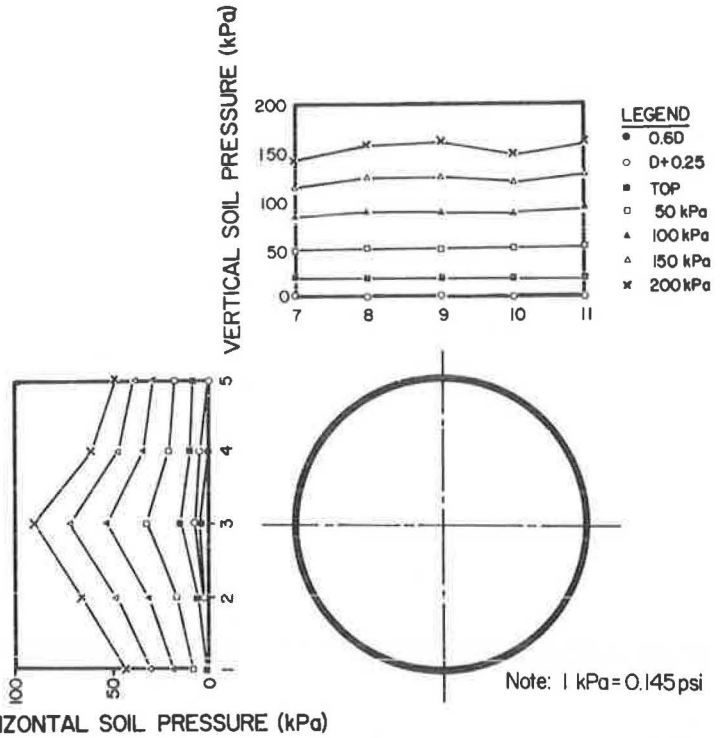

FIGURE 6 Vertical and horizontal soil pressure in the soil box, 1.27-kPa pipe in clay, Code A/ch installation design.

Code C than in sand and in higher-class installations. It can be seen in the figure that large initial deflections occurred in the more flexible pipe during installation (0.6*D*, Figure 8*a*). When soil construction is completed and surcharge pressure is applied, the installation deflections disappear and opposite deflections occur. When more rigid pipe and less compaction effort were applied, the initial deflections were negligible and the final deflections were relatively large (Figure 8*b*). This demonstrates that soil modulus or compaction degree affects pipe deflection more than pipe stiffness does over the tested range of relative soil and pipe stiffnesses. Proper soil compaction during installation also results in initial deflections, which are normally not accounted for in design. These

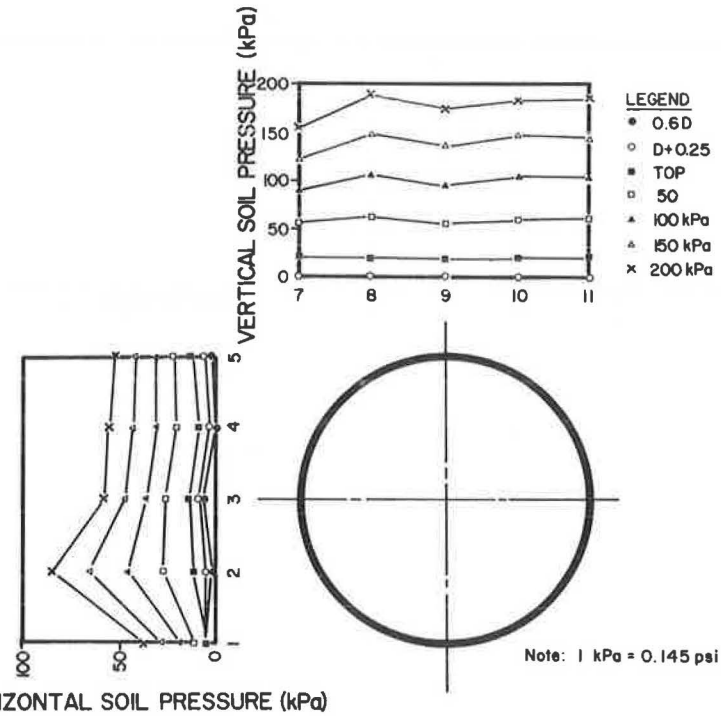

FIGURE 7 Vertical and horizontal soil pressure in the soil box, 4.62-kPa pipe in clay, Code B/ch installation design.

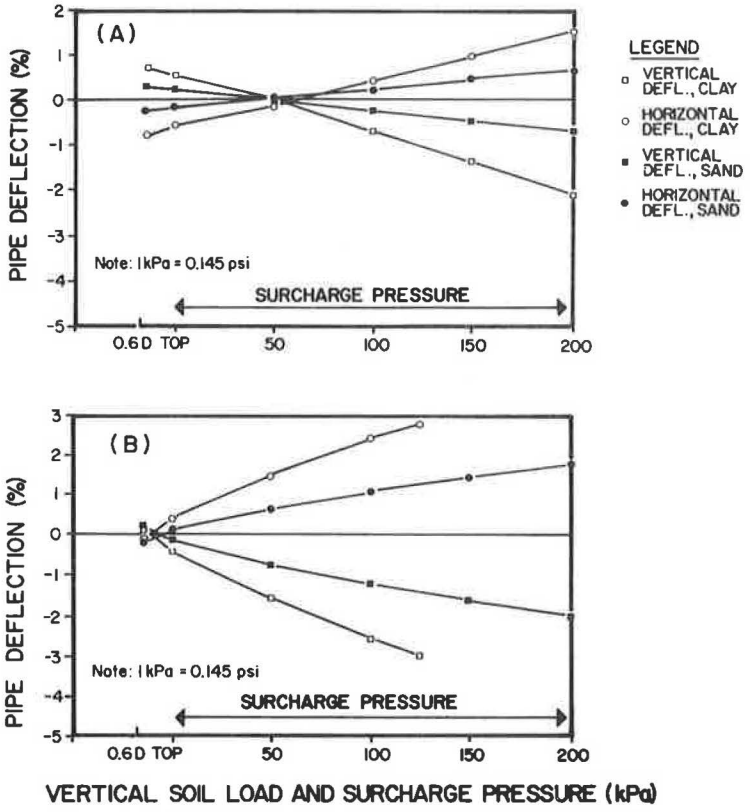

FIGURE 8 Vertical and horizontal pipe deflections in sand and clay: (A) 5.28-kPa pipe, Code B/ch installation design; (B) 10.84-kPa pipe, Code C/dh installation design.

installation deflections and the associated strains may contribute to better performance of the flexible pipe under full load.

Hoop Strains in the Pipe Wall

The measured hoop strains at the inner and outer surfaces of the pipe wall are shown in Figures 9 and 10. The distribution of strains expected in relatively rigid pipes (i.e., with extreme values at crown and spring line) was found only in the more rigid pipe placed in dumped clay (Figure 9). In all of the other tests (Figure 10) strain distributions were irregular at both the inside and the outside surfaces of the pipe. This phenomenon of irregular strain distribution, including the presence of a local minimum at the pipe invert and several zero points around the pipe, was also reported in an earlier study of flexible and semirigid pipes (*4*, *5*).

Another typical result of soil loading of nonpressure flexible pipes was the magnitude of the compression hoop strains induced by the surrounding soil. In all tests the compression (negative) hoop strains at any radial cross section of the pipe wall were much greater than the tensile (positive) strains at the same cross section (Figures 9 and 10). This was not found in a soil-pipe interaction study of relatively rigid asbestos-cement pipes (*5*).

Thrust and Bending Hoop Strains

The contribution of soil loading and backfill design to hoop strains in the pipe wall is better demonstrated by the induced bending

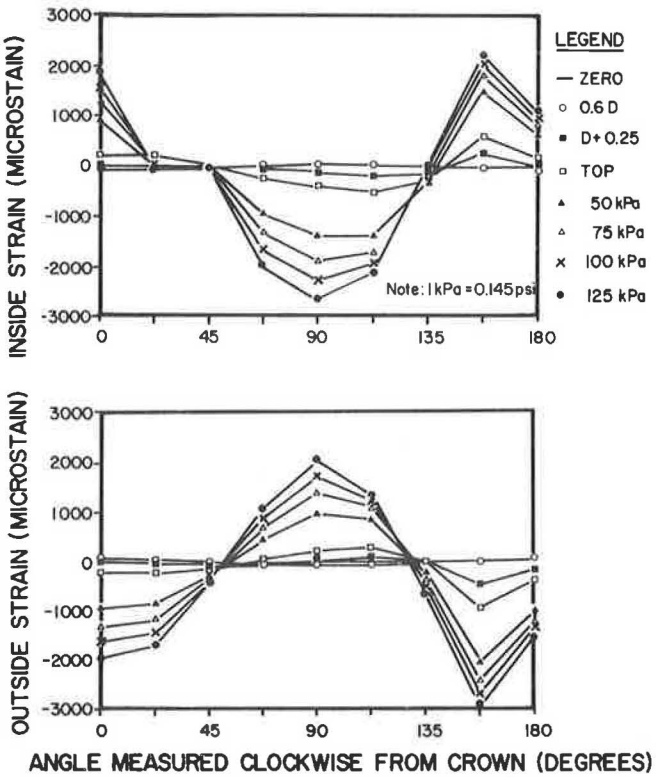

FIGURE 9 Inside and outside strains in 10.84-kPa pipe in clay, Code C/dh installation design.

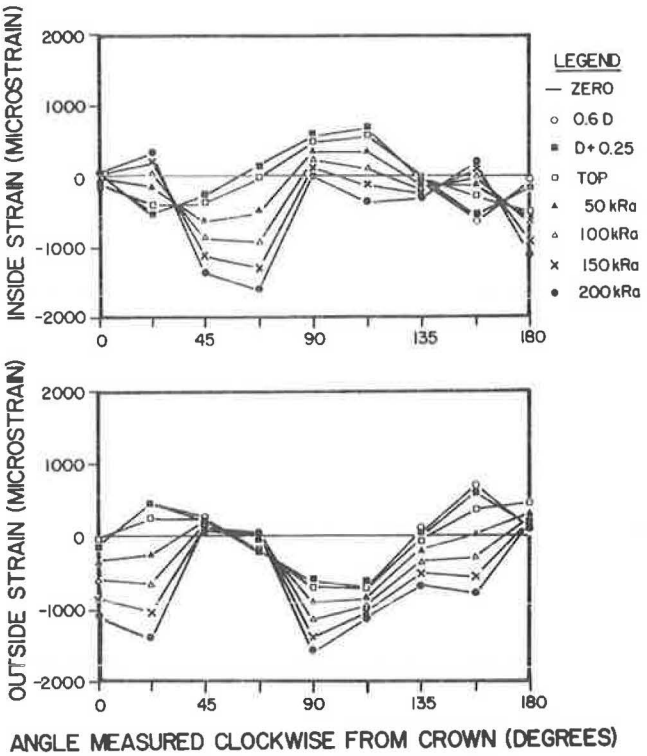

FIGURE 10 Inside and outside strains in 1.27-kPa pipe in sand, Code B/dh installation design.

moments. The strains (e_{in} and e_{out}), measured at the inner and outer surfaces of the pipe, give the sum of both those due to bending moments and those due to normal thrust in the wall of the pipe. Their separation into "thrust strains" and "bending strains" was calculated from the following expressions:

$$e_{thrust} = (e_{in} + e_{out})/2 \quad (1)$$

$$e_{bending} = (e_{in} - e_{out})/2 \quad (2)$$

Two illustrative examples of these equations are shown in Figures 11 and 12, in which the inside and outside strains are separated into thrust and bending strains. The magnitude of the thrust strains in flexible pipes and the irregular distribution of the bending strains can be clearly seen. In general, thrust strains and the ratio of thrust strains to bending strains increased with decreasing pipe stiffnesses. It can be shown (*1*) that irregular distribution is caused mainly by installation strains that reduce the final opposite strains under full load. The thrust strains, which reached a level of only a few microstrains in the case of asbestos-cement pipes (*5*), are of a significant magnitude in the flexible FRP pipes.

Installation Quality

The influence of installation quality is shown in Figure 13. As expected, better installation quality considerably reduces the hoop strains in the pipe wall. With well-compacted haunches (Figure 13*a*), maximum strains were recorded in the upper part of the pipe. The dumped haunches caused increasing strains in the lower part of the pipe (Figure 12*b*), and the maximum strains were shifted to the bedding area. However, the effect of poor haunches (or the difference between the extreme hoop stresses in the lower and the upper part of the pipe) was found to be less important in the higher stiffness ranges of the FRP pipes.

Split Backfill

Split backfill design was investigated in three test series. The first one was performed with a pipe of 4.62 kPa (0.67 lb/in.^{2}) stiffness, and compacted sand was filled up to 0.6 of the pipe diameter (Code B) and the rest of the soil box was filled with dumped clay. The strains in the lower part of the pipe were similar to those shown in Figure 14*a*, which shows the same pipe laid in sand of Code-B backfill design. In the upper part of the pipe, the strains of the split backfill test were as much as 50 percent larger than those obtained in sand. However, the maximum strains under full surcharge load of 200 kPa (29 lb/in.^{2}) were less than 1800 microstrains.

The split backfill design of compacted sand and dumped clay was repeated in a second test (Figure 14), but with a very flexible pipe (1.27 kPa). As a result, high strains occurred at a relatively low surcharge pressure (Figure 14*a*), and the upper part of the pipe lost its circular shape. In a third test, the dumped clay above the sand level of $0.6D$ was replaced by compacted clay, up to the $D + 0.25M$ (10 in.) level as in the Code-A backfill design. The results were impressive: the surcharge pressure was increased to its maximum value without reaching excessive strains (Figure 14*b*).

Radius of Curvature of the Deflected Pipes

The radii of curvature, measured by the RCM, give quantitative information about the shape of the deflected pipe at any tested point. Its changes from the state of "zero load" also indicate the magnitude of the bending strain or bending moment at a specific

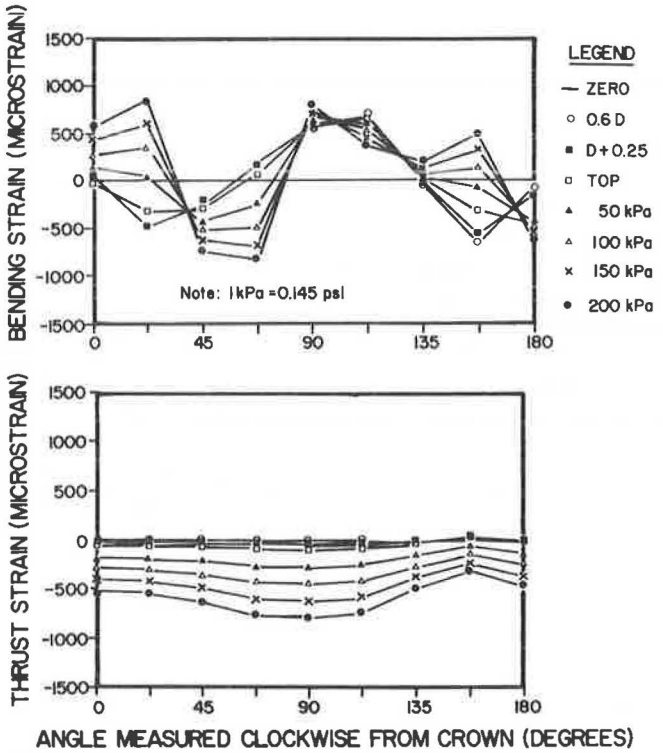

FIGURE 11 Bending and thrust strains in 1.27-kPa pipe in sand, Code B/dh installation design.

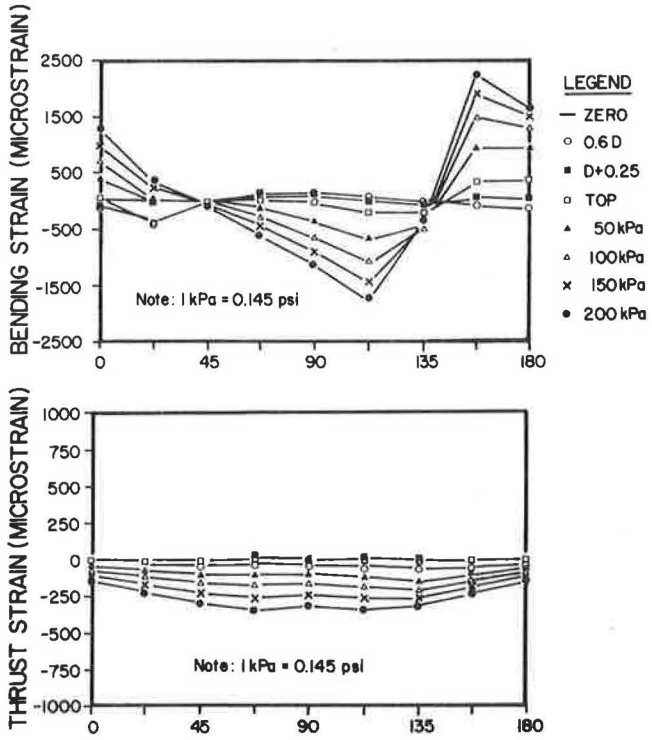

FIGURE 12 Bending and thrust strains in 10.84-kPa pipe in sand, Code C/dh installation design.

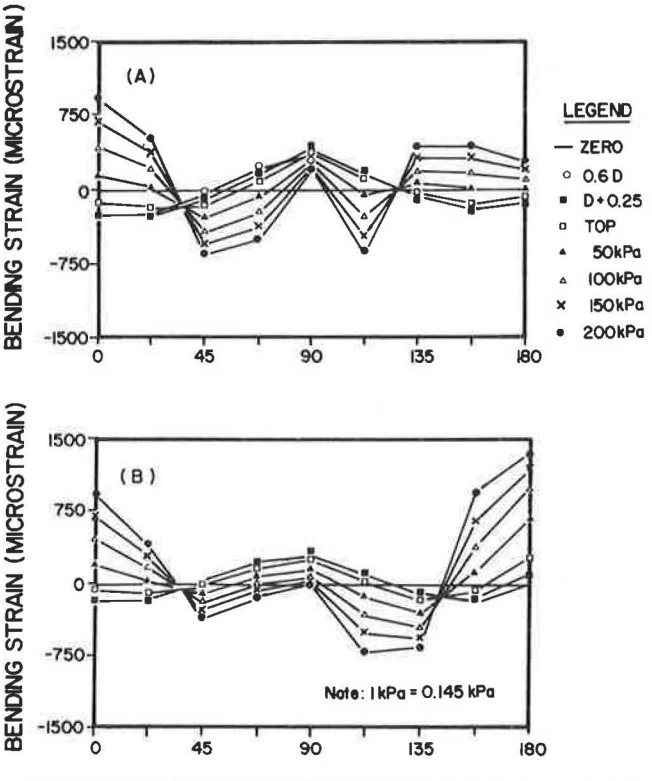

FIGURE 13 Bending strains in 4.62-kPa pipe in sand, Code B installation design: (A) compacted haunches and (B) dumped haunches.

point. Relatively large changes of the radius of curvature were measured during installation (0.6D backfill height) at the pipe spring line and invert. When backfilling was completed, the shape of the pipe was slightly rerounded. The RCM measurements also indicated whether dumped haunches were applied: the changes in the lower part of the pipe in this case were much greater than those that occurred when compacted haunches were applied. Thus the RCM served as a quick inspection tool during installation. An additional application of the RCM in cross checking strain measurements is shown in Figure 15.

Bending Strains Calculated from Radius of Curvature

The bending strains were calculated from strain measurements by Equation 2. Bending strains were also calculated from the measured radii of curvature and their alterations due to the various loads according to the following equation:

$$e_{\text{bending}} = (1/r - 1/r_0)t/2 \tag{3}$$

where

r = midwall radius of curvature of the deflected pipe,
r_0 = midwall radius of curvature of the undeflected pipe ("zero load"), and
t = wall thickness.

The bending strains based on (a) the strain gauge and (b) the RCM measurements are illustrated in Figures 15a and 15b, respectively. Fairly good compatibility is shown between the bending strains measured by the strain gauges and by the RCM. This

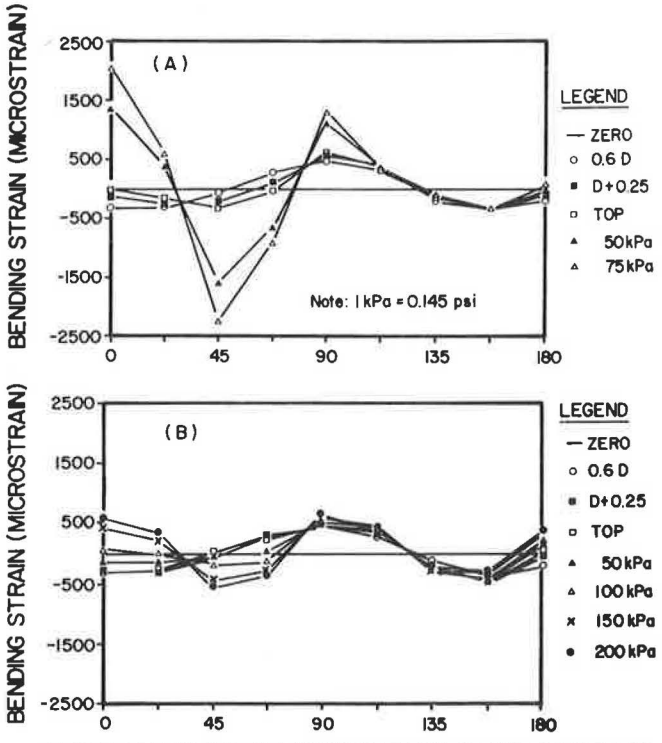

FIGURE 14 Bending strains in 1.27-kPa pipe in split backfill of sand and clay: (A) Code B/ch installation design and (B) Code A/ch installation design.

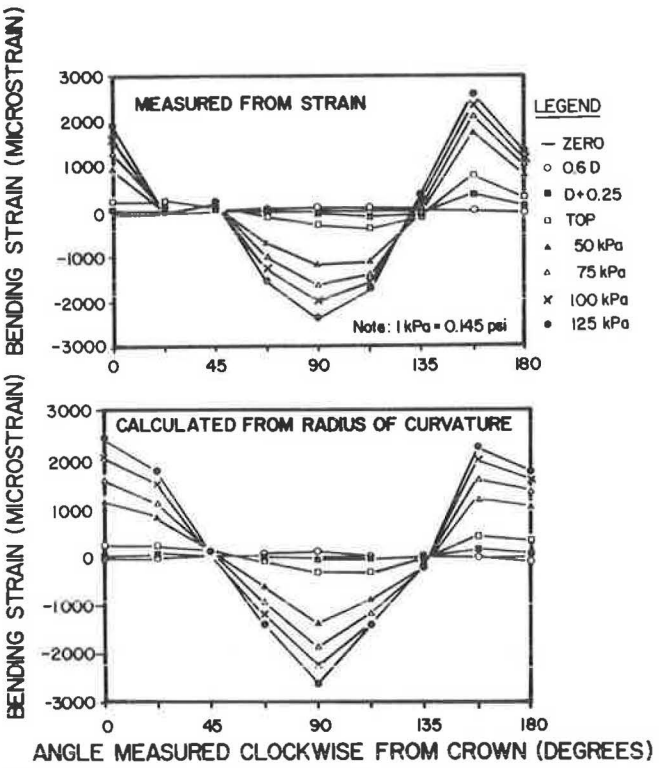

FIGURE 15 Bending strains in 10.84-kPa pipe in clay, Code C/dh installation design, measured from strains and calculated from radius of curvature.

compatibility, which was also found in the other tests, is of great importance as proof of the reliability of the test results. Some discrepancies between the two may be due to the fact that the two sets of measurements were taken around two different cross sections of the flexible pipe. An exception is observed in Figure 15 at an angle of 22.5 degrees from the crown. Here the discrepancy between the two measurements is due to malfunction of a strain gauge at the inner face of the pipe (see also Figure 9).

CONCLUSIONS

The main conclusions of the study can be summarized as follows:

- For the same installation design and surcharge pressure, soil stresses at the pipe-soil interface increase with pipe stiffness and are smaller in sand than in clay. The lateral soil pressure increases and the vertical soil pressure decreases when more flexible pipe and a higher degree of compaction are applied.
- Pipe deflections are reduced considerably with increasing soil modulus or degree of compaction. Proper soil compaction during installation is also associated with initial deflections that contribute to better performance of the flexible pipe under full load.
- Strain distribution around flexible pipes in well-compacted backfill is mostly irregular and the maximum strains do not always occur at the crown of the pipe or at its invert, as would be expected from a more rigid pipe. However, proper soil compaction considerably reduces maximum strains and deformations, in spite of the irregularities.
- The thrust strains in these pipes are of a significant magnitude. In the case of the more flexible pipes, they may reach the same order of magnitude as those due to bending. As a result, the extreme hoop strains in the wall of the nonpressure pipe are compressive (negative).
- Poorly compacted haunches result in higher strains, mainly in the lower part of the pipe. This effect of poor haunches appeared to be less important in the higher stiffness ranges of the FRP pipes.
- Split backfill of sand and clay, both well compacted, was quite successful. Such a backfill might safely be applied and recommended if results of prolonged tests were available.

The experience gained during the application of the radius of curvature meter (RCM) in this study suggests that the calculation of bending strains from the RCM measurements is simple and reliable. The RCM was utilized successfully for cross-checking the data obtained from strain gauge measurements. Additional potential use of the RCM is as a quick inspection tool for proper installation.

ACKNOWLEDGMENTS

This study was supported by the Israel Asbestos-Cement Corporation. The authors would like to acknowledge Shaul Bar-Shlomo, consultant to the pipe industry, for his assistance and fruitful contributions.

REFERENCES

1. N. Galili and I. Shmulevich. Testing of Buried Fiberglass-Reinforced Plastic Pipes. *Composite Materials Testing and Design*. STP 787. ASTM, 1982, pp. 559–578.
2. A. P. Moser, R. R. Bishop, O. K. Shupe, and D. R. Bair. "Deflection and Strain in Buried FRP Pipes Subjected to Various Installation Conditions." In *Transportation Research Record 1008*, TRB, National Research Council, Washington, D.C., 1985, pp. 109–116.
3. I. Shmulevich, N. Galili, and A. Foux. Soil Stress Distribution Around Buried Pipes. *Journal of the Pipeline Division*, ASCE, forthcoming.
4. N. Galili, I. Shmulevich, S. Bar-Shlomo, and A. Foux. *Soil-Pipe Interaction, Stages I and II, Final Report*. Publication 291. Agricultural Engineering, Technion City, Haifa, Israel, Nov. 1978.
5. I. Shmulevich and N. Galili. Deflections and Bending Moments in Buried Pipes. *Journal of the Pipeline Division*, ASCE, forthcoming.

Publication of this paper sponsored by Committee on Culverts and Hydraulic Structures.

Inelastic Flexural Stability of Corrugations

RAYMOND L. CARY

Empirically derived dimensional limits are presented for arc-and-tangent corrugated profiles to ensure local stability during inelastic bending; for example, during manufacture of culverts, storage bins, and conveyer covers. An empirical relationship for corrugation moment capacity is also presented. Twenty-four arc-and-tangent corrugated steel sheet specimens in eight corrugation and gauge combinations were tested in flexure with uniform moment. Test parameter ranges were arc inside radius-to-thickness ratios (3.7 to 27.7), tangent length-to-thickness ratios (4.4 to 23.6), and material yield strengths (40 to 50 ksi). Tangent length varied from 0.45 to 1.7 times the inside radius of the arc.

This study investigates the local stability of arc-and-tangent corrugated profiles when subjected to inelastic bending. Corrugated sheets are frequently curved to form products such as culverts, storage bins, and conveyer covers. The engineer must decide if the corrugated sheet can be satisfactorily curved without buckling. Certain structural installations may require the engineer to know the corrugation's critical flexural strain. Engineers have used experience and engineering judgment, based on elastic behavior, in developing dimensional limits for such corrugated products. Geometric limits based on elastic behavior may be unconservative, however, when corrugations sustain large inelastic strains. The engineer may also lack experience.

The only published research with some applicability to arc-and-tangent corrugated profiles deals with inelastic buckling of circular tubes. Sherman's research (*1*) is one example. Sherman conducted tests to determine the required outside diameter-to-thickness ratio (D/t) limit to prevent local buckling at fully developed plastic hinges. He concluded that members with D/t of 35 or less can sustain sufficient rotations to fully develop plastic hinges and failure mechanisms where F_y = 44 ksi. Maximum strains, however, were only about 2 percent. This is considerably less than many corrugated structures require to be successfully formed.

Sherman (*1*) also stated that critical strain and other inelastic buckling characteristics appears to be related to $(F_y)^{1/2}$ rather than to F_y or to a buckling parameter of $(t/D)^2$ (F_y/E) rather than (t/D) (F_y/E).

The current study presents empirically derived relationships from 24 flexural tests that relate critical corrugation dimensional limits to critical buckling strain, minimum curving radius, and ultimate moment capacity.

EXPERIMENTAL PROGRAM

Flexural tests of corrugated profiles and material tests to determine mechanical properties were conducted. Shown in Figure 1 with key dimensions are the three commonly available corrugated profiles tested. The corrugations and material thicknesses tested are given in the following table. Thickness equivalents for these U.S. standard sheet gauges are given in Table 1.

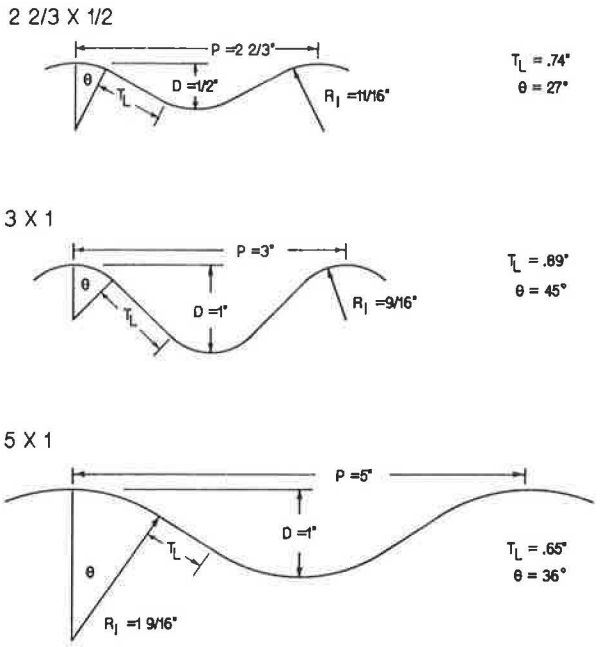

FIGURE 1 Test arc-and-tangent corrugated profiles with dimensions (T_L and Θ vary slightly with gauge).

Corrugation (in.)	*Thickness (gauge)*
2 2/3 x 1/2	8, 14, and 20
3 x 1	8, 16, and 20
5 x 1	12 and 16

Note that 5 x 1 are nominal dimensions. This is a metric corrugation (125 x 25 mm).

Arc inside radius-to-thickness (R_i/t) ratios, tangent length-to-thickness (T_L/t) ratios,and material yield strengths (F_y) are the major parameters that affect local stability of corrugation for any given material. The selected profiles and material gauges test a broad parameter range of R_i/t (3.7 to 27.7) and T_L/t (4.4 to 23.6). Material gauges were chosen to compare corrugation behavior when either of the dimensional parameters is nearly equal in different nominal profiles.

Material Tests

Material samples were cut from a tangent portion of each corrugated sheet test specimen. Average tensile properties are given in Table 2 for the eight profile and gauge combinations. Yield strength varied from approximately 40 to 50 ksi.

Armco Inc. Research Center, Middletown, Ohio 45043.

TABLE 1 ABRIDGED TABLE OF THICKNESS EQUIVALENTS FOR U.S. STANDARD SHEET GAUGES

Gauge No.	U.S. Standard Gauge for Uncoated Sheet (in.)
8	0.1644
12	0.1046
14	0.0747
16	0.0598
20	0.0359

TABLE 2 MATERIAL PROPERTIES

Corrugation	Gauge	Yield Strength (ksi)	Ultimate Tensile Strength (ksi)	Elongation in 2 in. (%)
3 x 1	8	43.5	55.4	30.8
3 x 1	16	47.7	59.0	30.6
3 x 1	20	41.5	55.2	32.2
5 x 1	12	48.5	60.1	25.8
5 x 1	16	43.3	56.7	27.6
2 2/3 x 1/2	8	48.7	60.0	25.3
2 2/3 x 1/2	14	43.9	55.1	27.6
2 2/3 x 1/2	20	42.3	54.2	29.1

Note: Average of six tensile tests for each gauge.

Flexural Tests

Test Specimens

Triplicate specimens were cut for flexural testing from each corrugation profile and gauge. Each specimen was 36 in. long and three or five corrugations wide, determined by the test fixture width. Specimens were cut along the profile neutral axis to ensure that the free edge would be unstressed in flexure.

Corrugations were measured across the entire width of each specimen and dimensions averaged to calculate appropriate design properties. Key buckling parameters R_i/t and T_L/t are listed in Table 3 as average measured values for triplicate specimens.

Flexural Test Procedure

The test setup is shown in Figures 2–4. Flexural specimens are subjected to a constant moment in the 3 1/2-in.-long region between the two center rollers. The two support rollers, 19 1/2 in. apart, and two center rollers are steel rounds machined and lubricated at each end to roll freely as the specimen deflects during the test. An 1/8-in.-thick neoprene cushion is bonded to each roller to distribute high local bearing pressures during the test over a portion of each arc. Figure 3 shows the fixture accommodating the large beam deflections necessary in this study.

A deflectometer, shown in Figure 4, is placed in the valley of test specimen corrugations to measure specimen curvature in the center region of constant moment. The specimen's deflected shape in the constant moment region is conservatively assumed to be a circular arc. The deflectometer consists of two pairs of legs each spanning 3 in. and a linear displacement transducer (LVDT) centered between one pair of legs. The LVDT measures deflections to the nearest 0.0001 in. in the circular arc over a fixed chord length of 3 in. between legs. With midchord deflections and chord length known, the mean arc radius of curvature can be calculated by Equation 1.

$$R_c = (4b2 + 9)/8b - d/2 \quad (1)$$

where

R_c = mean radius of curvature along the corrugated profile neutral axis,
b = LVDT deflection reading, and
d = corrugation depth.

With the arc radius of curvature determined, the extreme fiber strain can be calculated by the simple flexure Equation 2.

$$\varepsilon = (d + t)/2R_c \quad (2)$$

where ε is extreme fiber strain and t is material thickness.

Equation 2 overestimates ε for extreme bending to small radii of curvature. Because of neutral axis shift, the relationships in Equations 1 and 2 become complicated beyond the scope of this paper. However, any inaccuracy in the calculated strain (ε) is cancelled out whenever R_c is later back-calculated using strains developed from Equation 2.

Initially, strain gauges were also applied to test specimens to directly measure strains. Gauge debonding problems as well as cost discouraged the further use of strain gauges.

Loading was applied in deflection increments as recorded by the deflectometer at midspan and held steady at each increment until the load was stable for 1 min. Usually, a 4- or 5-min maximum hold stabilized loads at each increment.

A second LVDT measured fixture vertical displacement. This

TABLE 3 MEASURED AND NORMALIZED CORRUGATION BUCKLING PARAMETERS

Corrugation	Gauge	Measured[a]		Normalized[b]	
		R_i/t	T_L/t	R_i/t_n	T_L/t_n
3 x 1	8	3.8	4.5	4.3	5.2
3 x 1	16	10.8	15.1	12.9	18.2
3 x 1	20	17.0	23.5	19.1	26.3
5 x 1	12	15.1	9.0	18.4	10.9
5 x 1	16	26.5	15.4	30.4	17.7
2 2/3 x 1/2	8	4.3	4.4	5.2	5.4
2 2/3 x 1/2	14	10.0	9.7	11.5	11.2
2 2/3 x 1/2	20	18.2	20.0	20.6	22.7

[a]Average corrugation parameters for three specimens.
[b]Normalized to design F_y = 33 ksi by multiplying R_i/t and T_L/t $(F_y/33)^{1/2}$.

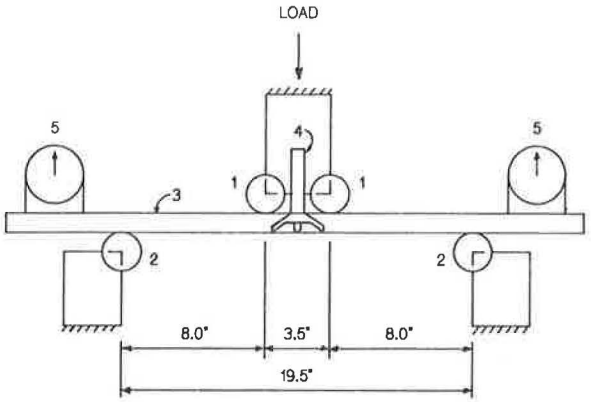

ITEM DESCRIPTION:

1. 1.75 IN. DIAMETER STEEL LOAD ROLLERS COVERED WITH .125 IN THICK NEOPRENE.
2. 1.75 IN. DIA. STEEL SUPPORT ROLLERS COVERED WITH .125 IN. THICK NEOPRENE.
3. CORRUGATED FLEXURAL TEST SPECIMEN.
4. DEFLECTOMETER TO MEASURE MIDSPAN CURVATURE.
5. MAGNETIC BASE INCLINOMETER TO MEASURE ANGULAR CHANGE OF ENDS.

FIGURE 2 Flexural test setup.

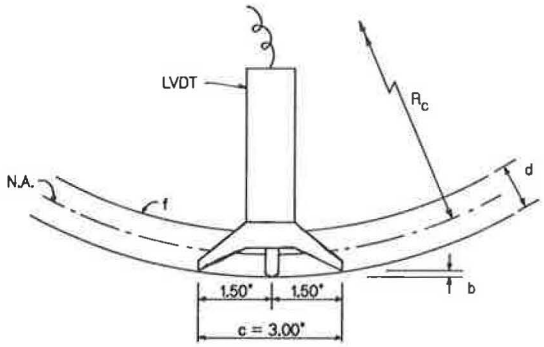

ITEM DESCRIPTION:

b = DEFLECTOMETER DEFLECTION READING

c = CHORD LENGTH OR DISTANCE BETWEEN DEFLECTOMETER LEGS

d = DEPTH OF CORRUGATED SPECIMEN

f = ASSUMED CIRCULAR ARC DEFLECTED SHAPE OF FLEXURAL SPECIMEN

LVDT = LINEAR DISPLACEMENT TRANSDUCER

N.A. = SPECIMEN NEUTRAL AXIS ASSUMED AT MIDDEPTH FOR ALL STRAIN LEVELS

R_c = MEAN RADIUS OF CURVATURE

FIGURE 4 Deflectometer for measuring curvature.

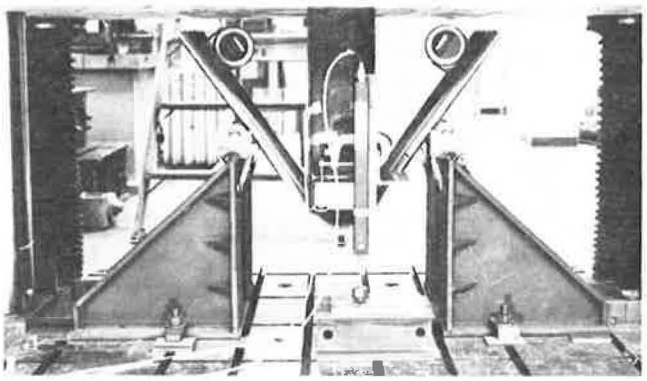

FIGURE 3 Flexural specimen during test.

displacement plus deflectometer reading, applied load, and panel rotations recorded by inclinometers enabled calculation of bending moments in the corrugated sheet. Bending moment equations are not shown because of the length and complexities caused by loads and reactions through the fixture rollers always being normal to the curved specimen. The raw data were input to a computer program that calculated bending moment, bending radius, and strain at each loading increment.

Critical Buckling Strains

The author detected initial buckling by feel, running his fingers over the multiple corrugation surfaces at each deflection increment. When surface irregularities were felt, the affected corrugation, buckled component, and deflections were recorded. Although this method is not sophisticated, it gave reasonably good replication of triplicate test results. Buckling always initiated at one of the corrugations nearest the free edge of the panel. To eliminate influence of free edges, the test specimen was not considered buckled until an interior corrugation buckled.

After testing the 3 x 1, 20-gauge specimens, it was obvious that the arcs of corrugations in compression had deformed at center load lines due to large bearing pressures from the rollers. Round bar inserts the size of the arc radius were cut 3/4 in. long. A segment equal to the corrugation height was inserted between the center rollers at each corrugation to help distribute loads more uniformly into the flexural specimen (Figure 5). The same three 20-gauge specimens were retested by cutting off the previously failed center portion and reloading. All exhibited increased strain capacity before buckling. One 3 x 1, 16-gauge specimen was retested in similar manner without a discernible difference in critical strain. Thus the other two 3 x 1, 16-gauge specimens were not retested. Thereafter all specimens tighter than 8 gauge were tested with inserts.

To account for effects from varying material yield strengths, specimen parameters R_i/t and T_L/t were normalized with respect to yield strength. As was reported by Sherman (*1*), less scatter was evident when data were normalized with $(F_y)^{1/2}$ instead of F_y. Thus R_i/t and T_L/t were normalized to use in design by multiplying by $(F_y/33)^{1/2}$, where F_y is the tangent tensile yield strength and 33 ksi is the AISI (2) and AASHTO (M218–82) design yield strength for buried corrugated steel structures. Normalized corrugation

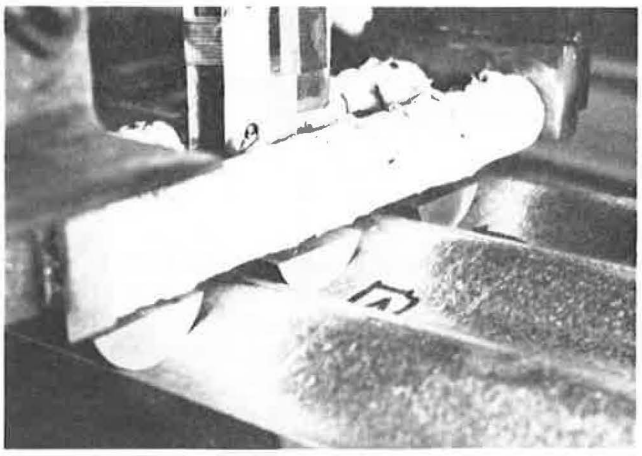

FIGURE 5 Corrugation support inserts.

parameters are shown in Table 3 along with average measured values for comparison.

Careful observation of the failure modes, critical buckling strain values, and review of numerous plots of critical strain versus normalized R_i/t and T_L/t, separately and combined, led to the conclusion that T_L/t does not significantly affect flexural buckling for the range of R_i to T_L relationships tested: $0.45\ R_i \le T_L \le 1.7\ R_i$. R_i/t is the dominant factor. If T_L is greater than R_i, buckling will be initiated in the tangents. If R_i is greater than or equal to T_L, buckling is initiated in the corrugation arcs. However, regardless of buckling mode, critical buckling strain appears to be unaffected.

Figure 6 shows a plot of nominal critical flexural strains versus normalized R_i/t (R_i/t_n). The three curves represent three possible choices for lower-bound predictions of critical strain. The first is a modified version of a lower bound for buckling of circular tubes suggested by Sherman (*1*). The coefficient has been modified to account for differences in design yield strengths. This curve proves

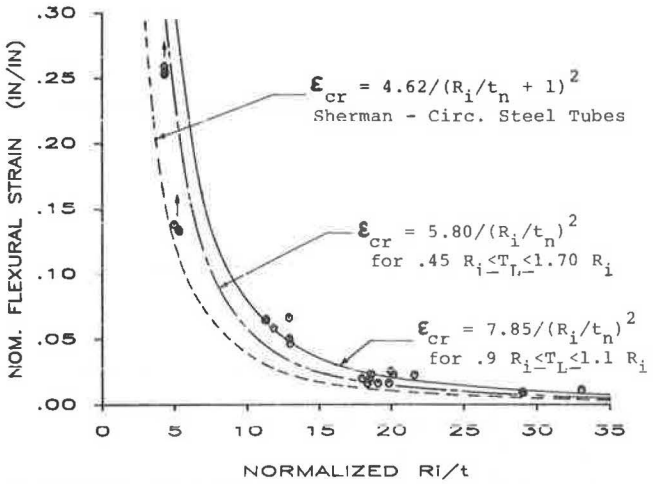

FIGURE 6 Critical flexural strain for arc-and-tangent corrugations.

to be too conservative for predicting critical strains of arc-and-tangent corrugated profiles.

The second is a general curve for the range of R_i to T_L relationships represented by the test data. Although six specimens of 8-gauge material fall below the second curve, none of the six experienced buckling. They were simply limited by the fixture geometry that would not permit additional strain to be induced. It is quite probable that corrugations with R_i/t_n of 5.5 or less will be limited by material elongation capacity rather than buckling.

The third curve appears to reasonably predict critical strains for profiles where T_L is within 10 percent of R_i values, the approximate relationship of 2 2/3 x 1/2 profile.

Ultimate Moment Capacities

T_L/t appears to be the most significant factor in determining the profile's maximum moment capacity for the range of R_i to T_L relationships tested. R_i/t factors are minor contributors. Two examples help support this conclusion. The first example compares 3 x 1, 20-gauge and 5 x 1, 12-gauge specimens. R_i/T_n factors are nearly equal, but T_L/t_n factors differ dramatically (see Table 3). The 3 x 1 T_L/t_n factors are about 26, and moment capacity averaged 94 percent of its calculated plastic moment. The 5 x 1 T_L/t_n factors are about 11, and moment capacity averaged 107 percent of its plastic moment. A second example compares the 5 x 1, 12-gauge with the 2 2/3 x 1/2, 14-gauge specimen. Here, R_i/t_n factors are different, 18.4 versus 11.5, but T_L/t_n factors for both are about 11. Both corrugations developed 107 percent of their calculated plastic moment capacity.

Figure 7 is a plot that compares maximum test moments with calculated plastic moments as a function of normalized T_L/t. Plastic moment capacity is calculated by multiplying the specimen's tangent tensile yield strength by its plastic modulus. The middle curve, labeled "M_{uc}," is the mean of the best fit generated by a curve-fitting program. All data points are within ±10 percent of the mean. The upper and lower curves are 95 percent confidence limits. For design, moment capacity (M_{uc}) should not exceed the plastic moment (M_p). Thus, for $T_L/t_n \le 16$, the moment capacity equals the plastic moment.

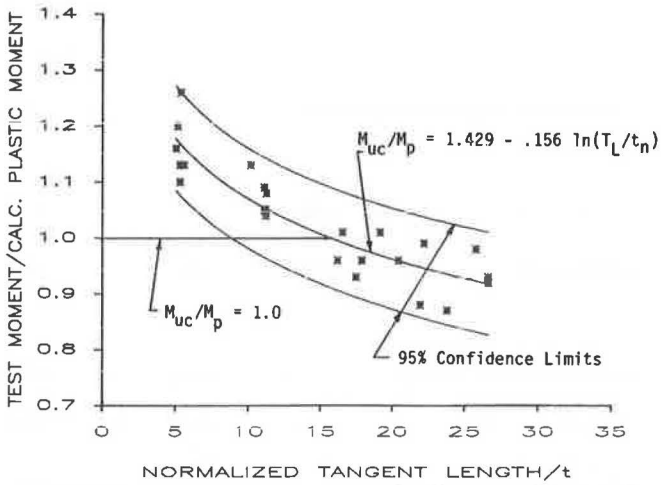

FIGURE 7 Bending moment capacity for arc-and-tangent corrugations.

DESIGN RECOMMENDATIONS

The following recommendations are based on limited test data and should not be used beyond the parameter range of $0.45\ R_i \le T_L \le 1.7\ R_i$ without further testing. Recommendations should be considered only as guidelines for corrugation design and are not intended to replace product testing.

Nominal Critical Flexural Strain

Two equations can be used for predicting nominal critical flexural strain in arc-and-tangent corrugated profiles. Equation 3 is for a specialized range of $0.9\ R_i \le T_L \le 1.1\ R_i$.

$$\varepsilon_{cr} = 7.85/(R_i/t_n)2 \qquad (3)$$

where

ε_{cr} = nominal critical flexural strain,
R_i/t_n = R_i/t normal by multiplying by $(F_y/33)^{1/2}$, and
F_y = material yield strength in ksi.

Equation 4 is for a broader range of $0.45\ R_i \leq T_L \leq 1.70\ R_i$.

$$\varepsilon_{cr} = 5.80/(R_i/t_n)^2 \quad (4)$$

In no case should ε_{cr} exceed that given in Equation 5.

$$\varepsilon_{cr} \leq \text{Material elongation limit} \quad (5)$$

To achieve maximum flexural strain capacity, corrugations should be designed with R_i/t and T_L/t nearly equal and as small as possible. In addition, material should be close to the minimum yield strength of 33 ksi.

The minimum curving radius can be calculated using Equation 6 when nominal critical flexural strain is known.

$$R_c = (d + t)/2\varepsilon_{cr} \quad (6)$$

where

R_c = mean radius of curvature of the corrugated profile,
d = corrugation depth, and
t = material thickness.

Ultimate Moment Capacity

Arc-and-tangent corrugation ultimate moment capacity can be calculated by Equation 7.

$$M_{uc} = [1.429 - 0.156 \ln (T_L/t_n)]\ M_p \leq M_p \quad (7)$$

where

M_{uc} = ultimate moment capacity,
M_p = calculated plastic moment, and
T_L/t_n = T_L/t normalized by multiplying by $(F_y/33)^{1/2}$.

When T_L/t_n exceeds 16 the ultimate moment capacity will be less than the calculated plastic moment (Figure 7).

SUMMARY AND CONCLUSIONS

Triplicate steel specimens in eight arc-and-tangent corrugation and gauge combinations were flexural tested to determine critical inelastic buckling strain levels and ultimate moment capacities. Specimens were 36 in. long and three or five corrugations wide. Key corrugation parameters were material yield strength (F_y), arc inside radius-to-thickness (R_i/t) and tangent length-to-thickness (T_L/t) ratios. F_y varied from 40 to 50 ksi, R_i/t from 3.7 to 27.7, and T_L/t from 4.4 to 23.6. All specimens were subjected to pure bending in the critical regions. Conclusions for arc-and-tangent corrugated steel profiles are, where $0.45\ R_i \leq T_L \leq 1.7\ R_i$,

1. Critical buckling strains area a function of $1/(R_i/t)^2$. T_L/t has little influence except in determining where buckling is first initiated.
2. Corrugations with R_i/t_n (normalized to 33 ksi yield strength) of 5.5 or less will probably be limited by material elongation rather than buckling.
3. Sherman's (I) equation for a lower bound of buckling in circular tubes is too conservative for corrugations.
4. Ultimate moment capacity is a function of the natural logarithm of T_L/t. T_L/t_n ratios (normalized to 33 ksi yield strength) must be 16 or less before the full plastic moment can be developed. R_i/t did not significantly affect moment capacity.

REFERENCES

1. D.R. Sherman. Tests of Circular Steel Tubes in Bending. *Journal of the Structural Division*, ASCE, Vol. 102, No. ST11, Nov. 1976, pp. 2181–2195.
2. *Handbook of Steel Drainage and Highway Construction Products*, 3rd ed. American Iron and Steel Institute, Washington, D.C., 1983.

Publication of this paper sponsored by Committee on Culverts and Hydraulic Structures.